# Electrical machine designs based on 3D flux paths with reuse & recycle magnet concepts for automotive applications

Pranshu Upadhayay

Communauté
UNIVERSITÉ Grenoble Alpes

# THÈSE

Pour obtenir le grade de

**DOCTEUR DE LA COMMUNAUTE UNIVERSITE GRENOBLE ALPES**

Spécialité : **Génie Electrique**

Arrêté ministériel : 25 mai 2016

Présentée par


## Pranshu UPADHAYAY


Thèse dirigée par **Afef KEDOUS-LEBOUC** et
codirigée par **Lauric GARBUIO** et **Jean-Claude MIPO**

préparée au sein du **Laboratoire de Génie Electrique de Grenoble (G2Elab),** en collaboration avec **Valeo Equipements Electriques Moteur (Valeo EEM)**
dans **l'École Doctorale Electronique, Electrotechnique, Automatique et Traitement du Signal (EEATS)**

# Conceptions de machines électriques à trajectoires de flux 3D pour application automobiles considérant la réutilisation et le recyclage des aimants

# Electrical machine designs based on 3D flux paths with reuse & recycle magnet concepts for automotive applications

Thèse soutenue publiquement le **11 Décembre 2018**,
devant le jury composé de :

**M. Guy FRIEDRICH**
Professeur à l'Université de Technologie de Compiègne, Président du jury
**M. Noureddine TAKORABET**
Professeur à l'Université de Lorraine, Rapporteur
**M. Bogi Bech JENSEN**
Professor, University of the Faroe Islands, Rapporteur
**Mme. Afef KEDOUS-LEBOUC**
Directrice de Recherche CNRS au G2Elab, Directeur de thèse
**M. Lauric GARBUIO**
Maître de conférences à Grenoble INP, Co-encadrant
**M. Jean-Claude MIPO**
Responsable de technologies avancées, Valeo EEM, Co-encadrant
**M. Peter Omand RASMUSSEN**
Associate Professor, Aalborg University, Invité
**M. Jean-Marc DUBUS**
Chef de projet avancé, Valeo EEM, Invité

# Acknowledgements

Absorb what is useful, reject what is useless, add what is specifically your own

- Bruce Lee

With these same words, I had concluded my presentation to the jury responsible for selection of Early Stage Researchers (ESRs) recruiting for the ETN DEMETER programme in 2015. Almost three years later, as I stand on the final step leading to my PhD, these words still resonate in my head.

When I came to France in the beginning of 2016, the transition was, to say the least, huge. My wife and I left our well established appointments in Mumbai, our families in Ahmedabad, our dear country and most importantly a well-defined path to a settled life. We set out, almost as vagabonds, with a completely clean slate, ready to begin again, just like children do, when entering a new school. France has been that new school, and contrary to public perception, she has been very welcoming. And entirely because of the incredible people we met on this journey. This section really is nothing else, but a tribute to all the persons who guided, supported, shaped, polished my journey for the attainment of this PhD.

Firstly, I would like to thank the thesis jury members, Prof. Noureddine Takorabet, Prof. Bogi Bech Jensen, Prof. Guy Friedrich and Prof. Peter O. Rasmussen, I was honored to have to help conclude this work. My heartfelt gratitude to you for accepting to be on the jury and for the feedback and proofreading of the manuscript.

The Project DEMETER team has an unequivocal role in the culminating of this thesis. I would like to thank Prof. Koen Binnemans (Coordinator), Prof. Peter Tom Jones (Valorisation Officer), Ms. Rabab Nasser (Project Manager) for their efforts and support right from the conception to culmination of this project. My thanks are also directed to all the other partner organizations and beneficiaries of the Project DEMETER.

I can't thank enough my supervisor, Prof. Afef Kedous-Lebouc, who has been instrumental at each and every step of this PhD journey. Her technical knowledge and expertise needs no introduction, however, what touched us most is her warmth and compassion as a person. Her untiring efforts to organize this thesis and the defense deserve special mention and credit.

I am most grateful to my co-supervisors, Mr. Jean-Claude Mipo (Valeo) and Prof. Lauric Garbuio (G2Elab) for their unceasing support and feedback that has shaped by research outlook and provided me with great insights to develop this project into a valuable PhD thesis.

I want to mention my very special gratitude to Mr. Jean-Marc Dubus (Valeo) who was the first person to welcome us in France. He ensured that my wife and I have the most comfortable start here. He is not only an inspiration of a full life, also his technical knowledge and suggestions have shaped my vision of research for the future. In Mr. Dubus I have gained a mentor for life.

I would also like to thank Valeo, France, and all the associates of Valeo, for providing the infrastructure and support during the three years of this PhD. My special thanks to Sophie P., Jerome L., Antoine T. K., Radu F., Mariam A., Radhoune K., Mamy R., Rijaniaina A., Benjamin L., Thomas B., Mohammed-Ali B., Mouheb D., Adham K., Reda B., Anand Francis C., Nitin G., Anil J., Ranjith, Michael C., Raouaa B., Jonathan, Thomas V., Thomas M., Katib O., Seung-Jun L., Maxime R., Ludovic Q., Vincent Y., Jacques P. for their immense support in different aspects of the project.
Muhammed A., Malik D., Allan W. from University of Birmingham for developing the recycled magnets and Thomas B. (Valeo), Justine B. (Université Paris Est-Creteil) and Redha F. (Université Paris Est-Creteil), for always supporting my wife and I with French translations.

During Project DEMETER, I have not only gained a PhD, I have made some friends for life. I will always have splendid memories of the bi-annual network

wide events and the time spent with all my ESR friends who provided the most congenial environment to discuss and stimulate research ideas. Special thanks to Amit J., Ziwei L. and Adolfo G. for being my closest associates in this work and also for initiating me into barbecuing.

Finally, my heartfelt gratitude to all those people who mean so much for me and my life. To my parents and family - no words can express the love and support I have had from you each step of my life and especially to my sister and brother-in-law for being friends who are family. To my wife's family - again, no words can express what it feels to have another family shower one with unconditional love and support. To my dear friend Fasil M. because of whom I found out about the Project DEMETER and who I turn to for guidance every time I am in a quandary.

And, last but not least the most important person, my life partner Neha, for her immense sustenance in my life; before, during and even after this part of my career and without her this would not have been possible at all.

Finally, going back to my favourite quote with which I started, I truly hope that I have succeeded in adding my specific value to this field of research, which if nothing else, is how we will 'drive' the future.

To all the above and the ones I was not able to mention, I will forever be grateful! Merci beaucoup.

# Contents

# List of Figures

# List of Tables

# List of Symbols

| Symbol | Description |
|---|---|
| $I_{dc}$ | DC load current |
| $V_{dc}$ | Battery voltage |
| $B_r$ | Magnetic remanence |
| $H_c$ | Magnetic coercivity |
| $R_g$ | Air gap reluctance |
| $R_{st}$ | Stator tooth reluctance |
| $R_{sy}$ | Stator yoke reluctance |
| $R_{ca}$ | Claw, axial reluctance |
| $R_{cr}$ | Claw, radial reluctance |
| $R_{cy}$ | Rotor yoke reluctance |
| $R_{ctl}$ | Tangential leakage reluctance |
| $R_{cal}$ | Axial between claws leakage reluctance |
| $R_{csl}$ | Slot leakage magnetic reluctance of the ring-shape DC excitation |
| $I_f$ | Field current |
| $p_1$ | Number of pole pairs |
| $W_1$ | Claw finger width at the broadest edge towards the rear end |
| $\Phi_{p1}$ | Fundamental of stator polar flux |
| $E_1$ | RMS value of the electromagnetic force (emf) fundamental |
| $\tau$ | Pole pitch |
| $l_{stack}$ | Stator stack length |
| $n$ | Speed in revolution per sec (rpm) |
| $a_p$ | Average rotor claw span |
| $B_{g1}$ | Flux density fundamental in the air gap |
| $B_g$ | Air gap flux density |
| $I'_f$ | Field current in stator frame |
| $F_{10}$ | MMF fundamental per stator pole |
| $K_c$ | Carter coefficient |
| $g$ | Air gap length |
| $\mu_0$ | Permeability of air |
| $F$ | Variable to represent EMF, current, flux linkages, etc. |
| $\theta$ | Angular displacement of the rotor *d*-axis w.r.t. the *a*-phase |
| $\psi$ | Flux linkage |
| $\psi_d$ | *d*-axis flux linkage |
| $\psi_q$ | *q*-axis flux linkage |
| $\psi_a$ | A-phase flux linkage |
| $\psi_b$ | B-phase flux linkage |

| | |
|---|---|
| $\psi_c$ | C-phase flux linkage |
| $I_d$ | $d$-axis current |
| $I_q$ | $q$-axis current |
| $I_a$ | A-phase current |
| $I_b$ | B-phase current |
| $I_c$ | C-phase current |
| $V_d$ | $d$-axis voltage |
| $V_q$ | $q$-axis voltage |
| $R_s$ | Stator phase resistance |
| $\omega$ | Speed |
| $T_e$ | Electromagnetic torque |
| $m$ | No. of phases |
| $P_{cu}$ | Copper losses |
| $I$ | RMS current |
| $R_{dc}$ | DC resistance |
| $P_{cu\text{-}s}$ | Stator copper losses |
| $I_s$ | Stator rms current |
| $R_{s\text{-}dc}$ | Stator phase DC resistance |
| $P_{cu\text{-}r}$ | Rotor copper losses |
| $R_{r\text{-}dc}$ | Rotor DC resistance |
| $H$ | Magnetic field |
| $P_i$ | Iron loss |
| $K_h$ | Hysteresis loss coefficient |
| $f$ | Frequency |
| $B_m$ | Peak flux density |
| $\alpha$ | Steinmetz constant |
| $K_e$ | Eddy current loss coefficient |
| $T$ | Time period corresponding to $f$ |
| $B$ | Flux density curve corresponding to an element in the machine |
| $T_{max}$ | Maximum p.u. torque |
| $T_{min}$ | Minimum p.u. torque |
| $T_{avg}$ | Average p.u. torque |
| $\%T$ | Percentage change in torque |
| $M, J$ | Magnetization |
| $T_w$ | Wheel torque |
| $m$ | Total mass |
| $a$ | Acceleration |
| $g$ | Gravity |
| $C_r$ | Coefficient of rolling resistance |
| $\rho_a$ | Density of air |

| | |
|---|---|
| $C_d$ | Coefficient of drag |
| $A_f$ | Vehicle frontal area |
| $v$ | Velocity of vehicle |
| $r_w$ | Radius of the wheel |
| $E_c$ | Total energy consumed |
| $E(t)$ | energy input as function of time |
| $t$ | Time |
| $EC_i$ | Energy cost index |
| $E_c(j)$ | Energy cost for Scenario $j$ |
| $Mag_c(j)$ | Magnet cost for Scenario $j$ |
| $E_c(b)$ | Energy cost for Scenario base |
| $Mag_c(b)$ | Magnet cost for Scenario base |
| $H_{cb}$ | Normal magnetic coercivity |

# Abstract

The research work presented in this thesis aims at developing a permanent magnet based claw-pole machine for automotive application with permanent magnet reuse and recycle concept. The aforesaid research is under the aegis of Project DEMETER which is in the framework of European Union's Horizon 2020 Marie Skłodowska-Curie actions. The project focuses on the recovery of rare earth permanent magnets utilized in automotive applications due to the prevailing problems of price fluctuations and supply-demand issues of these permanent magnets.

The claw-pole machine is employed in almost all of the automobiles in the world for alternator application. With the increase in power demands, the claw-pole machine is also being developed as a motor-generator utilized in the hybrid electric vehicles. At present the permanent magnet based claw-pole machine is being used in mild hybrid electric vehicles for energy savings. The literature is replete with various configurations of claw-pole machines that can be developed to achieve better performances. However, easy assembly and disassembly of various parts of the machine is also important for the reuse and recycle of magnets. In this research work two concepts have been developed; first, the direct reuse concept i.e. easy assembly/disassembly of the rotor and magnets, so as to easily take out the magnets for direct reuse or recycle and; second, the direct recycle concept i.e. utilization of recycled magnets in the machine to achieve the desired performance.

In the course of this research the base design of the claw-pole machine was developed, analyzed and optimized so as to attain best torque versus magnet-weight ratio. This helped in the reduction of magnet cost for almost the same torque. The optimization was carried out using 3-D numerical analysis. The optimized model was developed in a way that the assembly process of the magnets and claw-poles remained the same. However, during disassembly the magnets can easily be withdrawn without disassembling the complete rotor; therefore utilizing these magnets for direct reuse in other applications or sent for

recycling. In the direct recycle concept, the magnets used in the machine are recycled magnets with deteriorated performance. The type of recycling process is a strong determinant of the deterioration in performance of these recycled magnets. The aim of the direct recycle concept was to analyze the machine with virgin and recycled magnets, and evaluate the energy consumption of the machine under different drive cycles. It was observed that with utilization of recycled magnets in the claw-pole machine, the energy consumption was almost same as that of the machine with virgin magnets. Thus it can be concluded that for the permanent magnet based claw-pole machine, the utilization of recycled magnets is more sustainable for the environment as it can lead to consequential limits on the mining of rare earth materials. The price fluctuations and supply-demand problems can also be reduced with the increase in utilization of recycled magnets, albeit policy and norms are effectuated.

The prototype of the machine with virgin magnets have been fabricated and tested for performance. It has been observed that the experimental results match fairly well with the design analysis results, hence validating the design process and methodology.

# Résumé

Dans son dernier rapport publié en 2014, le groupe d'experts intergouvernemental sur les changements climatiques a déclaré: "Il est extrêmement probable que l'influence de l'homme ait été la principale cause du réchauffement observé depuis le milieu du XXe siècle". Nous avons eu quelques aperçus des effets importants profonds du changement climatique. Seize des dix-sept années les plus chaudes ont eu lieu depuis 2000. Les données empiriques de nombreuses études montrent que les gaz à effet de serre sont les causes majeures responsables de l'augmentation des températures mondiales: élévation du niveau des océans, incendies de forêt et cycles climatiques brusques.

Les gouvernements, ainsi que les groupes d'action composés d'industriels et d'universités, ont manifesté une volonté nouvelle de s'attaquer au problème des émissions excessives de gaz à effet de serre en adoptant des technologies plus écologiques et plus propres, non seulement au niveau de la production mais aussi de la consommation. Les émissions de véhicules constituent l'un des principaux facteurs des émissions mondiales de gaz à effet de serre. Il est impératif que la prochaine révolution automobile nous pousse vers des technologies moins polluantes et facilement adoptables à la fois. Compte-tenu avec du dynamique dans le domaine des technologies propres, la plupart des constructeurs automobiles s'orientent vers l'électrification des véhicules automobiles en introduisant sur le marché des véhicules hybrides et électriques. En raison des exigences concurrentielles de l'industrie automobile en matière de performances élevées dans des espaces restreints, les machines électriques requises pour ces applications doivent avoir des densités de puissance élevées. Pour atteindre ces densités de puissance élevées, la plupart des machines électriques utilisées dans les applications automobiles utilisent des aimants permanents à base de terres rares, en raison de leurs propriétés magnétiques élevées. L'utilisation de ces aimants permanents à base de terres rares s'est multipliée en raison des exigences susmentionnées des applications automobiles. Par conséquent, l'offre et la demande d'aimants à base terres rares ont été affectées au cours de la dernière

décennie. Cependant, la majorité des terres rares produites le sont en Chine. En 2011 des événements à caractère politique ont entraînés une très forte volatilité des coûts de ces matériaux .

Dans ce contexte, l'Union européenne a initié des travaux de recherches visant à réutiliser et recycler ces éléments critiques, à savoir: les matériaux magnétiques à base de terres rares. Cette thèse s'inscrit dans le cadre du projet Horizon 2020 MSCA DEMETER de l'Union européenne, qui se concentre sur la réutilisation et le recyclage des aimants permanents à base de terres rares utilisés dans les applications automobiles de trois manières:

- Réutilisation directe
- Recyclage direct
- Recyclage indirect

Les travaux de recherche présentés dans cette thèse visent à développer une machine à griffes à base d'aimants permanents (AP) pour les applications automobiles en tenant compte de la réutilisation et du recyclage des aimants permanents. Le projet se concentre sur le recyclage et la réutilisation des aimants permanents à base de terres rares utilisés dans les applications automobiles en raison des problèmes de fluctuations des prix et des problèmes d'offre et de demande de ces aimants permanents.

La machine à griffes est utilisée dans presque toutes les automobiles du monde pour les applications d'alternateur. Avec l'augmentation de la demande en puissance, la machine à griffes est également développée en tant que moteur-générateur utilisé dans les véhicules électriques hybrides. Actuellement, la machine à griffes à base d'aimants permanents est utilisée dans des technologies d'hybridation mild afin de réduire les émissions de $CO_2$. La littérature regorge de différentes configurations de machines à griffes pouvant être développées pour obtenir de meilleures performances. Cependant, le montage et le démontage

faciles des différentes parties de la machine sont également importants pour la réutilisation et le recyclage des aimants. Dans ce travail de recherche, deux concepts ont été développés; premièrement, le concept de réutilisation directe, c'est-à-dire le montage / démontage facile du rotor et des aimants, de manière à pouvoir retirer facilement les aimants pour les réutiliser ou les recycler directement; deuxièmement, le concept de recyclage direct, c'est-à-dire l'utilisation d'aimants recyclés dans la machine pour obtenir les performances souhaitées. Les figures R.1 et R.2 représentent respectivement le concept de réutilisation directe et le concept de recyclage direct dans le cadre de la machine à griffes.

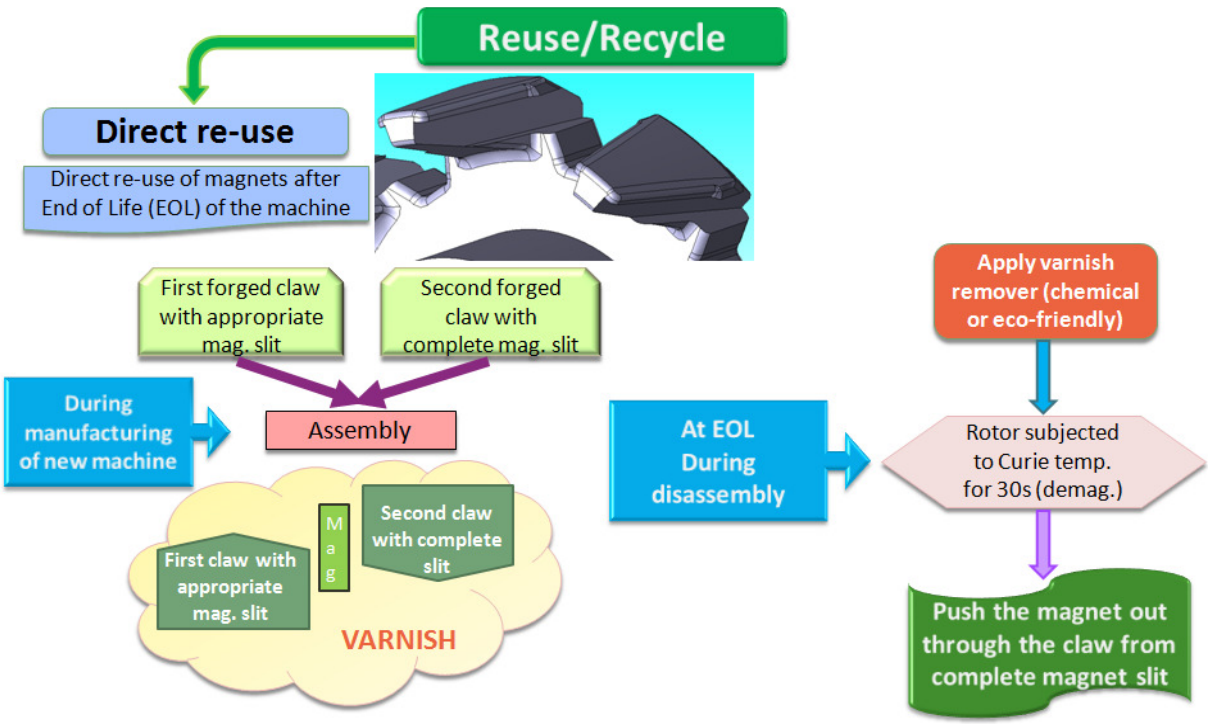


Fig. R.1 Méthodologie de réutilisation directe pour l'assemblage et le démontage d'aimants dans une machine à griffes

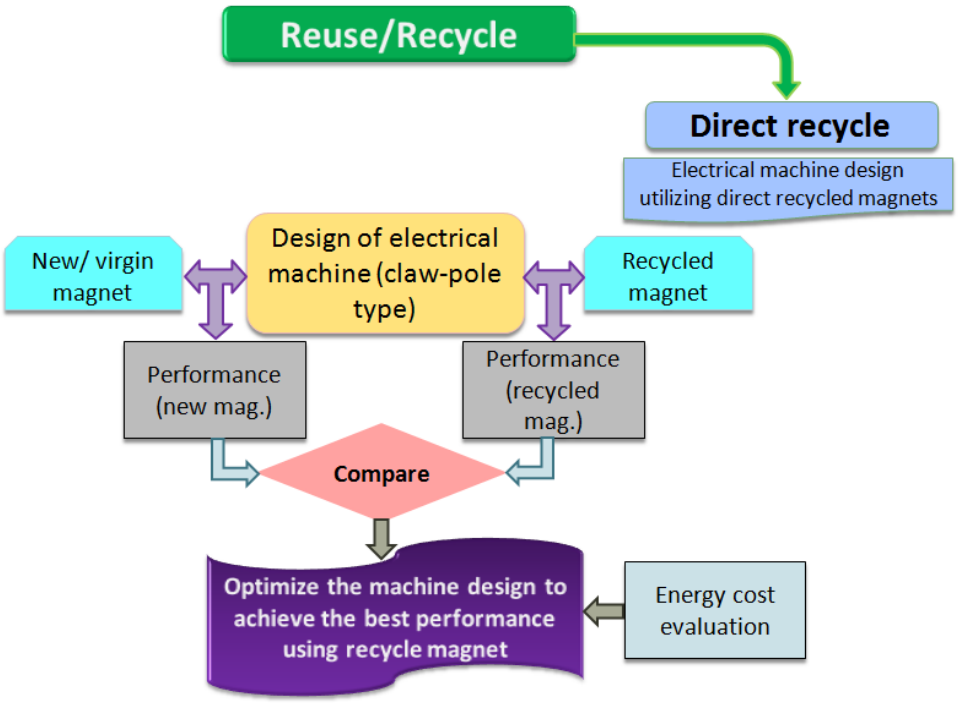


Fig. R.2 Méthodologie de recyclage direct pour la conception de machines électriques (type machine à griffes)

Au cours de cette recherche, la conception originale de la machine à griffes a été développée, analysée et optimisée de manière à obtenir le meilleur rapport couple / masse d'aimant. L'automatisation de la géométrie est réalisée sur l'éditeur de géométrie du logiciel d'analyse par éléments finis, de manière à obtenir une optimisation numérique tridimensionnelle de la géométrie des pôles à griffes pour obtenir le meilleur ratio couple / aimant. Cela a permis de réduire le coût des aimants pour presque le même couple. L'évaluation complète des performances est obtenue en utilisant des techniques de programmation, de manière à obtenir les cartographies du flux, du courant, la tension, des pertes et du rendement de l'enveloppe couple-vitesse. Le modèle optimisé a été développé de manière à ce que le processus d'assemblage des aimants et des griffes reste le même. Cependant, lors du démontage, les aimants peuvent être facilement retirés sans démonter le rotor complet; par conséquent, il est possible de réutiliser directement ces aimants dans d'autres applications ou procéder à leur recyclage.

Dans le concept de recyclage direct, les aimants utilisés dans la machine sont des aimants recyclés aux performances dégradées. Le type de processus de recyclage est un facteur déterminant dans la détérioration des performances de ces aimants recyclés. L'objectif du concept de recyclage direct était de comparer les performances de la machine avec d'un côté les aimants vierges et de l'autre côté les aimants recyclés et d'évaluer la consommation d'énergie de la machine selon différents cycles de conduite. On a observé qu'avec l'utilisation d'aimants recyclés dans la machine à griffes, la consommation d'énergie était presque identique à celle de la machine à aimants vierges. On peut donc en conclure que pour les machines à griffes à aimants permanents, l'utilisation d'aimants recyclés est plus durable pour l'environnement car elle peut réduire le besoin en extraction de terres rares. Les fluctuations de prix et les problèmes offre / demande peuvent également être réduits avec l'utilisation augmenté d'aimants recyclés.

Des indices de recyclage pondéré ont également été développés pour évaluer la machine en termes de recyclabilité. Le premier indice dépend de la standardisation et de la prise en compte des coûts, de l'assemblage et du démontage. Le deuxième indice dépend de la consommation d'énergie, en tenant compte du cycle de conduite. Le principe d'indexation a été utilisé pour évaluer la recyclabilité de la machine développée et la comparer aux autres topologies de machines développées dans le projet DEMETER.

Le concept de réutilisation directe et de recyclage direct des AP dans le contexte de la machine à griffes offre des avantages en termes de facilité de recyclage. Par conséquent, comme indiqué précédemment, l'utilisation de AP recyclés dans les machines électriques est également plus durable et contribue à réduire l'empreinte carbone en aidant à réduire les activités d'exploitation minière afin produire de nouveaux matériaux constitutifs d'AP. Comme cette machine est produite en gros volumes (des millions par an); l'utilisation d'aimants recyclés peut entraîner une réduction significative substantielle de l'exploitation minière. Cependant, pour une implémentation en douceur des concepts de réutilisation et

de recyclage; des politiques de réglementation doivent être mises en œuvre. Pour faire exister pleinement le concept de recyclage, il serait nécessaire que des directives politique soient lancées pour que le recyclage soit pris en considération depuis le début jusqu'à la fin de la chaine d'approvisionnement: du constructeur automobile au de-constructeur. Une fois le système en place, le recyclage deviendrait un processus naturel et offrirait de nombreux avantages pour que la planète reste verte et durable.

Enfin, une machine à aimants vierges est fabriquée avec les nouveaux pôles à griffes puis ses performances sont testées expérimentalement. De même, un rotor à griffes avec des aimants recyclés est également fabriqué pour la même machine. Les résultats expérimentaux correspondent assez bien aux résultats de la simulation, validant ainsi la méthodologie. La machine à aimants recyclés est beaucoup plus écologiquement durable car elle limite les activités d'extraction de nouveaux matériaux magnétiques et conduit à une moindre pollution de l'environnement.

# General Introduction

The Inter-Governmental Panel for Climate Change in its latest report released in 2014 said that "It is extremely likely that human influence has been the dominant cause of the observed warming since the mid-20$^{th}$ century." We have experienced a few glimpses of the far-reaching effects of climate change on our own. Sixteen of the 17 warmest years have occurred since 2000. Empirical evidence through numerous studies show that Greenhouse Gases are the major forces in driving up global temperatures which have had several detrimental spillovers like ocean levels rising, forest fires and abrupt climate cycles.

Governments, as well as action groups consisting of industry and academia, have exhibited a new resolve to tackle the problem of excess Greenhouse Gases emissions by moving towards the greener and cleaner technologies, not only at production levels but also at consumption levels. Vehicular emissions constitute one of the high contributors of global Greenhouse Gases emissions. It is imperative that the next automobile revolution pushes us towards technologies that are less polluting and easily adoptable at the same time. With this increased momentum in the field of clean technologies, most of the automobile manufacturers are moving towards electrification of the automotive vehicles by introducing hybrid and electric vehicles. Due to the competitive automotive requirements of high performance in constrained space, the electrical machines required for these applications need to have high power densities. To achieve these high power densities, most of the electrical machines used for automotive applications employ rare earth permanent magnets, due to their high magnetic properties. The utilization of these rare earth permanent magnets have multiplied due to the aforesaid requirements of automotive applications. Consequently, the supply/demand of rare earth magnets have been affected in the past decade. However, most of these rare earth materials are produced in China. It is observed that in 2011 politically motivated events led to very high volatility in the costs and supply/demand related problems to the rare earth magnetic materials.

Thus, in this context the European Union has started efforts in the reuse and recycling of these critical elements viz. the rare earth magnetic materials. This thesis is under the European Union's Horizon 2020 Project DEMETER which focuses on the recovery of rare earth permanent magnets utilized in automotive applications by the following three ways:

- Direct reuse
- Direct recycling
- Indirect recycling

The research in this thesis is concentrated on the direct reuse and recycle concept of Neodymium Iron Boron rare earth magnets used in a permanent magnet based claw-pole machine. The thesis is organized as follows:

**Chapter 1** presents the introduction and motivation for permanent magnet recyclability. It highlights the various critical raw materials identified by the European Commission, and depicts that Light Rare Earth Elements and Heavy Rare Earth Elements are the most critical materials as most of them are imported from China. The objectives and deliverables of Project DEMETER are highlighted and the need for reuse and recycle of permanent magnets is described in this chapter.

**Chapter 2** covers literature survey and bibliography study on hybrid and electric vehicles, claw-pole machines, reuse, recycling, assembly and disassembly of electrical machines. The state of the art architectures for various hybrid vehicles are explained along-with a typical electric vehicle architecture. The literature is replete with various configurations of claw-pole machines and its design analysis as well as for reuse, recycling, assembly and disassembly.

**Chapter 3** concentrates on the design and analysis of permanent magnet based claw-pole machine for automotive application. Geometry automation is carried out on the finite element analysis software's geometry editor, so as to obtain three dimensional numerical optimization of the claw-pole geometry for best torque to magnet weight ratio. The complete performance evaluation is obtained

by utilizing programming techniques, so as to obtain flux mapping, current mapping, voltage mapping, loss mapping and efficiency mapping for the complete torque-speed envelope.

**Chapter 4** is dedicated to elaborating the reuse and recycle magnet concept for the claw-pole machine. Two concepts have been developed; first, the direct reuse concept i.e. easy assembly/disassembly of magnets and; second, the direct recycle concept i.e. utilization of recycled magnets in the machine to achieve the desired performance. Weighted index of recycling has also been developed to score the machine in terms of its recyclability. First index is dependent upon the standardization and cost taking material, assembly and disassembly into consideration and second index is dependent upon energy consumption taking drive cycle into consideration. The claw-pole machine is also analyzed with recycled magnets developed at University of Birmingham with reduced performance, and it is seen that the machine performance does not drop substantially when compared to machine with virgin magnets. This result opens the possibility of utilizing recycled magnets for succeeding claw-pole machines.

**Chapter 5** presents the prototyping and experimental results of the developed claw-pole machine. A machine with virgin magnets is developed with the new claw-poles and tested for performance. Similarly an identical claw-pole rotor was fabricated and recycled magnets will be fitted into this for the same machine. The experimental results for the machine with virgin magnets rotor, match fairly well with the simulation results, hence validating the design and the development methodology. Similarly, the machine with recycled magnets is also assumed to perform comparable to the simulation results, hence validating the utilization of recycled magnets in next generation claw-pole machines. The machine with recycled magnets is much more sustainable from the environmental point of view as it limits mining activities for new magnet materials and leads to lesser environmental pollution. However, the demand of Neodymium would go up as the supplies for hybrid and electric vehicles increase.

# Chapter 1

# Permanent Magnet Recyclability: Introduction and Motivation

## 1.1 Critical Raw Materials: Rare-Earth Elements

Critical Raw Materials (CRMs) are those raw materials which are economically and strategically important for the European economy, but have a high-risk associated with their supply. In 2011 the European Commission (EC) published a report on CRMs for the European Union (EU) and highlighted the critical elements which are under supply risk and their impact on economy is higher compared to other raw materials [1]. Similarly in 2014 and 2017 the EC published updated reports of the CRMs in which new materials were added as critical elements [2]-[3]. Therefore, till date 27 raw materials have been listed as CRMs as per the EC which can be seen in Table. 1.1 [3]. The list has been generated to tackle challenges related to the access to CRMs. It is also an indirect tool to analyze investment needs to help in mitigating Europe's reliance on imports of raw materials, support research and innovation, transition to a low-carbon resource dependent economy and also incentivise the European production of CRMs by enhancing recycling activities.

Table. 1.1 List of 27 CRMs as per EC [3]

| Critical Raw Materials | | | |
|---|---|---|---|
| Antimony | Fluorspar | Natural graphite | Tantalum |
| Baryte | Gallium | Natural rubber | Tungsten |
| Beryllium | Germanium | Niobium | Vanadium |
| Bismuth | Hafnium | Phosphate rock | Platinum Group Metals |
| Borate | Helium | Phosphorus | Heavy Rare Earth Elements* |
| Cobalt | Indium | Scandium | Light Rare Earth Elements+ |
| Coking coal | Magnesium | Silicon metal | |

*HREE +LREE

Fig. 1.1 shows the CRMs and non-CRMs for EU as of 2017 in terms of supply risk and economic importance [4]. It can be observed from the EU CRM 2017 report that the global supply of majority CRMs like rare earth elements, magnesium, tungsten, antimony, gallium, germanium and few others is dominated by China [3]. Numerous other countries have leading supplies of specific raw materials, such as Brazil (niobium) and USA (beryllium and helium) [3]. Supply of platinum group metals is concentrated in Russia (palladium) and South Africa (iridium, platinum, rhodium and ruthenium) [3]. Low recycling rates and low substitution in several cases lead to the threat in the concentration and production of these raw materials. Therefore, reuse and recycle of as many CRMs as possible is a path to better sustainability and releasing pressure from the environment.

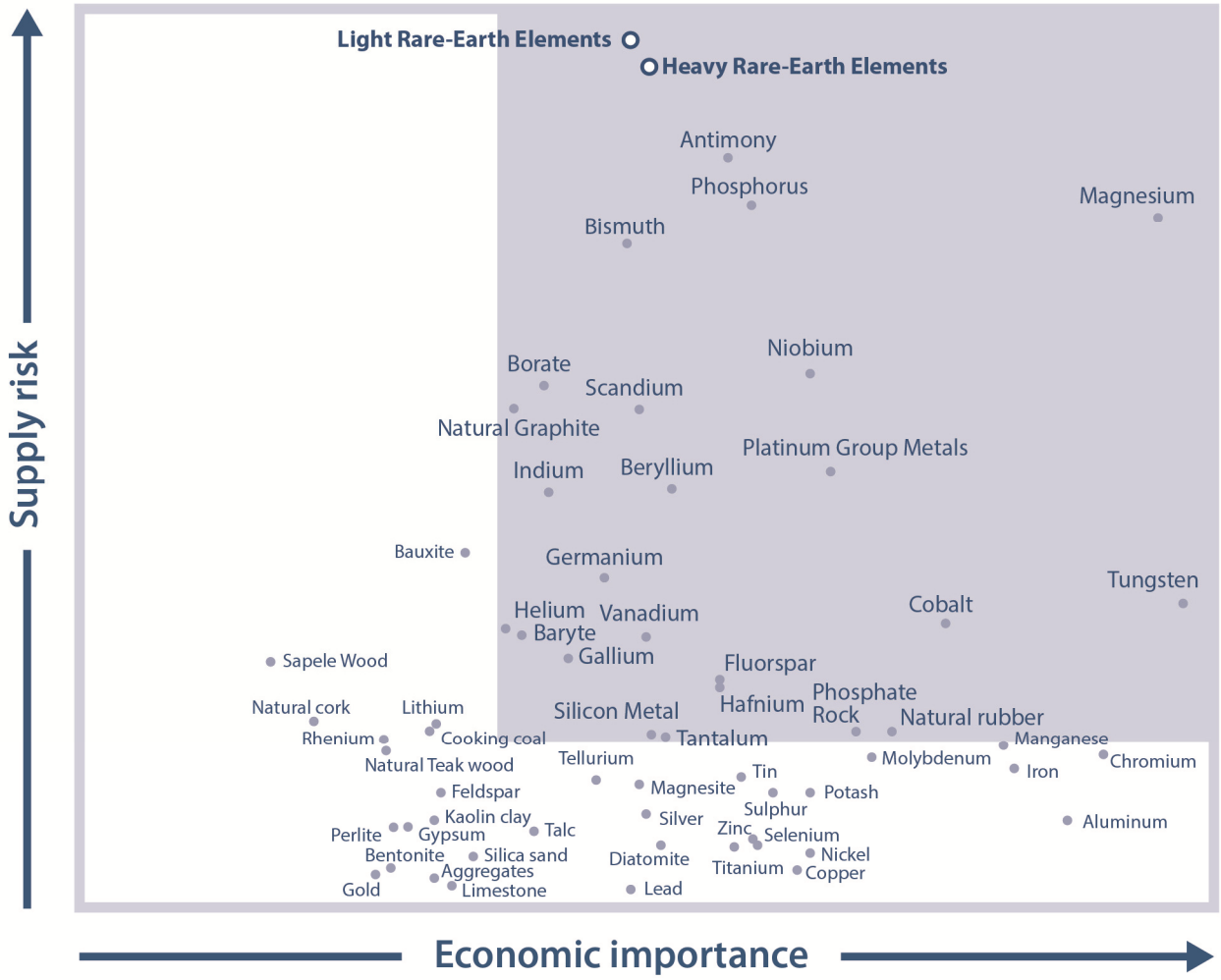


Fig. 1.1 List of CRMs and non-CRMs for EU as of 2017 [4] (credits image: redrawn by Paul McGuiness, available: https://new-mine.eu/eu-raw-materials-week/ )

### 1.1.1 Heavy Rare Earth and Light Rare Earth Elements

The rare earth elements (REE) are a set of seventeen chemical elements in the periodic table, i.e. the fifteen lanthanides including Scandium and Yttrium. Fig 1.2 depicts the 17 rare earth elements in the Periodic table [5].

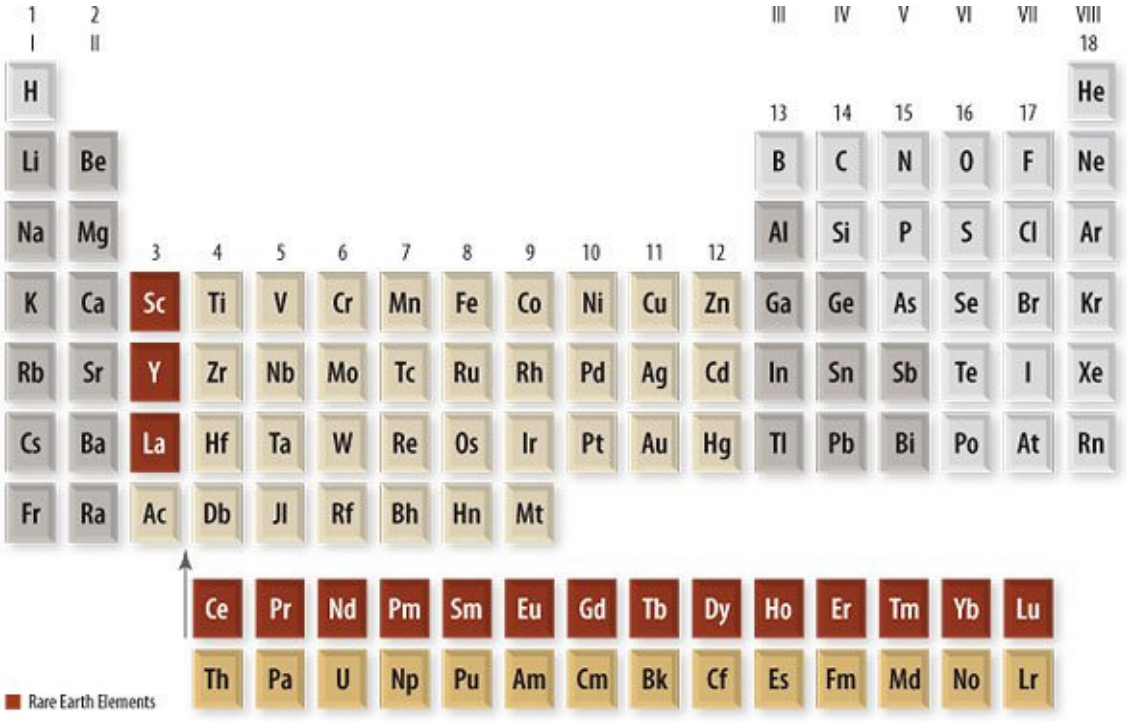


Fig. 1.2 Rare earth elements in the Periodic table [5]

The REEs are further sub-divided into two categories:

(i) **Heavy Rare Earth Elements (HREE)**, consisting of Europium (Eu), Gadolinium (Gd), Terbium (Tb), Dysprosium (Dy), Holmium (Ho), Erbium (Er), Thulium (Tm), Ytterbium (Yb), Luttetium (Lu) and Yttrium (Y).

(ii) **Light Rare Earth Elements (LREE)**, consisting of Lanthanum (La), Cerium (Ce), Praseodymium (Pr), Neodymium (Nd), Promethium (Pm) and Samarium (Sm).

The HREEs and LREEs are the most critical materials in terms of supply risk as both of them are 95% imported from China [4]. The rare earth permanent magnets are the strongest magnets available in the world till date. The term

'rare-earth' is used to refer to these permanent magnets (PM) due to the presence of REEs in these PMs. There are two types of rare-earth PMs:

(i) **Neodymium magnet**: - an alloy of neodymium, iron and boron to form the $Nd_2Fe_{14}B$ tetragonal crystalline structure.

(ii) **Samarium Cobalt magnet**: - an alloy of samarium and cobalt to form the $SmCo_5$ and $Sm_2Co_{17}$.

The NdFeB magnets also sometimes utilize praseodymium (Pr) and dysprosium (Dy) in their crystalline structure to improve their properties. Hence, due to the presence of Nd, Sm, Co, Pr and Dy in the rare-earth permanent magnets, they can also be indirectly considered as critical materials in the industry. The rare-earth PMs are used in various applications like not only limited to automotive, aerospace, electronics, magnetic resonance imaging devices, wind power, traction machines, computer hard drives, magnetic refrigeration, defence, microphones and speakers.

## 1.2 Rare-Earth Permanent Magnets in Automotive Applications

The electrical machines have been an integral part of an automobile since its inception and will be the most important component for future automotive applications. From the seasonally important wiper blades, to the glamorous power windows, from the totally indispensable CD player to the totally dispensable sun roof, (or maybe not); from the fuel pump to the starter motor, the list is endless. It is not endless, but it's very large and highlights the amount of RE PMs being used in automotive applications.

### 1.2.1 Electro-mobility in automotive applications

Electric Vehicles (EV) and Hybrid Electric Vehicles (HEV) are the new key developments in automotive industry with the implementation of new energy efficiency regulations and standards in various countries around the world. Electro-mobility (e-mobility) in automotive applications have picked up pace and

nowadays every automobile manufacturer is striving towards the development of EVs and/or HEVs. The EVs and HEVs provide benefits in the reduction of $CO_2$ emissions and help in environmental sustainability. Along-with EVs and HEVs, an automobile consists of large number of electrical machines for various other purposes. Fig 1.3 illustrates the large number of electric motors for various functions in an automobile. Most of these machines employ permanent magnets, whether it is ferrite magnets, AlNiCo magnets, NdFeB magnets or SmCo magnets. This provides a comprehension about the importance of PMs utilized in automotive applications.

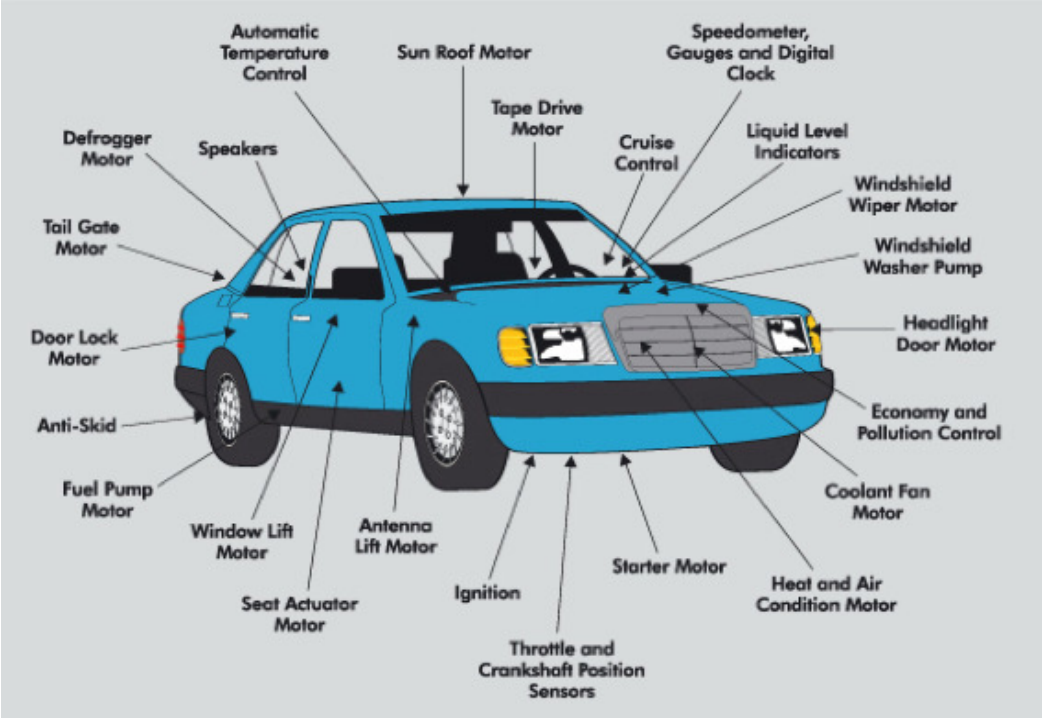


Fig. 1.3 Electric motors for various functions in an automobile [6]

### 1.2.2 Permanent magnets employed in electrical machines for automotive applications

Nowadays the most important component in advanced electrical machines used in automobiles is permanent magnets. For low power motor requirements of few Watts ferrite magnets are generally utilized. But with the stringent cost and space requirements in the automobiles high energy magnets need to be used so

as to fulfil the requirements. As highlighted in Section 1.1.1, rare earth magnets are the strongest magnet on earth till date, and sintered NdFeB magnets being strongest between SmCo and NdFeB. As a result, mostly NdFeB magnets are used in large number of EV/HEV applications. Fig. 1.4 shows the evolution of various PMs with respect to their energy product, and hence it can be observed that NdFeB magnets have the highest energy product till date.

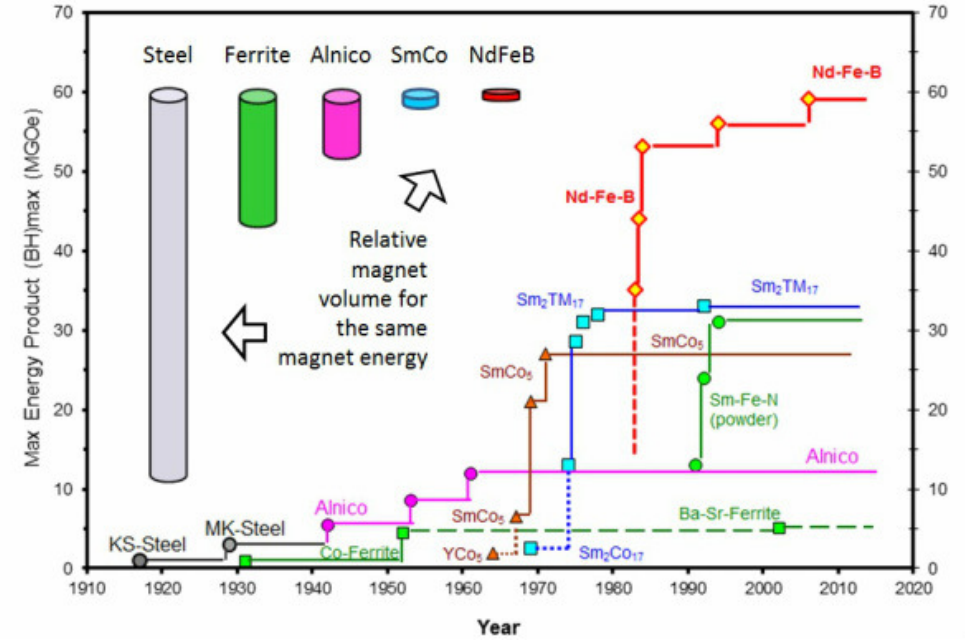


Fig. 1.4 Evolution of PMs with respect to their energy product [7]

The REE magnet industry consumes the major part of the LREEs i.e. Nd and Pr, while it consumes practically all of the produced HREE Dy. This makes the REE magnet industry and the various downstream sectors that utilise these magnets in their products and services extremely vulnerable to price fluctuations and shortages. The automotive sector is likely to become the main consumer of REE magnets in Europe, as it moves towards more HEVs and EVs [7].

## 1.3 Project DEMETER

Project DEMETER [8] is under the European Union's Horizon 2020 framework programme for research and innovation, and support researchers at all stages of their careers under Marie Skłodowska-Curie Actions (MSCA). DEMETER corresponds to European Training Network for the ***De****sign and Recycling of Rare-Earth Permanent* ***M****agn****e****t Mo****t****ors and G****e****ne****r****ators in Hybrid and Full Electric Vehicles.* During the rare-earth crisis of 2011, three possible solutions were investigated to alleviate the shortages; (1) increased recycling rates of REE-containing devices; (2) the search for new, mineable REE resources outside China, and; (3) the development of REE-free strong permanent magnets ("substitution"). Although Europe has access to some REE deposits, for instance Norra Kärr (Sweden) and Kvanefjeld (Greenland), these mining projects are still at an exploratory stage and it will take many years before these mines become operational. Secondly, the development of new REE-free permanent magnets requires a scientific breakthrough that has not come about, despite decades of research, not only in Europe, but around the world. Therefore, of the three potential options, only the first is likely to succeed from the European perspective on the short to medium term [8].

Concurrently, in the recently published report [9] of the European Rare Earth Competency Network (ERECON), which was set up under the auspices of Directorate-General (DG) Enterprise and Industry to lower the REE supply risk for the EU, it is pointed out that research focusing on the REE permanent magnets used in e-mobility should receive top priority with drive motors, power steering, stop-start motors, and regenerative braking generators being highlighted in particular. Combining the EU needs and the ERECON "call-for-arms", DEMETER, therefore, focuses on solutions for the large quantities of REE permanent magnets that are used in the motors and generators of EVs/HEVs, for which at present there is no clear pathway for reclaiming the REE magnets when they reach their End-of-Life (EoL) [8].

### 1.3.1 Objectives and Deliverables

The project focuses on the recovery of large (i.e. > 30 g) REE permanent magnets in the drive motor, the power-steering motor, the stop-start motor, and the regenerative braking and range extender generators in EVs/HEVs and in highly advanced internal combustion engine vehicles (ICEVs). There are three options with respect to the recovery of these devices.

I. The first option is **Direct Re-use**: magnets could be removed from EoL motors/generators and used again in new motors/generators. This is, however, not a realistic option at present, as the magnets in the current EVs/HEVs were never designed to be removed and are often difficult to extract. In DEMETER the first aim is to develop strategies based on Design for-Reuse with new generations of motors/generators that incorporate standard sizes of magnets that can be easily removed for re-use in new EVs/HEVs (and Advanced ICEVs) and also utilize recycled magnets in new generation electrical machines for these EVs/HEVs.

II. The second option is **Direct Recycling**, in which case the magnets are treated as a raw material for the production of new magnets, but using novel techniques such as hydrogen decrepitation (HD) processing, plasma/strip casting, and spark plasma sintering, to give new, ready-to-use, magnetic materials or a new master alloy that can be processed using existing magnet production facilities.

III. The last option is **Indirect Recycling**. In contrast with the alloy route in direct recycling, indirect recycling implies that the magnet scrap material is transformed to its elemental components. The REEs are recovered from the magnets and separated from each other for use in subsequent permanent magnet production or, possibly, in other existing or new applications such as magneto-caloric materials or lamp phosphors.

Fig. 1.5 depicts the above three ways to close the materials loop for rare earths from permanent magnets in EVs/HEVs. In DEMETER, not only NdFeB magnets, but also SmCo magnets are considered, as many magnet experts believe that

SmCo is the better choice in certain motor applications. DEMETER has a comprehensive strategy as it not only develops innovative, environmentally-friendly direct and indirect recycling strategies for the permanent magnet motors and generators in EVs/HEVs that are currently already on the market but also Design-for-Reuse solutions for the motors and generators in future EVs/HEVs.

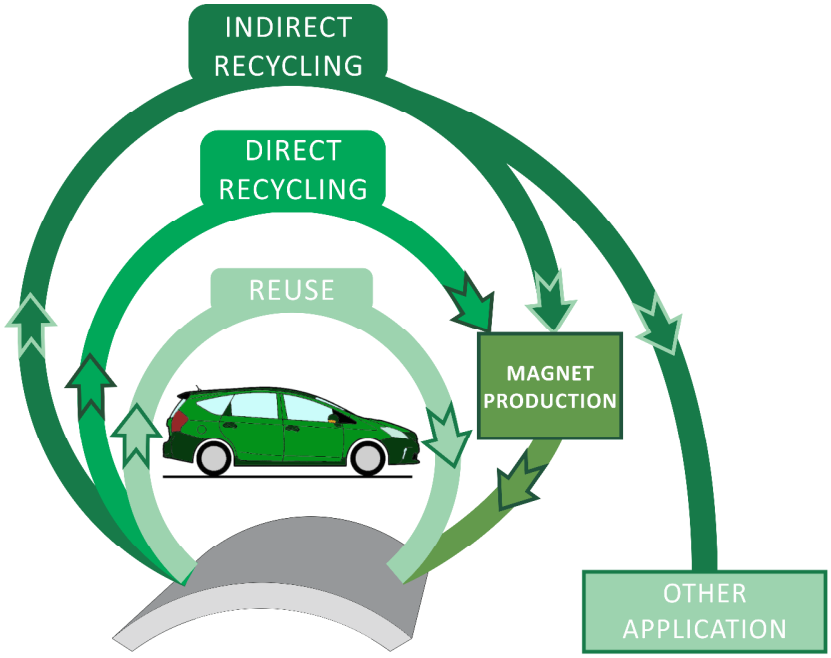


Fig. 1.5 Three ways to close the materials loop for rare earths from permanent magnets in EVs/HEVs (and Advanced ICEVs) [8]

DEMETER's science and technology (S/T) objectives are to:

- Develop innovative, eco-efficient direct and indirect recycling routes of NdFeB and SmCo magnets motors and generators from End-of-Life EVs/HEVs and Advanced ICEVs.
- Develop innovative processing techniques for production of high performance NdFeB and SmCo magnets.
- Design electric motors and generators for the next generation of EVs/HEVs and Advanced ICEVs to enable easy future reuse and recycle of NdFeB and SmCo magnets.
- Develop a complete, "(urban) mine-to-machine", lifecycle assessment (LCA) and lifecycle costing (LCC) methodology for REE permanent magnets to ensure that the most environmentally-friendly and economical routes are applied for recycling.

### 1.3.2 Collaborative work

In the project DEMETER consortium there are seven beneficiaries and three partner organizations. The seven beneficiaries host doctoral researchers who under their aegis work upon subjects related to project DEMETER's objectives and deliverables. These doctoral researchers are named Early Stage Researchers (ESRs) in the MSCA scholarship structure and there are fifteen ESRs working in the project for different beneficiaries. Consequently, due to the close-knit deliverables of the project, there is collaborative work possible between ESRs to achieve the goal of the project. Fig. 1.6 shows the possible integration of ESRs in the overall research programme of project DEMETER.

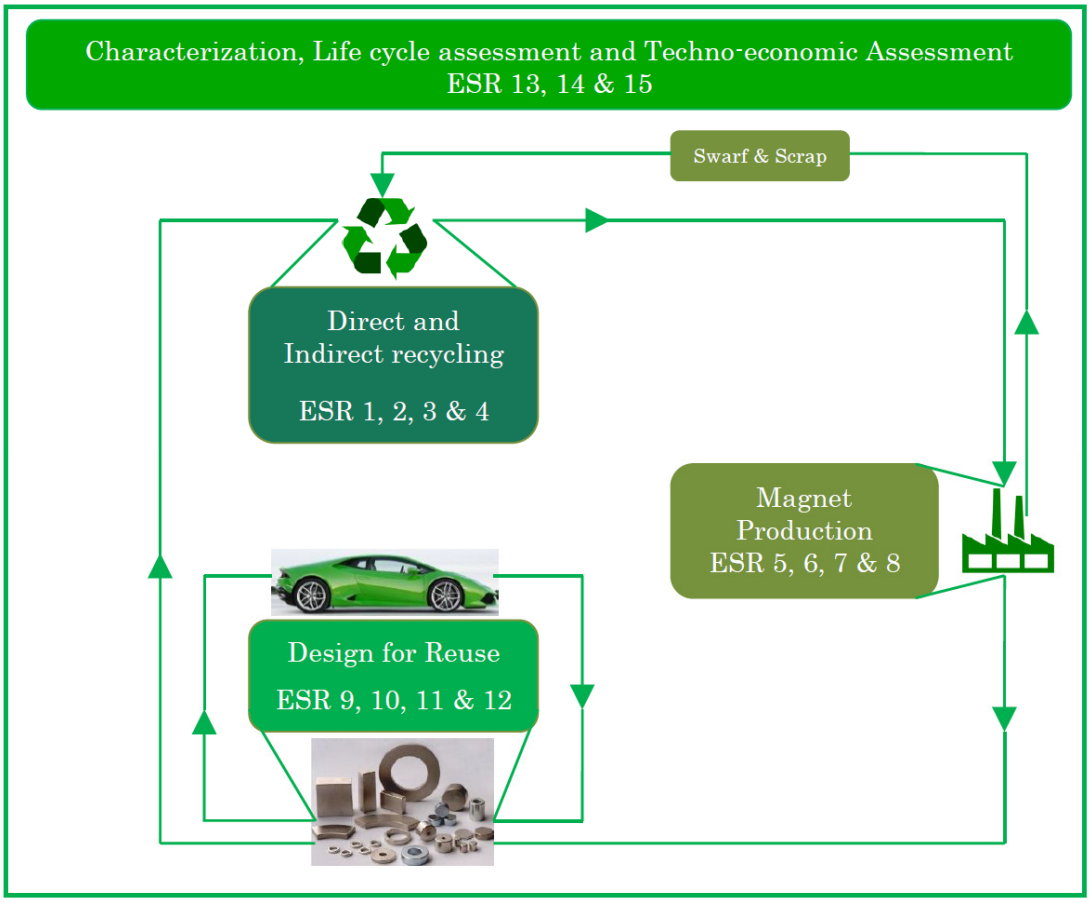


Fig. 1.6 Integration of ESRs in overall research programme [8]

This thesis is presented by ESR 11 whose deliverable was defined as to develop a claw-pole machine for HEV application where the permanent magnets can be extracted for reuse and also to develop a workable machine using recycled

magnets. Along-with the above objectives the machine should also meet the stringent performance and cost requirements of automotive applications.

During the course of the research work, ESR 11 worked closely with the group of ESRs 9 to 12 towards electrical machine designs with reuse and recyclability being the main driving force for different machine designs. As a result, recyclability index for electrical machines with respect to (w.r.t.) permanent magnets have been developed in the due course of the project by ESRs 9 to 12 which is detailed in Chapter 4. Four different machine designs have been developed and evaluated for their recyclability index w.r.t. to assembly/ disassembly and energy cost evaluation.

In additional collaboration with ESR 2 who is working on the development of recycled magnets from scrap magnetic materials, activities were undertaken for the recycling of magnets developed by their facility. ESRs 7 & 13 also helped in the final grinding and processing of these recycled magnets. These recycled PMs are planned to be assembled in the machine developed in the course of this research thesis. The results of this exercise are presented in Chapter 4 and they show that with the utilization of recycled magnets with reduced performance, there is negligible reduction in machine performance and energy consumed by the machine for different driving cycles.

There is also close integration with ESR 15 who works upon the LCA and LCC of magnet manufacturing and the complete supply-chain system. The results from the use-phase of the electrical machines will be utilized for the LCA and LCC research work of ESR 15.

As is evident, all the ESRs were connected to each other in some way or the other and this was an excellent opportunity to gain knowledge of different domains other than electrical machine design.

# Chapter 2

# Literature Survey and Bibliography Study

## 2.1 Hybrid and Electric Vehicle Technologies

All around the world environmental problems due to air, water and land pollution are creating huge health hazards. The main causes of air pollution are emissions from industries, transportation, agricultural activities, mining operations and indoor/household activities. Out of these, transportation is one of the major contributors due to the burning of fossil fuels by automobiles. As a result, many countries have started implementing new regulations and standards to curb this by emphasising the introduction of hybrid and electric vehicles. HEVs provide better fuel efficiencies than compared to conventional internal combustion engine (ICE) vehicles, whereas EVs are purely electric and hence sometimes termed as Zero Emission Vehicles (ZEV). There are various vehicle architectures employed in these HEVs and EVs so to achieve better fuel efficiencies in automobiles. Few of these are detailed in section below.

### 2.1.1 Hybrid Electric Vehicle architectures

Hybrid Electric Vehicles consist of an IC engine and one or more electrical machine to drive the automobile. Depending on the architecture the wheel power could be provided by IC engine or electrical machine or from both. Therefore, due to this combined effect, it is termed as 'Hybrid Electric Vehicle'. The IC engine could be a conventional fuel converter or the more contemporary advanced engines. The electrical machine can be of various types like direct current (DC) machines, induction machine, brushless DC machines, permanent magnet machines, synchronous reluctance machines, and many more. The electrical energy to the machine is generally provided by batteries installed in the automobiles. One of the main motivations for developing HEVs is the possibility

to combine advantages of pure electric vehicles, in particular zero local emissions, with advantages of ICE-based vehicles, namely high energy and power density. In principle, it is possible to [10]:

i. Downsize the engine and still fulfil maximum power requirements;
ii. Recover some energy during deceleration instead of dissipating it in friction braking;
iii. Optimize the energy distribution between the prime movers;
iv. Eliminate the idle fuel consumption by turning off the engine when no power is required (stop-and-start); and
v. Eliminate clutching losses by engaging engine only when speeds match.

The HEVs are generally categorized into three main types:

- **Series HEVs**: electrical machine (e-machine) provides power to the vehicle alone, and electrical energy to e-machine can be provided by battery or by engine-driven generator.
- **Parallel HEVs**: ICE and e-machine can power the vehicle individually or simultaneously.
- **Series-Parallel, or combined HEVs**: In this arrangement, mechanical and electrical link is present altogether and depending upon architecture the power is provided by ICE and e-machine.

#### 2.1.1.1 Series HEVs

In series HEVs, e-machine is the main unit to deliver power to wheels of an automobile. The electricity to e-machine is provided by battery, which is charged by a generator driven by an ICE. In some cases electric power to e-machine can be provided by battery and generator both depending upon the control strategy. Hence, ICE is an auxiliary power unit utilized only to drive the generator to charge the batteries or/and provide electricity via the generator. The engine

power and size is not dependent upon automobile power requirements directly. This type of architecture is a kind of EV assisted by an ICE to extend the electric driving range of the vehicle. As the engine and e-machine are decoupled, this configuration has the advantage of flexibility to place both components as per the vehicle design. But generally the efficiency of this architecture is lower compared to parallel HEVs. The series HEV becomes expensive when most of the components need to be designed for maximum sustained power if the series HEV is required to climb a long grade. On the other hand, when it is only needed to serve short trips as commuting to work and shopping, the corresponding ICE generator set can adopt a lower rating [12]. Fig. 2.1 (a) depicts a typical series HEV architecture [11].

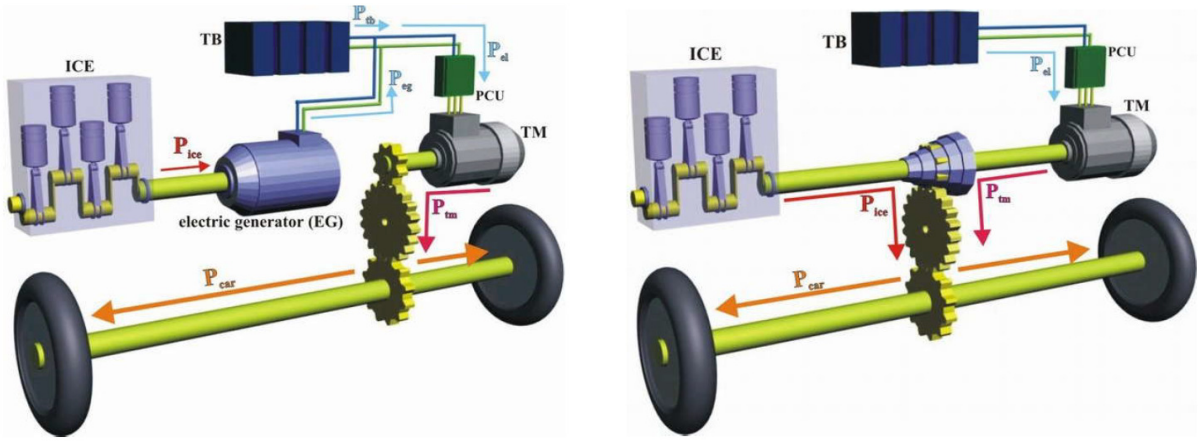


(a) (b)

Fig. 2.1 (a) Series HEV architecture (b) Parallel HEV architecture [11]
(where TB is battery, PCU is power control unit and TM is electric motor)

### 2.1.1.2 Parallel HEVs

The series HEVs has only one source of propulsion and that is the e-machine, hence can be considered as EV with a range extender, whereas in parallel HEVs, ICE and e-machine both can propel the automobile. While ICE and e-machine are generally paired together to the wheel transmission via clutches and gear, the driving force can be provided by ICE alone, or by e-machine alone or by both depending upon the configuration. Fig. 2.1 (b) shows a typical simple parallel HEV architecture [11]. Due to parallel nature of this configuration, there is an advantage that the ICE and e-machine can be optimized as per the drive control

design of the HEV. Another advantage is that the engine can be turned off during idling, and e-machine can be used to assist the ICE during peak loads. A disadvantage is the requirement of clutch, since ICE is mechanically linked to the drive train [10]. The e-machine can be used as a generator to charge the battery during regenerative braking or by the engine while normal driving. However, the power is divided between ICE and e-machine; both these components can be designed a little smaller so as to achieve same performance as a normal ICE vehicle. As a result, generally the fuel economy and efficiency of the complete system is higher than conventional gasoline powered vehicle, consequently less $CO_2$ emissions.

This architecture can further be subdivided to following categories (but not limited to the following):

- **Micro-hybrid**: These are generally defined as micro-hybrid because of the presence of automatic start-stop system. The start-stop system automatically shuts off ICE during idling and other non load conditions, and switches on ICE when the load requirement is induced. Regenerative braking is also possible but is limited in power. Hence due to this it provides marginal fuel savings. *(Power: 3-5 kW)*
- **Mild hybrid**: In this the e-machine is majorly utilized for start-stop, power assist to ICE, generation and regenerative braking operations. During peak loads the e-machine can provide boost to ICE so as to achieve more power and during normal running the e-machine can operate as generator for battery charging. During deceleration and descend at slopes, the e-machine can boost charge the battery by converting kinetic energy to electrical energy. This type of architecture provides good amounts of fuel savings. *(Power: 7-20 kW)*
- **Full hybrid**: Full hybrid has a powerful e-machine so that as certain drive schedules only the e-machine can power the wheels and ICE can be switched off. In this type the vehicle can work in various modes like EV mode (only e-machine operational), cruise mode (ICE powers the wheel, and e-machine charges the battery), boost mode (ICE and e-machine drive

the wheels during peak powers), regenerative braking and other modes depending on manufactures control design. They have substantially good fuel savings as compared to mild-hybrids. *(Power > 25 kW)*

- **Plug-in hybrid**: These are full hybrids with higher battery capacities and can also be charged from the grid via charging stations. These can be series or parallel or combined architectures. They have comparable fuel savings to full hybrids and sometimes even have higher savings than full hybrids. *(Power > 25 kW)*

#### 2.1.1.3 Series-Parallel, or combined HEVs

In series–parallel or combined hybrid, the arrangement incorporates the features of both series and parallel HEVs, but involving an additional mechanical link compared with the series hybrid and also an additional generator compared with the parallel hybrid. Although possessing the advantageous features of both the series and parallel HEVs, the series–parallel HEV is relatively more complicated and costly. Nevertheless, with the advances in control and manufacturing technologies, some modern HEVs prefer to adopt this system [12]. There are various architectures and configurations enlisted in number of literatures, which provides us with good inputs that HEVs can be optimized to achieve high-quality fuel savings [10]-[13].

#### 2.1.1.4 E-machine placement in a hybrid architecture

It can be noticed from section 2.1.1.1 to 2.1.1.3, the HEV architecture has lot of combinations to obtain required functions designed by various manufactures. The placement of e-machine and ICE can be played with to attain different HEV arrangements. Therefore, this section places attention on the placement of e-machine in HEV architecture. Fig. 2.2 illustrates various e-machine placement alternatives in HEV architecture. P0/P1 position demonstrates that the e-machine is always linked to the ICE via belt (P0) or on the crankshaft of ICE (P1). In P2 location the e-machine is linked to ICE on engine crankshaft but can

be decoupled by the clutch. At P3 position the e-machine is connected to ICE by gear transmission. The speed of e-machine is a multiple of ICE speed depending upon gear ratio and hence the e-machine can be decoupled as per requirements. In P4 locations the e-machine is mounted in driveline or in rear axle or in the wheels directly. In this location if engine is eliminated the HEV transforms into a pure EV.

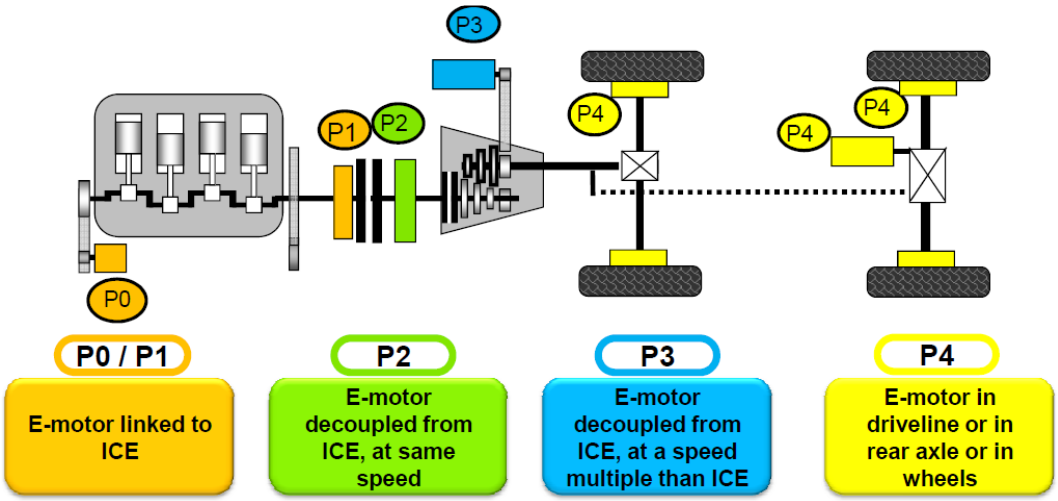


Fig. 2.2 Various e-machine placement alternatives in a HEV architecture [14]

Hence, it can be observed that with different placement of e-machine in HEV architecture, the e-machine would have different specifications. Each placement position has its own merits and demerits. For example, P0/P1 has start-stop, torque-assist and regenerative operations but no e-drive mode, P2/P3 has start-stop, torque-assist, regenerative and pure e-drive (certain distances) operations and P4 has start-stop, torque-assist, regenerative and pure e-drive (long distances) operations. The main aim of designers is to optimize the ICE and e-machines to achieve best efficiencies.

The e-machine in this thesis is based on 48 V mild-hybrid design for P0 position in the above HEV architecture.

### 2.1.2 Electric Vehicle architecture

Pure electric vehicles, in simple terms, convert stored electrical energy into mechanical energy for driving the automobile. The stored electrical energy is generally in the form of batteries, which convert the chemical energy into

electrical energy. Fuel cells, ultra-capacitors, and/or flywheels are some other sources of storage energy. The e-machine utilizes this electrical energy to produce mechanical movement. The EV has many advantages over the conventional ICE vehicle, such as absence of emissions, high efficiency, independence from petroleum, and quiet and smooth operation [13]. A simple modern EV architecture is depicted in Fig. 2.3 [13].

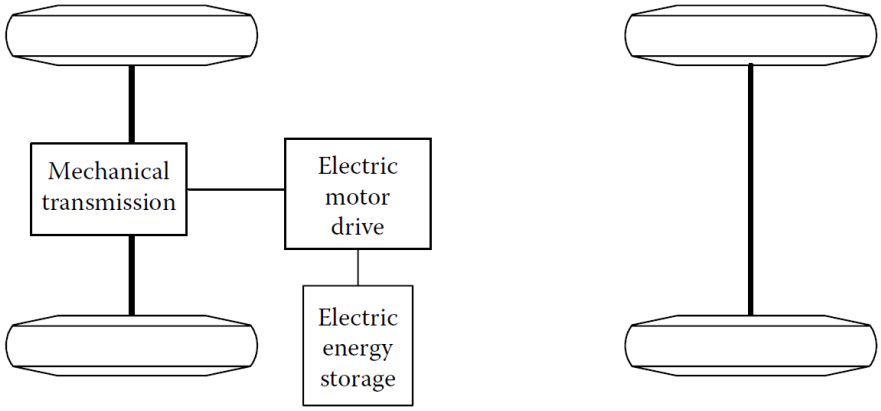


Fig. 2.3 A simple modern EV powertrain [13]

The e-machine is driven by an electronic controller which is programmed specifically for the function of driving with different performance patterns. The e-machine functions as a motor during powering mode and as a generator during deceleration or descend at slopes for regenerative braking. However, most times, the batteries need to be charged by the charging stations or sockets to get the batteries at maximum state of charge (SOC). The e-machine, electronic controller and battery capacities vary a lot depending on vehicle dynamics, size, weight, etc. Exhaustive literature is present in the domain of types of e-machine, electronic controller topologies and type of batteries used in various EVs. Various EV architectures are also detailed in [13] which portray that with the variation in characteristics of electric propulsion and energy sources, numbers of configurations are possible even for electric vehicles.

## 2.2 Claw-pole Machine

Increasing comfort and safety in cars, trucks, and buses, driven by combustion engines, require more installed electric power on board [15]. As of now, the claw-pole-rotor generator is the only type of automotive generator used in industry, with total power per unit up to 5 kW and speeds up to 18,000 rpm.

The solid rotor claw-pole structure with ring-shaped single DC excitation coil, though supplied through slip-rings and brushes from the battery on board, has proven to be simple and reliable, with low cost, low volume and low excitation power loss. In general, the claw-pole-rotor generator is a three-phase generator with three or six slots per pole and with 12, 14, 16 or, 18 poles, and a diode full power rectifier. Its main demerit is the rather large losses (low efficiency), which can be around 50-70% at full power and high speed. Producing electricity on board with such high losses is no longer acceptable as the electric power requirements per vehicle increase [16]. Improvements to the claw-pole-rotor (or Lundell) generator design for better efficiency at higher powers per unit are currently under aggressive investigation by both industry and academia, and encouraging results are continuously being published. Fig. 2.4 illustrates the position of the alternator in the complete powertrain unit.

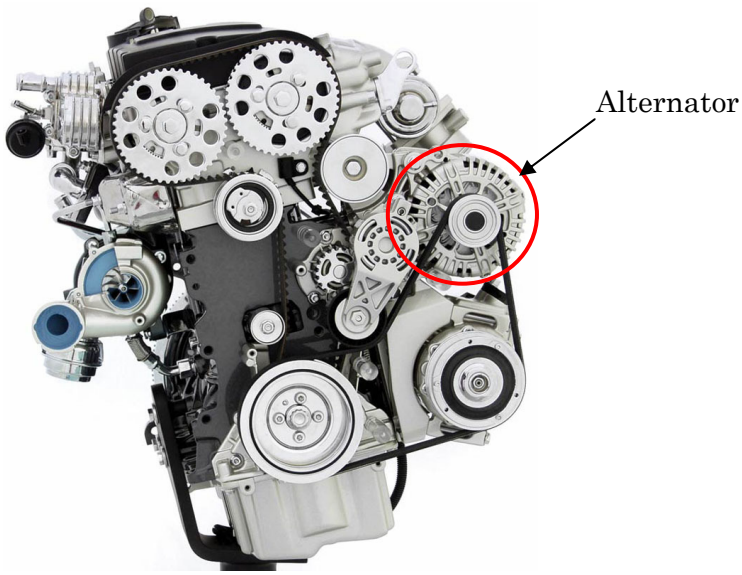


Fig. 2.4 Alternator position in the powertrain unit

### 2.2.1 Construction and Operation

#### 2.2.1.1 Construction

A cross-section of a typical industrial claw-pole-rotor generator is shown in Fig. 2.5. It contains the following main active parts:

- **STATOR**: Uniformly slotted laminated stator iron core.
- **STATOR WINDING**: Generally three-phase alternating current (AC) winding; typically one layer with q = 1, 2 slots per pole per phase, star or delta connection.
- **CLAW-ROTOR & WINDING**: Claw-pole rotor made of solid iron parts that surround the ring-shaped DC-fed excitation (single) coil.
- **SLIP RING & BRUSHES**: Copper slip-rings with low voltage drop brushes to transfer power to the DC excitation coil on the rotor.

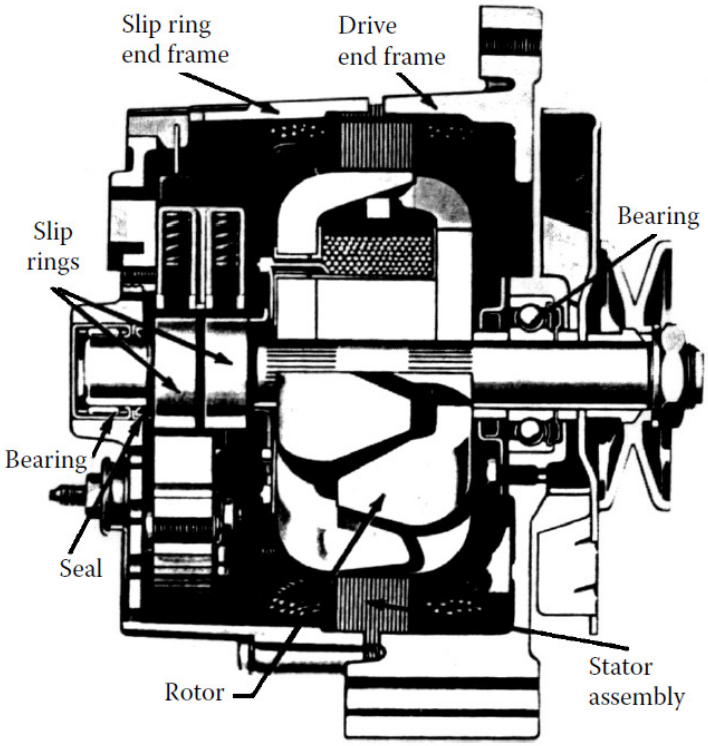


Fig. 2.5 Claw-pole-rotor (Lundell) generator [16]

Fig. 2.6 depicts a typical industrial Lundell generator system [16]. The Lundell generator AC output is rectified through a three- or four-leg diode rectifier and connected to the on-board battery. Today, 12 V DC batteries are used, but 42 and

48 V DC batteries are now adopted as the new standard for automotive application loads [16].

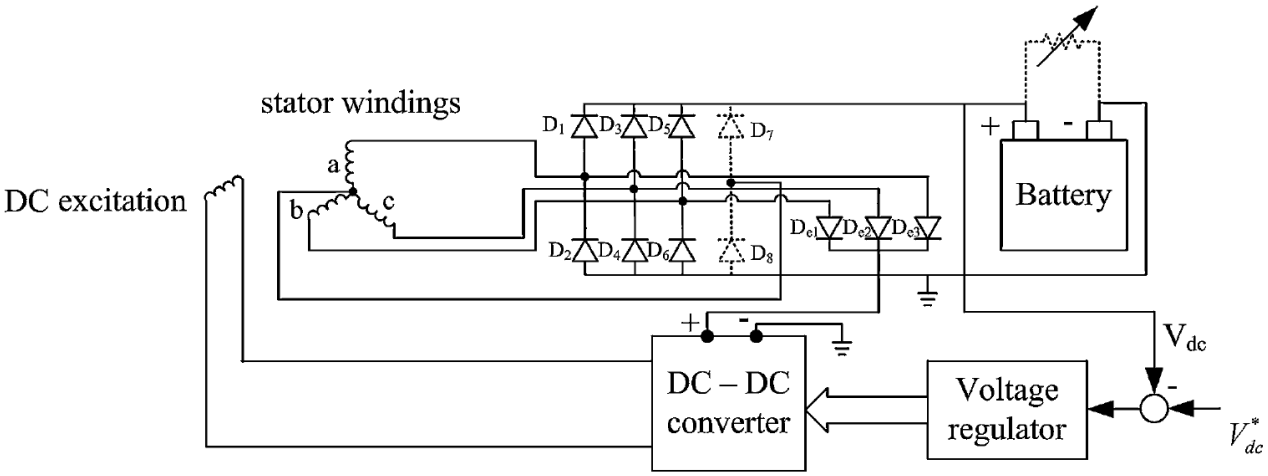


Fig. 2.6 Typical industrial Lundell generator system [16]

The diode rectifier serves the full-power output rectification and is designed for the maximum power of the generator. For large units (for e.g. trucks), three elementary diodes in parallel are mounted on radiator semi-legs to comply with the rather high current levels involved.

#### 2.2.1.2 Operation

Due to claw type rotor structure, the flux distribution in the machine is 3-dimensional (3-D) and hence requires 3-D numerical magnetic field analysis (finite element (FE)). The machine has axial fields and radial fields; as a result it is termed as 3D flux machine. Fig. 2.7 illustrates the geometry of a conventional claw-pole machine with its main flux path through the magnetic circuit and therefore we can observe the 3-D flux distribution [17].

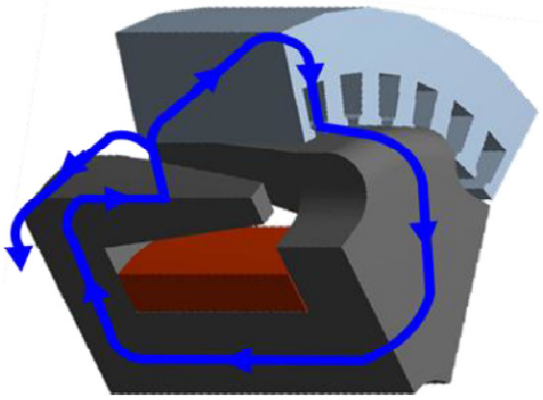

Fig. 2.7 Main 3-D flux path in a conventional claw-pole machine [17]

Hence, with no stator excitation and only DC field excitation the back electromotive force (EMF) increases with speed as well as with the increase in DC field current. The back EMF would saturate after a certain field current at a fixed speed as flux induction in the machine would saturate due to soft magnetic material properties. When stator is connected to a load like battery and resistors or inductors through the rectifier unit; current is induced in stator winding and provides load current to battery and other resistive or inductive loads. Typical DC load current ($I_{dc}$) vs. speed curves for given battery voltage $V_{dc}$, are shown in Figure 2.8 for three different Lundell automotive generators of increasing power [16].

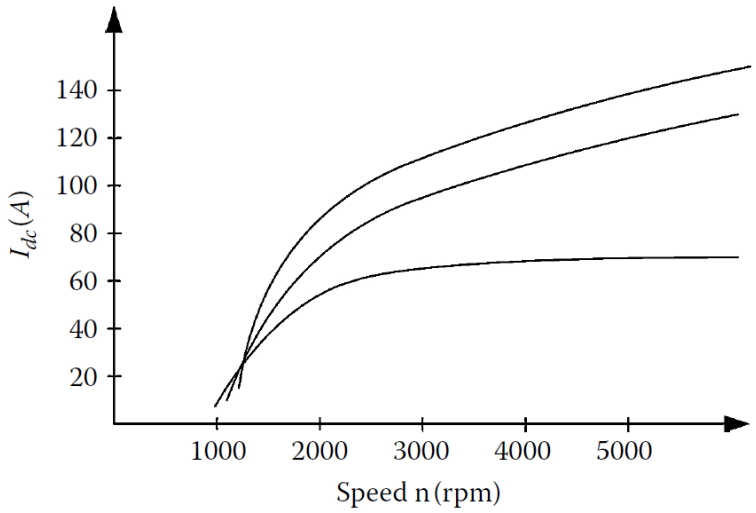


Fig. 2.8 Typical DC load output current vs. speed for constant battery voltage [16]

### 2.2.1.3 Permanent magnet based claw-pole machine

In a PM based claw-pole machine, the PMs are placed in the inter-claw region i.e. between the two claw poles, to provide increased magnetic flux and reduce flux leakage between the consequent claw poles [18]-[19]. Research work has also demonstrated that by utilizing Iron-Cobalt (FeCo) soft magnetic materials in the claw-pole alternator, there could be considerable gain in the output performance of the machine [20]. But due to high price of FeCo material the research in [20] shows that by utilizing them only in the rotor core also provides output power increment with fewer rises in machine cost. Fig. 2.9 shows the claw-pole rotor with the inter-claw magnets [21].

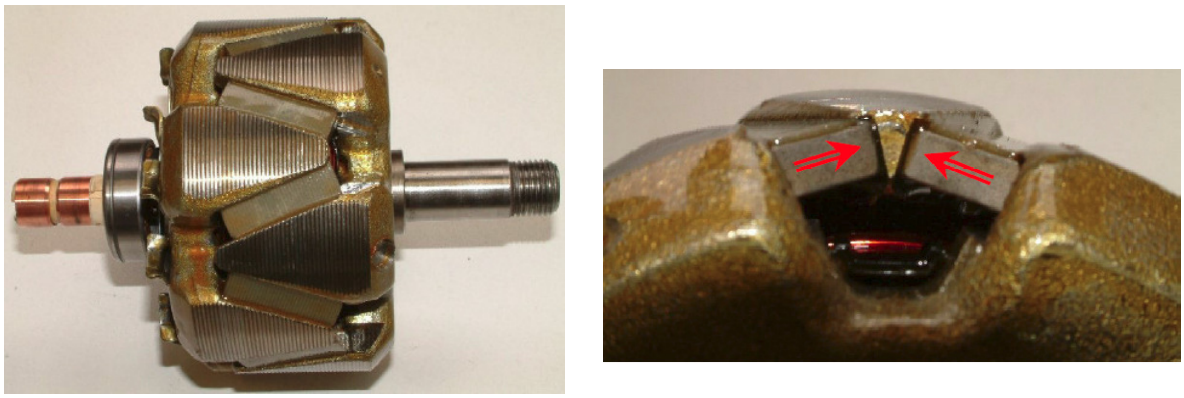

Fig. 2.9 Claw-pole rotor with inter-claw magnets [21]

Hence, the complete assembly of PM based claw-pole machine can be seen in Fig. 2.10. All the major parts like end brackets, electronics, claw-pole rotor with PMs, stator with windings and pulley are illustrated in the figure.

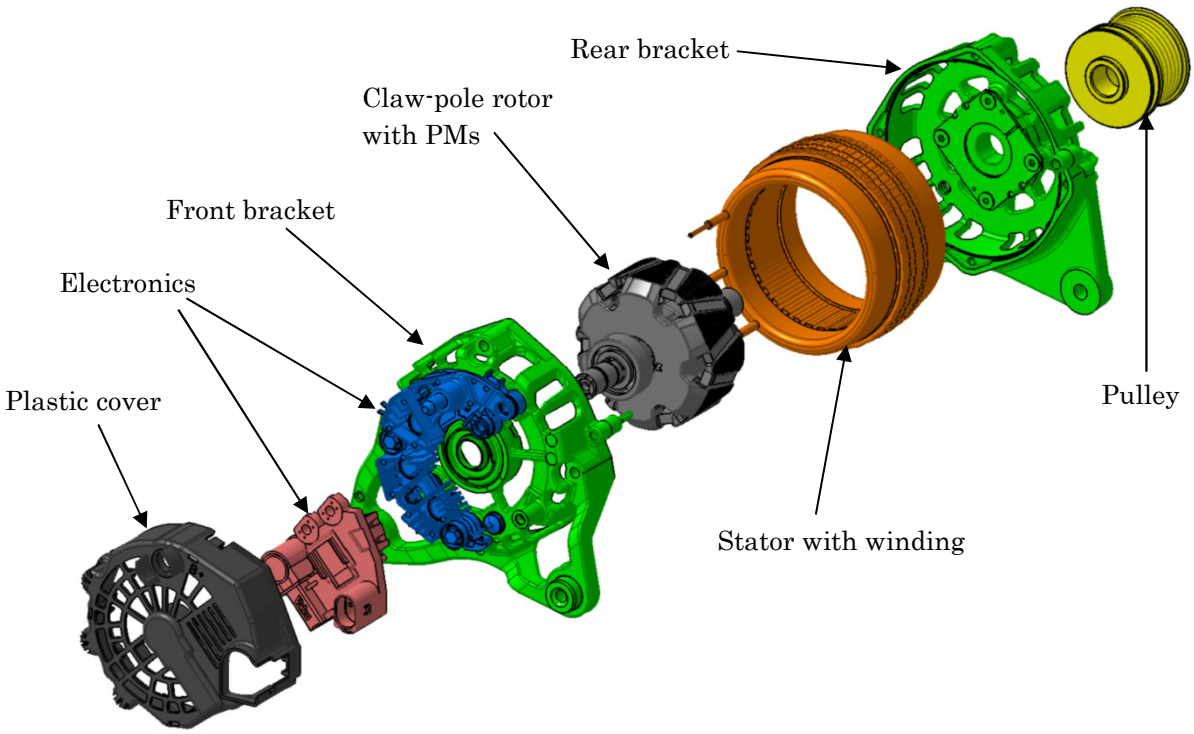


Fig. 2.10 Exploded view of the PM based claw-pole machine

### 2.2.1.4 Claw-pole machine as a motor-generator for HEV application

The claw-pole machines are nowadays being utilized as a motor-generator unit instead of only alternator operation, so as to be employed in micro or mild HEV architectures. The rectifier unit of claw-pole alternator is replaced by more

intelligent electronic controller so as to switch between motor and generator operations depending upon the driving situation. Its use as a starter motor presupposes inverter (frequency) control and, thus, implicitly controlled rectification capability during generating mode. The design accent will be placed on motoring mode with verifications for the generating mode [16].

Mild hybrid vehicles rely on the contribution of the starter/generator supplied from the 36 or 48 V DC battery. Three or four 12 V DC batteries in series, with a typical 100 to 300 A maximum current absorption, provide for a moderate cost battery. The battery also serves all the auxiliary equipment on board for a medium to large car. A 12 V DC bus is built through a special DC–DC converter to serve the low voltage loads [16]. A mild hybrid vehicle system architecture developed by Toyota with 42 V power net is illustrated in fig. 2.11 [16], [22].

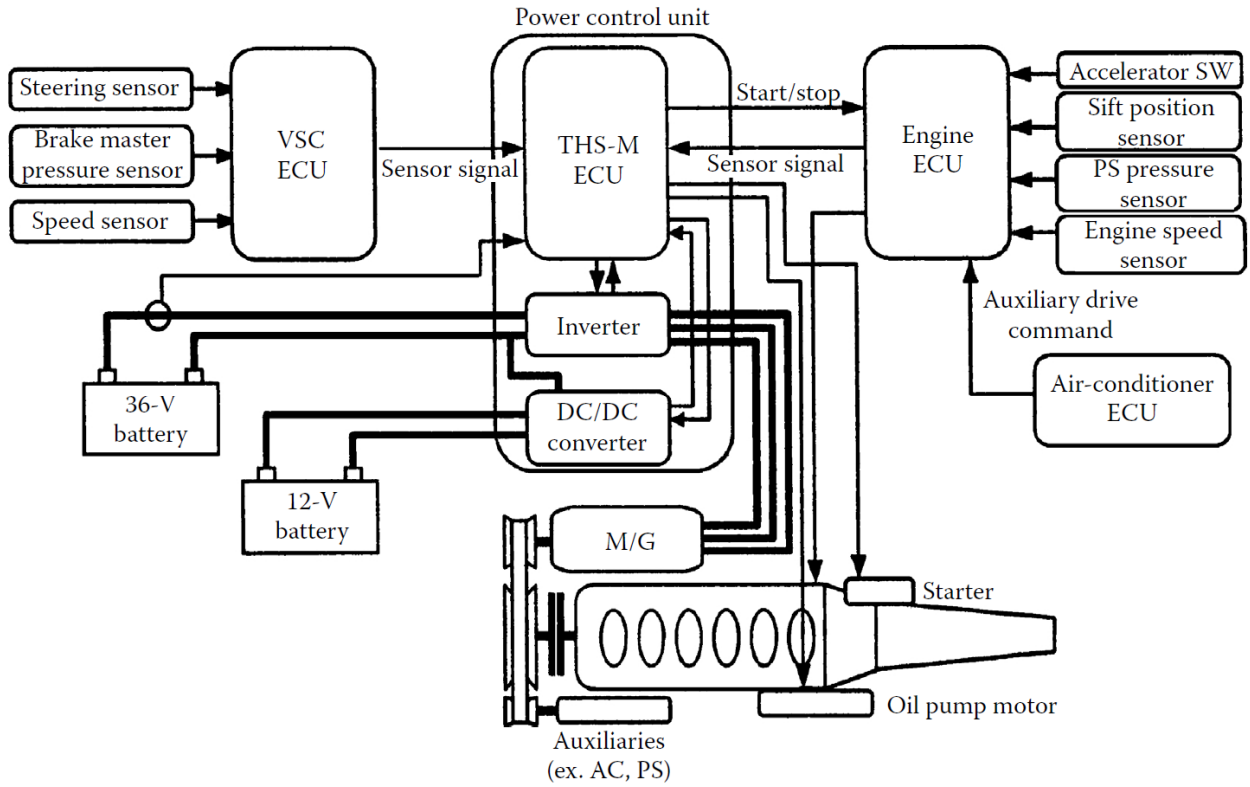


Fig. 2.11 A mild hybrid vehicle architecture by Toyota with 42 V power net [16], [22] (where, ECU is electronic control unit and VSC is variable speed controller)

The starter–alternator design should be worked on with the following objectives in mind [16]:

- Maximum motoring torque for starting and assisting the ICE at low speed, and for driving ICE air conditioner compressor load when the ICE is off.

- Maximum generating power vs. speed.
- Observation of the battery state and reduction of the losses in the system to obtain a reasonable battery life.
- Minimum possible machine volume and pulse-width modulator converter costs.

There are three ways to save fuel with the starter–generator system:

- Starting assistance of ICE.
- Energy saving during "idle stop," when the ICE is shut down at traffic lights or in traffic jams.
- Regenerative electric braking of the vehicle as much as the battery recharging permits.

The design, operation, analysis and detailed study of the mild hybrid operation are provided in reference [16] and [22]. This presents us with the impending advantages of HEV applications for fuel savings and environmental sustainability.

### 2.2.2 State-of-the-art for claw-pole machine

A lot of work has been carried out in the design and optimization of claw pole machines to improve their performance and achieve higher efficiencies at lower costs. This section details few state-of-the-art literature surveys on claw-pole machines.

#### 2.2.2.1 Design and analysis of claw-pole machines

Generally, the electromagnetic design and analysis of electrical machines can be obtained by analytical modelling and numerical modelling. In analytical modelling, the machine is modelled using reluctance network. The various parts of the machine are decomposed into separate reluctance equations and the solution of these equations provides the information related to machine design. In numerical modelling, the machine is generally modelled based on finite

elements. The FE method is a numerical analysis technique for obtaining approximate solutions to a wide variety of engineering problems. Now that computers are widely available, a more viable alternative is to retain the complexities of the problem and find an approximate numerical solution. The FE method envisions the solution region as built up of many small, interconnected sub regions or elements. A FE model of a problem gives a piece-wise approximation to the governing equations. The basic premise of the FE method is that a solution region can be analytically modelled or approximated by replacing it with an assemblage of discrete elements. Since these elements can be put together in a variety of ways, they can be used to represent exceedingly complex shapes [23].

Hence, analytical or lumped parameter models can provide quick and fast solutions but utilize high assumptions, as a result can produce approximate results. Whereas, numerical models can furnish accurate results but utilize time consuming iterations during simulations. V. Ostovic et al in [24] have presented a magnetic equivalent circuit (MEC) based model of a claw-pole alternator to compute its performance. The reluctance network is quite exhaustive with lot of elements but provides good agreement between calculated and measured results. Mamy Rokotova in [25] has developed a reluctance model of the claw-pole machine with comparatively less elements and provides rapid and good performance results. The electric circuit is also modelled in this as a model equivalent to the first harmonics, hence taking into account electromagnetic and electrical performances. Thermal calculations are also computed in [25] along-with electromagnetic calculations, hence providing data about the temperature of the machine. The results are validated with experimental results and they are in agreement with each other. Fig. 2.12 (a) depicts the MEC model developed by V. Ostovic et al. and Fig. 2.12 (b) illustrates the reluctance model developed by M. Rakotovao.

M. Hecquet & P. Brochet in [26] have also presented a permeance network based model, coupled to electric network for a claw-pole alternator, and the results are also validated with measured performances. H. Bai et al in [27] have developed a

lumped-parameter coupled-circuit model of a claw-pole alternator. The machine model is implemented in the simulation and analysis of an alternator/rectifier system using a state-model-based circuit analysis program. Comparisons with experimental results demonstrate the accuracy of the model in predicting the steady state and transient performance of the machine. Sang-Ho Lee et al. in [28] present magnetic field analysis of claw-pole machines using improved equivalent magnetic circuit (EMC) which considers magneto motive-force (MMF) source and permeance of 3-D main and leakage flux distribution. Nonlinear characteristics of magnetic core are also considered for precise analysis results. Calculated results are verified by FE analysis and as well as with experimental measurements and its comparison show the validity of improved EMC method. Similarly, L. Albert in [21] developed a reluctance network along-with electric coupling for design of claw-pole alternator. The optimization of the machine was also carried out using this reluctance tool with various design objectives and constraints like to maximize efficiency, to minimize mass, compromise between mass and yield, etc. and various design options were proposed.

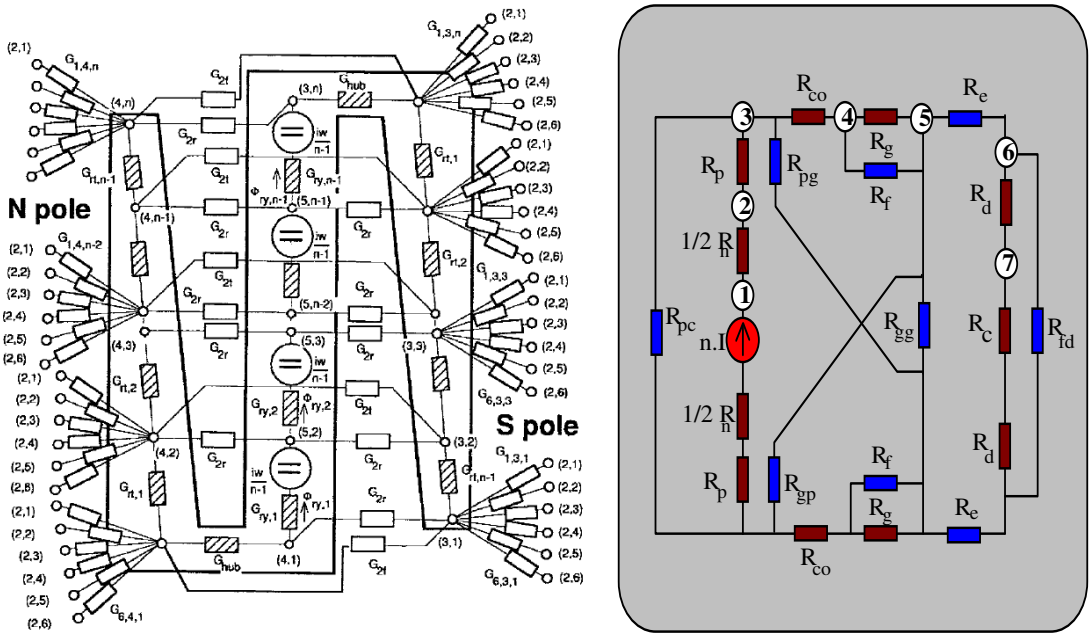


(a) (b)

Fig. 2.12 (a) MEC model by V. Ostovic [24] (b) Reluctance model by M. Rakotovao [25]

Sylvain Perez in [20] has also developed an accurate model to pre-design a claw-pole alternator taking different soft magnet materials into account in the claw-

poles. It is shown that replacing directly the material by another is not enough and optimization of the geometry as well as electric configuration are necessary to take profit of this change. Hence, it can be observed from various literatures above that analytical and semi-numerical design tools provide speedy solutions and are in reasonable agreement with test results, but final numerical check with FE analysis still needs to be obtained so as to assure minimum errors during manufacturing. As a result, diverse literature is also available in numerical analysis to attain close to manufactured product test results. Different authors like H. C. Lai et al. [29], G. Henneberger et al. [30], [31], C. Kaehler et al. [32], C. Barz et al. [33], [34], L. Melcesu [35], have worked upon numerical FE analysis of claw-pole machines. It has been observed that numerical simulations can present more detailed results related to local saturations, precise prediction of losses, accurate wave-shapes, harmonic content in various electrical quantities and proximal end results to experimental tests.

#### 2.2.2.2 Literature on different claw-pole concepts

Due to distinctive 3-D structure of the claw-poles in the claw-pole machine, different claw-pole concepts have been worked upon to achieve diverse solutions. Y. Kuroda et al. in [36] have mounted ferrite magnets in the claw-pole rotor just above the DC field windings, to increase the torque capability and reduce low field excitation losses. Fig 2.13 (a) shows the concept of the developed claw-pole machine with ferrite magnets in the rotor. J. Cros et al. in [37] have presented new claw-pole stator structures with soft magnetic composites (SMCs) and this can be seen in Fig. 2.13 (b).

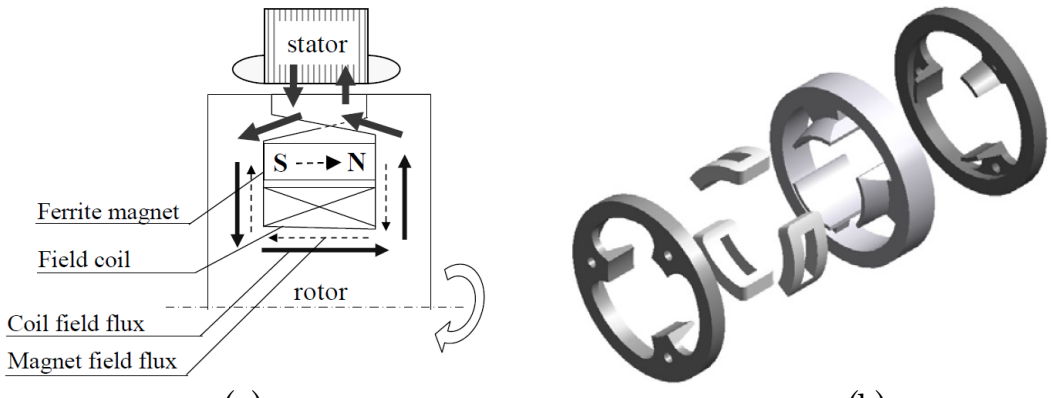


Fig. 2.13 (a) Claw-pole with ferrite magnet [36] (b) SMC Claw-pole stator [37]

The main advantages illustrated for different structures in [37] are that the electromagnetic, mechanical and thermal functions are integrated in the same stator parts. There is no end-winding and the copper volume can be minimized. These structures can be equipped with an integrated cooling system, with efficient air convection or water circulation. S. O. Kwon et al. in [38] have presented a double claw-pole structure as illustrated in Fig. 2.14 (a), to achieve higher power ratings, and exemplified a 2-D equivalent model for analysis. Fig. 2.14 (b) represents a claw-pole machine with DC field winding in the stator as developed in [17] by A. Ibala et al. The main advantage of this structure is the elimination of slip-ring and brush arrangement as compared to conventional claw-pole machine structure.

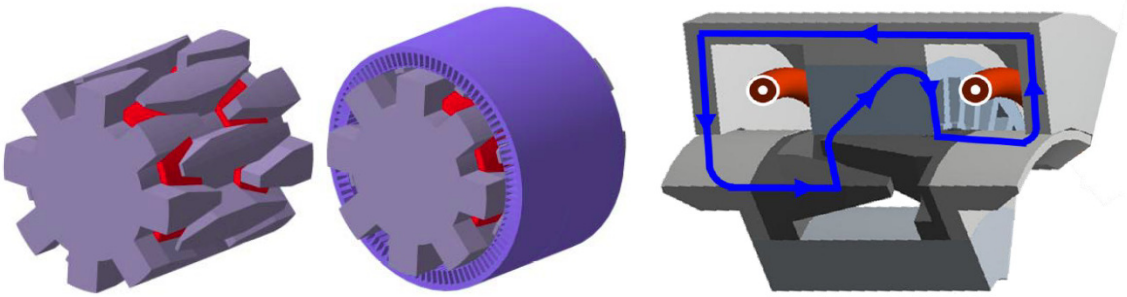

(a) (b)

Fig. 2.14 (a) Double claw-pole structure [38] (b) Claw-pole rotor with field in stator [17]

F. Zhang et al. in [39] presented a structure with inner claw-pole stator and outer PM rotor as seen in Fig. 2.15 (a). In this concept the claw stator need to be made of 2-3 stacks. The main advantage in this is that the brush and slip ring are eliminated and the different phases are isolated from each other, hence no mutual coupling. C. Liu et al. in [40] have presented a SMC claw-pole stator and four different radial flux PM rotors i.e. surface mounted PM rotor, surface inset PM rotor, V-type PM rotor, and flux concentrating PM rotor as seen in Fig. 2.15 (b). Motor with the flux-concentrating ferrite magnet rotor exhibits a very high ratio of torque to cost, making the best candidate for low-cost applications. For high-performance applications, the motor with surface-inset PM rotor has the highest torque density and flux weakening index.

R. Rebhi et al. in [41] illustrate a hybrid claw pole topology which is equipped by two excitation sources, such that: (i) PMs in both stator and rotor, and (ii) DC-

current in the stator. The PMs utilized in this study are ferrite magnets. It has been observed that with the following structure the power of the machine is enhanced and by using partial non-magnetic ring barrier in stator yoke helps in the homopolar flux cancellation and 3D flux enhancement. Fig. 2.16 (a) shows this hybrid excited claw-pole alternator with two ring PMs in stator and rotor.

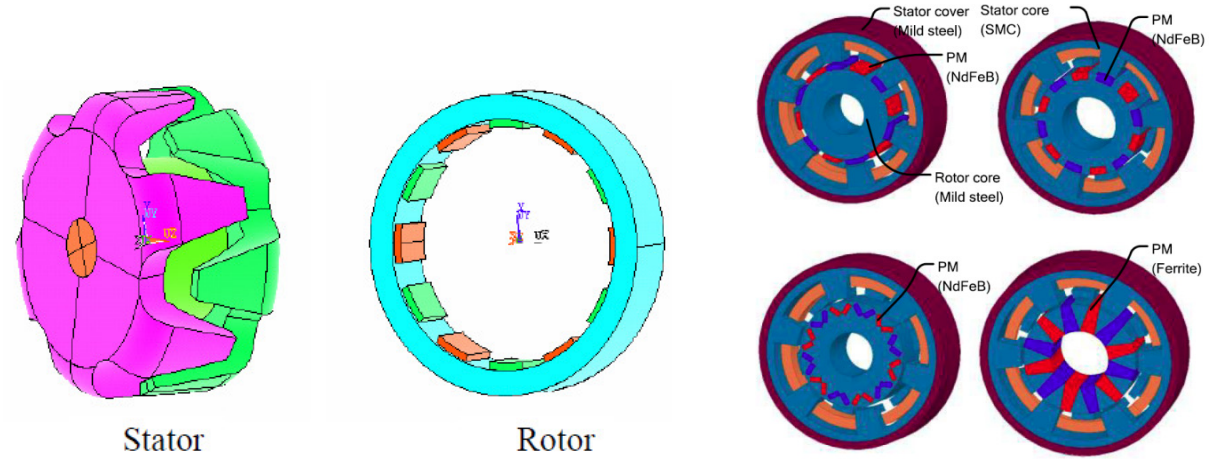


Fig. 2.15 (a) Outer PM rotor and inner claw-pole stator structure [39] (b) Claw-pole stator with different rotor structures [40]

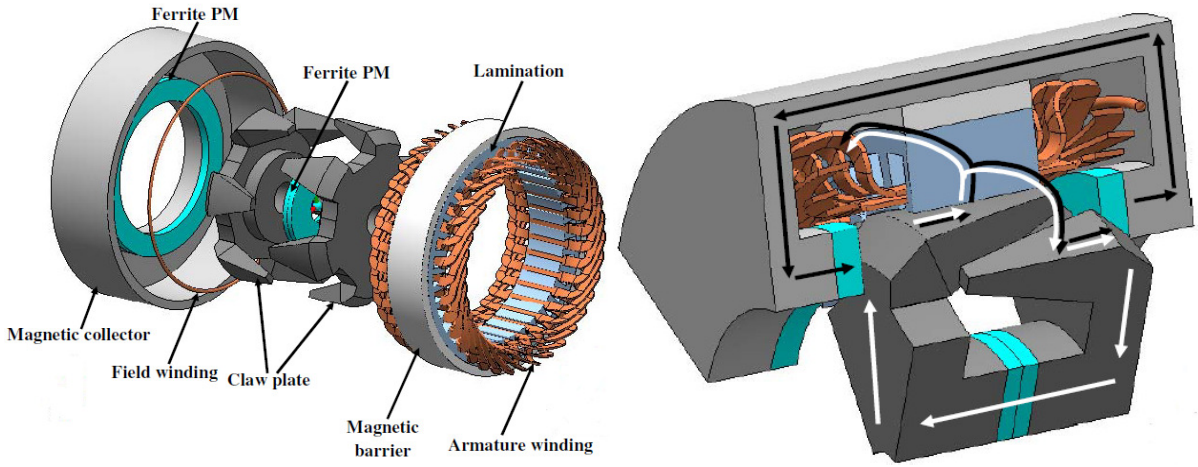


Fig. 2.16 (a) Hybrid excited claw-pole alternator with ring PMs in stator and rotor [41]

M. Wardach in [42] has presented a hybrid excited claw-pole alternator with skewed and non-skewed PMs in the claw-pole rotor fingers. In Fig. 2.16 (b) it can be observed that rectangular magnets are placed in the claw-pole rotor fingers and three different skew angles are seen i.e. 0°, 9° and 15°. It has been observed that cogging torque reduces till the skew angle of 9° and then increases, but the back EMF always decreases with increase in skew angle.

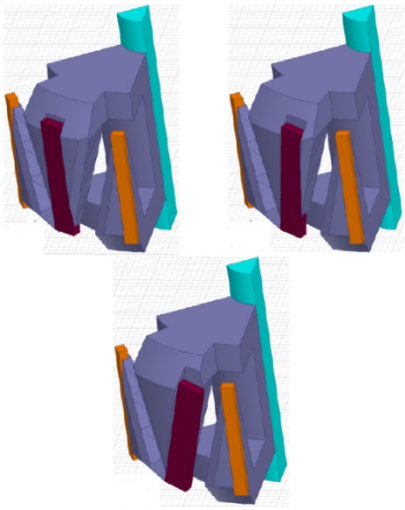

Fig. 2.16 (b) Hybrid excited claw-pole generator with skewed and non-skewed PMs [42]

G. Dajaku et al. in [43] have developed a hybrid excited claw-pole alternator by utilizing the space under the end-windings and adding two axial rotor magnets to increase the air gap flux density, higher power and better efficiency. Fig. 2.17 depicts the hybrid excited claw-pole rotor with axial PMs. Two different magnet materials (NdFeB and ferrite) were also used to analyze the effect in performance, and it has been observed that there is an enhancement of about 2 to 2.8 times in torque depending upon material type. In addition to torque density and efficiency improvements, the mechanical analysis shows that the new claw-pole alternator concept presents also a more rigid and robust structure.

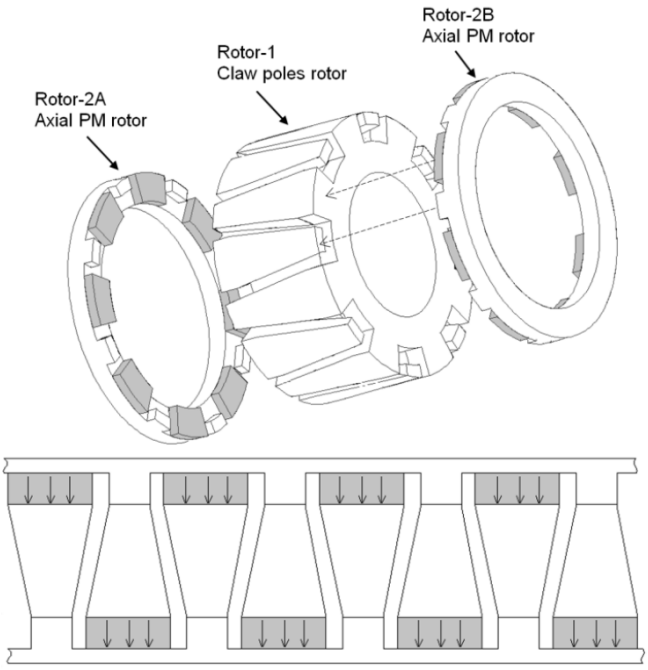


Fig. 2.17 Hybrid excited claw-pole rotor with axial PMs [43]

## 2.3 Recycling, Reuse, Assembly and Disassembly

Increase in the usage of e-machines in e-mobility due to implementation of standards and policies by various nations have also augmented the usage of PMs employed in them. Chapter-1 highlighted the motivation for recycle and reuse of these PM materials as they are considered CRMs by the EU. Hence, this section draws attention to literature study on recycling, reuse, assembly and disassembly of electrical machines and devices.

### 2.3.1 Recycle and reuse

In recent years, numerous studies are being carried out in recycling of critical materials, and NdFeB magnets contain a few of these critical materials i.e. Nd and Dy. K. Binnemans et al. in [44] have presented a critical review on recycling of rare earths. The paper provides an overview of developing efficient, fully integrated recycling routes, which can take advantage of the rich REE recycling literature; with emphasis on three main applications: permanent magnets, nickel metal hydride batteries and lamp phosphors. The state of the art in pre-processing of EoL materials containing REEs and the final REE recovery is discussed in detail. Both pyro-metallurgical and hydrometallurgical routes for REE separation from non-REE elements in the recycled fractions are reviewed. The relevance of LCA for REE recycling is emphasized. Fig. 2.18 shows the simplified recycling flow sheet for REE magnets as illustrated in the paper [44].

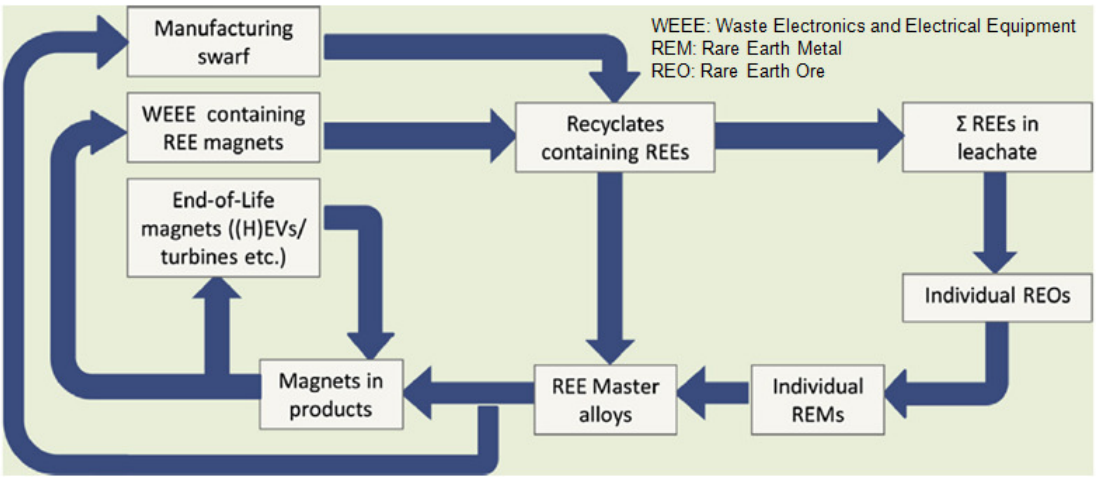


Fig. 2.18 Simplified recycling flow sheet for REE magnets [44]

The review corroborates that, in addition to mitigating the supply risk, REE recycling can reduce the environmental challenges associated with REE mining and processing.

Y. Yang et al. in [45] have detailed a critical review on REE recovery from EoL NdFeB PM scrap. This paper gives an overview of the sources of NdFeB permanent magnets related to their applications, followed by a summary of the various available technologies to recover the REEs from these magnets, including physical processing and separation, direct alloy production, and metallurgical extraction and recovery. At present, no commercial operation has been identified for recycling the EoL NdFeB permanent magnets and the recovery of the associated REE content. Most of the processing methods are still at various research and development stages. It is estimated that in the coming 10–15 years, the recycled REEs from EoL permanent magnets will play a significant role in the total REE supply in the magnet sector, provided that efficient technologies will be developed and implemented in practice. It is believed that no single metallurgical process can be successful for the efficient recovery of the REEs from their EoL secondary resource, and a combination of hydrometallurgical, pyro-metallurgical, and/or electrochemical technologies will be the future solution.
M. Zakotnik et al. in [46], [47] have demonstrated method of recycling NdFeB sintered magnets using HD/degassing process and also improved the properties of recycled magnets by multiple recycling with the addition of Nd hydride. It has been observed that the magnetic properties of recycled magnets deteriorate due to surface demagnetization effects and slight oxidation of the powder during degassing. Whereas in [47] it has been illustrated that with the addition of Nd hydride in multiple recycling steps; the magnetic properties can be improved to a great extent. Fig. 2.19 (a) shows the demagnetizing curves of the recycled magnets for up to four times of recycling cycle. In this there is no addition of Nd hydride. The starting material has remanence ($B_r$) of 1.18 T and coercivity ($H_c$) of 870 kA/m, while at 4$^{th}$ cycle the recycled magnet has $B_r$ of 1.05 T and $H_c$ of 343 kA/m, hence approximately 11% reduction in $B_r$ and 60% reduction in $H_c$. The main reason for this degradation is (a) increasing porosity and diminishing of Nd-

rich material and (b) build up in the oxygen and carbon content. The $B_r$ reduction may not be a great threat for certain applications but the $H_c$ reduction is certainly high as this could lead to magnet demagnetization at certain load levels. Fig. 2.19 (b) depicts the demagnetizing curves of recycled magnets blended with 1at% Nd additions, added on 2nd, 3rd, and 4th cycle. Here it can be observed that the $B_r$ of starting material and 4th cycle recycled magnet are almost similar and the $H_c$ reduction is around 20%, which is quite acceptable for certain load applications. Therefore, HD together with blending with Nd hydride provides an effective means of recycling sintered NdFeB magnets.

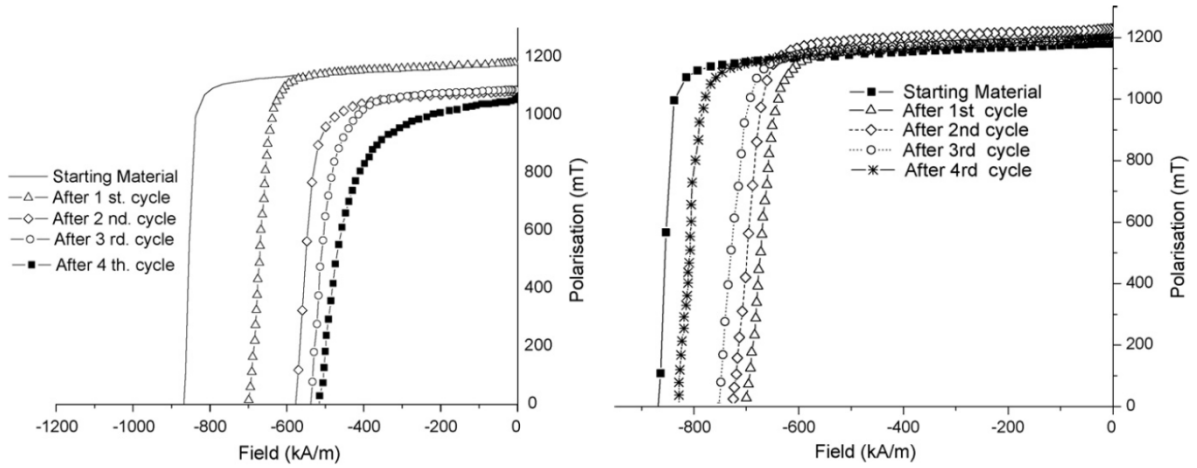


(a) (b)

Fig. 2.19 (a) Demagnetizing curves of magnets recycled up to four times [47] (b) Demagnetizing curves of recycled magnets blended with 1 at.% Nd additions, added on 2nd, 3rd, and 4th cycle [47]

R. S. Sheridan et al. in [48], [49] have shown that anisotropic magnetic powder can be produced successfully from NdFeB scrap magnets by utilizing a combination of the HD and Hydrogenation Disproportionation Desorption Recombination (HDDR) processes. Varying disproportionation temperature alone causes a large variation in magnetic properties. Each disproportionation pressure has an optimum processing temperature and vice versa. Increasing disproportionation temperature requires increased disproportionation pressure. The starting material has $B_r$ of 1.36 T and $H_c$ of 860 kA/m, whereas the recycled material has $B_r$ of 1.08 T and $H_c$ of 840 kA/m. Hence, approximately 20% reduction in $B_r$ and only 2.3% reduction in $H_c$; as a result highlighting good recycle capabilities for PM scrap materials.

Stig Högberg in his doctoral work [50] has worked upon the direct reuse of rare earth PMs from rotating machines. In this exhaustive work direct reuse of bonded RE PMs, direct reuse of sintered RE PMs and magnet coating integrity has been researched and presented in detail. Fig. 2.20 (a) shows the typical production flow chart for sintered NdFeB magnets, Fig. 2.20 (b) shows the typical recycling paths and Fig. 2.20 (c) shows the alternative reuse path for RE PMs. It can be observed that during the HD/HDDR, machining and final application steps the PMs can be utilized for recycling if proper tools, steps, systems and processes are established and maintained.

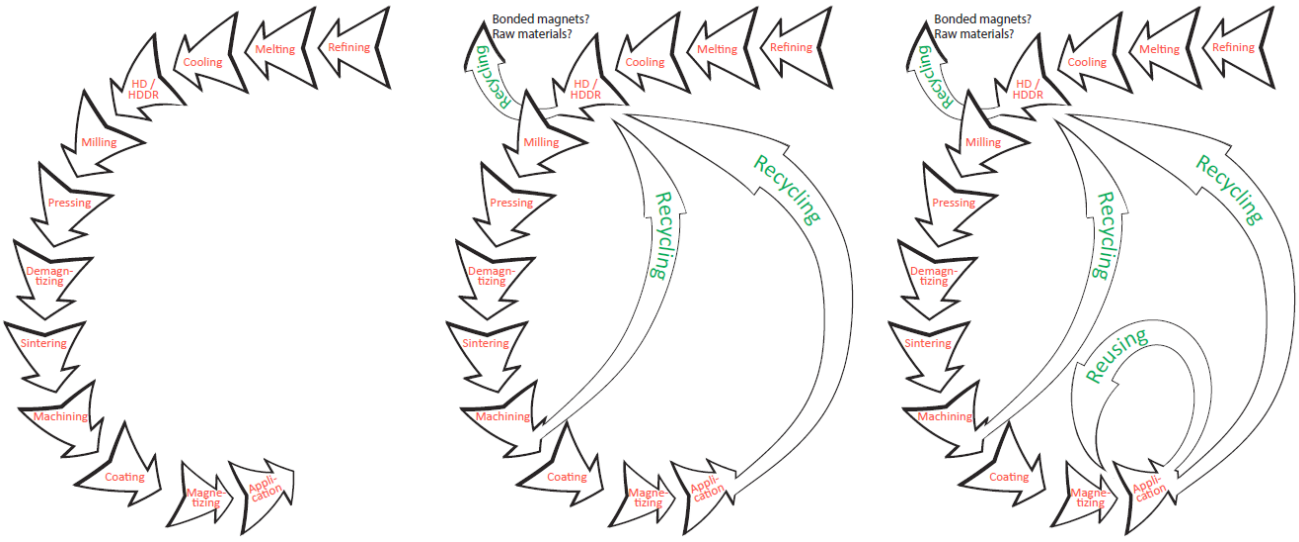


Fig. 2.20 (a) Typical production flow chart for sintered NdFeB magnet (b) Typical recycling paths shown (c) Showing reuse as an alternative recycling path [50]

Comprehensive literature is available on the reuse and recycle of RE PMs, and the above bibliography study in reuse and recycle is only a certain extract so as to emphasize the importance of these steps in future studies.

### 2.3.2 Assembly and disassembly

Several European organizations and universities like Siemens, Daimler, Umicore, Vaccumschmelze, Universitat Erlangen-Nurnberg, Technische Universitat Clausthal, Oko-Institut and Fraunhofer, came together for MORE project (Motor Recycling) which aimed for recycling of components and strategic

metals from electric traction drives [51]. In the project report many routes and ways were investigated for the easy assembly and disassembly of PMs from electric motors. Three strategies for recovering PMs from surface mounted PM motor have also been investigated, and Fig. 2.21 (a) shows these three strategies i.e. thermal demagnetization, removal of bandages and disassembling the magnets. The three steps can be operated in various configurations to obtain the magnets from the rotor, and these different steps are also highlighted in Fig. 2.21 (a). A sophisticated automatic disassembly machine for surface PMs was also developed and used for removal of magnets, which can be seen in Fig. 2.21 (b).

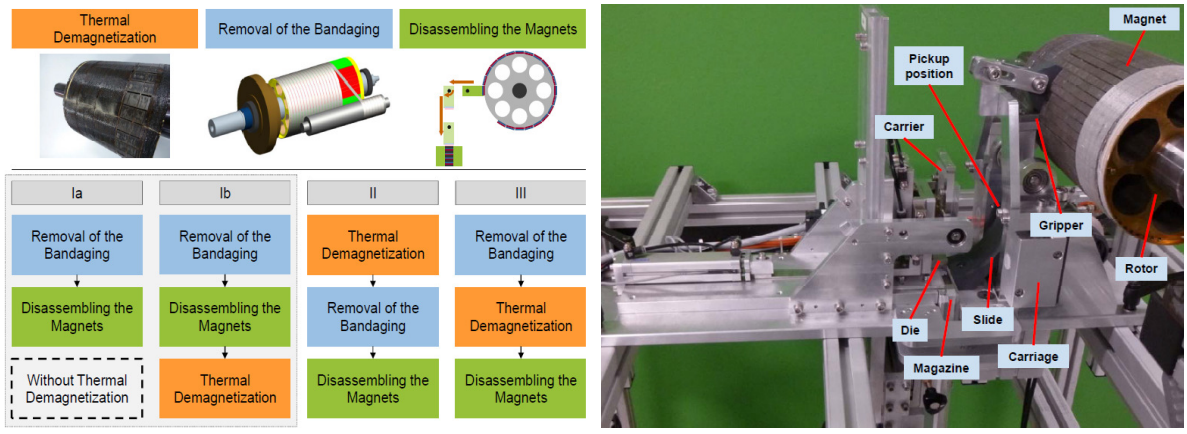


(a) (b)

Fig. 2.21 (a) Three strategies for recovering PMs from surface mounted PM motor [51] (b) Sophisticated disassembly machine for surface mounted magnets

Similarly, disassembly concept for internal permanent magnet machine has also been developed in [51], which is accomplished by using different pressing and sliding mechanism to achieve the task. But it has also been commented that the use of these magnets in secondary markets as second-life magnets needs to be investigated. Additionally the properties of dismounted magnet bodies have to be compared to unused originals. And finally, there is still some uncertainty in the price development of rare earth materials.

J. Franke et al. in [52] presents alternative approaches for the automation of difficult assembly processes regarding issues like, the manufacture of complex new winding bobbin geometries and the development of highly efficient automation processes for magnet assembly. The authors have presented a Robot-Based Winding-Process which offer potential for the economic production of

conventional coils as well as for the flexible manufacturing of innovative winding products. The authors have also explained the logistic chain for processing magnet material, i.e. starting with lab measurement principles and concepts and then requirements for inline tests. The first concept handles the examination of preassembled magnet bodies, the second pays attention towards the finished product at the end of the rotor production line. Therefore a new concept integrating hall sensors in a line array was presented. This enables automated inline measurements of assembled rotary drives.

B. Karlsson & J. O. Jarrhed in [53] presents a robotized workstation for EoL treatment of electrical motors with an electrical effect of about 1 kW. The first step is an inspection whereby the functionality of the motor is checked and classification either for re-use or for disassembly is done. In the second step the motors classified for disassembly are disassembled in a robotized automatic station. By measuring the rotation speed and the current and voltage of the three phases of the motor classification for either reuse or disassembly can be done. During the disassembly work, vision data are fused in order to classify the motors according to their type. The vision system also feeds the control system of the robot with various object coordinates, to facilitate correct operation of the robot. Finally, tests with a vision system and eddy-current equipment are performed to decide whether all copper has been removed from the stator. Fig. 2.22 shows the developed recycling shop in [53].

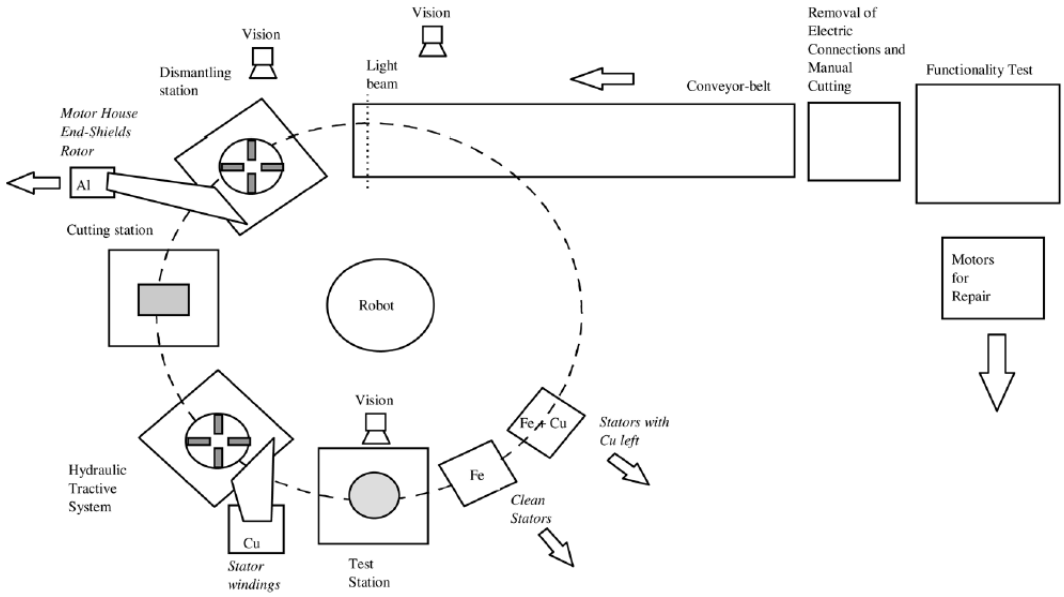


Fig. 2.22 A schematic drawing of the recycling shop [53]

T. Yuksel & I. Baylakoglu in [54] studies development of recycling method of a washing machine and oven. In the study, the recycling systems have been evaluated and a methodology has been presented to find the cost that producers should bear according to the different collection targets. This is determined in developing the best solution methodology in between the automatic disassembly, manual disassembly and recycle with shredders. It has been broadly concluded that the best results can be obtained by developing optimization of automatic-manual methods and correct optimization method can provide the efficient usage of resources and also provide benefits for logistics and tracking. M. Bdiwi et al in [55] propose a robotized workstation for automatic disassembly of electric vehicle motors. Fig 2.23 depicts the screw detection algorithm used in [55].

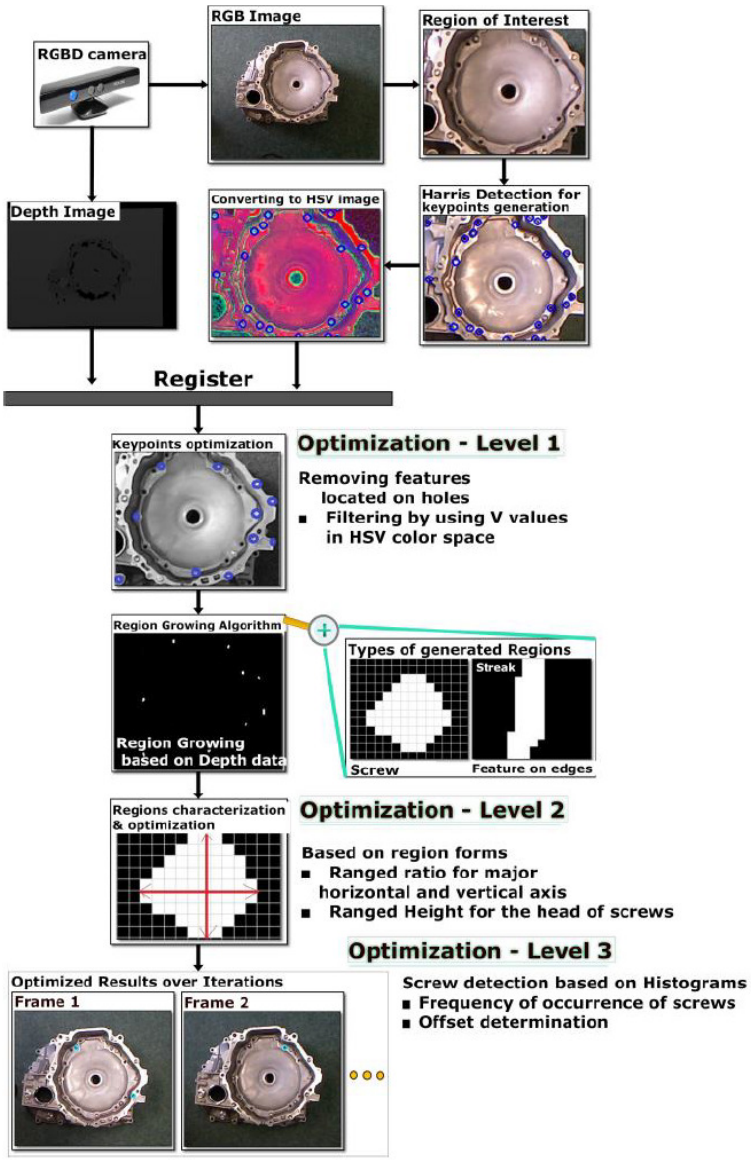


Fig. 2.23 Screw detection algorithm [55]

A novel image processing algorithm is utilized for autonomous detection of motor screws, to automate the task of motor disassembly. Instead of having a database of templates for matching, the screws are detected based on their characteristics with respect to its gray scale, depth and HSV (hue, saturation, value). Furthermore, with frame iterations, the accuracy of the system is increased, mean while reducing its runtime. The algorithm is successfully tested and implemented and yields highly accurate results [55].

T. Elwert et al. in [56] discuss the current developments in the recycling of traction batteries, electric motors, and power electronics, which constitute the key components of HEVs. Both technical and ecological aspects are addressed. As e-mobility is a new trend, no recycling routes have been established at an industrial scale for these components. The implementation is complicated by small return flows and a great variety of vehicle concepts as well as components. Furthermore, drastic changes regarding design and material compositions can be expected over the next decades. Due to hazards and high weights, there is a strong research emphasis on battery recycling. Most pilot-scale or semi-industrial processes focus on the recovery of cobalt, nickel, and copper due to their high value. Electric motors and power electronics can be fed into established recycling routes if they are extracted from the vehicle before shredding. However, these processes are not capable of recovering some minor metals such as rare earth elements and antimony.

S. T. Lundmark & M. Alatalo in [57] and M. Alatalo et al. in [58] present the design of a claw-pole motor, considering recycling of its components i.e. the suggested design has segmented core parts of soft magnetic composites which yield a design very suitable for recycling as the core material is brittle and it thus simplifies the access of the copper winding. However, SMC are generally not utilized in the rotors due to their low mechanical strength and brittle nature. The machine components that are primarily considered as valuable to recycle are copper and permanent magnet material but also the core material is considered. It is observed that in comparison with the commercial motor (Toyota Prius

motor); the claw-pole motor has similar performance, a higher core and magnet weight and a lower copper weight. But it also has an expected advantage regarding manufacturing cost and cost of recycling and it has lower copper loss. In [58] it is shown possible to make an electric motor that is relatively easy to recycle, without losing much of the overall performance (compared to a similar sized reference AROS motor). A claw pole motor design is suggested which can have permanents magnets (of SmCo) that can be recycled. The stator and rotor core are of a recyclable material (SMC) that by its brittleness, simplifies the recycling of the copper coils. Fig. 2.24 illustrates the one phase of the claw-pole motor and Fig. 2.25 depicts the various steps of assembling the motor, hence portraying good recycling aspects.

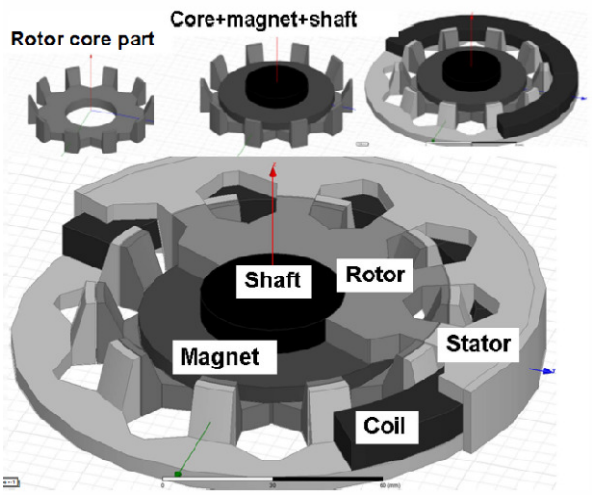


Fig. 2.24 The design of one phase of the claw-pole motor [57]

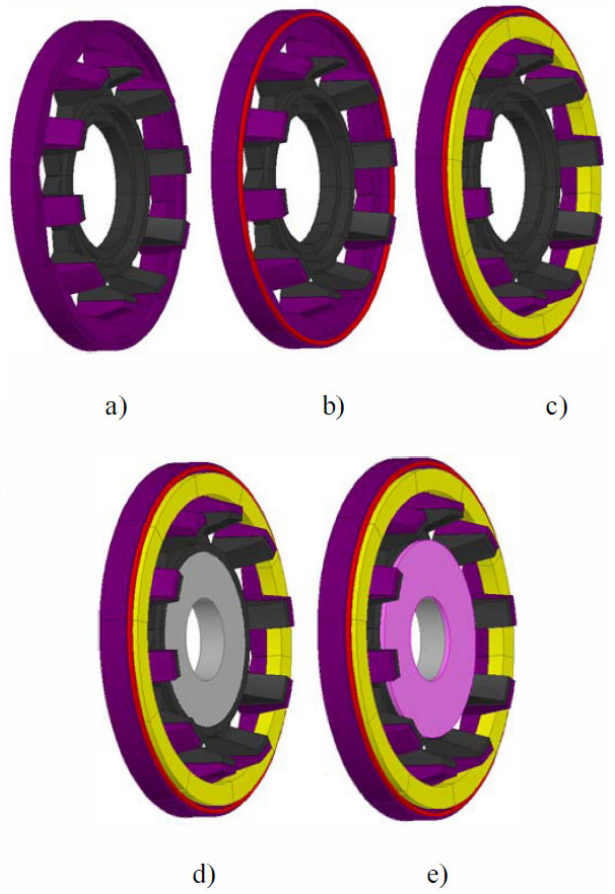


Fig. 2.25 Half a stack of the claw-pole motor with (a) 10 segments of rotor and stator SMC parts, b) an added ring that keeps stator segments in place, c) the ring coil is added, d) the steel ring of the rotor is added, and e) the ring magnet is added to the rotor [57]

## 2.4 Conclusion

Significant amount of literature was explored during the course of the research work and it has been observed that lot of work has been carried out on the design, analysis and experimental testing on claw-pole alternators. It has also been observed that good amount of research work is also being carried out on the reuse, recycling, assembly and disassembly of electrical machines. Therefore, the culmination of all the above literature provides a good insight towards the research work to be utilized in this thesis.

# Chapter 3

# Design and Analysis of Permanent Magnet based Claw-pole Machine for Automotive Application

## 3.1 Electromagnetic Design

The design of an electrical machine can be segregated into electromagnetic design, thermal design, mechanical design and system level design (i.e. along with electronic controller). In this section main focus is given to the electromagnetic design and analysis of the claw-pole machine for 48 V mild hybrid motor-generator applications. As discussed in Chapter 2, section 2.2.2.1, electromagnetic design and analysis can be achieved by analytical modelling and numerical modelling. Both the methods have their advantages and disadvantages, viz. analytical modelling provides quick solutions however with lot of approximations, whereas numerical modelling provides accurate results however with certain time consuming iterations. Nevertheless, analytical modelling is preferred for initial design and sizing of the machine and subsequent final verifications can be obtained using numerical FE analysis. The section below provides an overview of magnetic equivalent circuit modelling of the claw-pole machine.

### 3.1.1 Magnetic Equivalent Circuit modelling [16]

The magnetic equivalent circuit (MEC) modelling generally utilizes the reluctance or permeance network to model the machine. As the claw-pole machine is 3-D in structure due to claw-poles, the MEC should be based on the 3D magnetic flux path. A typical magneto-motive force (MMF) field flux path of the claws is shown in Fig. 3.1 (a) and the simplified MEC is shown in Fig. 3.1 (b). It corresponds to no-load conditions (zero stator current).

Each flux path section is characterized by a magnetic reluctance:

- Air gap: $R_g$
- Stator tooth: $R_{st}$
- Stator yoke: $R_{sy}$
- Claw, axial: $R_{ca}$
- Claw, radial: $R_{cr}$
- Rotor yoke: $R_{cy}$

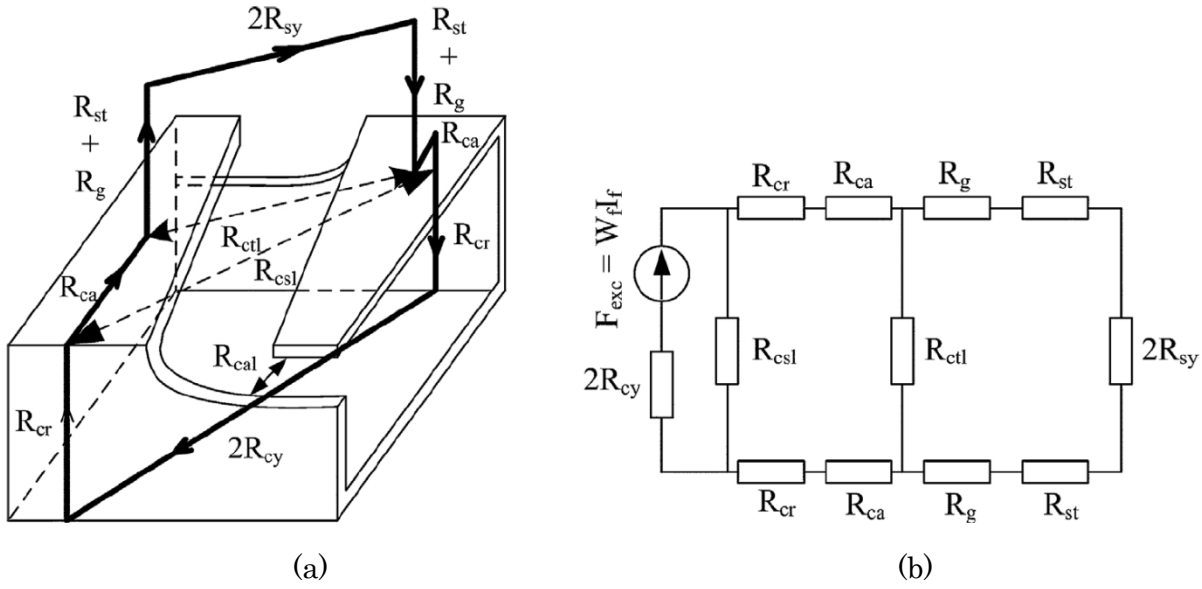


Fig. 3.1 (a) Typical MMF field flux path (b) simplified MEC of the claw-pole [16]

Besides, there are at least two essential leakage paths for this main flux line: one tangential and the other axial between claws: $R_{ctl}$ and $R_{cal}$. In addition, there is the "slot" leakage magnetic reluctance of the ring-shape DC excitation coil: $R_{csl}$.

In the simplified MEC for no load shown in Fig. 3.1 (b), the axial inter-claw leakage flux $R_{cal}$ was neglected, for reluctance simplicity. Analytical expressions for all these magnetic reluctances have to be adopted. While for the stator sections ($R_{sy}$, $R_{st}$) and the air gap ($R_g$) the formulae are rather straightforward (with zero slot openings), for the rotor sections ($R_{cr}$, $R_{ca}$, $R_{cy}$, $R_{ctl}$), the magnetic reluctance expressions, including magnetic saturation effects, are cumbersome, if good precision is expected, because the claw pole cross-section varies axially and so does the magnetic permeability in them. See for details reference [59], pp. 125–127.

Acceptable no-load magnetization curves may be obtained this way:

$$E_1\left(I_f\right) = \pi\sqrt{2}.n.p_1.W_1.\Phi_{p1}\left(I_f\right); \quad \Phi_{p1} = B_{g1}.\frac{2}{\pi}.\tau.l_{stack} \tag{3.1}$$

where,

$I_f$ is the field current

$p_1$ is the number of pole pairs

$W_1$ is the claw finger width at the broadest edge towards the rear end

$\Phi_{p1}$ is the fundamental of stator polar flux

$E_1$ is the rms value of the electromagnetic force (emf) fundamental

$\tau$ is the pole pitch

$l_{stack}$ is the stator stack length

$n$ is the speed in revolution per sec (rpm)

The relationship between the polar flux $\Phi_{p1}$ and the field current has to account for the approximated air gap flux density distribution at no load which can be observed in Fig. 3.2.

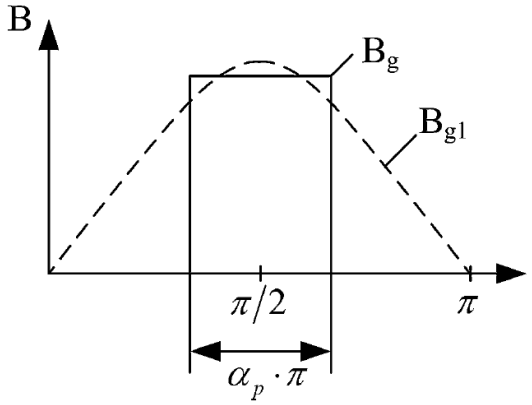


Fig. 3.2 Ideal no-load air gap flux density [16]

The rectangular distribution, calculated with the average rotor claw span $\alpha_p$ = 0.45 to 0.6 (Fig. 3.2) leads to an ideal flux density fundamental in the air gap $B_{g1}$ of the following:

$$B_{g1} = \frac{4}{\pi}.B_g.\sin\alpha_p.\frac{\pi}{2} \quad = \quad K_{\alpha_p}.B_g \tag{3.2}$$

where,

$$K_{\alpha_p} = \frac{4}{\pi}.\sin\alpha_p.\frac{\pi}{2} \tag{3.3}$$

and similarly,

$$\Phi_{p1} = K_{\alpha_p}.\Phi_p \tag{3.4}$$

Reducing the field current $I_f$ to the stator frame $I'_f$ is also required for the machine fundamental equation:

$$K_{\alpha_p}.I_f.W_f = 2.F_{10}\ ; \quad F_{10} = \frac{3.W_1.I'_f.\sqrt{2}}{\pi.p_1} \tag{3.5}$$

$F_{10}$ is the mmf fundamental per stator pole of a three-phase current $I'_f$ that produces the same air gap field as the DC field current $I_f$ and $W_f$ is the number of turns in the field coil.

$$I'_f = I_f.K_{if}\ ; \quad K_{if} = \frac{W_f.K_{\alpha_p}}{\frac{6.W_1.\sqrt{2}}{\pi.p_1}} \tag{3.6}$$

In general, to limit the DC excitation losses, the air gap is kept small (g = 0.35 to 0.5 mm), but, to reduce the machine reactances and volume, the magnetic circuit is saturated for rated field current. Also, the solid iron claw poles serve as a damper winding during transients and during commutation in the rectifier. However, air gap field harmonics produce additional eddy currents in the claw poles even during steady state. These additional losses increase with speed up to a point and pose a severe limitation on machine output.

In the above approximations, the stator slot openings were neglected. To a first approximation, they may be considered by increasing the air gap magnetic reluctance $R_g$ per pole by the known Carter coefficient $K_c > 1$ :

$$R_g \approx \frac{1}{\mu_0}.\frac{g.K_c}{\alpha_p.\tau.l_{stack}} \tag{3.7}$$

The Carter coefficient produces a rough approximation that is also global in the sense that the tangential actual distribution, strongly disturbed by the stator slot openings, is not visible.

For no load, however, the emf measured harmonics are smaller than 10%, even for rated field current, when heavy magnetic saturation occurs and tends to

"induce" a third harmonic in the emf. This saturation-produced third harmonic may be interpreted as if the inverse air gap function contains a second harmonic, besides the constant value.

While the above MEC is suitable for no load, a more complicated one is needed to take care of the local magnetic saturation as well as the inverse air gap function variation with rotor position and along axial direction (due to the tapering shape of claws). Such a comprehensive model is presented in reference [24], where the on-load operation is considered directly.

It is a 3-D model in the sense that the permeance of air gap varies along axial and tangential directions, while the stator and rotor permeances vary along radial and tangential directions. Axially and in the radial plane, the areas are divided into a few sections of almost uniform (but different) permeability (in iron). The more elements that are considered, the better precision is obtained, but the computation time increases notably. The magnetic permeance approximations are, in general, analytical functions of rotor position (of time). Each slot and tooth is modelled by one (or two) element. Axially, the machine is divided into a few sections. The connection of phases is arbitrary. Remarkably good agreement between calculated and measured phase and neutral (for eight-diode rectifier) current is obtained with a few minutes of time on a laptop computer [24]. In the same time, the distribution of air gap flux density along circumferential directions is properly, though approximately, simulated.

## 3.2 Computer-Aided-Design and Analysis of the machine

Computer-Aided-Design (CAD) refers to the utilization of computers in modelling, creation, design and analysis of any component or system. Currently, numerous CAD softwares are available to develop products, components, processes and varied user defined requirements. With the advancement in new computer systems; complex geometries and components can be modelled to design and analyze in a short time. To utilize this advantage, CAD and analysis of the claw-pole machine is conceptualized in this section so as to obtain various performance results and optimize the complex 3-D geometry of the machine.

### 3.2.1 Geometry Modelling

The geometry of claw-pole machine is typically complex due to its two claws and therefore requires 3-D geometry modelling. Consequently, the two-dimensional (2-D) symmetry in the Z-plane for the claw-pole machine is unfeasible and involves 3-D CAD modelling on commercially available CAD softwares like CATIA™, Solidworks™, etc. After CAD modelling, the geometry needs to be imported in commercially available FE softwares (like JMAG® or Altair Flux® or ANSYS® Maxwell®) for electromagnetic analysis. As a result, this operation maybe repeated a number of times for parametric geometry variations and optimization analysis of the claw-pole machine; therefore this leads to an escalation in design and analysis time for one specification. The above process is repeated again for various other specifications, thus cumulatively increasing design and analysis time.

In view of this problem, the best solution would be to model the geometry directly in the FE analysis software's geometry modeller itself, and thereby reduce the time for each parameter variation by systematic design approach. This can be achieved by modelling the claw-pole machine with variables and equations incorporated in the geometry modeller, which can be utilized easily to vary parameters and observe their changes rapidly and efficiently.

#### 3.2.1.1 Geometry modelling in JMAG®

For electromagnetic design and analysis of the claw-pole machine, commercially available FE software viz. JMAG® has been utilized. For the purpose of modelling in JMAG®, a built in geometry modeller is incorporated in the software named 'Geometry Editor'. The Geometry Editor has the following functions:

- It is a history based modelling tool.
- This tool can be used for 2-D and 3-D models.

- This tool can be used for creating solid models and mesh models.
- A CAD model created using CAD software from another supplier can be edited using the Geometry Editor (with certain limitations).

But in spite of various advantages in modelling via Geometry Editor, there are other disadvantages related to CAD modelling. The Geometry Editor has limited commands/operations/tools for modelling as compared to dedicated CAD softwares like CATIA™ or Solidworks™, therefore building geometries in it can be sometimes difficult. The modelling of claw-pole machine in Geometry Editor is carried out in a number of steps so as to achieve the desired claw-pole profile. The geometry modelling is detailed in Appendix A1. Fig. 3.3 depicts the developed claw-pole machine in .

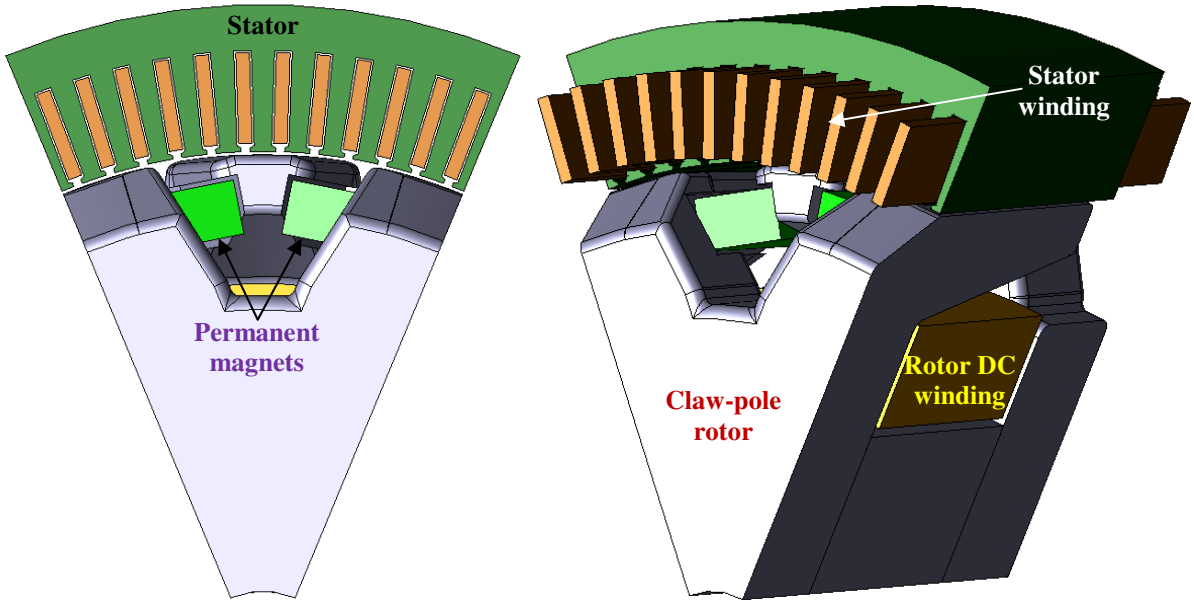


Fig. 3.3 The developed claw-pole machine in JMAG®

Therefore, utilizing equations and variables, two examples are enlisted below which illustrate the quick change in geometry for different value of variables.

Fig. 3.4 (a) shows the machine model with claw outer radii as 55 mm and in Fig. 3.4 (b) 56 mm.

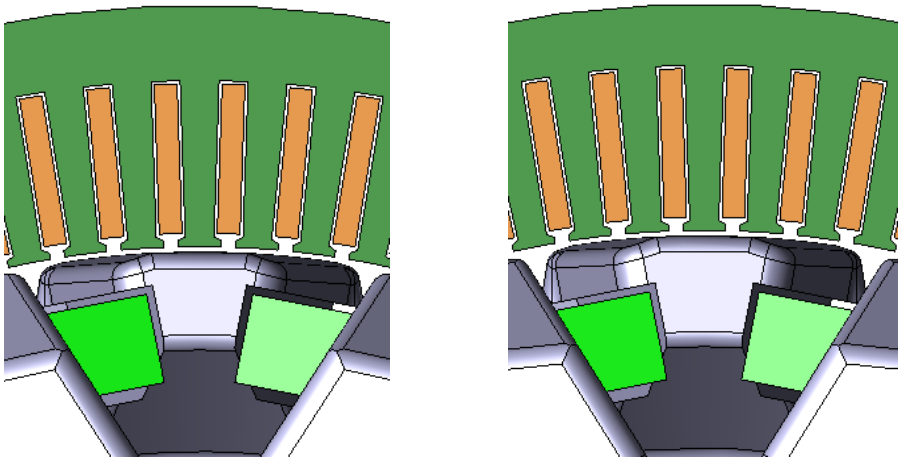

(a) (b)

Fig. 3.4 Machine models with different claw outer radii (a) with 55 mm & (b) 56 mm

Fig. 3.5 (a) shows the machine model with 24 mm as claw core outer radii and in Fig. 3.5 (b) 32 mm. Consequently, just by changing variable values we can obtain quick geometry variations.

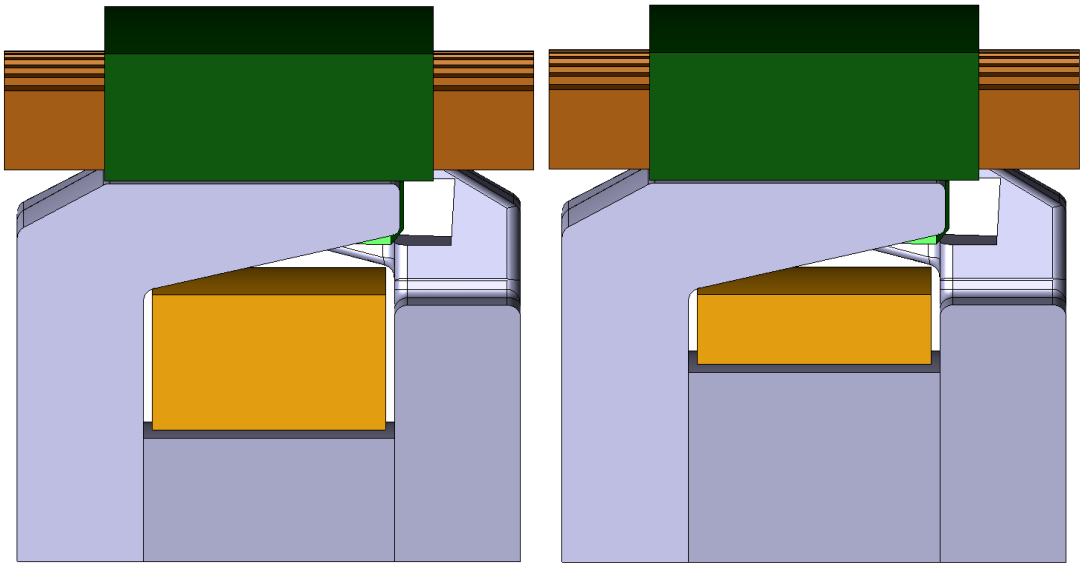

(a) (b)

Fig. 3.5 Machine models with different claw core outer radii with (a) 24 mm & (b) 32 mm

Similarly various other geometric parameters can be varied easily to get different values of the claw pole geometry as well as the stator geometry. Hence trouble-free geometry editing is possible by utilizing the defined variables and the equations related to these variables in the JMAG® geometry editor.

### 3.2.2 Numerical Analysis of the base design

The numerical design analysis of the developed claw-pole machine is necessary to obtain the various performance characteristics. The machine is designed and modelled as per the specifications provided by the research & development department of Valeo. The machine is to be developed for a 48 V mild hybrid motor-generator application utilized in automobiles. The maximum speed for the machine is 18,000 rpm and peak power is around 14 kW. The stator material is M800-50A, rotor material is SAE 1005 and magnet is N42SH sintered NdFeB. The numerical analysis carried out uses JMAG® FE analysis software by JSOL Corporation, Japan.

The design analysis of the machine has been carried out using classical electrical machine analysis theory using Park's transformation and FE analysis to evaluate the machine performance at various speeds [60]. The *d-q* transformation equations utilized are as follows [60]:

$$\begin{bmatrix} F_d \\ F_q \\ F_0 \end{bmatrix} = \frac{2}{3} \begin{bmatrix} \cos\theta & \cos\left(\theta - \frac{2\pi}{3}\right) & \cos\left(\theta + \frac{2\pi}{3}\right) \\ -\sin\theta & -\sin(\theta - \frac{2\pi}{3}) & -\sin\left(\theta + \frac{2\pi}{3}\right) \\ \frac{1}{2} & \frac{1}{2} & \frac{1}{2} \end{bmatrix} \begin{bmatrix} F_a \\ F_b \\ F_c \end{bmatrix} \tag{3.8}$$

where, variable $F$ can represent any of the following, i.e. electromotive force (EMF) $e$ in volts, current $(I)$ in Amps and flux linkage $(\psi)$ in Wb. $\theta$ is the angular displacement of the rotor *d*-axis w.r.t. the *a*-phase.

Due to the complex 3-D geometry of the claw-pole machine, 3-D time stepping motion FE analysis is time consuming. Therefore, in order to have quick performance analysis with accurate results, Park transformation equations along with static FE analysis can yield to favourable performance results. In Eq. 3.8, utilizing flux linkage $\psi$ in place of $F$ can provide the values of *d*-axis flux linkage $(\psi_d)$ *and* *q*-axis flux linkage $(\psi_q)$ from phase flux linkages $\psi_a$, $\psi_b$ and $\psi_c$ for different values of *d*-axis current $(I_d)$, *q*-axis current $(I_q)$ and field current $(I_f)$. Hence, transforming three-phase time varying quantities to constant DC *d-q*

quantities. Fig. 3.6 illustrates an example of Park transformation of 3-phase flux linkages into DC *d-q* flux linkages.

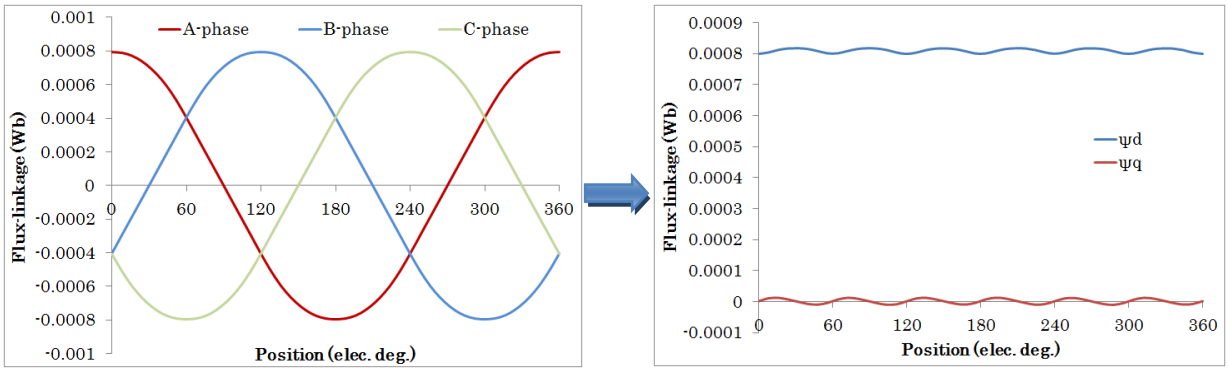


Fig. 3.6 Park transformation of 3-phase flux linkages to DC *d-q* flux linkages

The claw-pole machine developed in this research work is a double 3-phase topology with 30° phase shift between phase-1 set and phase-2 set. The double 3-phase topology helps in reducing the torque ripple and the electronic controllers' device current carrying capacity. It also assists in increasing the machine power. A current source excitation is utilized to evaluate the steady state performance results of the machine and Fig. 3.7 shows the circuit utilized in the FE software.

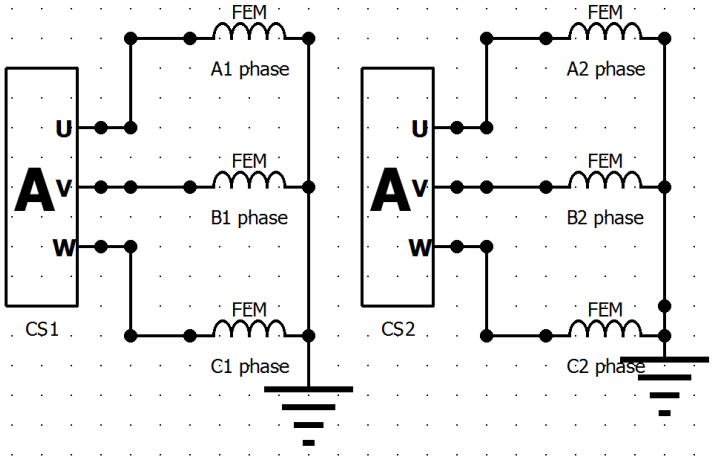


Fig. 3.7 Current source excitation for steady state analysis

The stator currents ($I_{a1}$, $I_{b1}$, $I_{c1}$, $I_{a2}$, $I_{b2}$ and $I_{c2}$) and $I_f$ are varied to obtain the flux linkages in the stator windings i.e. $\psi_{a1}$, $\psi_{b1}$, $\psi_{c1}$, $\psi_{a2}$, $\psi_{b2}$ and $\psi_{c2}$ and thereafter using Park transform equations $\psi_d$ and $\psi_q$ is calculated. Fig. 3.8 shows the flux map of the machine, where Fig. 3.8 (a) depicts the $I_d$ vs. $I_q$ vs. $\psi_d$ matrix and Fig. 3.8 (b) depicts $I_d$ vs. $I_q$ vs. $\psi_q$ matrix for $I_f$ = 10A in motoring mode.

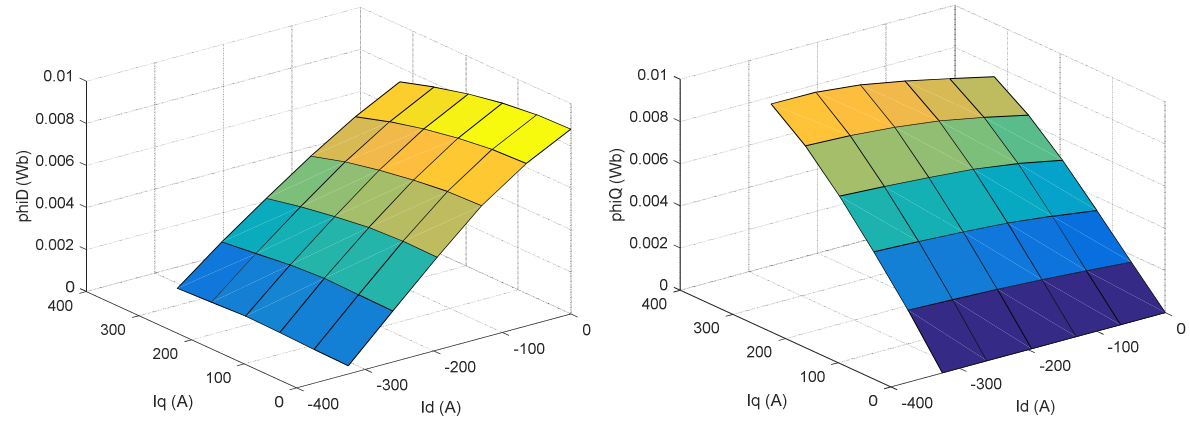


(a) (b)

Fig. 3.8 Flux map of the machine for $I_f$ = 10 A (a) $I_d$ vs. $I_q$ vs. $\psi_d$ (b) $I_d$ vs. $I_q$ vs. $\psi_q$

Flux density and vector plot of the developed claw-pole machine for $I_d$ = 0 A, $I_q$ = 325 A and $I_f$ = 10 A can be seen in Fig. 3.9. This operating condition is during peak torque performance and hence it can be observed that the machine is saturated in most of the parts.

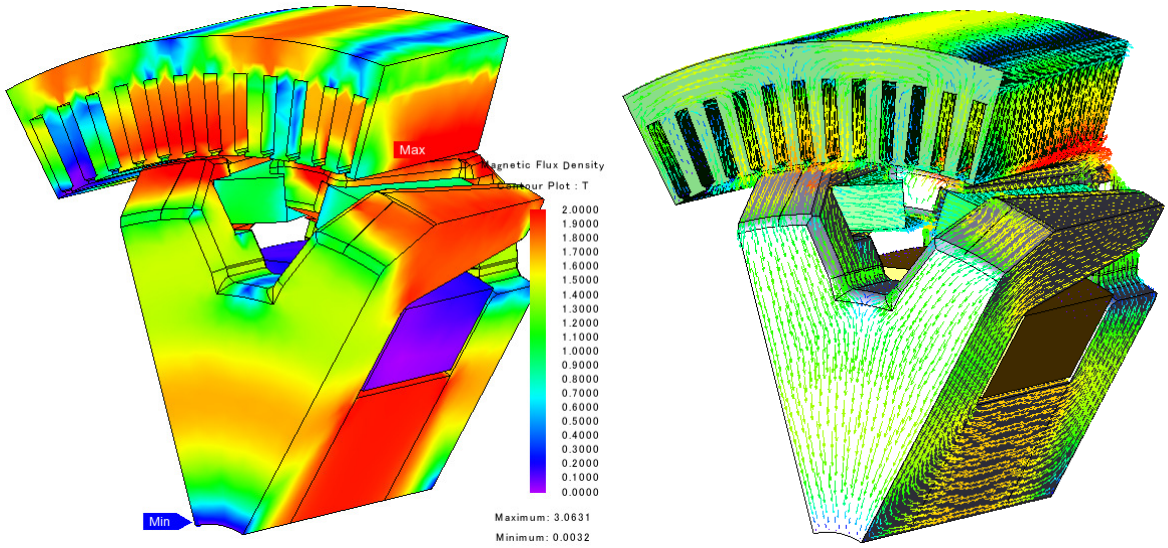


Fig. 3.9 Flux density and vector plot of the machine for $I_d$ = 0 A, $I_q$ = 325 A & $I_f$ = 10 A

By the variation of $I_d$, $I_q$ and $I_f$, different winding voltages and torque can be obtained. But it is important to maintain the voltage under the specification limit and power should be steady in the constant power region. Fig. 3.10 depicts an ideal torque/power vs. speed characteristics. In the constant torque region, the $I_d$ is small, $I_q$ is close to maximum value and $I_f$ is also maximum to achieve the maximum torque, whereas in the constant power region or field weakening

region, $I_d$, $I_q$ and $I_f$ need to be optimized so as to attain steady power and limit the voltage to the specified value.

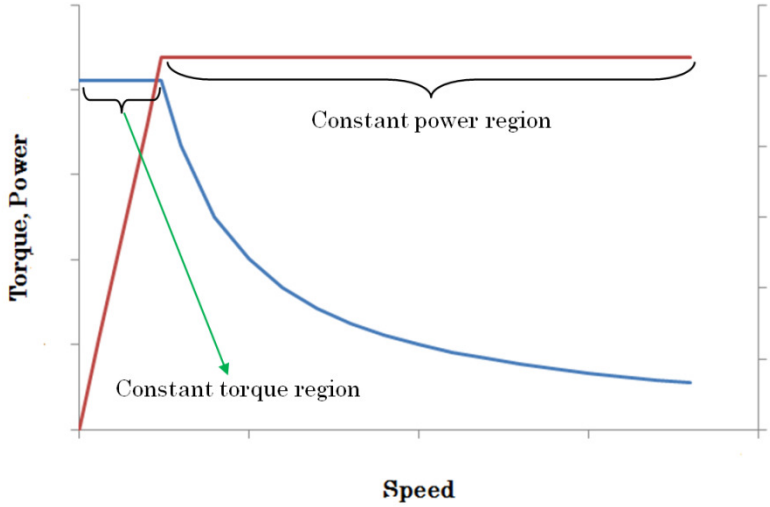


Fig. 3.10 Ideal torque/power vs. speed characteristics

The voltage equations at steady state are defined as follows [60]:

$$V_d = R_s I_d + \frac{d\psi_d}{dt} - \omega\psi_q \tag{3.9}$$

$$V_q = R_s I_q + \frac{d\psi_q}{dt} + \omega\psi_d \tag{3.10}$$

where, $V$ is the voltage in volts, $R_s$ is the stator phase resistance in ohms and $\omega$ is the speed in rad/s.

Finally the torque $T_e$ in Nm is as below [60]:

$$T_e = \frac{m}{2} p_1 \left(\psi_d(I_d, I_q, I_f).I_q - \psi_q(I_d, I_q, I_f).I_d\right) \tag{3.11}$$

where, $m$ is the number of phases and $p_1$ is the number of pole pair.

In Table 3.1 $I_d$, $I_q$ and $I_f$ for four different speeds were injected into the machine to evaluate the torque and voltages. $V_s$-dq and $T_e$-dq corresponds to voltage and torque using static FE analysis respectively and $V_s$-FE and $T_e$-FE corresponds to time stepping motion FE analysis respectively. It can be observed that the voltage and torque for static and time stepping motion analysis are matching fairly well with each other. This encourages in utilizing static FE analysis for complete performance evaluation and optimization of the machine.

Table 3.1 Evaluation of torque and voltages using static and time stepping FE analysis

| $I_d$ (A) | $I_q$ (A) | $If$ (A) | $\psi_d$ (Wb) | $\psi_q$ (Wb) | Speed (rpm) | $Vs$-$dq$ (V) | $Vs$-$FE$ (V) | $T_e$-$dq$ (p.u.) | $T_e$-FE (p.u.) |
|---|---|---|---|---|---|---|---|---|---|
| 0 | 325 | 10.0 | 0.00806 | 0.00703 | 600 | 7.53 | 8.41 | 1.01 | 1.00 |
| 0 | 325 | 10.0 | 0.00806 | 0.00703 | 2440 | 23.86 | 24.36 | 1.01 | 1.00 |
| -310 | 60 | 8.0 | 0.00164 | 0.00196 | 10000 | 23.68 | 23.96 | 0.27 | 0.26 |
| -315 | 35 | 6.8 | 0.00055 | 0.00127 | 18000 | 23.24 | 23.87 | 0.16 | 0.16 |

*Copper losses:*

The stator and rotor copper loss calculations are purely dependent upon the currents, resistances and temperatures. The DC copper losses at a particular temperature are calculated by the following equation:

$$P_{cu} = I^2 R_{dc} \tag{3.12}$$

where, $P_{cu}$ is the copper losses, $I$ is the rms current and $R_{dc}$ is the DC resistance.

Consequently, the stator copper losses at a particular temperature can be computed as below:

$$P_{cu-s} = m.{I_s}^2 R_{s-dc} \tag{3.13}$$

where, $P_{cu\text{-}s}$ is the stator copper losses, $m$ is the number of phases $I_s$ is the stator rms current and $R_{s\text{-}dc}$ is the stator phase DC resistance.

Similarly, rotor copper losses at a particular temperature can be computed as below:

$$P_{cu-r} = {I_f}^2 R_{r-dc} \tag{3.14}$$

where, $P_{cu\text{-}r}$ is the rotor copper losses, $I_f$ is the rotor field current and $R_{r\text{-}dc}$ is the rotor DC resistance.

AC copper losses can be predominant as compared to DC copper losses at higher frequencies. Due to high computational time required to calculate the AC copper losses using FEM; they are neglected in this study and considered as future work.

*Iron losses:*

Iron losses are generated in electrical machines due to the changing magnetic field in the stator and rotor cores. For ferromagnetic materials, the iron losses are often separated into hysteresis losses and eddy current losses. The former describes the losses due to the hysteresis properties of the magnetic material. If a magnetic material is first slowly magnetized with an increasing magnetic field $H$ and afterwards demagnetized with an opposing magnetic field $-H$, the magnetization curve does not describe the same path back. Instead, a hysteresis curve is created. The area enclosed by this hysteresis curve is equal to the specific energy for each cycle and thus proportional to the hysteresis losses. Eddy currents are created by the induced voltages in the conducting magnetic materials due to the changing magnetic flux, leading to dynamic iron losses. These eddy currents counteract the variations (time and direction) of the magnetic fields. They lead to a broadening of the hysteresis curve and thus increase the $H_c$ [61].

The challenge with determination of the value of iron losses is that it is not possible to measure them directly. Indirect thermal measurements (inverse thermal models and calorimetric measurements), magnetic field measurements (search coil windings, hall sensors, etc.) or loss separation calculations (subtracting all known other losses from the total losses) are the applied possibilities to determine indirectly iron losses in ferromagnetic materials for electrical machines [61]. Fig. 3.11 depicts the *BH* curves for the soft magnetic materials used in the machine viz. (a) M800-50A and (b) SAE 1005.

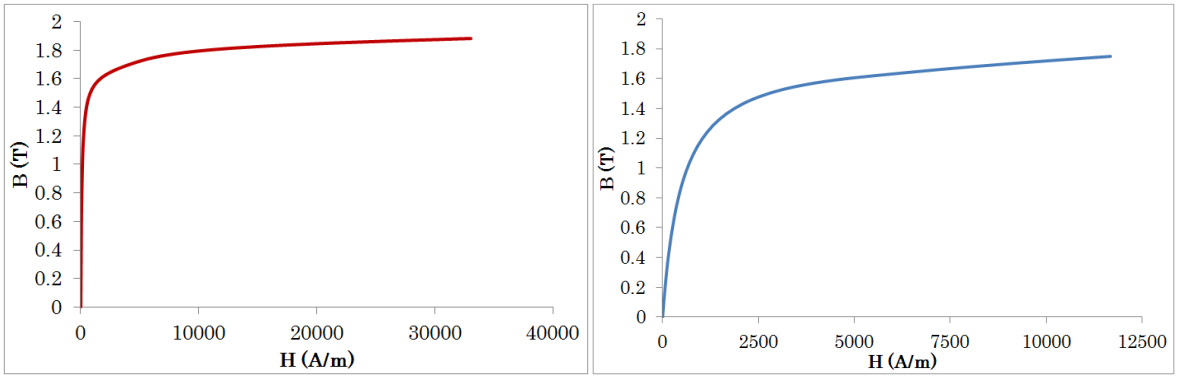


(a) (b)

Fig. 3.11 *BH* curves of (a) M800-50A and (b) SAE 1005 soft magnetic materials

The iron losses can be depicted as per the equation below, considering their simple decomposition into hysteresis losses contribution and classical eddy current contribution. The excess losses contribution as modelled by Bertotti is not considered [62].

$$P_i = K_h . f . {B_m}^{\alpha} + K_e . \frac{1}{T} \int_0^T \left(\frac{dB}{dt}\right)^2 \, dt \tag{3.15}$$

where, $P_i$ is the iron loss, $K_h$ is the hysteresis loss coefficient, $f$ is the frequency, $B_m$ is the peak flux density, $\alpha$ is like Steinmetz constant, $K_e$ is the eddy current loss coefficient, $T$ is the time period corresponding to $f$ and $B$ is the flux density curve corresponding to an element in the machine.

As a result, utilizing the above methodology, equation and analysis results, performance of the machine can be computed for the entire torque-speed range. The above section will be utilized to evaluate the machine performance and efficiency map in Section 3.5.

## 3.3 Impact on Performance by Geometric Variations

Design optimization of claw-pole machine requires rigorous design iterations by geometric parameter variations. This result into huge time consuming optimization algorithms to be run in parallel to obtain appropriate results for the complete torque-speed curves. Therefore, this section illustrates the effect of variation in geometric parameters of the claw-poles on the performance of the machine in the complete operational speed range of 600 rpm to 18,000 rpm and hence provides information that geometry optimization could only be concentrated in the constant torque region and not for the complete speed range. The different geometric parameters utilized for the study are claw core outer diameter, claw inside radius, claw side plate thickness and claw undercut angle. These parameters are varied within a specific range of minimum and maximum, taking the manufacturing and production design into consideration. It has been observed that there is a significant variation in torque during low speed

operation with the alteration in the above stated geometric parameters of the claw-poles. Fig. 3.12 provides the details of various claw-pole geometry parameters utilized in the study i.e. claw core outer radius, claw inside radius, claw side plate thickness and claw undercut angle.

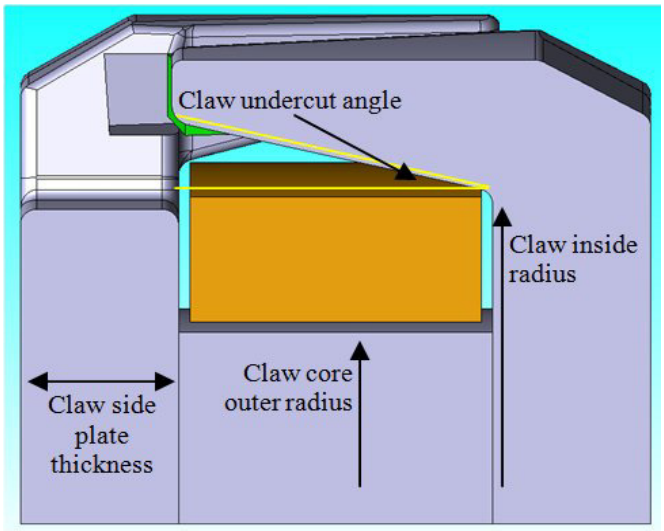


Fig. 3.12 Various geometric parameters of the claw-pole used for the study

The study in this section is mainly concentrated on the motoring mode of the 48 V mild-hybrid automotive application. As the main functions of integrated belt motor-generator are (a) to start and boost the ICE by running as inverter driven motor and (b) generating electric power during generator mode by controlled rectification through the inverter; therefore, the low speed operation during motoring mode is important as the machine needs to provide an adequate starting torque to crank the ICE during initial starting. Along with the importance of low speed operation, there is also a need to evaluate the performance of the machine in constant power region, to verify the machine's capability to deliver sufficient power at higher speeds. The design study for peak output power of the machine in motoring mode has been carried out for the entire speed range to obtain torque vs. speed and power vs. speed curves. Therefore, the performance analysis is carried out for the following two investigations: (i) at low speed operation of 600 rpm and (ii) at complete speed range from 600 rpm to 18,000 rpm.

One of the major challenges in automotive applications is having minimum size and weight of the machine albeit with improved or increased performance. This makes it necessary to have manufacturing and production related design into consideration during parameterization and optimization of the machine. Hence, geometric parameters of the claw-poles are varied within a specific range of minimum and maximum, i.e. claw core outer radius is varied from 24 mm to 33 mm, claw inside radius is varied from 37 mm to 45 mm, claw side plate thickness is varied from 11 mm to 19 mm & claw undercut angle is varied from 10° to 18°. In the below study, when one geometric parameter is varied, the other geometric parameters are kept constant as the base design values.

### 3.3.1 At Low Speed Operation (600 rpm)

Torque at low speed of 600 rpm is evaluated for all the geometric parameter variations, which are as below:

#### 3.3.1.1 Claw core outer radius

The claw core outer radius is varied from 24 mm to 33 mm, thereby modifying claw core area and rotor winding area. With the increase in claw core outer radius, there is reduction in rotor winding area. The number of turns of the rotor winding has to be suitably designed so as to maintain approximately constant current density in the rotor winding while also maintaining about 80% of the rotor winding slot fill factor. As a result, in this case the number of turns of the rotor winding is varied so as to maintain approximately 11.6 A/mm$^2$ as the current density in the rotor winding.

Fig. 3.13 shows the flux density plot of the machine with claw core outer radius at 24 mm and 33 mm respectively. It is observed that the claw core is highly saturated at 24 mm as compared to 33 mm with the same maximum scale of 2.2 T for the flux density value. Fig. 3.14 illustrates the variation of torque with

change in claw core outer radius, and it can be observed that the torque increases initially from 24 mm to 30 mm radius and then decreases rapidly till 33 mm.

The initial increase of torque is mainly due to reduction of claw core saturation till 30 mm and there after the claw core is totally unsaturated. However, the effective ampere-turns in rotor winding are reduced due to less availability of rotor winding area; in turn less amount of flux generation is possible through the claw core.

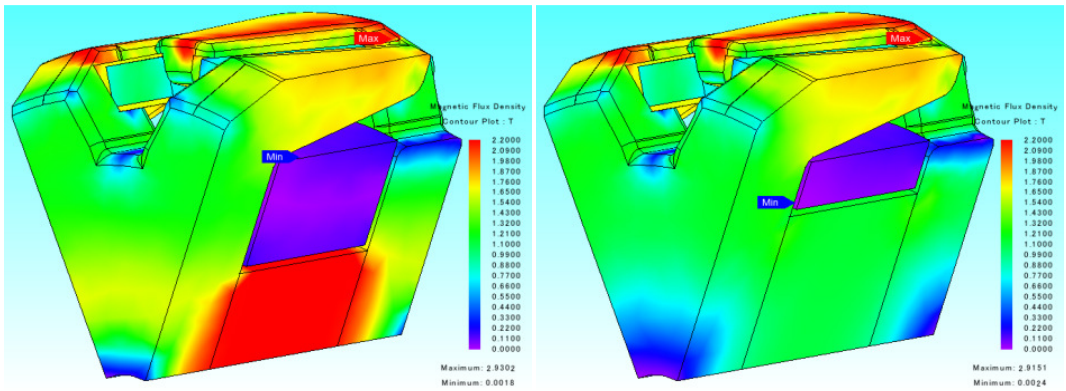


Fig. 3.13 Flux density plot of the machine with 24 mm and 33 mm as the claw core outer radius respectively

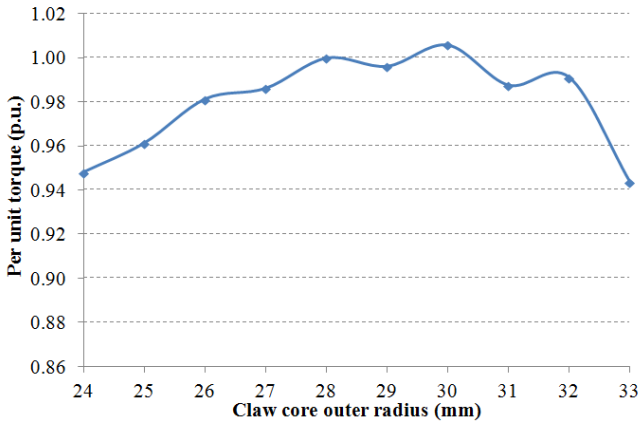


Fig. 3.14 Variation of torque with change in claw core outer radius

### 3.3.1.2 Claw inside radius

The claw inside radius is varied from 37 mm to 45 mm, therefore modifying the rotor winding area. With the increase in claw inside radius, there is an increment in rotor winding area. The number of turns of rotor winding has to be

appropriately designed in the same way as discussed in the previous section 3.3.1.1. In this study also the current density in the rotor winding is maintained at approximately 11.6 A/mm$^2$.

Fig. 3.15 shows the flux density plot of the machine with claw inside radius at 37 mm and 45 mm respectively. It is observed that the claw core saturation changes slightly from 37 mm to 45 mm as compared to the saturation on the claw fingers which increases drastically from 37 mm to 45 mm for the same maximum scale of 2.2 T of flux density value. Fig. 3.16 illustrates the variation of torque with change in claw inside radius, and it can be observed that the torque increases from 37 mm to 42 mm and then decreases till 45 mm. The initial increase of torque is mainly due to unsaturated claw fingers till 42 mm and thereafter they are totally saturated in spite of increase in the effective ampere-turns in rotor winding, therefore, flux increment in the air gap is restricted due to saturation of claw fingers.

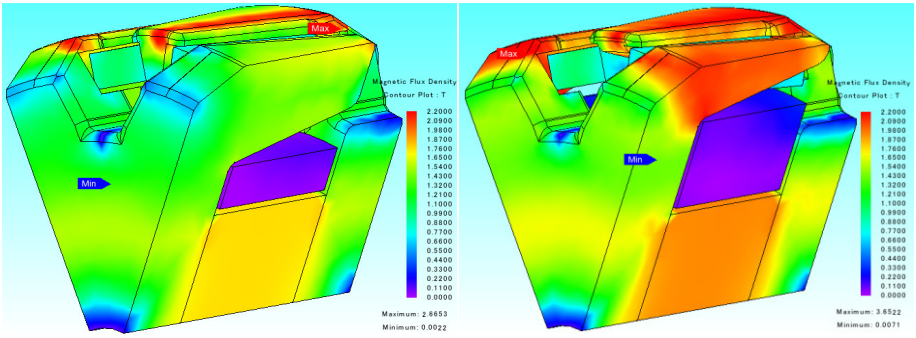


Fig. 3.15 Flux density plot of the machine with 37 mm and 45 mm as the claw inside radius respectively

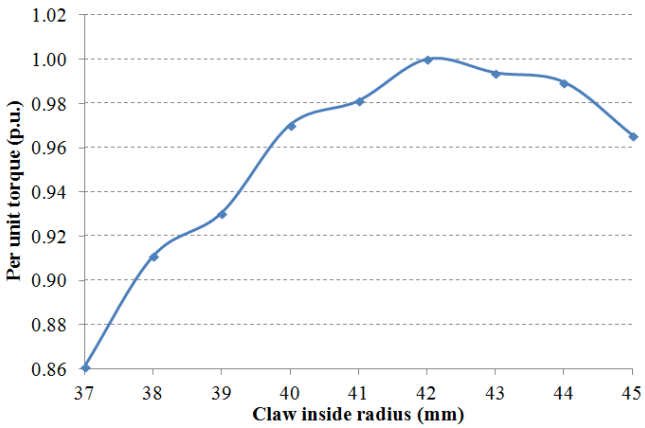


Fig. 3.16 Variation of torque with change in claw inside radius

### 3.3.1.3 Claw side plate thickness

The claw side plate thickness is varied from 11 mm to 19 mm, hence modifying the side plate area and not altering the rotor winding area. Fig. 3.17 shows the flux density plot of the machine with claw side plate thickness at 11 mm and 19 mm respectively. It is observed that the claw side plates are less saturated at 11 mm thickness as compared to at 19 mm thickness where they are totally unsaturated. It is also observed that the claw core is unsaturated at 11 mm thickness and it gets saturated at 19 mm thickness. Fig. 3.18 illustrates the variation of torque with change in claw side plate thickness, and it can be observed that the torque increases from 11 mm to 19 mm thickness. The gradient of increment is more from 11 mm till 14 mm thickness in contrast to thickness from 14 mm till 19 mm and this is due to the start of saturation of claw core with the increase in claw side plate thickness.

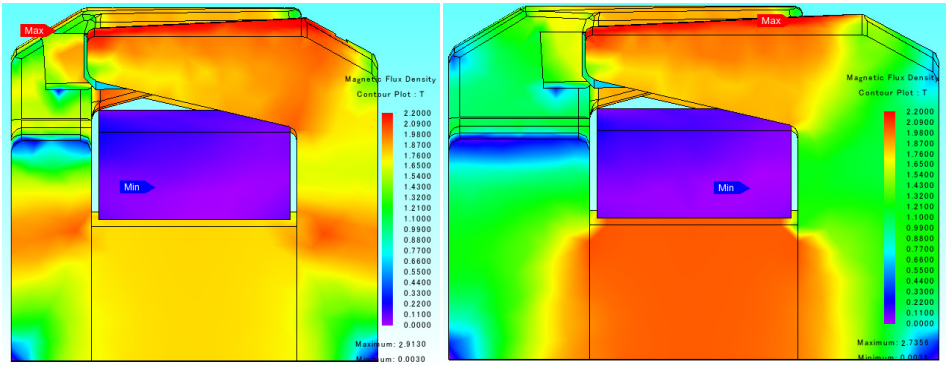


Fig. 3.17 Flux density plot of the machine with 11 mm and 19 mm as the claw side plate thickness respectively

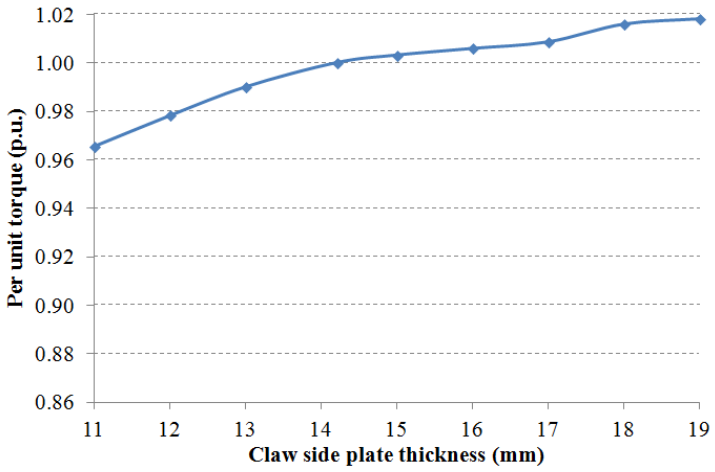


Fig.3.18 Variation of torque with change in claw side plate thickness

### 3.3.1.4 Claw undercut angle

The claw undercut angle is varied from 10° to 18°, hence modifying the claw finger area and not altering the rotor winding area. Fig. 3.19 shows the flux density plot of the machine with claw undercut angle at 10° and 18° respectively and it is observed that there is small deviation in the flux density level of claw core area as well as in claw finger area. Fig. 3.20 illustrates the variation of torque with change in claw undercut angle and it can be observed that there is only slight modification in torque from 10° to 18°, and it is mainly due to the little variation in flux at claw core, claw fingers and air gap areas.

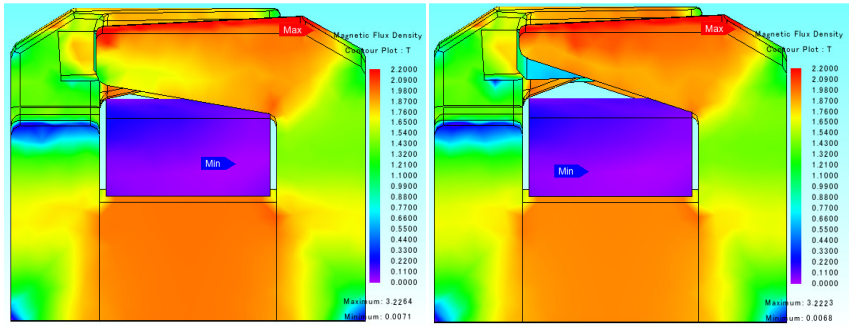


Fig. 3.19 Flux density plot of the machine with 10° and 18° as the claw undercut angle respectively

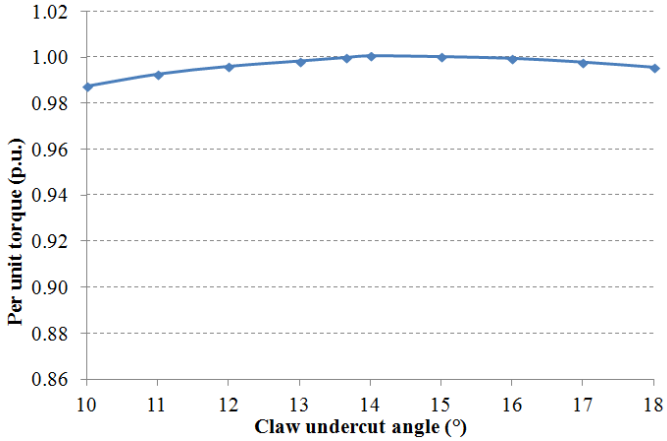


Fig. 3.20 Variation of torque with change in claw undercut angle

Consequently, we can observe from the aforementioned four cases that with the variation of geometric parameters, there is alteration in torque of the machine at low speed. To quantify the above analysis, percentage change in torque is calculated for all the aforesaid cases in the following way:

$$T_{avg} = \frac{T_{max} + T_{min}}{2} \tag{3.16}$$

$$\%T = \frac{(T_{max} - T_{\min}) * 100}{T_{avg}} \tag{3.17}$$

where for each case, $T_{max}$ and $T_{min}$ are the per unit (p.u.) maximum and minimum torque, $T_{avg}$ is average p.u. torque which is calculated by (3.16), and $\%T$ is percentage change in torque which is calculated by (3.17).

Table 3.2 shows $T_{max}$, $T_{min}$, $T_{avg}$ and $\%T$ for all the geometric parameters and it can be observed that for claw core outer radius, claw inside radius, and claw side plate thickness the $\%T$ varies from 5% to 15% which is a significant value.

Table 3.2 $T_{max}$, $T_{min}$, $T_{avg}$ and $\%T$ for all the geometric parameters

| Geometric Parameter | $T_{max}$ (p.u.) | $T_{min}$ (p.u.) | $T_{avg}$ (p.u.) | %T (%) |
|---|---|---|---|---|
| Claw core outer radius | 1.006 | 0.944 | 0.975 | 6.38 |
| Claw inside radius | 1.000 | 0.861 | 0.931 | 14.92 |
| Claw side plate thickness | 1.018 | 0.965 | 0.992 | 5.30 |
| Claw undercut angle | 1.001 | 0.988 | 0.994 | 1.32 |

### 3.3.2 At Complete Speed Range Operation (600 to 18,000 rpm)

To obtain the complete torque vs. speed and power vs. speed curves for the claw-pole machine, it is very important to optimize the $I_d$, $I_q$ and $I_f$, so as to obtain the constant torque and power region without exceeding the voltage limit of 48 V DC. Multi-objective genetic algorithm methodology was adopted for performance evaluation in the complete speed range. The objective functions in this analysis were (i) to maximize the torque and (ii) to limit the voltage at 48 V DC. The FE models of all the geometric variations were realized and performance parameters were evaluated at various speeds, which are as below.

#### 3.3.2.1 Claw core outer radius

Fig. 3.21 illustrates torque vs. speed and power vs. speed curves in p.u. with change in claw core outer radius, respectively. It can be observed that the

modification of torque is higher in constant torque region as compared to constant power region.

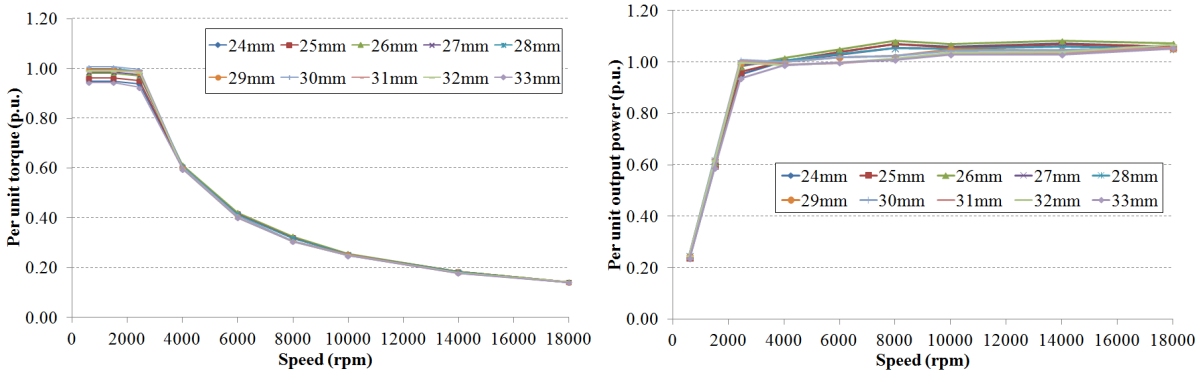


Fig.3.21 Torque vs. speed and power vs. speed with change in claw core outer radius, respectively

### 3.3.2.2 Claw inside radius

Fig. 3.22 illustrates the torque vs. speed and power vs. speed curves in p.u. with change in claw inside radius, respectively. It can also be observed that the change in torque is larger in constant torque region as compared to the constant power region, comparatively similar to previous case of claw core outer radius parameter.

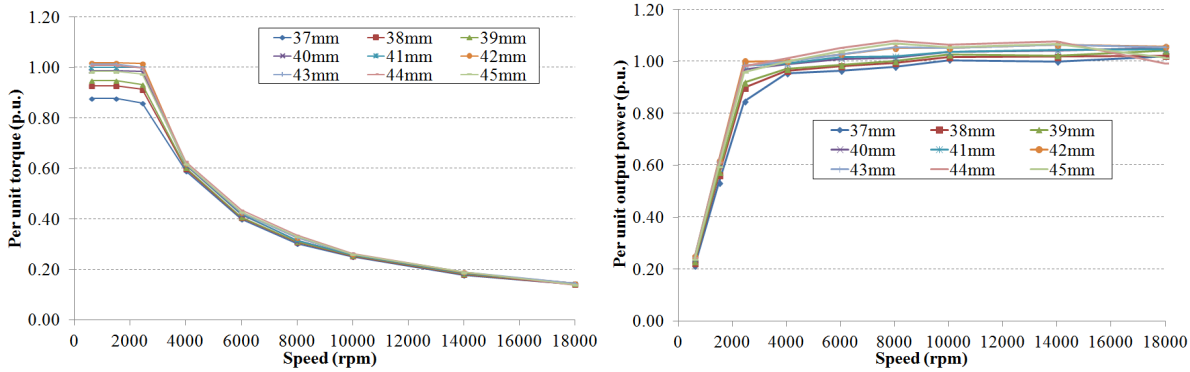


Fig. 3.22 Torque vs. speed and power vs. speed with change in claw inside radius, respectively

### 3.3.2.3 Claw side plate thickness

Fig. 3.23 illustrates the torque vs. speed and power vs. speed curves in p.u. with change in claw side plate thickness, respectively. It can again be observed that

the variation of torque is greater in constant torque region as compared to the constant power region, rather similar to previous two cases of claw core outer radius and claw inside radius parameters.

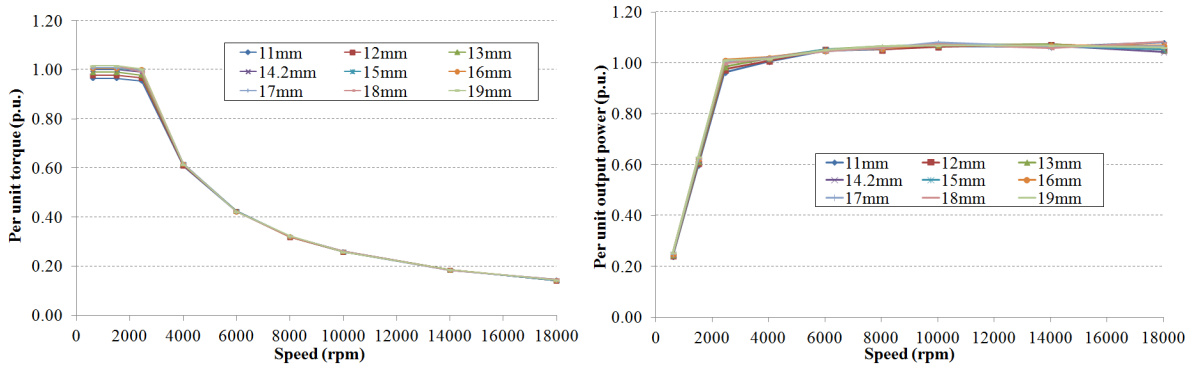


Fig. 3.23 Torque vs. speed and power vs. speed with change in claw side plate thickness, respectively

### 3.3.2.4 Claw undercut angle

Fig. 3.24 illustrates the torque vs. speed and power vs. speed curves in p.u. with change in claw undercut angle, respectively. It can be observed that in both the constant torque and constant power region there is almost no alteration in torque and power for the entire speed range.

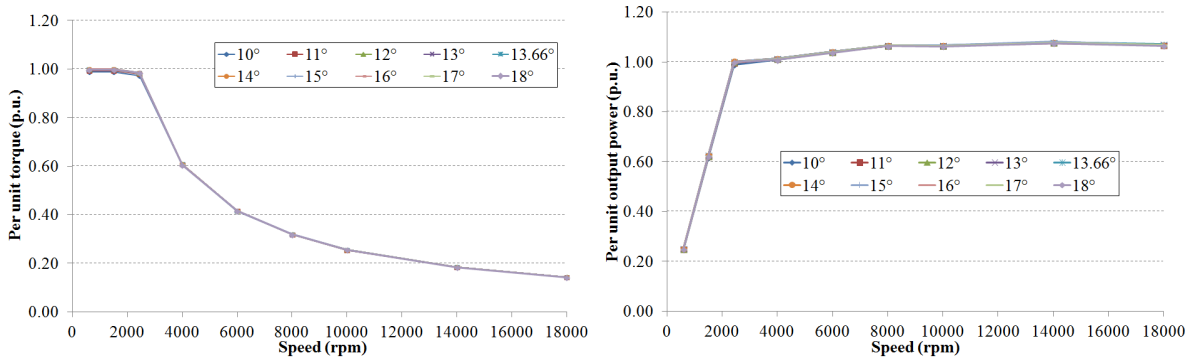


Fig. 3.24 Torque vs. speed and power vs. speed with change in claw undercut angle, respectively

As a result we can observe from the above four cases that with variation of above geometric parameters, there is consequent modification of torque in constant torque region, thereby emphasizing that geometry optimization of the claw-pole machine can fully be concentrated in the low speed range, and verification of

performance can be carried out for the complete speed range after optimization convergence.

## 3.4 Design Optimization of the machine

In this section emphasis is set on the design optimization of the claw-pole machine by 3-D numerical analysis. As observed in the previous section that the performance variation is more in the constant torque region as compared to constant power region with geometry parameter variations; the optimization will be carried out only to maximize the torque at low speed. Final verification for complete torque vs. speed envelope will be computed after the optimization convergence. Various optimization algorithms are utilized nowadays for design optimization of electrical machines viz. genetic algorithm, quadratic surface response, non-dominated sorting genetic algorithm (NSGA), direct search, particle swarm and many others. In this study genetic algorithm is used for the optimization. The genetic algorithm is a method for solving both constrained and unconstrained optimization problems that are based on natural selection, the process that drives biological evolution. The genetic algorithm repeatedly modifies a population of individual solutions. At each step, the genetic algorithm selects individuals at random from the current population to be parents and uses them to produce the children for the next generation. Over successive generations, the population "evolves" toward an optimal solution [63].

### 3.4.1 Problem definition and optimization methodology

As the main problem definition of this thesis work is reuse and recycle of PMs, hence optimization is this section is only concentrated in the rotor parameters. The stator geometry is unaltered and optimization for complete machine is considered for future work. The various geometry parameters varied in the optimization are depicted in Fig. 3.25, viz. claw core outer radius, claw inside

radius, length of the claw, claw side plate thickness, claw top step (pole pitch), magnet width, magnet height and magnet length.

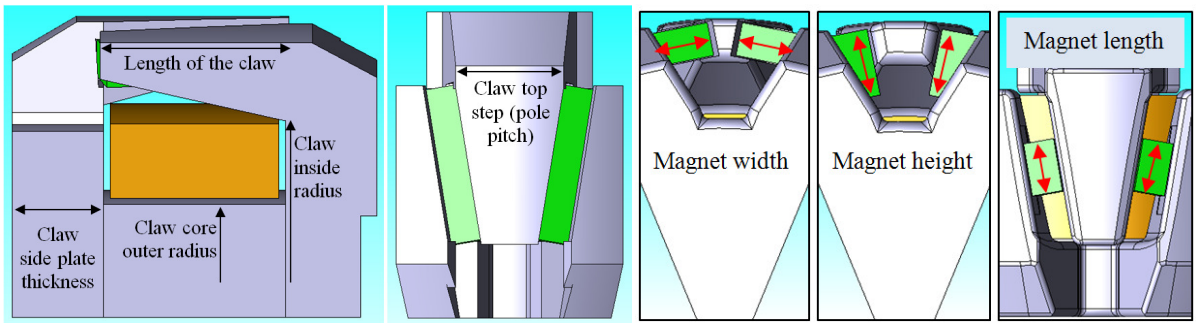


Fig. 3.25 Various parameters utilized for the optimization

Few salient points considered for the optimization are as follows:

- ✓ Prototype to be made with virgin magnets and look into the possibility of utilizing recycled magnets.
- ✓ Stator geometry unchanged. Overall dimensions unchanged.
- ✓ Temperature of stator winding, magnet and rotor winding @ 120°C.
- ✓ Number of turns in rotor DC coil varied according to coil fill factor.

Fig. 3.26 depicts the optimization methodology adopted to obtain the most favorable design. A large set of geometry parameter ranges are used and design of experiments (DOE) is employed to obtain reduced ranges to be utilized for the optimization. Genetic algorithm is utilized with a defined objective function and constraints to attain various results for a number of iterations. In the end best design in terms of performance and cost is selected for the final analysis.

### 3.4.2 Optimization to maximize torque by magnet weight

In this optimization methodology the main focus is given on the average torque at low speed and the magnet volume. It has been observed in the research work in Appendix A2, that with the increase in magnet weight there is an augmentation in torque, but this rise is not linear as compared to some PM based machines. Hence, along with certain claw dimensional parameters, PM dimensions are also varied so as to observe the change in average torque of the machine. Due to high

production volumes of this type of machine; even small amount of cost reduction builds up into huge amount of cost savings in total revenues.

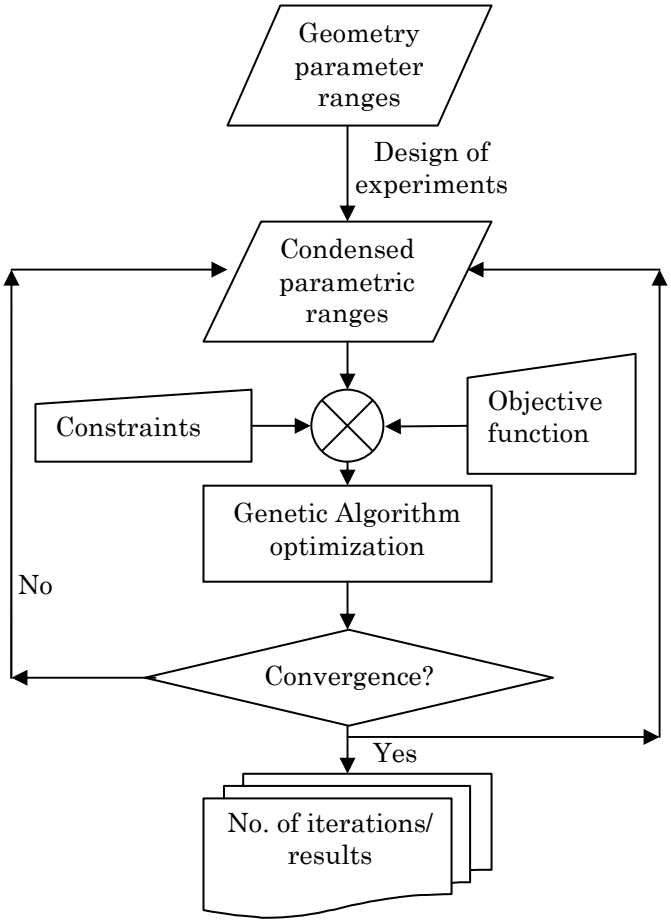


Fig. 3.26 Flowchart for optimization methodology

The objective function is:

- To maximize the average torque by magnet weight

The constraints are:

- DC voltage limit ≤ 48 V
- Rotor DC coil fill factor ≤ 75 %
- Magnet weight < 240 g

The fixed parameters are:

- Speed = 600 rpm
- Stator current $I_s$ = 230 $A_{rms}$

Fig. 3.27 (a) and Fig. 3.27 (b) show respectively the evolution of per unit torque and the evolution of magnet weight in the process of optimization.

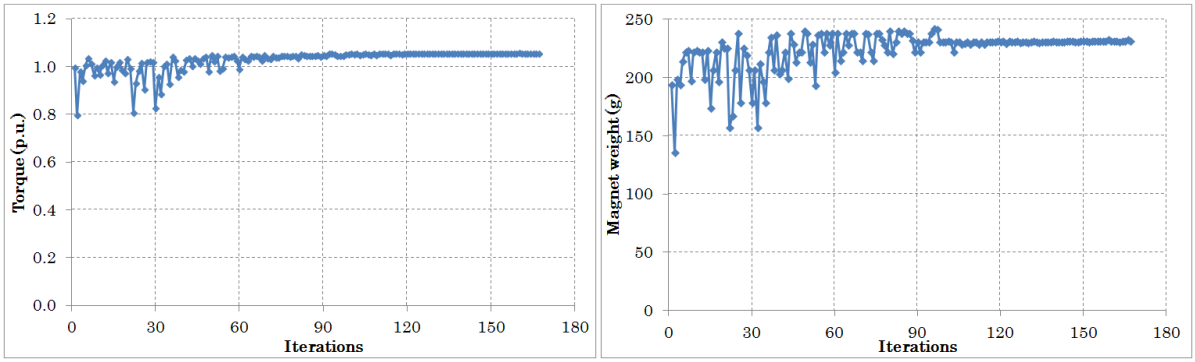


(a) (b)

Fig. 3.27 Evolution of torque (p.u.) and magnet weight in the process of optimization

Similarly, Fig. 3.28 (a) shows the evolution of torque/magnet weight and Fig. 3.27 (b) shows the evolution of rotor number of turns (p.u.) in the process of optimization.

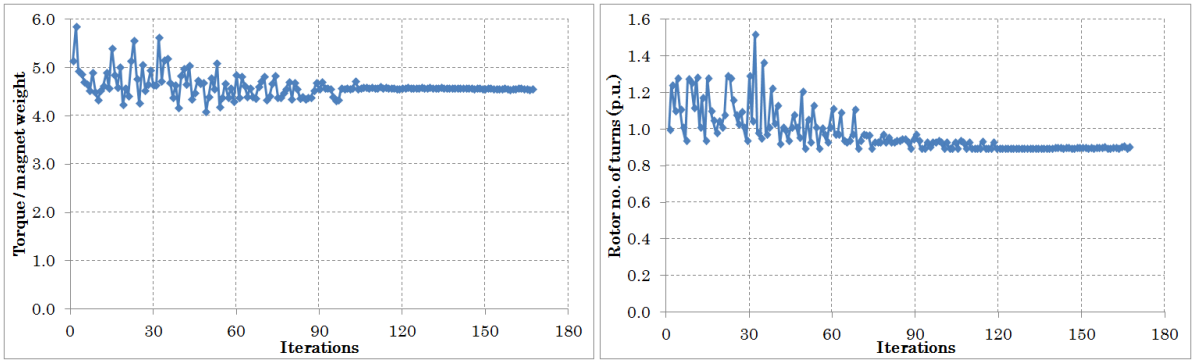


(a) (b)

Fig. 3.28 Evolution of torque/magnet weight and rotor number of turns (p.u.) in the process of optimization

It can be observed from Fig. 3.27 that, the torque (p.u.) has increased during the final iterations, but the magnet weight has also increased for the corresponding duration. So, it is important to observe the torque/magnet weight. It can be observed from Fig. 3.28 (a), that the torque/magnet weight becomes constant after iteration no. 100 and so on. But it is also important to observe the torque

(p.u.) and torque/magnet weight simultaneously, as at some cases the torque/magnet weight could be higher, but the actual torque could be much lower than base torque. Similarly, as the claw dimensions are changing in the optimization process, the number of turns in the rotor also change accordingly so as to maintain the same fill factor during the complete optimization, and this can be observed from Fig. 3.28 (b).

After a careful selection of certain designs depending upon torque, magnet weight, claw-pole dimensions, manufacturability and design experience; selected designs are shown in Table 3.3. It gives a comparison w. r. t. torque and magnet weight. It can be observed that % difference in torque (% diff. T), % difference in magnet weight (% diff. mag. wt.) and torque/magnet weight (T/mag_wt) are the important factors to decide the final design for prototype fabrication. Case 2 and case 4 have the same % diff. T but with opposite polarities. Case 2 has 2.54 % increment in torque but also 3.07 % increase in magnet weight. Whereas Case 4 has 2.54 % decrease in torque however 16.40 % decrement in magnet weight. This escalates into cost savings as magnet material prices are more expensive as compared to iron and copper. Therefore, next step would be to compare Case 2 and Case 4 along with the base design for the complete torque-speed envelope, so as to have a final confirmation of the performance in field weakening region.

Table 3.3 Design comparisons w.r.t. torque and magnet weight

| Case | Torque (p.u.) | Magnet weight (g) | % diff. T | % diff. mag. wt. | T/mag_wt |
|---|---|---|---|---|---|
| **Base** | 1.00 | 194 | 0.00 | 0.00 | 5.15 |
| **1** | 1.05 | 220 | 4.74 | 13.45 | 4.75 |
| **2** | 1.03 | 200 | 2.54 | 3.07 | 5.12 |
| **3** | 0.98 | 172 | -2.11 | -11.70 | 5.71 |
| **4** | 0.97 | 162 | -2.54 | -16.40 | 6.00 |
| **5** | 0.97 | 159 | -2.95 | -18.02 | 6.09 |

Fig. 3.29 depicts the torque-speed comparison of the base design, Case 4 and Case 2 designs. It can be observed that the field weakening region is not affected

much due to DC field current control and hence it confirms that utilizing Case 4 design for final prototype development is a good compromise between torque and magnet weight. It also provides high T/mag_wt and less reduction in constant torque region performance.

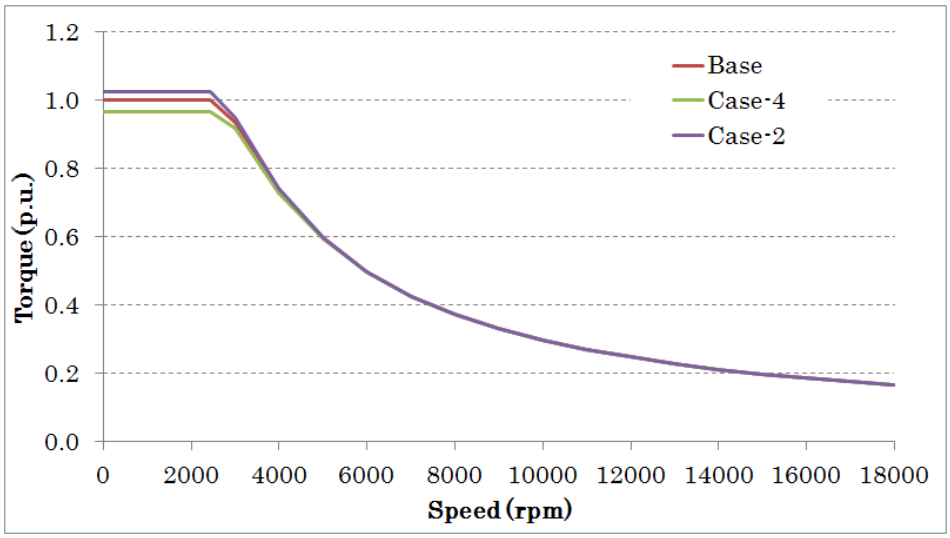


Fig. 3.29 Torque-speed comparison of the base, Case 4 and Case 2 designs

## 3.5 Performance Evaluation and Efficiency Mapping for Motor and Generator mode

After the design optimization of the machine it is important to obtain the performance results in the complete torque vs. speed envelope. Efficiency at rated or part load points provides only a certain amount of information related to machine performance. Hence, efficiency or loss map presents a better understanding of the machine performance in the complete torque-speed curve. For this reason in this section a methodology to evaluate the torque vs. speed curve along with the efficiency map in the motor and generator mode is presented. Fig. 3.30 shows the methodology to obtain the performance curves of the machine and in turn to get the efficiency map.

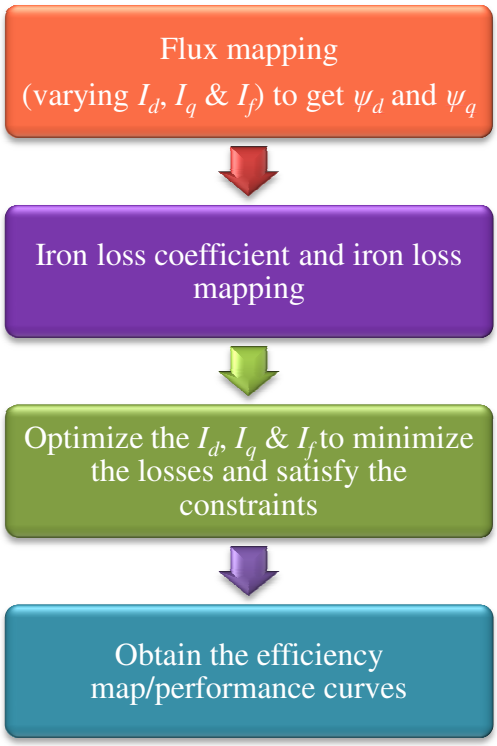


Fig. 3.30 Methodology to obtain the performance curves of the machine

### 3.5.1 Flux and iron loss mapping

Static FE analysis using JMAG® is utilized to get the flux map for different values of $I_d$, $I_q$ and $I_f$ as explained in Section 3.2.2. Fig. 3.8 (a) depicts the $I_d$ vs. $I_q$ vs. $\psi_d$ matrix and Fig. 3.8 (b) depicts $I_d$ vs. $I_q$ vs. $\psi_q$ matrix for $I_f$ = 10A. It can be observed from the above figures that the flux matrix is evaluated for coarse values of $I_d$, $I_q$ and $I_f$. The above figures shown are for only one value of $I_f$, but the actual flux matrix contains all values of flux linkages from 0 A to 10 A of $I_f$. Subsequently, interpolation method is used to obtain the exact values of flux linkages for any value of $I_d$, $I_q$ and $I_f$, hence reducing the time for generation of finer flux matrix using FE analysis only.

The next step is to evaluate the iron loss coefficients and integrate the same into iron loss mapping. The iron loss equation for electrical machine is used as per Eq. 3.15 detailed in section 3.2.2. 3-D time stepping motion FE analysis of the claw-

pole machine is carried out for three random operating points of the machine and iron losses at these points are recorded. The flux density values at specific points in the machine are also recorded for the three operating points. Using the above three values of $P_i$, $B_m$, $B$ and $f$; optimization algorithm is utilized to fit $K_e$, $K_h$ and $\alpha$ for these values and to obtain the three iron loss coefficients. Using the above iron loss coefficients, iron loss mapping can be obtained for any other values of $B$ and $f$ of the machine. The $B_m$ and $B$ values from static FE analysis are used to generate the flux density wave-shape by utilizing hybrid electromagnetic analysis model as described in [64], Chapter 3.

### 3.5.2 Optimization to obtain performance curve/efficiency map for minimum losses

The most important step is the optimization of $I_d$, $I_q$ and $I_f$ to minimize the total losses and satisfy the constraints. For this purpose, optimization algorithm *fmincon* of MATLAB® is utilized [63].

The objective function being:

- To minimize the total losses (copper and iron losses)

The constraint function being:

- DC voltage limit ≤ 48 V
- Stator current $I_s \leq 230$ $A_{rms}$

The optimization algorithm is setup to evaluate the objective functions and satisfy the constraint function for the entire torque vs. speed envelope. After the successful convergence of the optimization algorithm different performance curves can be obtained like efficiency map, loss map, voltage map, current map for the entire torque vs. speed envelope. Fig. 3.31 illustrates the various current maps i.e. $I_d$, $I_q$, $I_f$ and $I_{s\text{-}rms}$ as a function of torque and speed of the machine.

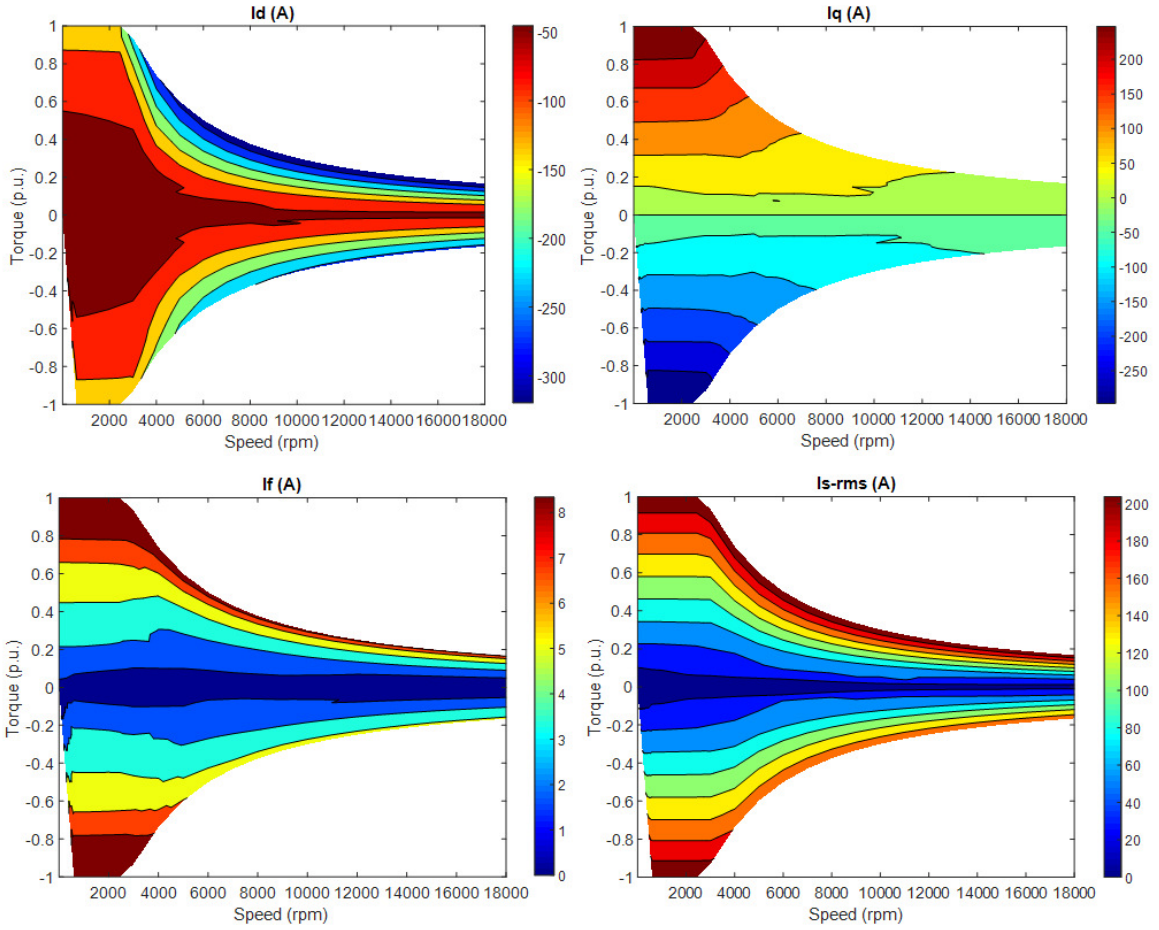


Fig. 3.31 $I_d$, $I_q$, $I_f$ and $I_{s\text{-}rms}$ map as a function of torque and speed

Similarly, Fig. 3.32 shows the copper and iron losses of the machine as a function of torque and speed, and Fig. 3.33 depicts the efficiency map of the machine.

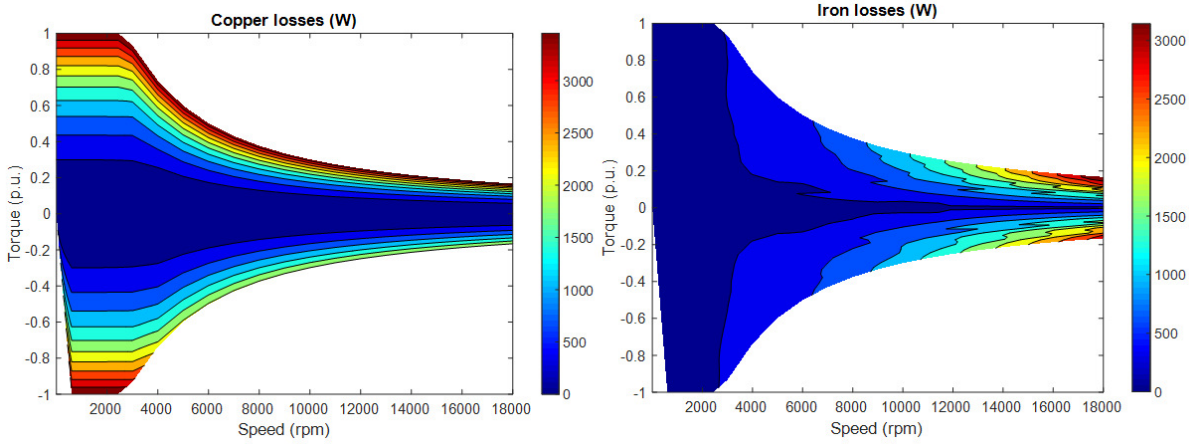


Fig. 3.32 Copper and iron loss map as a function of torque and speed

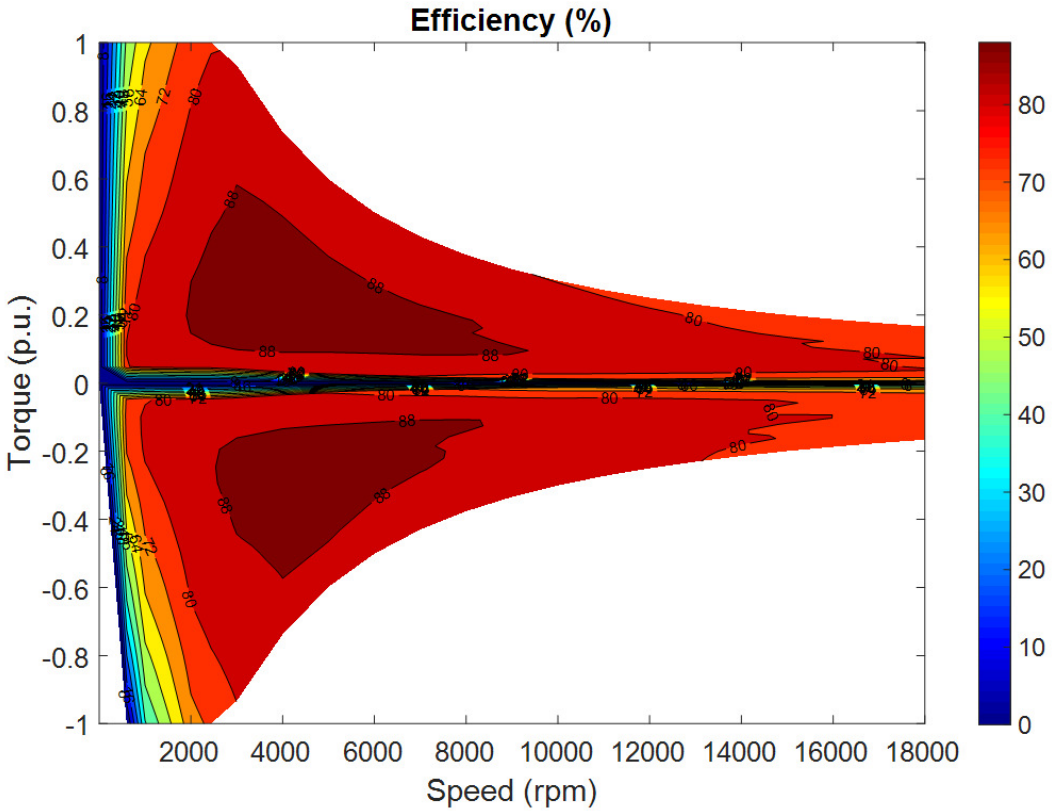


Fig. 3.33 Efficiency map as a function of torque and speed

It can be observed that the stator rms current $I_{s\text{-}rms}$ and field current $I_f$ are maximum near the highest torque and then start reducing as the torque decreases. The $I_{s\text{-}rms}$ is distributed accordingly between $I_d$ and $I_q$, so as to achieve the desired torque and maintain the DC voltage below 48 V. The copper losses dominate during the constant torque region at higher level of torques, whereas the iron losses dominate at high speeds. It can be observed that the peak efficiency of the machine is around 88 % for certain operating region, and can be as low as 50-60 % for certain operating region of peak performance for short period of time.

The cartographic representation of the performance results provides detailed insight of the operating points of the machine at various loads. However, the above mapping is based upon a particular type of optimization algorithm, and various other methods can also be evaluated to obtain different results. In this study, pulse width modulation (PWM) technique has been adopted in the entire mapping region. Another optimization technique could be to utilize PWM

strategy from low speeds to some medium speeds and then switching to full wave technique till maximum speeds. In this method, it can be observed that there is a torque increase from the medium speeds as the voltage limit at the winding terminals is increased as compared to PWM technique. Similarly, the optimization methodology can be used for minimization of losses in certain operating points where the machine operates most of the time. For this technique, more information is needed regarding the ICE operating points and a complete system simulation could help in retrieving this data. This would result in more optimized control technique as the efficiency optimization is considered only in the most important regions and not in the entire torque-speed envelope. The above methodology can also be improved by incorporating analytical thermal model so as to obtain the continuous performance curve as per the machine and inverter cooling topology.

Incorporation of electromagnetic FE simulations along with surface response mapping effectively provides good cartographic results in reasonably quick time. As a result, electrical machine design and development landscape can be build up to generate designs from initial analytical and FE models, and finally obtain performance maps as per the specification requirements. This in turn can help in obtaining various design results to fulfil different customer prerequisites and provide faster solutions for their applications.

## 3.6 Conclusion

Therefore, automation of the geometry modeling was achieved by utilizing variables and associated equations in the geometry editor of the numerical analysis software. Genetic algorithm was utilized for the design optimization of the machine so as to achieve maximum torque to magnet weight ratio. Various claw parameters and magnet dimensions were varied to achieve the above objective. It was observed that the new optimized claw-pole and magnets provide fairly the same torque as the original machine with at least 16 % reduction in magnet weight.

# Chapter 4

# Reuse and Recycling: In the context of Claw-pole Machine

## 4.1 Reuse/Recycle methodology for Claw-pole machine

The reuse and recycle of permanent magnets in electrical machines is considered imperative now due to various reasons detailed in Chapter-1 and Chapter-2, viz. supply and demand, price fluctuations, environmental factors and many others. Various recycling routes have been detailed so as to recover the REEs from waste electronics and electrical equipments and automotive applications. Lot of technological processes viz. physical processing and separation, direct alloy production, metallurgical extraction and recovery are also detailed. Easy assembly & disassembly is also considered as a significant step in e-machines used for automotive applications, as it helps in trouble-free recovery of PMs.

In this chapter, emphases are provided on the reuse and recycle methodology adopted for the PM based claw-pole machine. The main motivation to use this machine for reuse and recyclability are:

(i) At present approximately, 95 million cars per year are manufactured with this machine type used as a generator or motor-generator. Hence, cumulatively large no. of magnets utilized that can be recovered after EoL.

(ii) Project DEMETER's objective is to recover > 30 g of magnets, and this machine utilizes around 160-200 g magnets.

(iii) Presently, no reuse or recycle of PMs for e-machines is being worked up extensively.

(iv) Three other motor topologies being designed in project DEMETER for reuse and recyclability, hence a global perspective w.r.t. to e-machine designs.

Direct reuse methodology is the first concept developed for the claw-pole machine, so as to have unsophisticated recovery of PMs. The second concept is

the utilization of magnets produced by direct recycling in the claw-pole machine design. To evaluate the impact of reuse and recyclability, a novel recycle index is also developed depending upon easy assembly and disassembly, and also taking energy consumption of the machine for particular drive cycle into account.

### 4.1.1 Concept of Direct Reuse of magnets in the machine

Direct reuse is defined as easy assembly and disassembly of permanent magnets after EoL of the machine and reuse in other applications or reuse as an input material in the manufacturing of new magnets. At present, in the claw-pole machine, the two claw-poles are generally identical in construction related to magnet placement between the inter-claws. The inter-claws have appropriate magnet slits so as to maintain the magnets in the desired position. Fig. 4.1 shows the claw-poles and magnets along with the highlighted appropriate magnet slit at the end of each claw-pole in order to maintain the magnets in the desired position. As a consequence, this arrangement hinders the disassembly of magnets at EoL unless the complete assembly is dismantled using special tools and techniques.

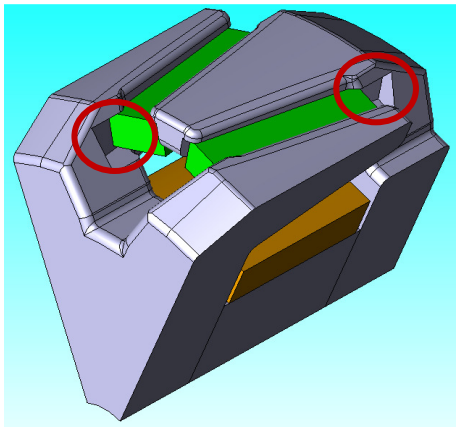

Fig. 4.1 Claw-poles and magnets with the *appropriate magnet slit*

After assembly of the rotor is finished, varnish is applied on the complete rotor assembly i.e. the claw-poles, rotor winding, magnets and shaft. In the present design, varnish is important because it helps in the following issues:

- Vibration issues
- Corrosion issues (magnets are non-coated)

- Thermal issues (to some extent)

There are various varnish removers available in the market according to their removal capabilities and toxic levels. Following is the list of few varnish removers as per extant literature available:

1. **Methylene chloride**
   - Toxic but very quick in removal
2. **Dimethyl sulfoxide**
   - Medium level toxic and moderately quick in removal
3. **Eco-organic solvents like terpenes from pine, citric acid, benzyl alcohol**
   - Less toxic but slow in removal

The Fig. 4.2 illustrates the direct reuse methodology for assembly and disassembly of magnets in claw-pole machine.

The steps for direct reuse methodology are as follows:

During manufacturing assembly:

a) First forged claw-pole with appropriate magnet slit is placed in the manufacturing setup.
b) Magnets are inserted in the desired position of the inter-claw till the end of the appropriate magnet slit.
c) It is proposed in the reuse methodology to have second forged claw-pole with complete magnet slit till the end as seen in Fig. 4.2. Subsequently, the second claw-pole is placed over the first claw-pole and magnets.
d) Varnish is applied to the complete rotor assembly.

At EoL, i.e. during disassembly:

a) Varnish remover is applied on the complete rotor assembly. Depending upon the needs, chemical based or eco-friendly varnish remover can be applied.

b) The rotor is subjected to Curie temperature for 30 seconds so as to demagnetize the magnets before disassembly. This temperature treatment also helps in loosening of the varnish.

c) Push the magnet out through the complete magnet slit.

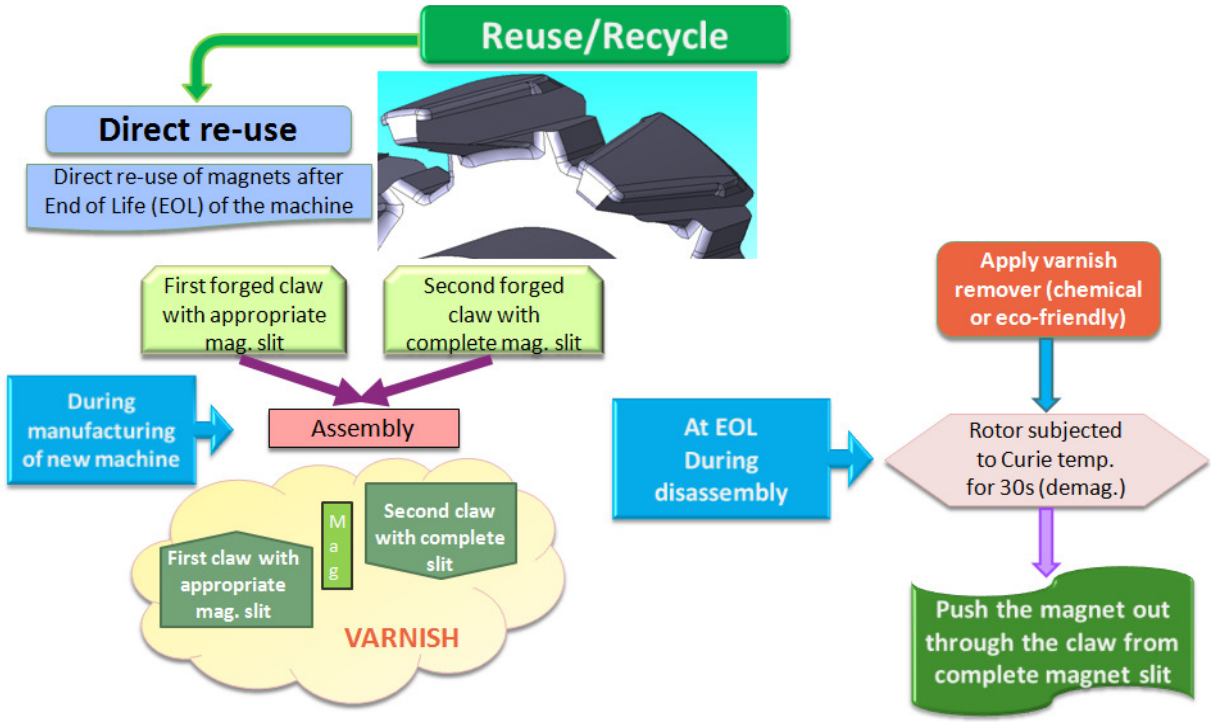


Fig. 4.2 Direct reuse methodology for assembly and disassembly of magnets in claw-pole machine

Therefore, it can be observed that with the above detailed process steps; there is no change in the present assembly process. There is certain change in the rear claw-pole design as the two claw-poles are no more identical, hence needs re-development. In general, both claw-poles are not identical in many other designs also, as there are certain modifications in the chamfers and manufacturing related process. The extra process of disassembly is an added procedure, and needs small investment. But due to large quantities of these machines being produced, the recovery of PMs would be large, and provide recycling benefits. The direct reuse concept provides prominence to directly use the PMs for similar shapes in some other applications depending upon their quality or use the scrap PMs for reprocessing so as to obtain new recycled magnets.

### 4.1.2 Concept of utilizing Direct Recycled magnets in the machine

Direct recycle is defined as utilizing directly recycled permanent magnets in design of new electrical machines developed for automotive applications. Direct recycling of permanent magnets refers to the treatment of scrap magnets as a raw material for the production of new magnets, but using novel techniques such as HD and HDDR processing, chemical treatments, and many more, to give new, ready-to-use, magnetic materials or a new master alloy that can be processed using existing magnet production facilities. Literature has shown that the magnetic properties of recycled magnets may differ by 3% to 20% when compared to that of the original magnetic material used for production of new magnets. Consequently, with the change in magnetic properties, the performance of electrical machine is also altered. For example, decreased magnetic performance of recycled PMs may lead to large variation in machine performance of surface mounted PM radial flux machine, but less variation in machine performance for PM assisted synchronous reluctance machine. This is because the contribution of PMs in magnetic circuit is more in a surface mounted design than in PM assisted synchronous reluctance machine design. Hence, direct recycle methodology for design of electrical machine (claw-pole type) has been proposed in Fig. 4.3.

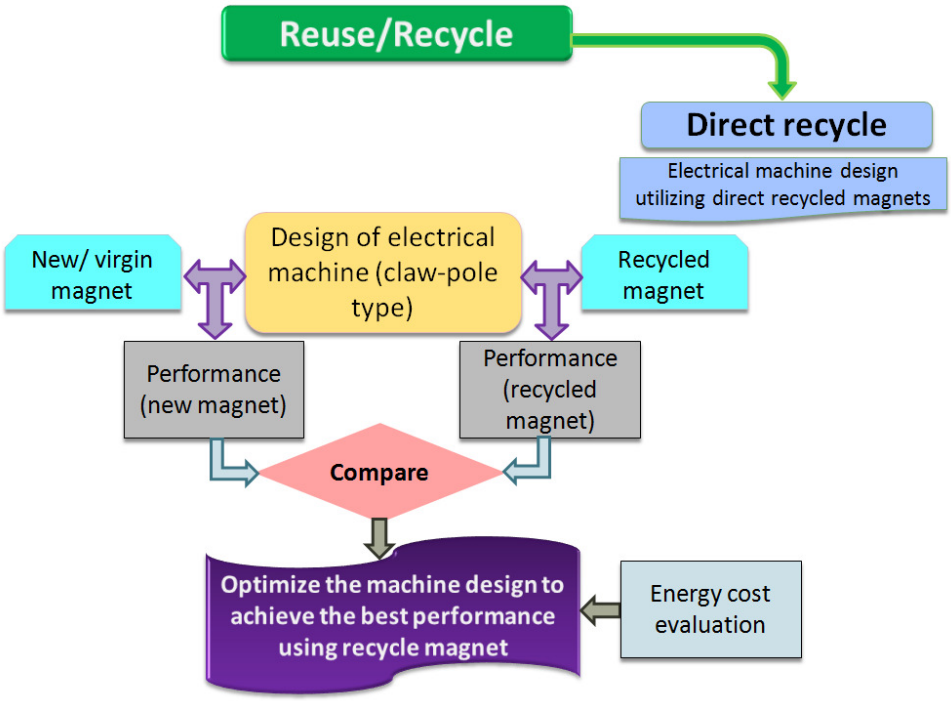


Fig. 4.3 Direct recycle methodology for design of electrical machine (claw-pole type)

The steps for direct recycle methodology are as follows:

a) Existing electrical machine designs utilizing new/virgin permanent magnets are analyzed and the performance of these machines are recorded in a dataset.
b) In the electrical machine design of step 1, recycled magnet material properties are used for analysis and performance parameters are recorded in another dataset.
c) The machine performances with new/virgin magnet and recycled magnets are compared using data analysis.
d) Finally the machine design is optimized so as to achieve the best performance utilizing the recycled magnet properties.
e) Evaluation of energy and fuel consumption to check for economic viability.

## 4.2 Weighted Index of Recycling and Energy concept

Weighted Index of Recycling and Energy (WIRE) concept is a tool that have been developed for analyzing the recycling index of electrical machine. At present there are no techniques or tools to define the reusability or recyclability of electrical machines. In the framework of DEMETER project, one of the tasks was also to develop a recycling index so as to score the different machine designs with respect to their reuse and recycle capabilities. For this reason, in this section a weighted index for recycling has been developed and it is divided into two parts. Fig. 4.4 illustrates these two parts of the WIRE concept. Part-1 defines the recyclability considering standardization and cost of materials, assembly and disassembly. While part-2 considers the energy consumption evaluation of electrical machine over a drive cycle. A weighted index of recycling for part-1 and energy index for part-2 are first developed for a commercially available outer rotor HUB motor. The methodology and tool for this are detailed in the section below. Then the WIRE indexes for the claw-pole machine and the other motors developed in DEMETER project are worked upon by the consortium researchers.

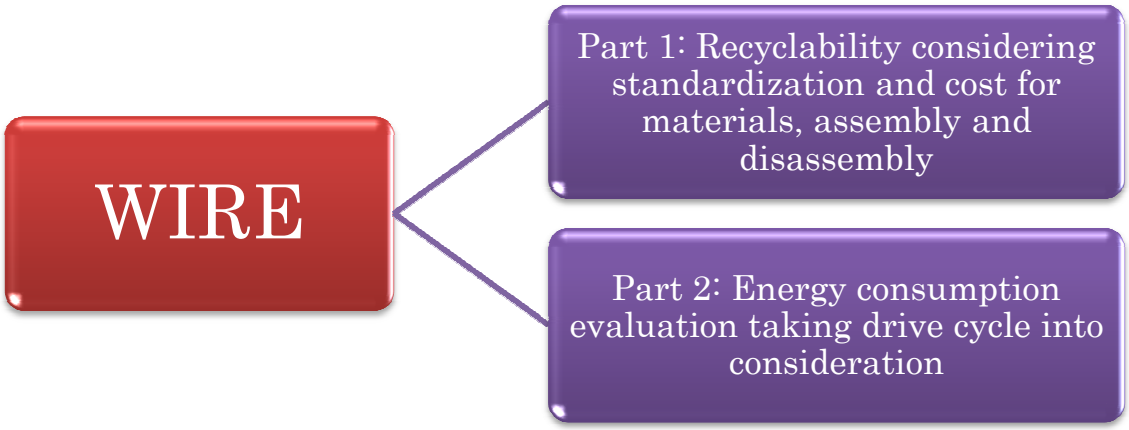


Fig. 4.4 Weighted Index of Recycling and Energy (WIRE) concept

### 4.2.1 Recycle index for standardization and cost taking material, assembly and disassembly into consideration

In this part the recycle index is generated so as to achieve easy assembly and disassembly, as it leads to good reuse and recyclability. The main elements scored are standard and cost for electrical machines materials, assembly and disassembly. Standard is defined as existing or available materials/components/ processes and cost is defined as the price of the materials/components/processes with its impact on recycling. Fig. 4.5 depicts the sample evaluation sheet developed for assessing the scores for various sections. It can be observed in this that the standard and cost category is sub-divided into two scoring patterns i.e. Score (S) and Importance (I). The S depends on its relative scale of 1-5 in respective section while I depend on the materials/process relative criticality in terms of recyclability of materials on the scale of 1-5. The final score is the product of both S and I i.e. (SxI). For evaluation of WIRE it is recommended to have a group of 5-6 people from different fields, involved in design and manufacturing process of the motor. In Fig. 4.5 only the material section is visible and similar sheet is also available for assembly and disassembly, and hence the cumulative score for all the section accounts into the final score of the machine. Although, the assessment largely depends on the mutual agreement of the group formed for evaluation; certain guidelines are also formulated to evaluate different sections and are enlisted in the form of a data-list.

Furthermore, the process/materials in different sections are different depending on the criticality of the material/process.

| Scoring pattern | 0-5 | 1 - Lowest score | 5 - Highest score | |
|---|---|---|---|---|
| | | 1 - Lowest score | 5 - Highest score | 3 = neutral score |

| MOTOR ID | Hub motor for in-wheel application | | | | | | | | | | |
|---|---|---|---|---|---|---|---|---|---|---|---|
| Component/ Parts | | | Standard | | | | Cost | | | | Recyclability SCORE |
| | | Remarks | S | I | SxI | Remarks | S | I | SxI | Remarks | |
| **Materials** | | | | | | | | | | | |
| **- Stator** | | | | | | | | | | | |
| | Lamination S | segmented stator | 5 | 5 | 25 | good for recycle not reuse | 1 | 5 | 5 | | 30 |
| | Copper | SWG 24 | 5 | 5 | 25 | | 2 | 1 | 2 | | 27 |
| **- Rotor** | | | | | | | | | | | 0 |
| | Steel R | MS steel | 5 | 5 | 25 | good for recycle not reuse | 1 | 4 | 4 | | 29 |
| | Magnets | NdFeB-rect shape | 5 | 4 | 20 | Because of shape | 5 | 1 | 5 | Because of coating | 25 |
| **-Shaft** | | | | | | | | | | | 0 |
| | Shaft | Steel | 4 | 5 | 20 | shaft with hole for wires | 1 | 2 | 2 | | 22 |
| **-Endshileds** | | | | | | | | | | | 0 |
| | Drive Side | aluminium die cast | 2 | 5 | 10 | prepare new die | 1 | 2 | 2 | | 12 |
| | Non-Drive side | aluminium die cast | 2 | 5 | 10 | prepare new die | 1 | 2 | 2 | | 12 |
| | | | | 34 | 135 | | | 17 | 22 | | 157 |
| | section score | | | | 79.41% | | | | 25.88% | | |

Fig. 4.5 Sample evaluation sheet for assessing the scores for various sections

The complete methodology explanation is detailed in ref. [65], where the definitions of standard for material, assembly, disassembly and cost for material, assembly and disassembly are defined. Calculation of the recyclability index is also defined as per the weighted indexing principle so as to easily compare different topologies of machines by a single tool. General guidelines for scoring have also been defined for various categories viz. materials for standard, assembly/disassembly for cost, importance of assembly/disassembly process and score for materials. The developed methodology is flexible in adapting for new categories and different guidelines by diverse users. Hence, this provides a new starting tool to design and process engineers to keep recyclability into mind.

#### 4.2.1.1 Recycle index of sample HUB motor

This methodology is now utilized to evaluate a commercially available outer rotor HUB PM motor. The motor was disassembled using standard tools and instruments in a step-by-step process and all the parameters were noted down.

After the disassembly, the team evaluated the machine as per the WIRE assessment sheet for standard and cost with material, assembly and disassembly taken into account. Fig. 4.6 shows the various components and parts of the sample HUB motor along-with the various disassembly steps.

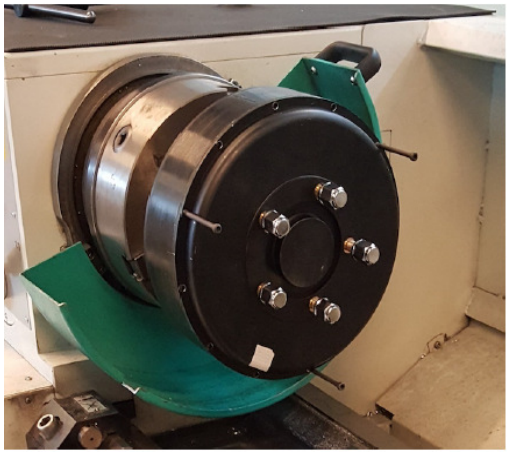

(a) Hub PM Motor

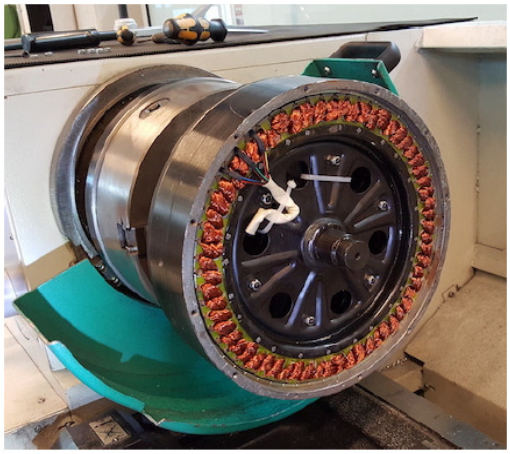

(b) Motor without end shields

(c) Stator with disassembled windings

(d) Rotor with magnets

Fig. 4.6 Sample outer rotor HUB PM motor

The recycling index distribution for standard and cost category of the sample HUB motor is depicted in Fig. 4.7. It can be observed that the material category in the standard section has the highest score due to the usage of standard materials, and assembly category has the lowest score as the assembly of the machine is done so as to avoid recycling. Whereas in cost section the material category is lowest as the materials used in the machine are standard products with less return of the cost value. The disassembly category in the cost section is highest as the machine was comparatively easy to disassemble with standard tools at relatively low cost.

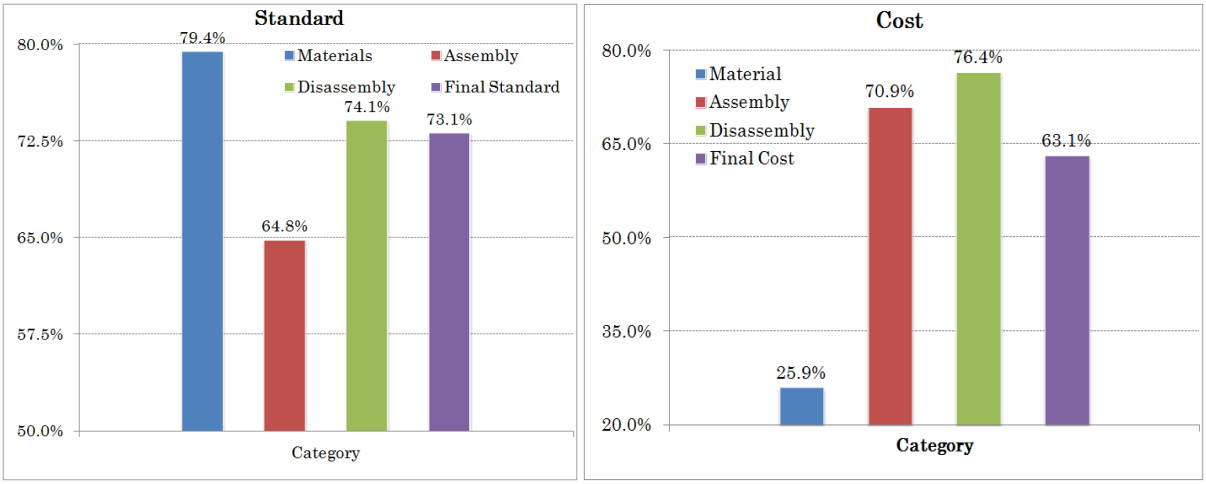


Fig. 4.7 Recycling index distribution for standard & cost category of sample HUB motor

The final score for standard section is 73.1 % and cost section is 63.1 %, which depicts that the machine is developed with standard materials and assembly/disassembly. Whereas, in cost section it is little lower due to low recyclability kept in mind while designing the sample HUB motor.

#### 4.2.1.2 Recycle index of claw-pole machine

Utilizing the above described methodology, the claw-pole machine was also evaluated within the team for all the categories in the evaluation sheet. Fig. 4.8 illustrates the recycling index distribution for standard and cost category of the developed PM based claw-pole machine.

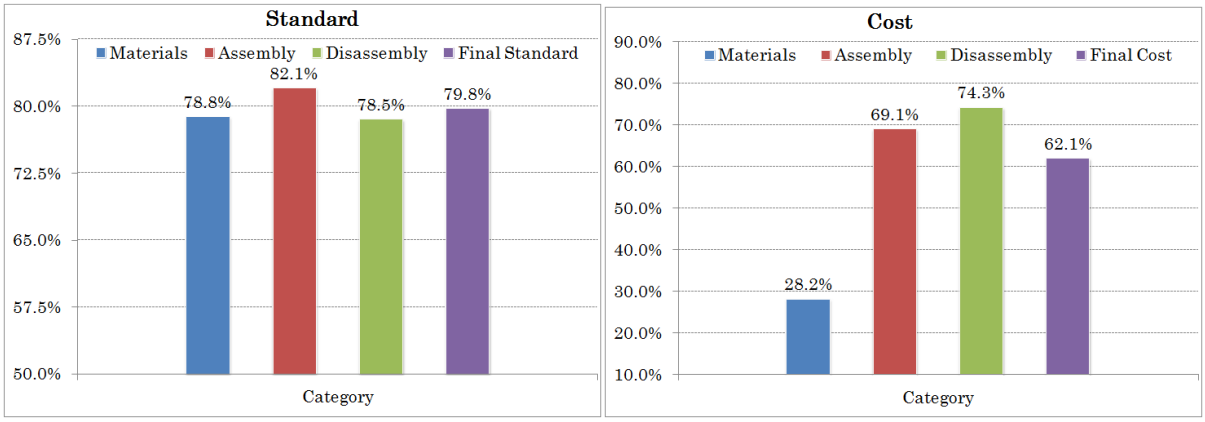


Fig. 4.8 Recycling index distribution for standard & cost category of the developed claw-pole machine

It can be observed that almost all the categories in the standard section are high and above 78 %, which portrays that the machine is quite standard in materials and assembly/disassembly. In the cost section, the material score is low due to standard products with low return value for recyclability for a single machine. But as this machine is developed in high quantities (millions), the amount of return value is much higher when compared to some other machine types. The assembly cost is lower than the disassembly cost in terms of recyclability due to the utilization of automated tools for the assembly of PMs and the claw-poles. But due to the new reuse concept of the claw-poles as described in section 4.1.1, the disassembly cost score is higher as compared to assembly cost score. This corroborates the WIRE index evaluation, as it can be seen that the new claw-pole concept is designed for easy disassembly, hence it is fruitful in recycling of the magnet after EoL. In ref. [65] four different machines of DEMETER project are evaluated using the WIRE sheet and the scores are compared for all the categories providing the authors a good way forward on the developed methodology.

### 4.2.2 Recycle index for energy consumption taking drive cycle into consideration

The second part of evaluating the recycle index is by energy consumption assessment taking drive cycle into account. In this section also the sample PM based HUB motor is used to evaluate the above methodology development. The benchmarking of sample HUB motor is done by disassembly, experimentation and FE analysis. The efficiency map and energy consumption of sample HUB motor with virgin magnets for urban part of New European Driving Cycle (NEDC) i.e. ECE-15 [66] is evaluated. Similarly, machine performance and energy consumption with recycled magnets for the same ECE-15 drive cycle is evaluated. Finally, comparison in energy consumption between virgin magnets and recycled magnets for sample HUB motor is done to obtain the energy cost index.

#### 4.2.2.1 Benchmarking of sample electric vehicle motor

The sample motor is utilized in medium speed electric 2-wheeler or small compact low speed city cars. The DC bus voltage for the sample motor is 72 V, maximum speed of 700 rpm and output power up to 3.5 kW. The motor controller is a standard three-phase power electronic inverter with hall sensor inputs used for position sensing.

*Experimental measurements:*

The motor was assembled on a test bench with high precision torque transducer connected to the shaft. The input power measurements were recorded using an industrial grade power analyzer so as to limit the uncertainties in measurement. Fig. 4.8 (a) shows the experimental test setup utilized for the measurements and performance evaluation. Two machines were assembled back to back and a resistive load was connected to the machine which would operate as a generator and load the test machine. Different resistance values were used with a set of speed variations to get the torque, speed, voltage, output power and input power of the test machine. Fig. 4.9 (b) depicts the experimental torque vs. speed with the corresponding efficiency values.

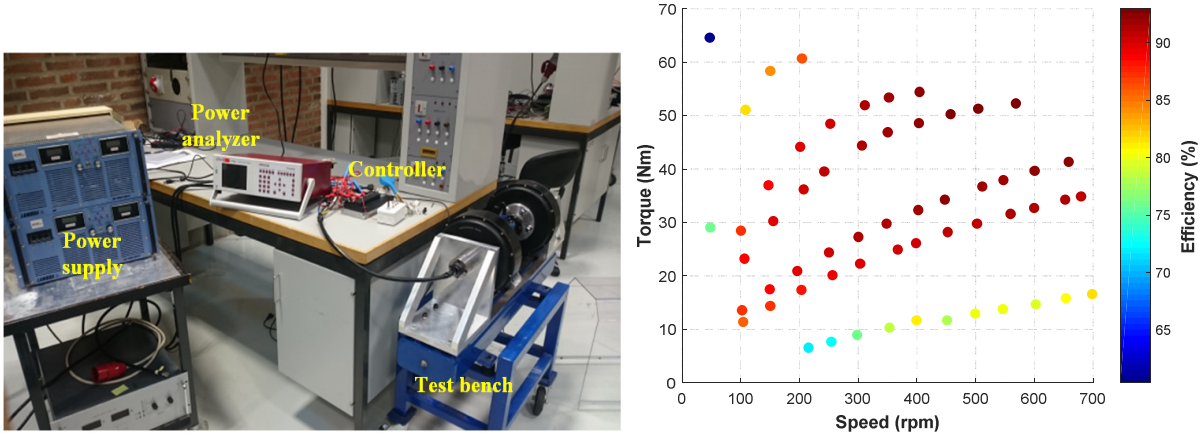


(a) (b)

Fig. 4.9 (a) Experimental test setup for performance evaluation, (b) Experimental torque vs. speed with corresponding efficiency values by virgin magnets

*Disassembly and dimensions:*

The major dimensions, weight and materials were identified by disassembling the machine in a step by step process. Fig. 4.10 shows the disassembled machine

and the magnets. Table 4.1 depicts the main machine dimensions which would be utilized later on for 2-D FE analysis so as to obtain simulated performance of the machine.

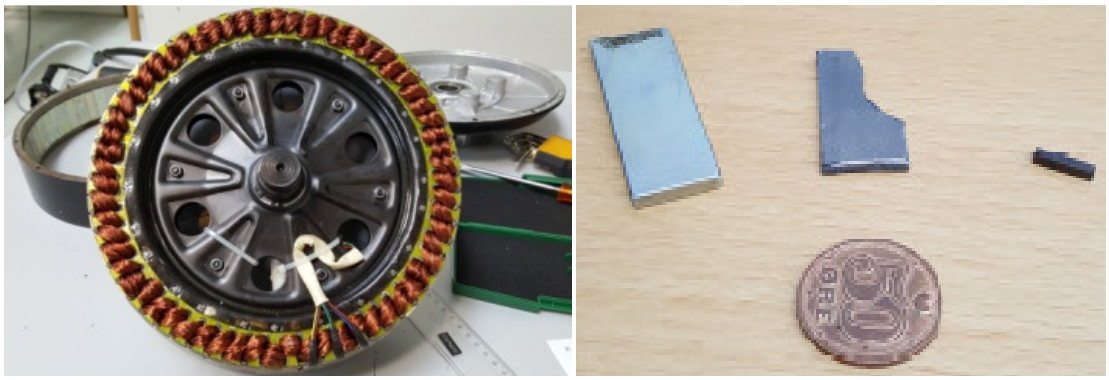

Fig. 4.10 Disassembled machine and permanent magnets

Table 4.1 Main dimension of the sample HUB motor

| Parameters | Value |
|---|---|
| Stack length [mm] | 40 |
| Maximum speed [rpm] | 700 |
| Air-gap length [mm] | 0.6 |
| Magnet axial length [mm] | 40 |
| Magnet thickness [mm] | 3 |
| Magnet width [mm] | 14 |
| Stator outer diameter [mm] | 253 |
| Number of poles | 56 |
| Number of slots | 63 |

The PMs were shaped in appropriate sizes so as to be analyzed for their magnetic properties. They were put to test in Magnetic Property Measurement System (MPMS®) from Quantum Design. It was observed that the magnetization *(M)* of the magnet at zero applied field *(H)* is around 130 emu/g which corresponds to around 1.2 T as $B_r$ at temperature of approximately 300 K (27 °C).

*Finite element analysis & comparison with test results:*

The machine was modelled on commercially available FE analysis software by using the dimensional details obtained in earlier. The magnet properties were utilized from the MPMS® measurements with 1.2 T as the $B_r$ value. The stator lamination was a standard silicon iron soft magnetic material with loss of around 5 W/kg at 1.5 T, 50 Hz. Time stepping 2-D motion analysis was carried out to get

the various performance parameters like back EMF, cogging torque, electromagnetic torque, iron losses, copper losses and winding voltages. Fig. 4.11 (a) shows the 2-D model along with the flux density plot at no-load by FE analysis. The experimental winding current values were fed as an input in the FE analysis at various speed points to get the developed torque and losses of the machine. Finally the input power, output power, voltage and efficiency were evaluated by simulation results. In Fig. 4.11 (b) it can be noticed that the comparison of simulated and experimental results for torque vs. speed with corresponding efficiency values of the machine. It can be observed that the simulated and experimental results match fairly well and there is a maximum percentage discrepancy of 9 % in torque and 5 % in efficiency values.

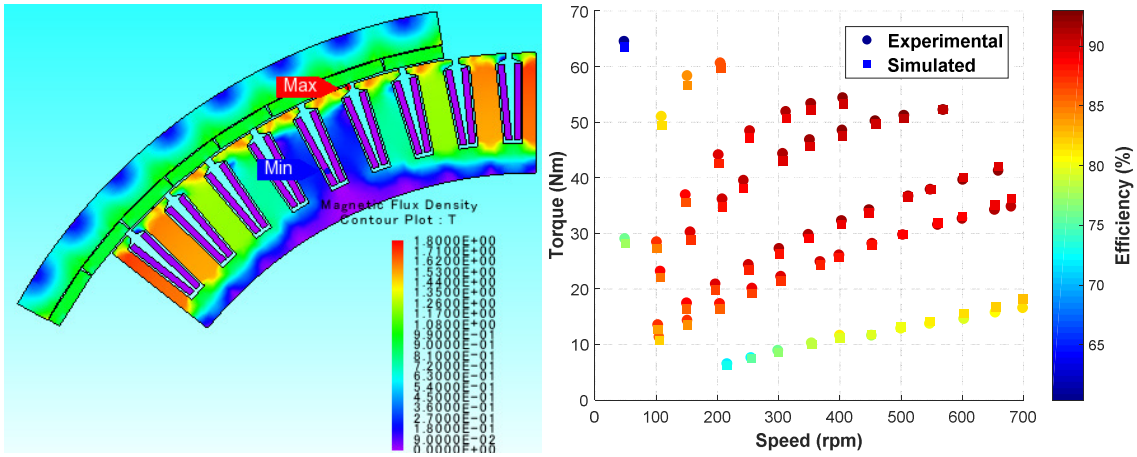


(a) (b)

Fig. 4.11 (a) Flux density plot of the sample HUB motor with virgin magnets, (b) Comparison of experimental & simulated torque vs. speed with corresponding efficiency values by virgin magnets

### 4.2.2.2 Efficiency map and energy evaluation of the sample hub motor with virgin magnets

Energy consumption for a reference drive cycle requires performance parameters of the machine for the complete torque vs. speed envelope. As a result, efficiency map of the motor needs to be evaluated so as to acquire the precise torque and efficiency points for the corresponding speed values in the reference drive cycle.

*Methodology for energy consumption evaluation:*

A methodology has been developed to evaluate the energy consumed by the machine for a particular drive cycle. Various articles/papers/studies depict the importance of evaluating the energy consumption of a machine for different drive cycles with diverse vehicle dynamics [67]-[76]. Fig. 4.12 shows the flow diagram of the developed methodology. In this, the machine performance is evaluated using FE analysis and utilizing the flux map of the machine, efficiency map is generated. Along with this, vehicle parameters like wheel radius, vehicle weight, rolling resistance, air density, drag coefficient and frontal area are used as input for deriving torque vs. time curve from speed vs. time of drive cycle. Now, these are used as input to the efficiency map and energy consumption for one cycle of the drive cycle is evaluated. Finally, total energy consumed in the lifetime of the machine is estimated by assuming that the motor operates for 2 hours daily during 10 years as the vehicle assumed is a compact city car with the vehicle parameters as listed in Table 4.2.

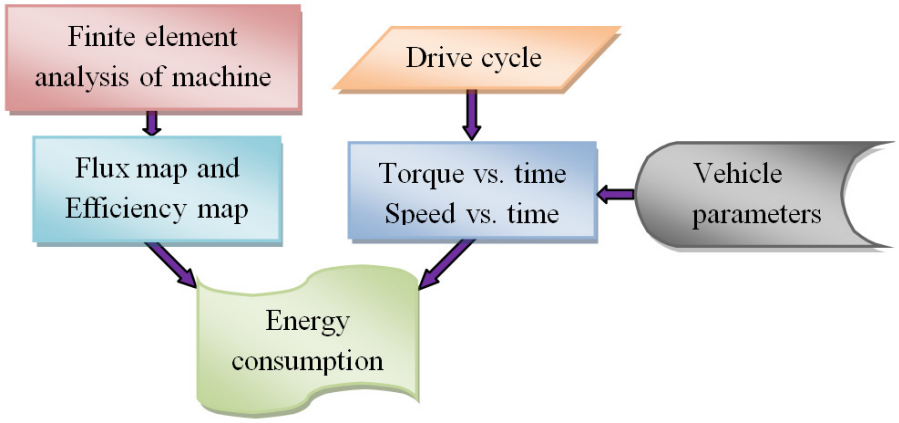


Fig. 4.12 Flow diagram for energy evaluation methodology

Table 4.2 Vehicle parameters

| Parameters | Value |
|---|---|
| Vehicle weight [kg] | 920 |
| Density of air [kg/m$^3$] | 1.225 |
| Frontal area [m$^2$] | 1.85 |
| Drag coefficient | 0.4 |
| Coefficient of rolling resistance | 0.01 |
| Tyre radius [m] | 0.21 |

*Efficiency map and energy consumption:*

The efficiency mapping of the machine is evaluated by utilizing the flux map with different values of $I_d$ and $I_q$. Similarly, iron loss mapping is also required for various values of machine flux density and current levels. Therefore, by utilizing optimization algorithm, the efficiency mapping is obtained for the sample motor. Fig. 4.13 illustrates the efficiency map of the sample motor with virgin magnets.

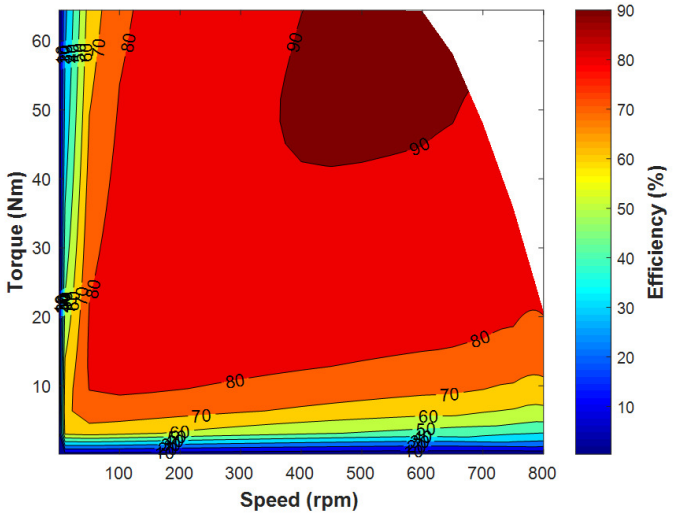


Fig. 4.13 Efficiency map of the sample HUB motor with virgin magnets

The drive cycle selected for this study is the urban part of the NEDC i.e. ECE-15 [68]. Fig. 4.14 (a) shows the speed vs. time profile of the ECE-15 drive cycle. The instantaneous wheel torque can be derived by using the following equation:

$$T_w = \left(ma + mgC_r + \frac{1}{2}\rho_a C_d A_f v^2\right) r_w \tag{4.1}$$

where, $T_w$ is wheel torque, $m$ is total mass, $a$ is acceleration, $g$ is gravity, $C_r$ is coefficient of rolling resistance, $\rho_a$ is density of air, $C_d$ is coefficient of drag, $A_f$ is vehicle frontal area, $v$ is velocity of vehicle and $r_w$ is radius of the wheel. Hence, using Eq. (4.1), vehicle parameters as in Table 4.2 and ECE-15 drive cycle, the wheel torque vs. time profile can be obtained. Fig. 4.14 (b) shows the wheel torque vs. time profile for the selected vehicle and ECE-15 drive cycle.

In typical EVs, the electrical machine is coupled to the wheels via transmission hence they have high speeds and high efficiencies. But here, it can be observed that maximum torque required at wheel is around 220 Nm. The maximum motor

torque which can be delivered is around 65 Nm. Hence, it is assumed that four motors would be used in the vehicle with direct drive in-wheel configuration to achieve required vehicle wheel torque.

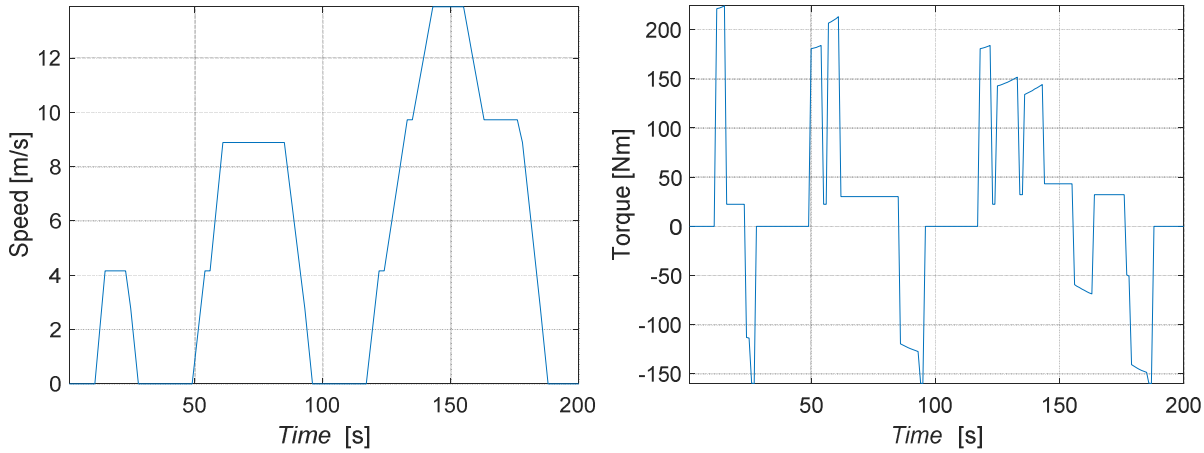


(a) (b)

Fig. 4.14 (a) Speed vs. time profile of the ECE-15 drive cycle, (b) Wheel torque vs. time profile for the specified vehicle and ECE-15

As per the flow diagram in Fig. 4.11, this torque vs. speed profile and efficiency map are employed together to get the energy consumed by one motor during the lifetime of 10 years with 2 hours of daily operation. The energy consumption can be calculated as:

$$E_c = \int_0^t E(t)dt \tag{4.2}$$

where $E_c$ is total energy consumed, $E(t)$ is energy input as a function of time and $t$ is time. The regenerative braking and negative torque values are assumed to be zero in the energy calculations. As a result, for the sample HUB motor with virgin magnets, the total energy consumed for the complete lifetime is 3071 kWh from Eq. (4.2). The harmonized electricity price for Europe region is considered as 0.22 €/kWh [77]. Therefore, the energy cost for one motor with virgin magnets is € 676 for the entire assumed lifetime. The weight of total magnet in the motor is 0.7 kg, and NdFeB material price considered is 45 €/kg [78], consequently the total magnet price is € 31.5 in one motor. The study has utilized ECE-15, but the methodology can be used to assess any drive cycle like NEDC, Urban Dynamometer Driving Schedule, and Worldwide Harmonized Light Vehicles Test Procedure (WLTP), etc.

#### 4.2.2.3 Machine performance with recycled magnets

Research is been carried out in recycling the PM scrap from various sources and fabricate recycled magnets by HD and HDDR processes [47]-[49]. In this study, magnetic property of recycled magnet considered is around 0.96 T as $B_r$. This is as per reference [49], where new magnet material has 1.36 T as $B_r$ and recycled magnet has 1.08 T as $B_r$, hence 20% reduction in the $B_r$. In this study virgin magnet has 1.2 T as $B_r$, and taking 20% reduction for recycled magnet, the $B_r$ evaluated is 0.96 T.

*Performance characteristics:*

For the evaluation of machine performance with recycled magnets in sample motor, the methodology utilized is similar to performance calculated with virgin magnets as in earlier section. The sample motor's dimensional parameters are kept same as that with virgin magnets; only magnet properties are altered with recycled magnet properties i.e. having 0.96 T as $B_r$ and increased length of the motor to achieve same torque as obtained with virgin magnets. The length of stator, rotor and magnets is increased from 40 mm to 46 mm. Henceforth, 2-D time stepping FE analysis is carried out to get the performance characteristics. Performance has been evaluated with similar current values as used in test and simulations during the study with virgin magnets in earlier section. Fig. 4.15 shows simulated torque vs. speed with corresponding efficiency values by virgin and recycled magnets.

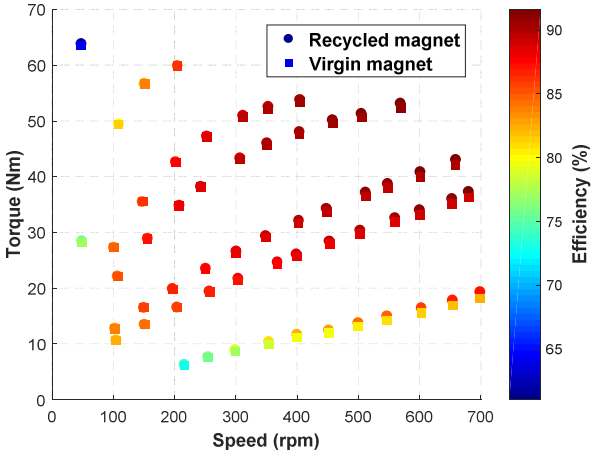


Fig. 4.15 Simulated torque vs. speed with corresponding efficiency values by virgin and recycled magnets

It can be observed that torque values match fairly well for virgin and recycled magnets. But the efficiency at certain points has increased with recycled magnets due to cumulative decrease of total losses, as iron losses have reduced but copper losses have increased.

*Efficiency map and energy consumption:*

The efficiency map and energy consumption of the sample motor with recycled magnets is evaluated similarly as was done while using virgin magnets in earlier section. By utilizing the flux map with different values of $I_d$ and $I_q$ and iron loss map for various values of machine flux induction and current levels, the efficiency map is generated for the motor with recycled magnets. Fig. 4.16 illustrates the efficiency map of the sample motor with recycled magnets.

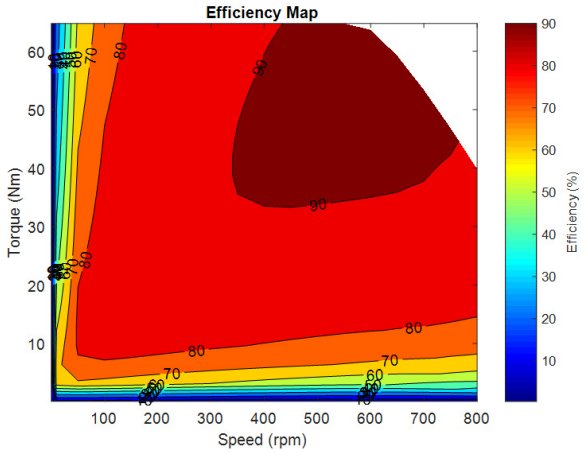


Fig. 4.16 Efficiency map of the sample HUB motor with recycled magnets

Hereafter employing the flow diagram in Fig. 4.12, torque vs. speed profile and efficiency map together can provide energy consumed by one motor during the lifetime of 10 years with 2 hours of daily operation with recycled magnets. Consequently, for sample motor with recycled magnets, total energy consumed for complete lifetime is calculated as 2995 kWh from Eq. (4.2). Similarly, assuming the harmonized electricity price for Europe region as 0.22 €/kWh [77], the energy cost for one motor with recycled magnets is € 659 for the assumed lifetime. It is difficult to comment on the price of recycled magnets as it is subject to ongoing research. But as it is assumed to be prepared from scrap PMs the price is assumed to be lower when compared to virgin PMs. Due to increased

length the PM weight increases from 0.7 kg to 0.81 kg with recycled magnets. Therefore, assuming the price of recycled magnet material as approximately the half of virgin magnets i.e. 22.5 €/kg, the total PM price calculated would be € 18.23 since the motor contains 0.81 kg of magnets.

#### 4.2.2.4 Energy cost index and comparison between virgin and recycled magnets

Energy cost evaluation considering the machine performance on a particular drive cycle or duty cycle gives more insights than evaluating machine performance at rated loads. Since machine performance could be optimized for rated conditions but their operation may not be subjected to rated conditions during a specific duty cycle. Therefore, comparing machine performance at a particular drive cycle with different magnet scenarios would provide information about the importance of energy and magnet cost. For this purpose, an index has been proposed to compare the energy cost in relation to magnet cost. The temperature for both the machines has been assumed the same. For instance, in this study energy consumption cost with virgin magnets is € 676 and magnet cost is € 31.5 for the sample motor. Considering this as the base scenario and naming it as Scenario 1 and/or Scenario base. The energy cost computed with recycled magnets is € 659 and magnet cost is € 18.23 for the sample motor; and naming it as Scenario 2. The energy cost index is defined as follows:

$$EC_i = \left(\frac{E_c(j)}{E_c(b)}\right).\left(\frac{Mag_c(j)}{Mag_c(b)}\right) \tag{4.3}$$

where, $EC_i$ is the energy cost index, $E_c(j)$ is energy cost for Scenario $j$, $Mag_c(j)$ is magnet cost for Scenario $j$, $E_c(b)$ is energy cost for Scenario base and $Mag_c(b)$ is magnet cost for Scenario base. As a result, energy cost index for Scenario 2 as per Eq. (3) is evaluated as 0.564. Various other sample scenarios have also been evaluated in ref. [84] which indicates the variation of the index with the deviation in energy cost and magnet cost. From Fig. 4.17 it can been observed that the design with recycled magnets has low efficiency in low speed high torque region and high efficiency in high speed low torque region as compared to efficiencies with virgin magnets. However, the drive cycle has most of the points in high speed low torque region; hence energy consumption is low with recycled

magnets for this drive cycle. Hence, it can be deduced that energy consumption depends on both drive cycle and machine design.

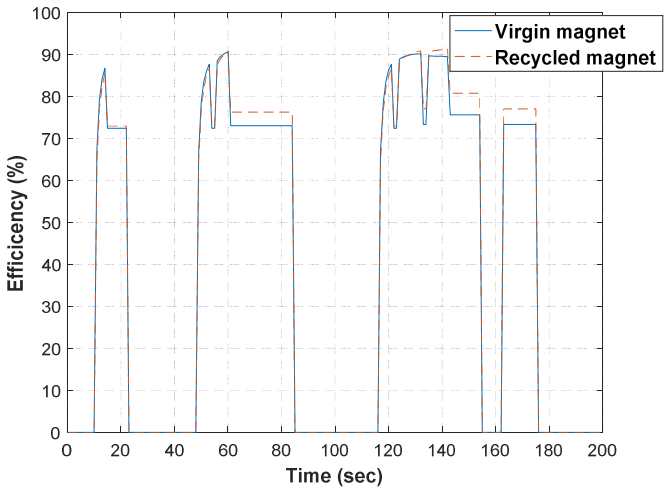


Fig. 4.17 Efficiency vs. time profile for virgin and recycled magnets

A general representation of the index is tabulated in Table 4.3, where energy cost index varies with the cost of virgin and recycled magnets. In this the $E_c$ virgin magnet is € 676, $E_c$ recycled magnet is € 659 and weight of virgin magnet is 0.7 kg and weight of recycled magnet is 0.81 kg. Hence, it can be observed that as the PM material price varies for virgin and recycled magnets the index varies accordingly. The greener is the index; the better it is economically when compared to red coloured cells in Table 4.3.

Table 4.3 Energy cost index with varying magnet costs

| | | | VIRGIN MAGNETS | | | | | |
|---|---|---|---|---|---|---|---|---|
| | PM. mat. price(€/kg) | | 20 | 35 | 50 | 65 | 80 | 95 |
| | | PM. cost (€) | 14.0 | 24.5 | 35.0 | 45.5 | 56.0 | 66.5 |
| RECYCLED MAGNETS | 5 | 4.05 | 0.282 | 0.161 | 0.113 | 0.087 | 0.071 | 0.059 |
| | 20 | 16.20 | 1.128 | 0.645 | 0.451 | 0.347 | 0.282 | 0.237 |
| | 35 | 28.35 | 1.974 | 1.128 | 0.790 | 0.607 | 0.494 | 0.416 |
| | 50 | 40.50 | 2.820 | 1.611 | 1.128 | 0.868 | 0.705 | 0.594 |
| | 65 | 52.65 | 3.666 | 2.095 | 1.466 | 1.128 | 0.917 | 0.772 |
| | 80 | 64.80 | 4.512 | 2.578 | 1.805 | 1.388 | 1.128 | 0.950 |
| | 95 | 76.95 | 5.358 | 3.062 | 2.143 | 1.649 | 1.340 | 1.128 |

Similarly, hypothesis can be generated with variable energy costs for different grades of magnets and the index would indicate the cases which are economically more advantageous.

Besides the above cited advantages, with recycled magnets one can observe an additional advantage, that they have low environmental impact as compared to virgin magnets. The mining of rare earth materials have negative repercussions in terms of environmental and human conditions. The preparation of recycled magnets has lower implications on human labour aspects as no mining is required. Additionally they have environmental benefits like reduction in air and water pollution. It can be argued that even for the preparation of recycled magnets a number of environmental hazards are possible like storage of hydrogen gas and its use in HD and HDDR process, and use of certain chemicals for separation of materials. However, if both the circumstances are weighed together, as assumed in [79], the mining would have higher negative impact on the environment than producing recycled magnets from scrap.

## 4.3 Design Analysis with recycled magnets in the machine

Utilization of recycled PMs in electrical machines is now being researched upon so as to explore the advantages of reuse/recyclability, i.e. less pressure on mining, fewer environmental impacts and small amount of supply-demand problems [80]. In this section, first the synthesis of recycled magnets using HD processing is presented, then comparison in torque-speed at peak performance with virgin and recycled magnets is presented and thereafter, energy consumption is evaluated for NEDC and WLTP drive cycles.

### 4.3.1 Recycled magnet synthesis at University of Birmingham

Researchers at the University of Birmingham have shown that hydrogen can be used to separate NdFeB magnets from hard disk drive scrap [81]. In this work, hydrogen is used to extract NdFeB magnets from automotive motor scrap in the form of hydrogenated NdFeB powder. This powder was then purified by various separation techniques (e.g. magnetic separation and sieving) for production of sintered magnets with good magnetic properties. However, the polymeric coating

on some of the magnets used in drive motors could not be fully removed by these techniques. Previous work has shown that carbon has a negative influence on the magnetic properties; however this influence depends upon the rare earth material composition as well as the carbon content [82].

In this work, the magnets were extracted from drive motors of EoL vehicles and demagnetized by heating to 350 °C in the air and the polymeric coating was removed by grinding the surfaces followed by HD. The HD powder was then milled under Argon to below 45 µm particle size using a knife mill after the addition of 5at% freshly prepared neodymium hydride ($NdH_{2.7}$). Finally the powder was aligned in 1.3 T field using a permeameter, iso-statically pressed into a green compact and sintered at 1080 °C for 1 hour under vacuum (~$10^{-5}$ mbar). These recycled magnets were then compared in terms of magnetic properties and density with commercially produced sintered N42SH magnets. Fig. 4.18 shows the schematic of possible re-processing routes as developed in ref [81].

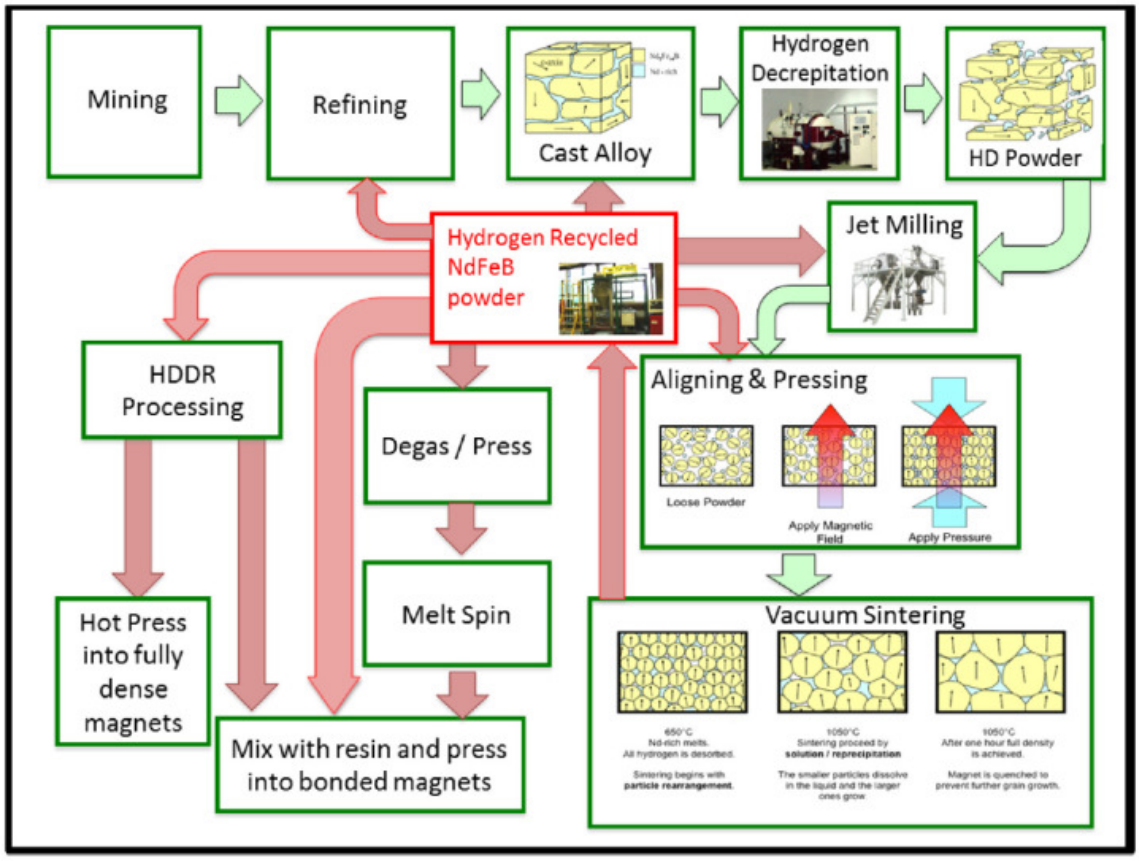


Fig. 4.18 Schematic of possible re-processing routes. Green boxes show the primary route for manufacturing a sintered NdFeB magnet. Red boxes and arrows demonstrate where the hydrogen extracted powder can be fed back in to recycle the material [81]

Fig. 4.19 (a) and (b) depict the measured *JH* and *BH* curve of virgin N42SH and recycled magnet at 25 °C and 150 °C temperature respectively. Table 4.4 illustrates the magnetic properties i.e. $B_r$ and normal coercivity ($H_{cb}$) of virgin and recycled magnets at 25 and 150 °C temperatures.

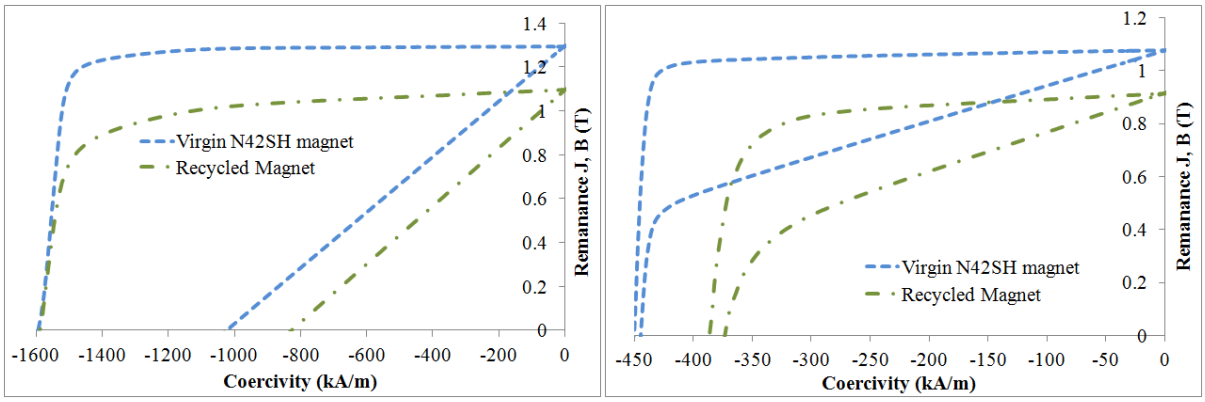


(a) (b)

Fig. 4.19 Measured *JH* and *BH* curves of: (a) virgin N42SH and recycled magnet at 25 °C temperature, (b) virgin N42SH and recycled magnet at 150 °C temperature

Table 4.4 Magnetic properties of virgin and recycled magnets at different temperatures

| | Temperature | Virgin magnet | Recycled magnet | % diff. |
|---|---|---|---|---|
| $B_r$ (T) | @ 25 °C | 1.30 | 1.10 | 15.4 |
| | @ 150 °C | 1.08 | 0.92 | 14.8 |
| $H_{cb}$ (kA/m) | @ 25 °C | -1025 | -830 | 19.0 |
| | @ 150 °C | -445 | -375 | 15.7 |

It can be observed that the relative difference in $B_r$ @ 25 °C is 15.4 % and @ 150 °C is 14.8 %, and relative difference in $H_{cb}$ @ 25 °C is 19.0 % and @ 150 °C is 15.7 %. The percentage reduction in $B_r$ for recycled magnets is in the range of around 14-16 %, which would mainly affect the machine flux induction and torque; and reduction in $H_{cb}$ is around 15-19 %, which would affect the magnet operating point at elevated temperatures. Hence, it is pertinent to check machine performance at higher temperatures for recycled magnets as the reduction in $H_{cb}$ is high and could lead to an irreversible demagnetization of magnets.

### 4.3.2 Performance evaluation using recycled magnets

Virgin magnets used in this study are commercially available N42SH PMs with the magnetic properties as listed in Table 4.4. The recycled magnets utilized are developed at a lab scale as described in the above section and with magnetic properties as listed in Table 4.4. 3-D FE analysis and MATLAB programming were carried out to obtain the machine performance in the complete torque-speed envelope. Fig. 4.20 illustrates the comparison of torque-speed curve with virgin and recycled magnets at peak performance. It can be observed that there is a reduction of 5.26 % in peak torque during constant torque region, and almost negligible change in torque at constant power region. This decrease is mainly due to the reduction in recycled magnet's magnetic performance and can be overcome by optimizing the machine design.

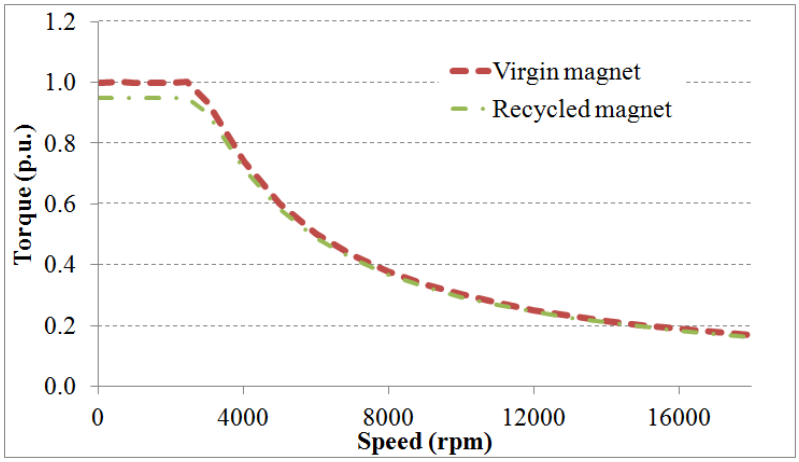


Fig. 4.20 Torque-speed curve at peak performance with virgin and recycled magnets for the PM based claw-pole machine

### 4.3.3 Energy consumption evaluation with drive cycle incorporation

Energy consumption during the machine operation in the automobile for a particular drive cycle is an important parameter to be considered. The methodology to obtain the energy consumption by the machine is presented in section 4.2.2.2 and similar methodology would be utilized for different drive cycle and vehicle parameters. To compare the energy consumption of the machine with virgin and recycled magnets, it is important to obtain the efficiency map of the

machine with recycled magnets. The machine peak torque with recycled magnets is reduced by 5.26 %; hence it is vital to obtain the same peak torque value as the machine with virgin magnets, so as to have fair comparison for energy consumption. The stator current is increased by approximately 7.8 %, so as to achieve the same peak torque values. As a result, Fig. 4.21 shows the efficiency map of the machine with recycled magnets in motor and generator mode.

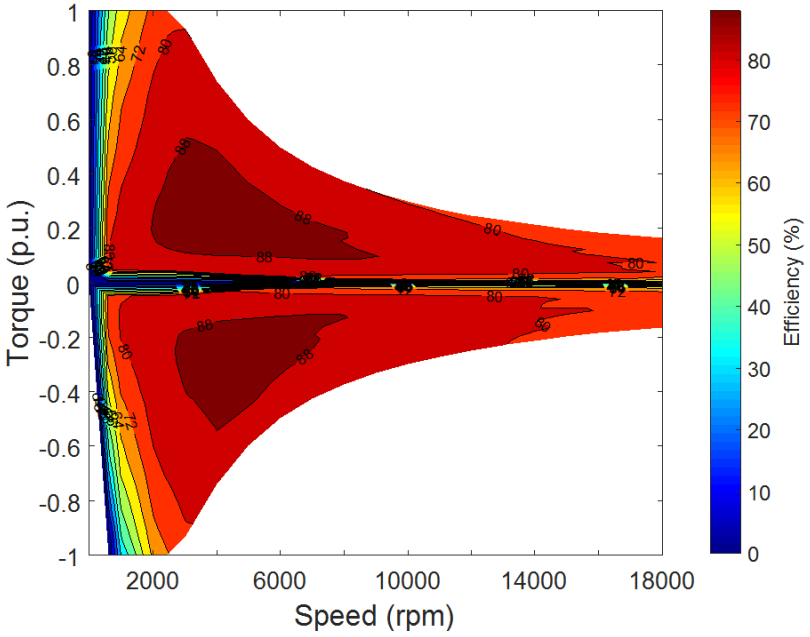


Fig. 4.21 Efficiency map of the machine with recycled magnets

To evaluate fuel consumption of the machine it is required to analyze the complete system simulation with ICE, clutch and gear mechanism, etc. Hence, in this section it is assumed that the machine performs in pure EV mode in an EV automobile and is coupled to the wheels by gear transmission. It is assumed that the vehicle is a compact 2-seater city car with the vehicle parameters as enlisted in Table 4.5 [67].

Table 4.5 Vehicle parameters for compact 2-seater city car

| Parameters | Value |
|---|---|
| Vehicle weight [kg] | 500 |
| Density of air [kg/m$^3$] | 1.25 |
| Frontal area [m$^2$] | 1 |
| Drag coefficient | 0.3 |
| Coefficient of rolling resistance | 0.007 |
| Tyre radius [m] | 0.273 |
| Gear ratio | 10:1 |

Two different drive cycles are utilized in this section for energy consumption evaluation viz. NEDC and WLTP which can be seen in Fig. 4.22 (a) and (b) respectively. The NEDC cycle is the most widely used drive cycle for Europe. But it has been criticized because it doesn't take into account many of the real world driving conditions. The WLTP drive cycle has started to be incorporated by many vehicle manufacturers for their new automobiles. The WLTP includes more realistic driving, higher average and maximum speeds, longer distance, shorter stops, more dynamic and representative accelerations and decelerations. As a result, in this study both the drive cycles are used for the study.

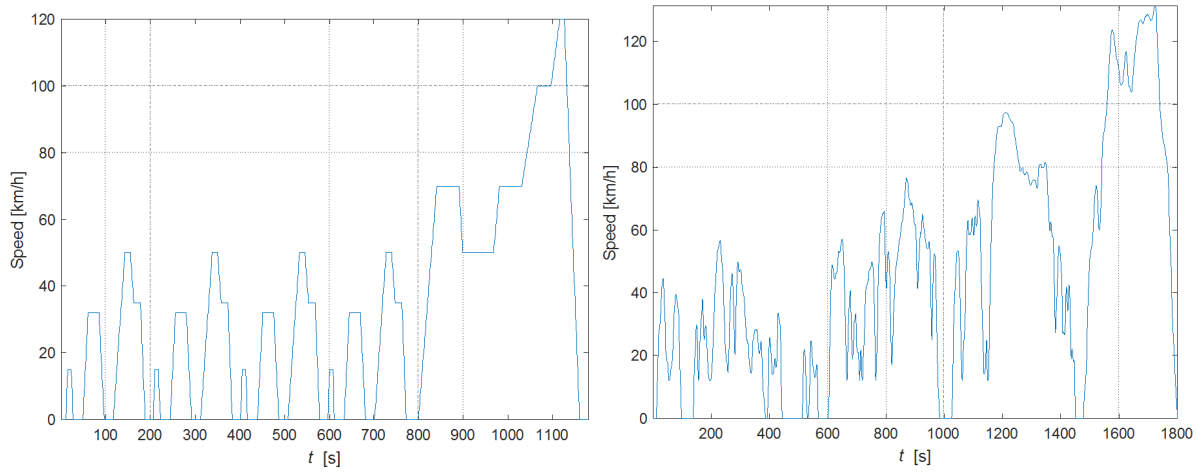


(a) (b)

Fig. 4.22 (a) NEDC drive cycle (b) WLTP drive cycle

Consequently, using the vehicle parameters given in Table 4.5 and NEDC & WLTP cycles, the operating points of both the drive cycles can be obtained by utilizing the flow diagram as shown in Fig. 4.12. The gear ratio of 10:1 is selected due to the fact that all the operating points of NEDC and WLTP cycle are placed nearly below the continuous performance region of the machine. This is because the machine should operate in its thermal equilibrium continuously for the complete drive cycle. Fig. 4.23 depicts the torque-speed envelope of the machine for peak and continuous performance along with NEDC operating points. Similarly, Fig. 4.24 shows the torque-speed envelope of the machine for peak and continuous performance along with WLTP operating points.

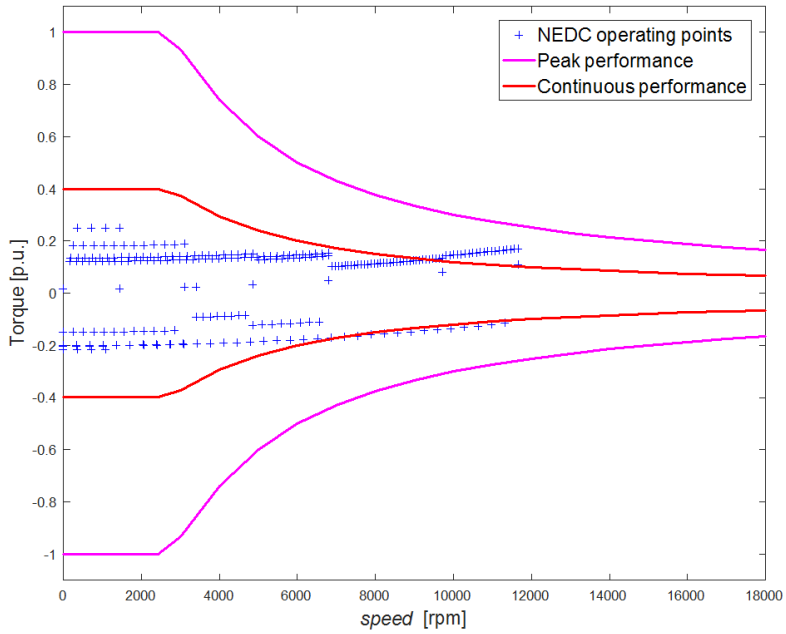


Fig. 4.23 Torque-speed envelope of the machine with NEDC operating points

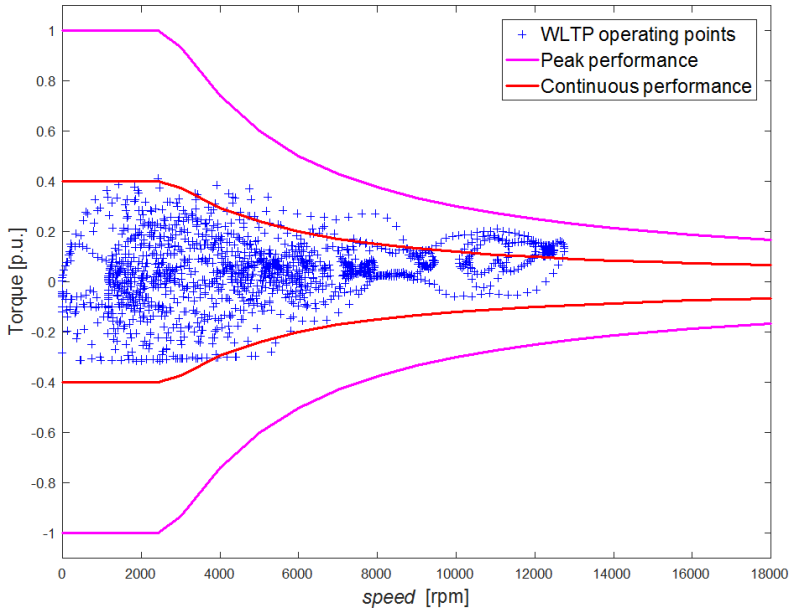


Fig. 4.24 Torque-speed envelope of the machine with WLTP operating points

As per the flow diagram in Fig. 4.12; the torque vs. speed profile and efficiency maps are employed together to get the energy consumed by the machine during the lifetime of 10 years with 2 hours of daily operation. The energy consumption is calculated as per Eq. 4.2. The harmonized electricity price for Europe region is considered as 0.22 €/kWh [77].

As a result, the energy consumption and energy cost by the machine with virgin and recycled magnets for NEDC and WLTP drive cycle with the above assumed lifetime are listed in Table 4.6.

Table 4.6 Energy consumption and energy cost by the machine with virgin and recycled magnets for NEDC and WLTP drive cycle

| Parameters | NEDC | | WLTP | |
|---|---|---|---|---|
| | Virgin magnet | Recycled magnet | Virgin magnet | Recycled magnet |
| Energy used - Motor mode (kWh) | 12,048 | 12,088 | 19,804 | 19,851 |
| Energy recuperated - Generator mode (kWh) | -2,428 | -2,419 | -3,451 | -3,436 |
| Total Energy (kWh) | 9,619 | 9,669 | 16,353 | 16,415 |
| Energy cost (€) | 2,116 | 2,127 | 3,598 | 3,611 |
| Distance travelled (km) | 244,983 | 244,983 | 339,450 | 339,450 |
| Total energy/distance (kWh/km) | 0.03927 | 0.03947 | 0.04817 | 0.04836 |

It can be observed that, for NEDC cycle the total energy consumed by the machine is 9619 kWh with virgin magnets and 9669 kWh with recycled magnets. Similarly, it can be observed that the total energy consumed by the machine is 16,353 kWh with virgin magnets and 16,415 kWh with recycled magnets for WLTP cycle. Thus, in the two cases the increment in energy with recycled magnets as compared to virgin magnets remains very small i.e. 0.51 % for NEDC and 0.38 % for WLTP. As the distance travelled by WLTP cycle is more compared to NEDC cycle; the total energy/distance provides a good comparison of energy consumption for different cycles. As a result the total energy/distance with virgin and recycled magnets for NEDC cycle is 0.03927 kWh/km and 0.03947 kWh/km respectively, and similarly this is 0.04817 kWh/km and 0.04836 kWh/km with virgin and recycled magnets for WLTP cycle respectively. The total energy/distance for WLTP cycle is higher as compared to NEDC cycle for both types of magnet since they are subject to increased real world driving conditions. Finally, it can be concluded that the machine performance with recycled magnets in different drive cycles at various operating points is almost the same as the performance with virgin magnets. The above investigation gives insight upon the utilization of recycled magnets in new age electrical machines of this application

for these power ratings. The claw-pole machine could be easily optimized to obtain the little reduction in energy and torque-speed performance to obtain results equivalent to a machine with virgin magnets. The price of recycled magnets is assumed to be lesser than virgin magnets, hence providing cost benefits for the machine. Even if the price of recycled magnets is similar to virgin magnets, the environmental impact of recycled magnets is much lower due to reduced mining activities. Life cycle assessment of NdFeB magnet production by magnet-to-magnet recycling for EV motors shows that PMs fabricated from magnet scrap can have up to 64-96 % lower environmental impacts, depending on the specific impact categories under investigation [79].

The energy cost index can be evaluated for the claw-pole machine by utilizing Eq. 4.3. Thus, Table 4.7 (a) and (b) provides energy cost index with varying magnet costs for NEDC and WLTP drive cycles. Here, the $E_c$ for virgin and recycled magnets are respectively € 2116 and € 2127 for NEDC cycle; while they are € 3598 and € 3611 for WLTP cycle. The weight of both virgin and recycled magnet is 0.16 kg.

Table 4.7 Energy cost index with varying magnet cost for (a) NEDC and (b) WLTP cycles

(a)

| | | | NEW MAGNETS | | | | | |
|---|---|---|---|---|---|---|---|---|
| | PM. mat. Price(€/kg) | | 20 | 35 | 50 | 65 | 80 | 95 |
| | | PM. cost (€) | 3.2 | 5.6 | 8.0 | 10.4 | 12.8 | 15.2 |
| RECYCLED MAGNETS | 5 | 0.8 | 0.251 | 0.144 | 0.101 | 0.077 | 0.063 | 0.053 |
| | 20 | 3.2 | 1.005 | 0.574 | 0.402 | 0.309 | 0.251 | 0.212 |
| | 35 | 5.6 | 1.759 | 1.005 | 0.704 | 0.541 | 0.440 | 0.370 |
| | 50 | 8.0 | 2.513 | 1.436 | 1.005 | 0.773 | 0.628 | 0.529 |
| | 65 | 10.4 | 3.267 | 1.867 | 1.307 | 1.005 | 0.817 | 0.688 |
| | 80 | 12.8 | 4.021 | 2.298 | 1.608 | 1.237 | 1.005 | 0.846 |
| | 95 | 15.2 | 4.775 | 2.728 | 1.910 | 1.469 | 1.194 | 1.005 |

(b)

| | | | NEW MAGNETS | | | | | |
|---|---|---|---|---|---|---|---|---|
| | PM. mat. Price(€/kg) | | 20 | 35 | 50 | 65 | 80 | 95 |
| | | PM. cost (€) | 3.2 | 5.6 | 8.0 | 10.4 | 12.8 | 15.2 |
| RECYCLED MAGNETS | 5 | 0.8 | 0.251 | 0.143 | 0.100 | 0.077 | 0.063 | 0.053 |
| | 20 | 3.2 | 1.004 | 0.573 | 0.401 | 0.309 | 0.251 | 0.211 |
| | 35 | 5.6 | 1.756 | 1.004 | 0.703 | 0.540 | 0.439 | 0.370 |
| | 50 | 8.0 | 2.509 | 1.434 | 1.004 | 0.772 | 0.627 | 0.528 |
| | 65 | 10.4 | 3.262 | 1.864 | 1.305 | 1.004 | 0.815 | 0.687 |
| | 80 | 12.8 | 4.014 | 2.294 | 1.606 | 1.235 | 1.004 | 0.845 |
| | 95 | 15.2 | 4.767 | 2.724 | 1.907 | 1.467 | 1.192 | 1.004 |

Similarly, it can be observed that as the PM material price varies for virgin and recycled magnets the index varies accordingly. The greener the index, better it is economically when compared to red coloured cells in Table 4.7. The trend for energy cost index varies in similar direction depending upon energy cost and magnet cost as also seen in Table 4.3. The differentiating factor is that in Table 4.3, the magnet weight for virgin and recycled magnet are different, hence the index for similar priced magnets is higher in Table 4.3 as compared to in Table 4.7. Therefore, the recycle index of energy consumption provides an idea for recyclability of magnets utilized in electrical machines.

*Consumption evaluation with HEV configuration:*

As the developed claw-pole machine is meant for a mild hybrid application, the fuel consumption evaluation is also important for this configuration. The HEV configuration utilized for this study is for P0 type architecture as it can be seen in Fig. 2.2 in Chapter-2. The e-machine is belt driven by the ICE and is always engaged to the ICE crankshaft. The supply voltage is provided by a 48 V battery with 10 Ah rating. The automobile used for evaluation is a C-segment vehicle like Volkswagen Golf or Peugeot 308 or similar with 1.2 litre engine and 5-speed gearbox. The simulation schematic utilized is similar to as shown in Fig. 4.25 [12].

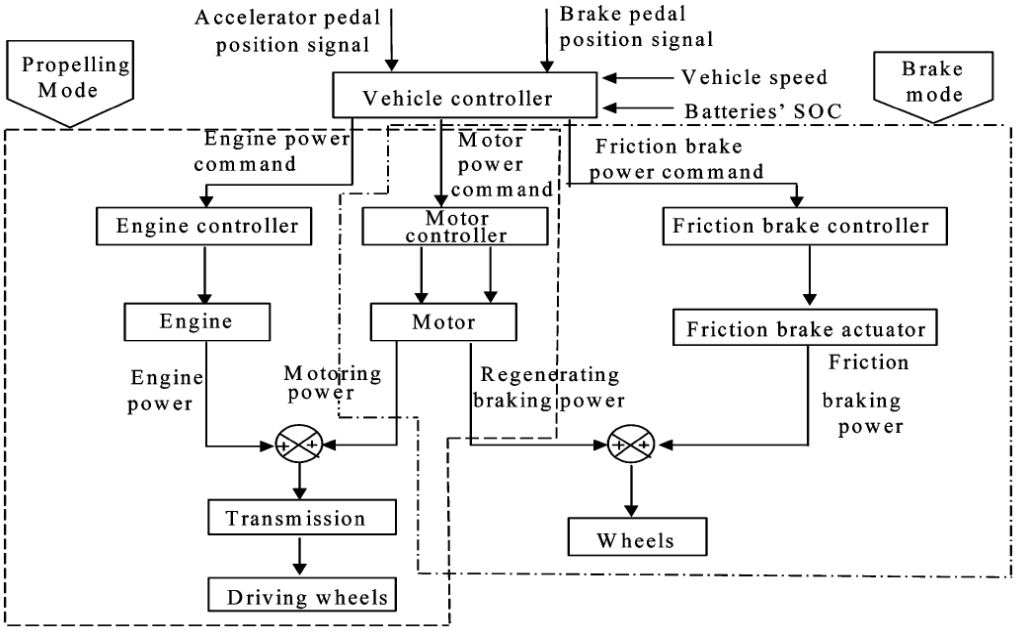


Fig. 4.25 HEV simulation schematic utilized for fuel consumption simulations [12]

The drive cycle utilized for this study is for WLTP cycle with the above mentioned vehicle type. The e-machine efficiency map is fed along with engine efficiency map to obtain the fuel consumptions. The evaluation is carried out for the vehicle without e-machine and with e-machine for virgin and recycled magnets. The initial and final battery state of charge considered is 60 %. The study is carried out by the system simulation team working at Valeo EEM, Creteil, with experience into HEV system simulations. The consumption evaluation for only ICE vehicle and HEV automobile are listed in Table 4.8.

Table 4.8 Consumption evaluation for only ICE and HEV automobile

| Parameters | Only ICE | HEV | | % diff bn only ICE & virgin | % diff bn virgin & recycled |
|---|---|---|---|---|---|
| | | With virgin PM | With recycled PM | | |
| Fuel consumption (l/100 km) | 5.3571 | 5.0072 | 5.0080 | -6.53 % | 0.016 % |
| $CO_2$ emissions ($gCO_2$/km) | 125.89 | 117.67 | 117.69 | -6.53 % | 0.016 % |
| Electrical energy used in ZEV [kJ] | | 580.77 | 575.81 | | -0.855 % |
| Electrical energy used in torque assist [kJ] | | 1102 | 1092 | | -0.899 % |
| Electrical energy recovered on regenerative braking [kJ] | | -1845 | -1838 | | -0.391 % |
| Electrical energy recovered on generation [kJ] | | -295 | -289 | | -1.932 % |

It can be observed that there is at least 6.53 % of fuel saving and $CO_2$ emission reduction between an only ICE and HEV automobile with virgin magnets. This is as expected from a mild hybrid automobile of this power rating and vehicle segment, hence substantiating the use of HEVs for reduced emissions and fuel savings around the world. The interesting point to be observed is that the fuel consumption and $CO_2$ emissions difference between the machine with virgin and recycled PMs is only 0.016 %. This is almost negligible and corroborates well with the results obtained earlier with pure EV mode. As a result it can easily be concluded that recycled magnets with lower performances can be incorporated into new age electrical machines of these ratings so as to provide two main advantages: (a) release pressure on mining activities and (b) tackle the supply-demand balance problem. Hence, utilizing recycled PMs would make e-machines more sustainable in nature as compared to e-machines with virgin magnets.

*Demagnetization study:*

The magnet demagnetization is an important aspect to be considered for PM based machines. At elevated temperatures the PM performance curve degrades and the knee point of the *BH* curve lies in the second quadrant. If the machine operates near this knee point at these temperatures, irreversible demagnetization of the magnet can occur. Due to this, the machine gets derated permanently and hence loses its performance. Therefore to avoid this, prior investigation of magnet demagnetization is necessary so as to observe the machine behaviour during high temperatures with peak demagnetizing currents as the worst case scenario. The demagnetization study is more imperative in the case of recycled magnets due to the reduced $H_{cb}$ as compared to virgin magnets as observed in the earlier section at Table 4.4.

In this section, first the machines' developed torque at base speed with peak current would be observed. Then as a worst case scenario, maximum field current and only negative $I_d$ current at 150 °C temperature would be injected and the magnet demagnetization would be observed. This demagnetized magnet would again be used to calculate the new developed torque and compare it to the one obtained with non-demagnetized PM. This procedure would be carried out for the machine with virgin and recycled magnets. In Fig. 4.26, the magnetic field distribution in virgin magnets with $I_d$ = -325 A and $I_q$ = 0 A is shown.

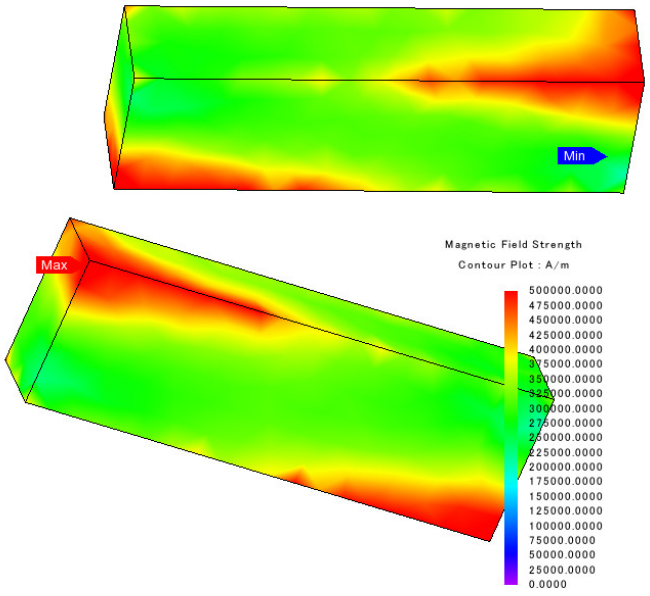


Fig. 4.26 Magnetic field distribution in virgin magnets at $I_d$ = -325 A and $I_q$ = 0 A

It can be observed that at PM corners the magnetization is above the knee point of the *BH* curve and only small area seems to be demagnetized. Fig. 4.27 depicts the developed torque with non-demagnetized and demagnetized virgin PMs. It can be observed that there is almost no change in the torque and hence the machine is capable to handle the worst case scenario without downgrading.

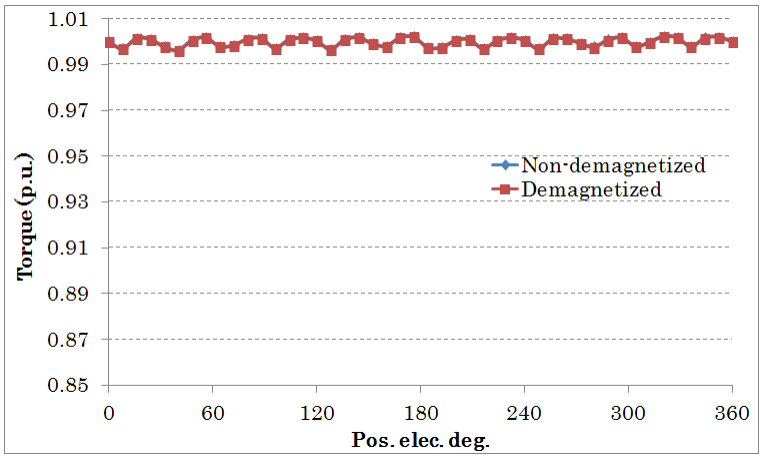


Fig. 4.27 Developed torque with non-demagnetized and demagnetized virgin PMs

Similarly, in Fig. 4.28 the magnetic field distribution in recycled magnets with $I_d$ = -325 A and $I_q$ = 0 A can be observed. The recycled PM gets demagnetized more towards the corners and move inwards as compared to virgin PMs as the $H_{cb}$ for recycled PMs is around 15 – 19 % lower than the virgin PMs. The developed torque with non-demagnetized and demagnetized recycled PMs in the machine can be seen in Fig. 4.29.

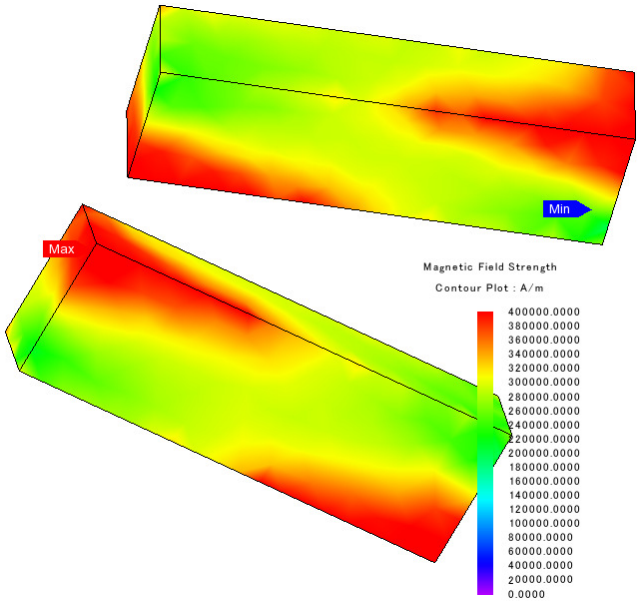


Fig. 4.28 Magnetic field distribution in recycled magnets at $I_d$ = -325 A and $I_q$ = 0 A

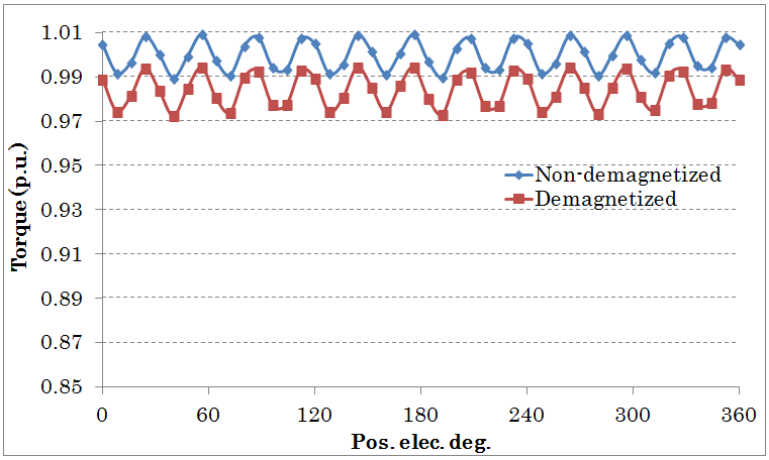


Fig. 4.29 Developed torque with non-demagnetized and demagnetized recycled PMs

It can be observed that the developed torque is reduced by 1.6 % for demagnetized PMs as compared to non-demagnetized PMs. The percentage reduction in torque is very less as the PMs are not the main source of induction in this machine but still the e-machine design needs to be taken care for this reduction during designing the new e-machines. This reduction can easily be surpassed by systematic optimization of the e-machine in order to achieve the performance and as well as to take into account magnet demagnetization affects.

Finally, it can be concluded that utilization of recycled magnets in the PM based claw-pole machine can be adopted with minor improvement in machine designs. The direct reuse and direct recycle concept of PMs in the context of claw-pole machine provides advantages towards easy recyclability of PMs. Consequently as stated before, the utilization of recycled PMs in e-machines is also more sustainable in nature and helps in reducing the carbon footprint by aiding in the reduction of mining activities to recover new PM materials. As this machine is produced in high volumes (millions); utilizing recycled magnets can lead to a substantial reduction in mining.

However, for a smooth implementation of reuse and recycle concept; policy and regulations need to be put into operation. To penetrate recycling into the

complete supply chain system, it would be necessary to execute guidelines from the bottom to top level viz. from scrap yards to automobile manufacturers. Once the system is in place the recycling would become a natural process and provide numerous benefits to keep the planet green and sustainable.

## 4.4 Conclusion

The direct reuse concept and the direct recycle concept have been developed in this chapter, and they emphasis upon the reusability and recyclability of the magnets used in the claw-pole machine. The weighted index of recycling and energy concept has also been developed and proposed; and the machine's score in all the categories for standardization section is above 78 % and the score for disassembly category in cost section is 74 %, hence favoring the machine design for easy assembly and disassembly. It can also be observed that the energy consumption of the machine in pure electric vehicle mode and hybrid electric vehicle mode for virgin and recycled magnets is almost the same i.e. the deviation is less than 0.5%. Thus, substantiating the use of recycled magnets in new claw-pole machines as they are ecologically sustainable due to the fact that they assist in reduced mining of new rare earth magnet materials.

# Chapter 5

# Prototyping and Experimental Results

## 5.1 Prototype Fabrication

One of the deliverables of the project was to develop and fabricate a prototype of the designed electrical machine and test the performance parameters. Prototyping and experimental testing provides more insights about the machine's manufacturing process and actual test measurements. Two sets of claw-poles for the new design were fabricated, so as to assemble two rotors; one with virgin magnets and the other with recycled magnets. The virgin magnets were procured as per the N42SH specification from the supplier and the recycled magnets were developed by the School of Metallurgy and Materials, University of Birmingham, UK in their laboratory. Fig. 5.1 shows the fabricated front claw-pole with the appropriate magnet slit.

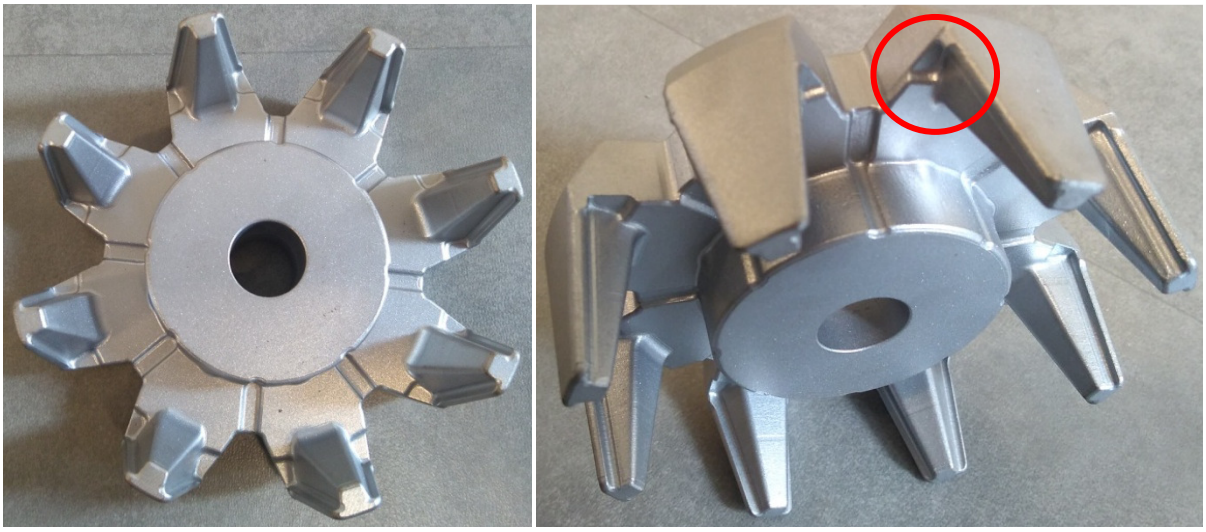

Fig. 5.1 Front claw-pole with the appropriate magnet slit

Fig. 5.2 shows the fabricated rear claw-pole with complete magnet slit. Hence it can be observed that through this complete magnet slit it is possible to recover the magnets after EoL as per the direct reuse concept of Fig. 4.2.

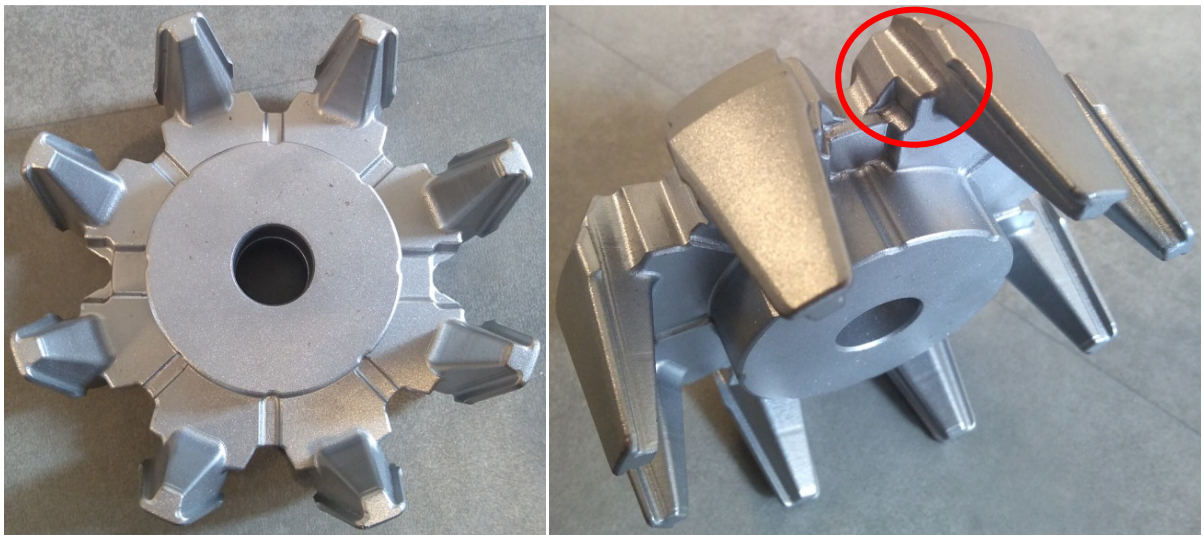

Fig. 5.2 Rear claw-pole with the complete magnet slit

One complete machine is fabricated at Valeo's manufacturing unit with stator, stator windings, end shields, electronic controller, and other components required for the prototyping. In Fig. 5.3 the complete assembled machine can be observed. The aim is to first assemble the rotor with virgin magnets in this machine and test it for the performances and then assemble the rotor with recycled magnets and again test it for performances. Hence, it will be possible to compare the simulated and experimental results for both virgin and recycled magnets, and also observe easy assembly and disassembly of magnets in the new claw-poles.

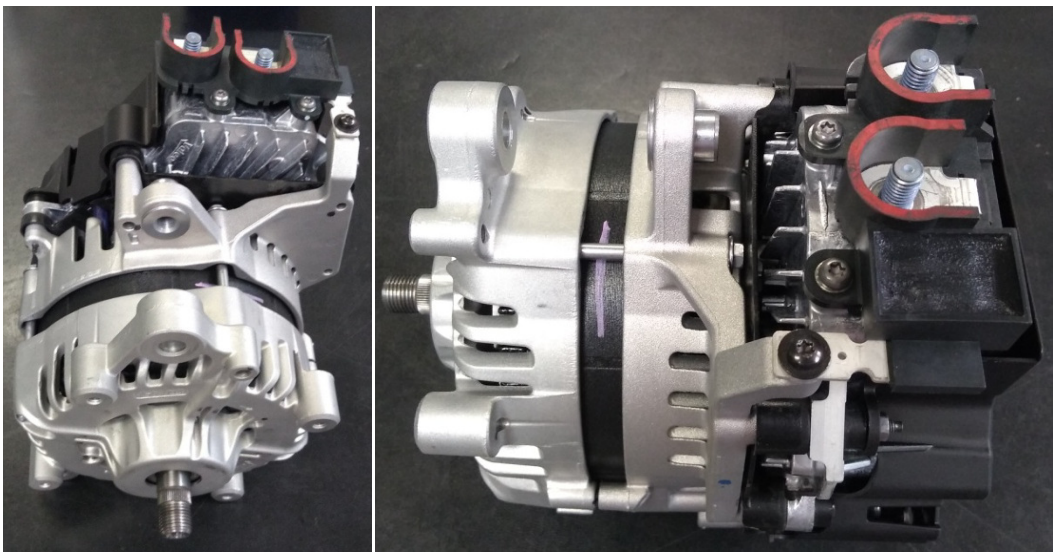

Fig. 5.3 Complete assembled prototype machine

### 5.1.1 Prototype for 48 V application with virgin magnets

One set of claw-pole rotor with virgin magnets is assembled and developed in the proto-shop of Valeo. Fig. 5.4 shows the prototype claw-pole rotor with virgin magnets. The assembly process was similar to the existing process as the front claw-pole design is similar to the existing claw-poles, so as not to modify the present assembly process.

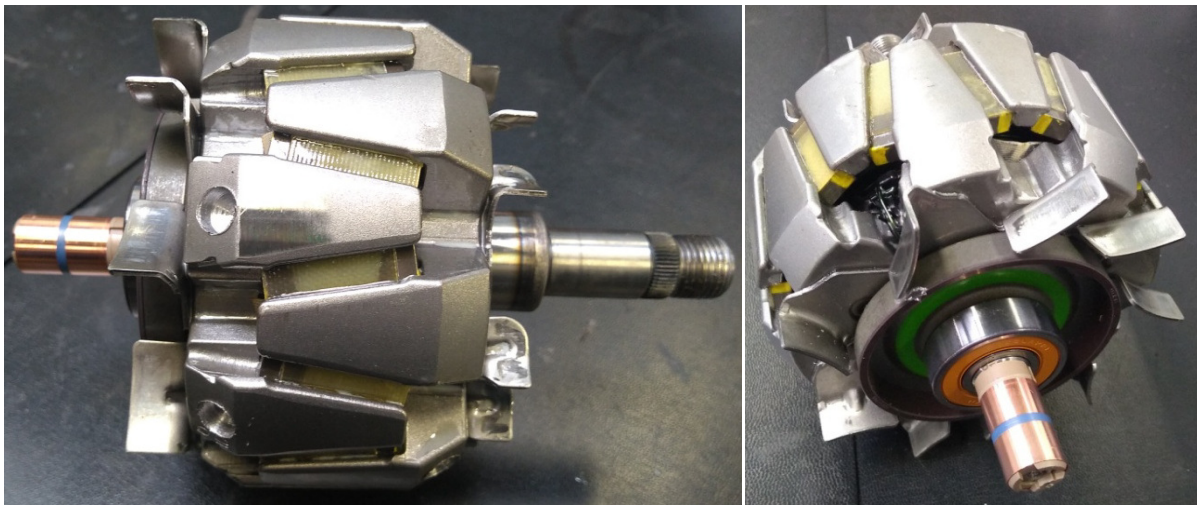

Fig. 5.4 Prototype claw-pole rotor with virgin magnets

### 5.1.2 Prototype for 48 V application with recycled magnets

Similarly, another set of claw-pole rotor for recycled magnets is assembled and developed in the proto-shop of Valeo. As the recycled magnets are still in the machining and grinding stage, the claw-pole rotor is assembled without the recycled magnets. Fig. 5.5 shows the prototype claw-pole rotor for recycled magnets, but without the magnets. It has been planned to slide the recycled magnets into the claw-poles through the complete magnet slit when they are finally fabricated for the proper shape and size. At present, due to existing manufacturing process, the rear fan hinders sliding in and out of magnets and obstructs the path for the entry and exit of the magnet. In the future designs, the fan blades can be redesigned so as not to hinder the entry and exit of the

magnets. This is possible by redesigning the number of fan blades as per the number of rotor poles so that the blade comes just behind the claw finger and provides a good path for the magnets. However, this needs further investigation into thermal management of the machine as the fan blade design affects the cooling of the machine.

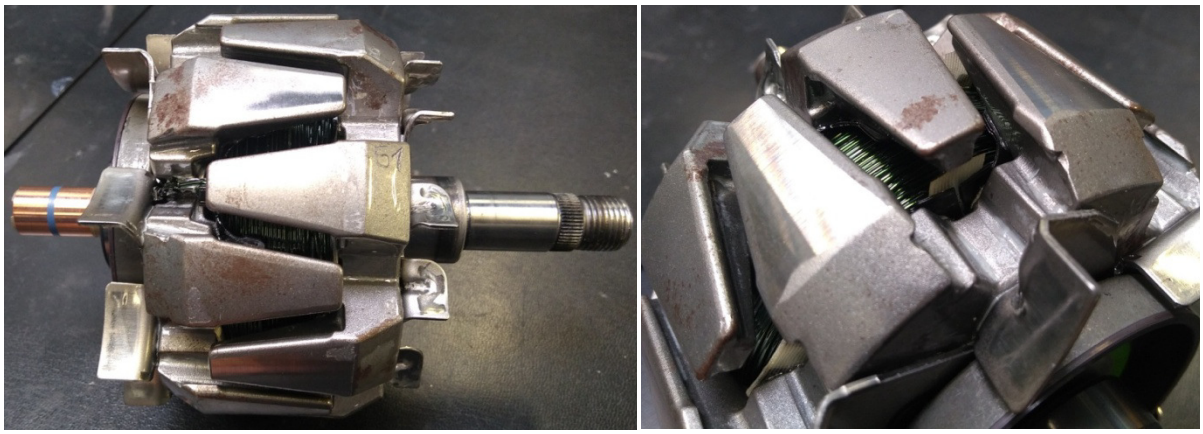

Fig. 5.5 Prototype claw-pole rotor for recycled magnets but without the magnets

## 5.2 Experimental Testing

As the prototype is fabricated for the validation of a new concept, the experimental testing is carried out for most essential tests viz. resistance measurement, open circuit back EMF test and load test at various test points. Other tests like temperature rise test, test on application, reliability tests, and many more are also needed to validate a prototype for the complete product. However, these are comprehensive tests with an extended timeline and would be carried out as the prototype validation is complete. Measurement instrumentation is also a very important step during experimental testing, as improper measurements can lead to inaccurate results. Therefore, while measuring the experimental results, the existing test bench of Valeo has been utilized and this has been calibrated for their routine product testing.

### 5.2.1 Resistance measurement

As the developed machine has a double 3-phase stator winding with star connection, the phase to phase resistance is measured using a micro-ohm meter. Similarly, the resistance of rotor winding is also measured and documented. The instantaneous ambient temperature also needs to be observed and noted down. Table 5.1 depicts the measured stator and rotor winding resistances.

Table 5.1 Measured stator and rotor winding resistances

| Stator Winding | | | | |
|---|---|---|---|---|
| **Phase-Phase** | **Resistance (mΩ)** | **Phase-Phase** | **Resistance (mΩ)** | **Temperature (°C)** |
| U1-V1 | 16.42 | U2-V2 | 16.36 | 25 |
| V1-W1 | 16.60 | V2-W2 | 16.53 | |
| W1-V1 | 16.66 | W2-V2 | 16.62 | |

| Rotor winding | |
|---|---|
| **Resistance (Ω)** | **Temperature (°C)** |
| 2.22 | 25 |

### 5.2.2 Open circuit back EMF test

Open circuit back EMF test is conducted to analyze the machine's electromagnetic performance with no stator excitation. The machine is externally driven by a motor to a speed of 1000 rpm and the voltage values are observed at the stator winding terminals with varying field current. The back EMF voltage are also observed and recorded in an industry grade oscilloscope to check the integrity of the phases and the wave-shape. The test is carried out at two ambient temperatures i.e. at room temperature of 25 °C and high temperature of 105 °C, so as to verify the difference in voltage due to remanence change in magnets at high temperatures. Fig 5.6 shows the machine on the test setup for back EMF measurement. Fig. 5.7 (a) and (b) show the measured back EMF waveform at 0.1 p.u. and 1 p.u. field current respectively @ 25 °C ambient temperature.

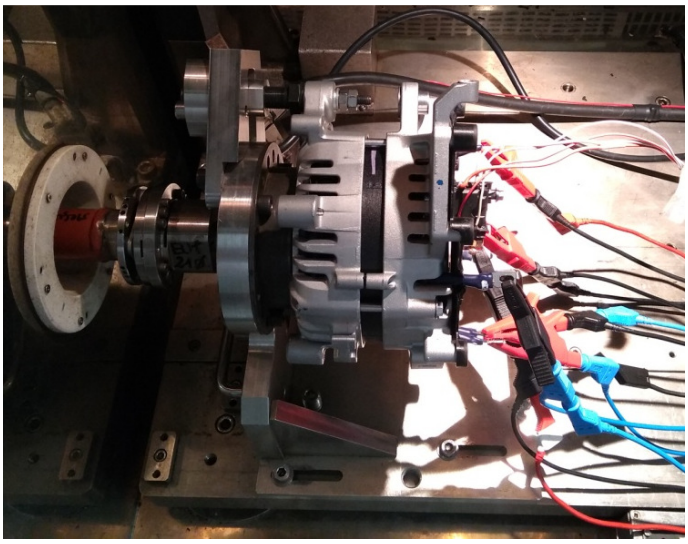

Fig. 5.6 Machine assembled on the test bench for back EMF measurement

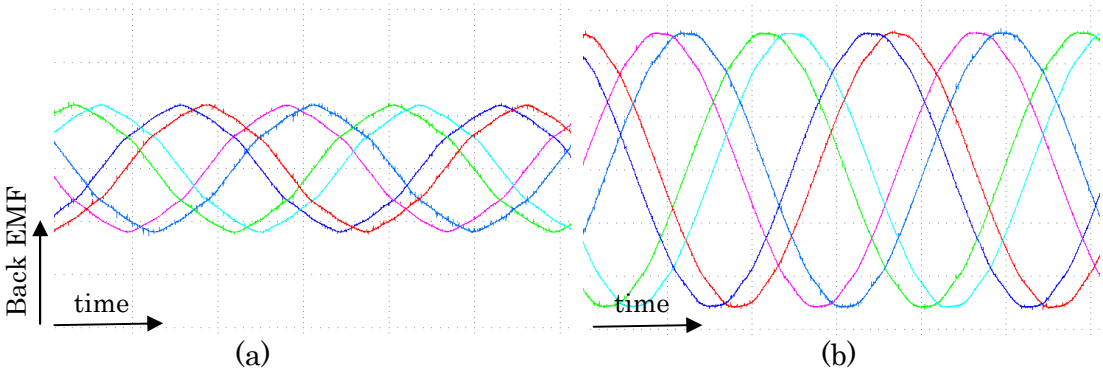


Fig. 5.7 Measured back EMF waveform @ 25 °C: (a) 0.1 p.u. & (b) 1 p.u. field current

In Fig. 5.8 the p.u. back EMF voltage is depicted with varying field current at 25 °C and 105 °C ambient temperatures. It can be observed that there is approximately 3% reduction in back EMF at high temperature and this is mainly due to remanence reduction of magnets.

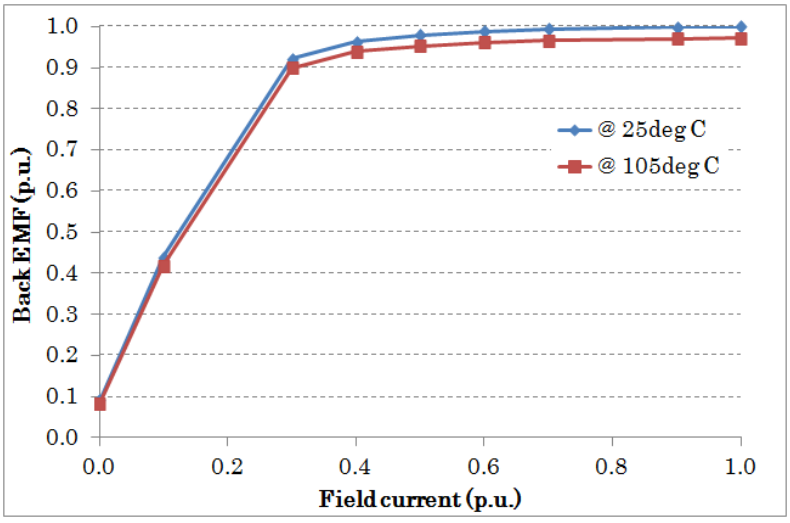


Fig. 5.8 Measured p.u. back EMF with varying field current @ 25 °C & 105 °C temp.

### 5.2.3 Load test

Load test is carried out on the machine to evaluate the performance along with electronic controller at various test points to observe the torque, speed, voltages, currents, input power, output power and efficiency. The machine is assembled on the same test bench where the back EMF test had been conducted. In this test the electronic controller is also assembled with the machine and appropriate control algorithm is programmed into the controller so as to test the machine at various test points. Fig. 5.9 depicts the machine in the test bench along-with the electronic controller for load test.

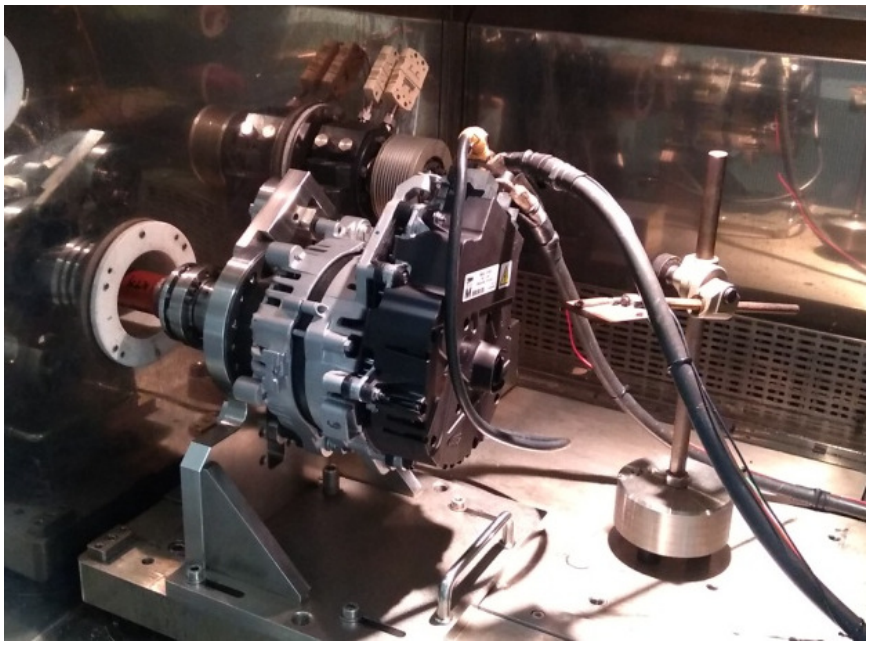

Fig. 5.9 Machine assembled on the test bench for load test along with controller

In this test, different $I_d$, $I_q$ and $I_f$ are injected in the machine by the electronic controller for various speeds and the torque, speed, currents, voltages, input power and output power are measured in the instrument panel. The test is carried out from low speed of 50 rpm to high speeds of 10,000 rpm. Due to test setup limitations, the test for higher speeds till 18,000 rpm could not be conducted. However as the field weakening operation starts from 2300 rpm, the machine performance at constant power region could be measured till 10,000 rpm. The test was conducted at 105 °C ambient temperature, so as to observe the machine performance at elevated temperatures. Fig. 5.10 depicts the measured

torque, power, $I_d$, $I_q$, $I_f$ and $I_{s\text{-}rms}$ (all in p.u.) as a function of speed and efficiency of the machine.

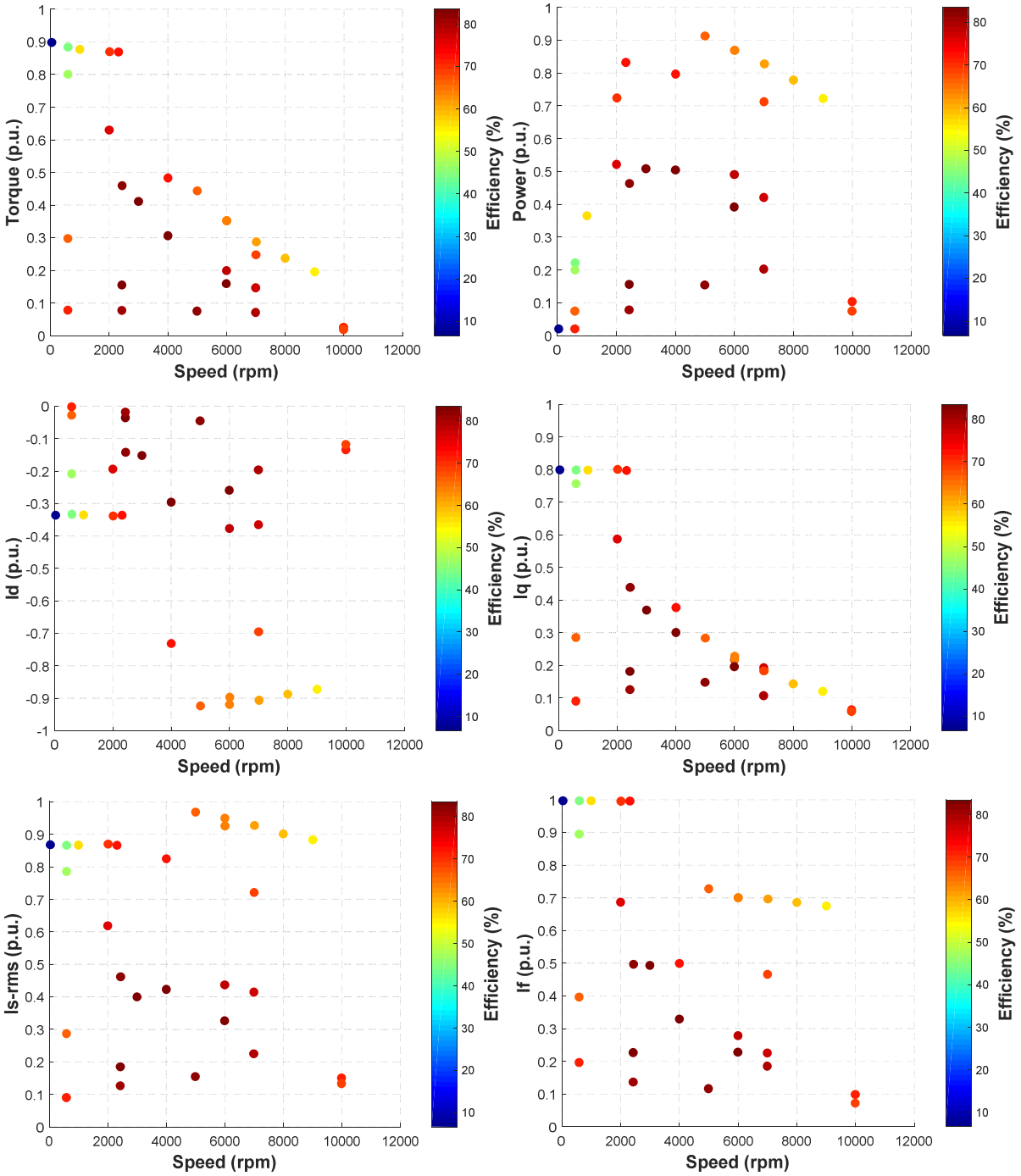


Fig. 5.10 Measured torque, power, $I_d$, $I_q$, $I_f$ and $I_{s\text{-}rms}$ (all in p.u.) as a function of speed and efficiency of the machine

It can be observed that the peak efficiency of the machine along with controller is around 84 %. The torque and power varies according to the $I_d$, $I_q$ and $I_f$ variation, as it can also be observed by the above measurement results. The next step is the

validation of simulation results by comparing them with these measurement results.

## 5.3 Comparison of measured and simulated results

The main aim of this section is to compare the measured and simulated results, so as to validate the design methodology. The open circuit back EMF test and load test results are compared for the same operating conditions.

### 5.3.1 Open circuit back EMF test

The calculated open circuit back EMF of the machine is simulated for the same value of field currents as measured in Section 5.2.2 and at a speed of 1000 rpm. Fig. 5.11 depicts the comparison between simulated and measured p.u. back EMF with varying fields for (a) 25 °C and (b) 105 °C temperature. It can be observed that the simulated and measured results are matching very closely and have a maximum deviation of only 2 %. At certain field currents there is no deviation between simulated and measured results. Hence, it validates the machines electromagnetic performance at open circuit and also corroborates the quality of magnet material and its magnetization level.

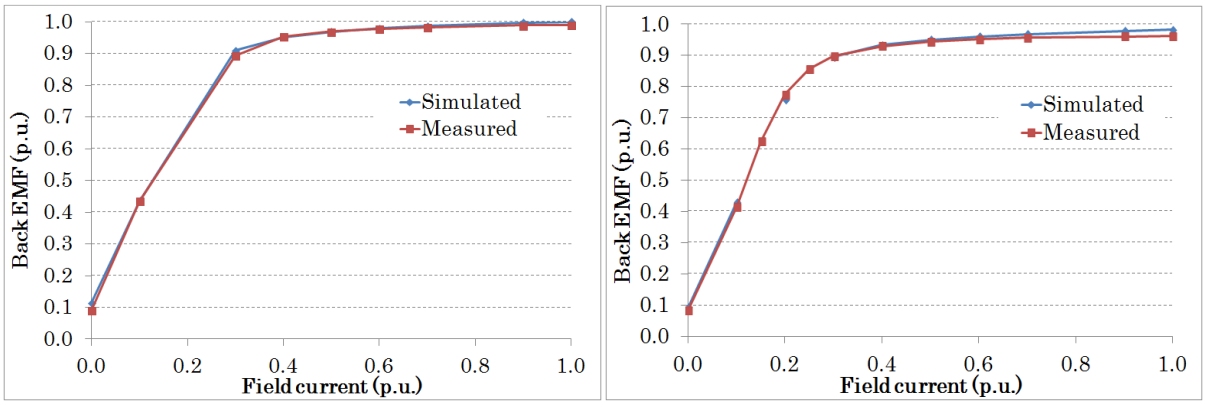


(a) (b)

Fig. 5.11 Simulated and measured p.u. back EMF with varying field current: (a) 25 °C and (b) 105 °C temperature

Fig. 5.12 also illustrates the simulated and measured back EMF waveform for (a) 0.1 p.u. and (b) 1 p.u. field current at 105 °C temperature. The wave-shape and the amplitude are precisely close to each other and hence providing a substantial validation of the design in terms of its' unloaded electromagnetic performance.

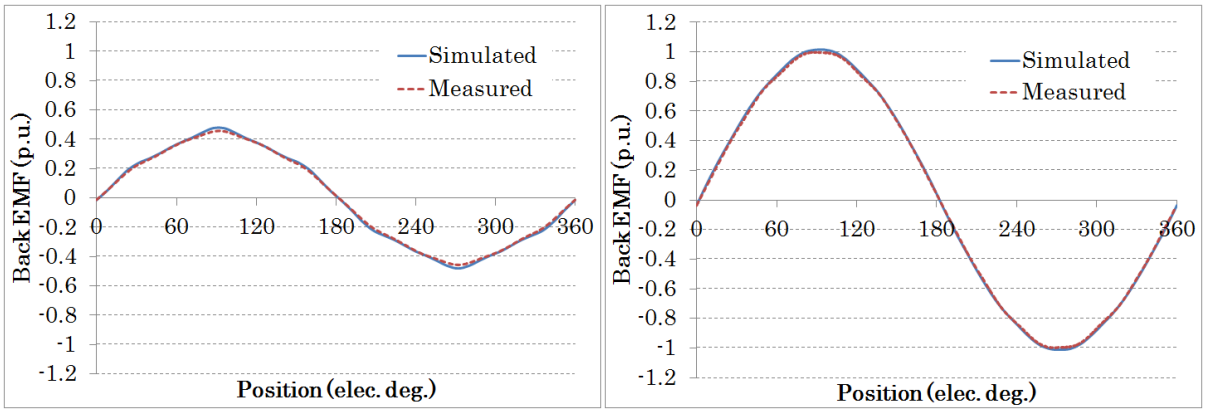


(a) (b)

Fig. 5.12 Simulated and measured back EMF waveform at 105 °C: (a) 0.1 p.u. and (b) 1 p.u. field current

### 5.3.2 Load test

In this section the calculated performance on load was simulated by utilizing the same $I_d$, $I_q$ and $I_f$ for the similar speeds as tested experimentally in section 5.2.3, so as to fairly compare the simulated and measured performance during loaded condition. Fig. 5.13 shows the simulated and measured p.u. torque, speed and efficiency of the machine. Similarly, Fig. 5.14 depicts the simulated and measured p.u. power, speed and efficiency of the machine. It can be observed that the simulated and measured p.u. torque and p.u. power match fairly well with each other, and the maximum deviation is around 7 %. However, in 21 test points out of the total 29 test points, the deviation in torque and power is less than 5 %. This demonstrates a very good agreement between simulated and measured results for the machine performance during loaded condition. Although the deviation in simulated and measured efficiency is higher as compared to deviation in simulated and measured torque and power.

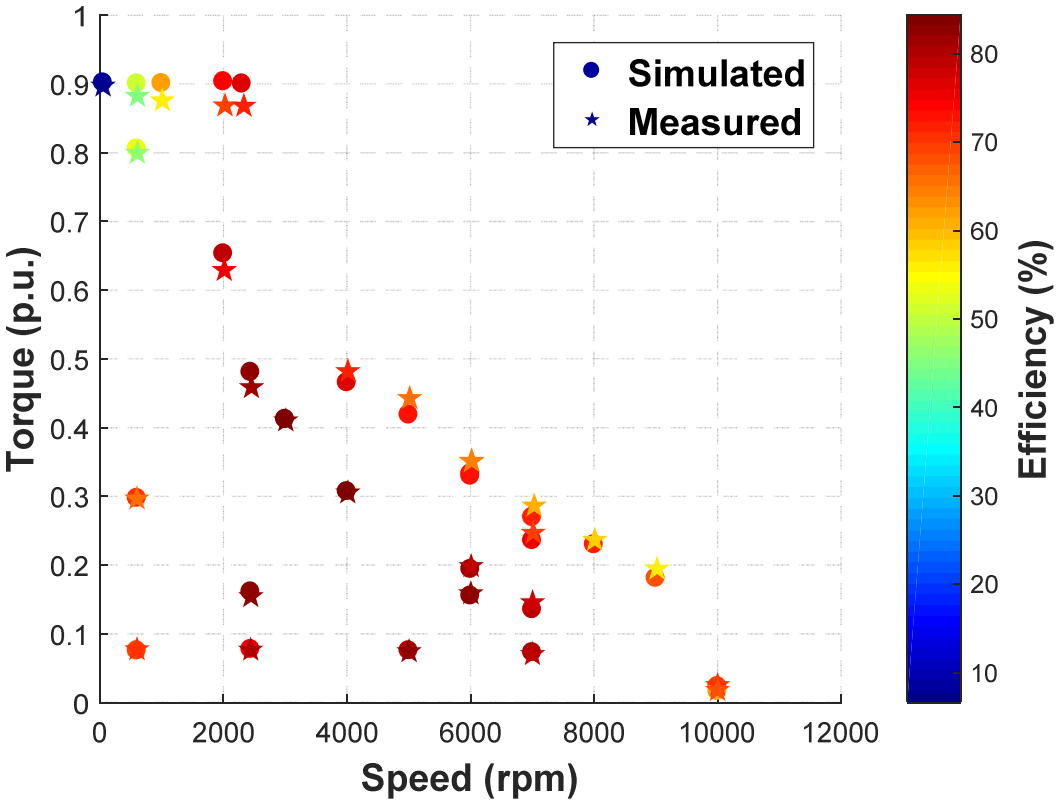


Fig. 5.13 Simulated and measured p.u. torque, speed and efficiency of the machine

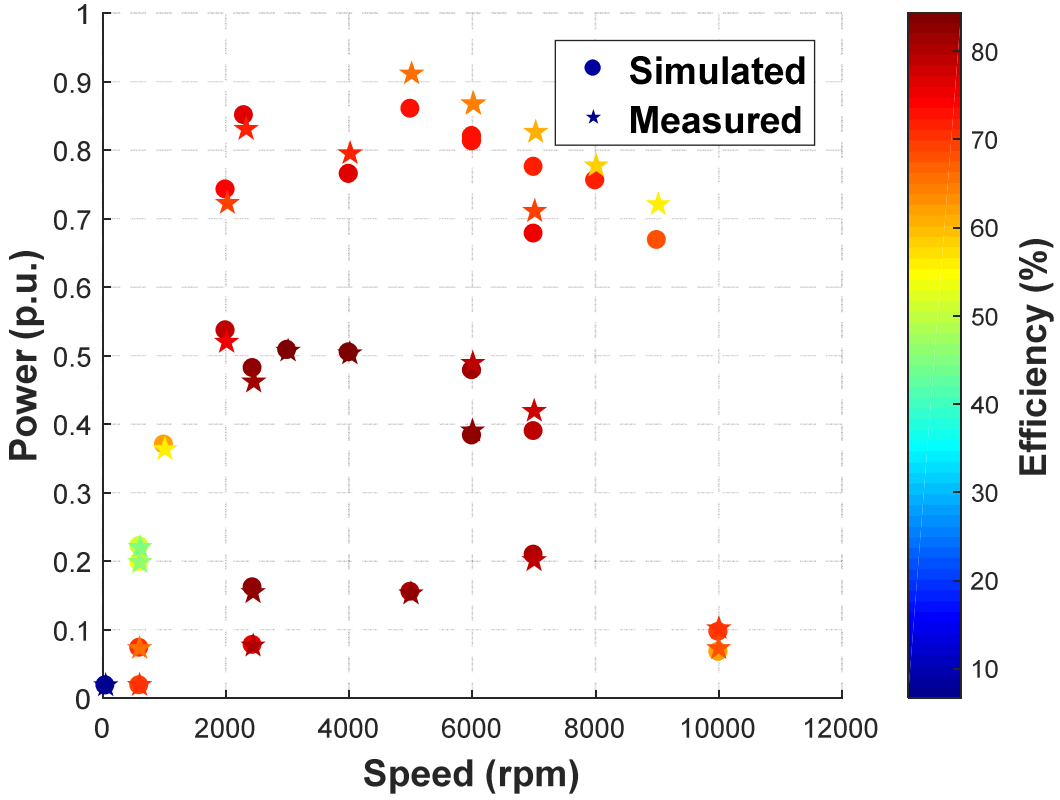


Fig. 5.14 Simulated and measured p.u. power, speed and efficiency of the machine

There is a maximum deviation of around 20-23 % in the simulated and measured efficiency. However, in 19 test points out of the total 29 test points, the deviation in efficiency is less than 10 %. This varying deviation in efficiency could be due to the assumptions in the calculated efficiency in the simulations. In fact, in this latter case, it is assumed that the converter efficiency is constant 95 % for the complete test. The stray load losses are also assumed to be constant and the calculated iron losses are based upon simple decomposition into hysteresis and eddy current loss model. Whereas during actual experimental testing, the converter losses depend upon the current level and switching strategy; and the stray load losses also vary according to the loading conditions.

The complete comprehensive experimental testing has helped in validating the new design and the performance results calculated by simulations. This facilitates in developing various other new models and designs for other specifications and later on with the help of experimental correction factors predict the future test results. Thus, the above good agreements in simulated and experimental results also substantiates that the machine which will be developed with recycled magnets would be able to deliver the performance as predicted by the simulated results. For this reason, it can be concluded that utilization of recycled magnets in claw-pole machines would result in reducing the carbon footprint by aiding in the reduction of mining activities to recover new PM materials, hence making the e-machine more ecologically sustainable.

## 5.4 Conclusion

It has been observed that the simulated and measured back EMF results correlate with each other with a maximum deviation of only 2 %. During the load test, the simulated and measured torque and power are in the range of 5-7 %, hence substantiating the proximity between design and experimental results. The deviation in simulated and measured efficiency is in the range of 5-23%, and this is mainly due to the assumptions present in simulated results viz. controller efficiency, iron losses and stray load losses.

# Conclusion

In today's world, the importance of developing reuse and recycle technologies cannot be over-emphasized. Changing climate and depleting natural resources propel the need for design concepts which can produce the traditional performance, albeit with reused or recycled raw materials. It is with this objective that the Project DEMETER was conceived to reduce the dependence on new mining of rare earth materials and developing technologies which enhance the reusability of these materials.

This thesis is the culmination of research work which was carried out with the main objective of developing a permanent magnet based claw-pole machine for automotive applications considering reuse and recyclability of magnets. Significant amount of literature was explored during the course of the research work and it has been observed that lot of work has been carried out on the design, analysis and experimental testing on claw-pole alternators. Various automotive original equipment manufacturers produce claw-pole machines as a motor-generator for micro/mild hybrid applications, but there is limited literature on design, analysis and testing of claw-pole machine as a motor-generator. Therefore, in this thesis the claw-pole machine is developed for a 48 V mild hybrid automotive application.

The numerical analysis of the claw-pole machine is quite rigorous and time-consuming due to the 3-D flux paths in the geometry. Due to this, geometric design optimization is a prolonged activity with numerous iterations. Hence, automation of the geometry modeling was achieved by utilizing variables and associated equations in the geometry editor of the numerical analysis software. Genetic algorithm was utilized for the design optimization of the machine so as to achieve maximum torque to magnet weight ratio. Various claw parameters and magnet dimensions were varied to achieve the above objective. It was observed that the new optimized claw-pole and magnets provide fairly the same torque as the original machine with at least 16 % reduction in magnet weight. This is a

substantial reduction as the machine would be developed in millions of quantities, hence a huge amount of cost savings.

In this research work two concepts have been developed and proposed for reuse and recyclability of magnets. First, the direct reuse concept i.e. easy assembly/disassembly of the rotor and magnets, so as to easily take out the magnets for direct reuse or recycle. Second, the direct recycle concept i.e. utilization of recycled magnets in the machine to achieve the desired performance. Weighted index of recycling and energy (WIRE) concept has also been developed and proposed to score the machine in terms of its recyclability. First index is dependent upon the standardization and cost taking material, assembly and disassembly into consideration and second index is dependent upon energy consumption taking drive cycle into consideration. Consequently, the results exhibit that:

- ✓ With the direct reuse concept, the magnets can easily be withdrawn out from the complete magnet slit without disassembling the complete rotor and then they can be sent for reuse or recycling.
- ✓ For the first part of WIRE index, the machine's score in all the categories for standardization section is above 78 % and the score for disassembly category in cost section is 74 %, hence favoring the machine design for easy assembly and disassembly.
- ✓ For the second part of WIRE index, the energy consumption of the machine in pure electric vehicle mode and hybrid electric vehicle mode for virgin and recycled magnets is almost the same i.e. the deviation is less than 0.5%. Thus, substantiating the use of recycled magnets in new claw-pole machines as they are ecologically sustainable due to the fact that they assist in reduced mining of new rare earth magnet materials.

The new optimized claw-poles with virgin magnets were fabricated and a prototype of the complete machine was developed for experimental testing. It has been observed that the simulated and measured back EMF results correlate with each other with a maximum deviation of only 2 %. During the load test, the simulated and measured torque and power are in the range of 5-7 %, hence

substantiating the proximity between design and experimental results. The deviation in simulated and measured efficiency is in the range of 5-23%, and this is mainly due to the assumptions present in simulated results viz. controller efficiency, iron losses and stray load losses.

Thus, the implementation of reuse and recycle concept of rare earth magnets in electro-mobility has been accomplished in this thesis and this initiates new prospects to expand the work for new electrical machines and complete system incorporation, so as to achieve the global goal of recyclability.

# Future work

As the research work carried out for this thesis was mainly concentrated upon reuse and recyclability of rare earth magnets in the claw-pole machine, a good amount of future work is possible which are listed below:

- Although the magnetic properties of the recycled magnets are measured experimentally in the lab; experimental testing of the claw-pole machine with recycled magnets would substantiate the direct recycle concept.
- The WIRE index could be improved by incorporating more information regarding manufacturing process, tools and quality requirements along with finer scaling for the scoring patterns.
- Design optimization of the claw-pole machine can be performed by taking the stator, stator winding, number of poles and number of phases into consideration. The objective function can be varied for different goals.
- The cartographic representation of the results viz. efficiency map, loss map, current map and voltage map can be improved by incorporating the converter losses, AC copper losses and analytical thermal models so as to achieve more accurate simulated results.
- A complete hybrid electric vehicle system could be developed for the evaluation of energy and fuel consumption of the machine for various hybrid configurations and automobiles.

# Appendix A1

# Geometry modelling in JMAG®

## A1.1 Geometry Editor Interface

Fig. A1.1 shows the main interface of the JMAG® Geometry Editor with various interface sections highlighted upon it like the model manager, toolbar, graphics window and status bar.

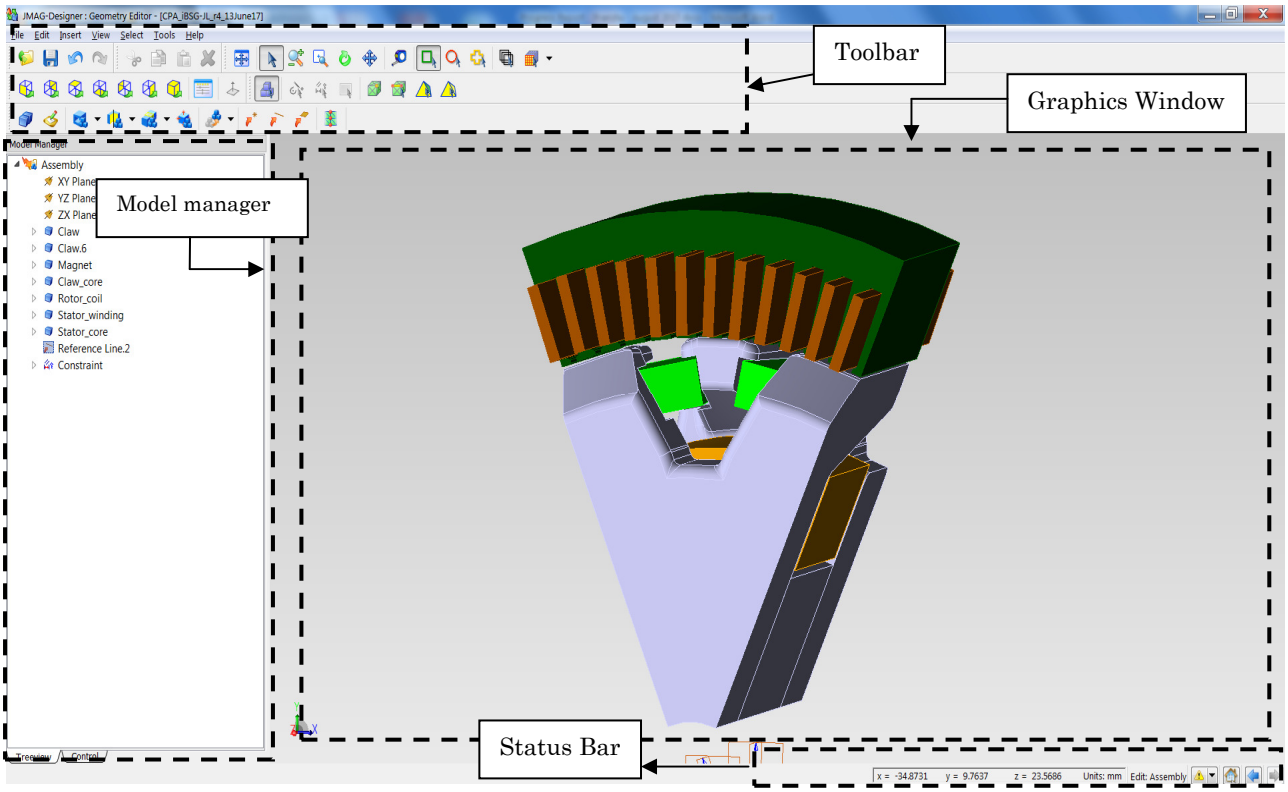


Fig. A1.1 JMAG® Geometry Editor interface

All the geometric operations like creation of 2-D and 3-D geometries, extrude, chamfer, boolean, reference point or line or plane, extrude cut, fillets, etc. are listed upon in the Model Manager, and hence all the information regarding the model generation is available in this tab.

Therefore, utilizing the various toolbar options and constraint feature of JMAG®, the complete geometry of the claw-pole machine was modelled, and all the parts are enlisted below along with the related figures.

## A1.2 Claw-poles

Fig. A1.2 shows the developed claw-poles modelled in JMAG® geometry editor. In the model manager it can observed that various operations like extrude, chamfer, boolean, fillets, etc. have been utilized to model the said topology.

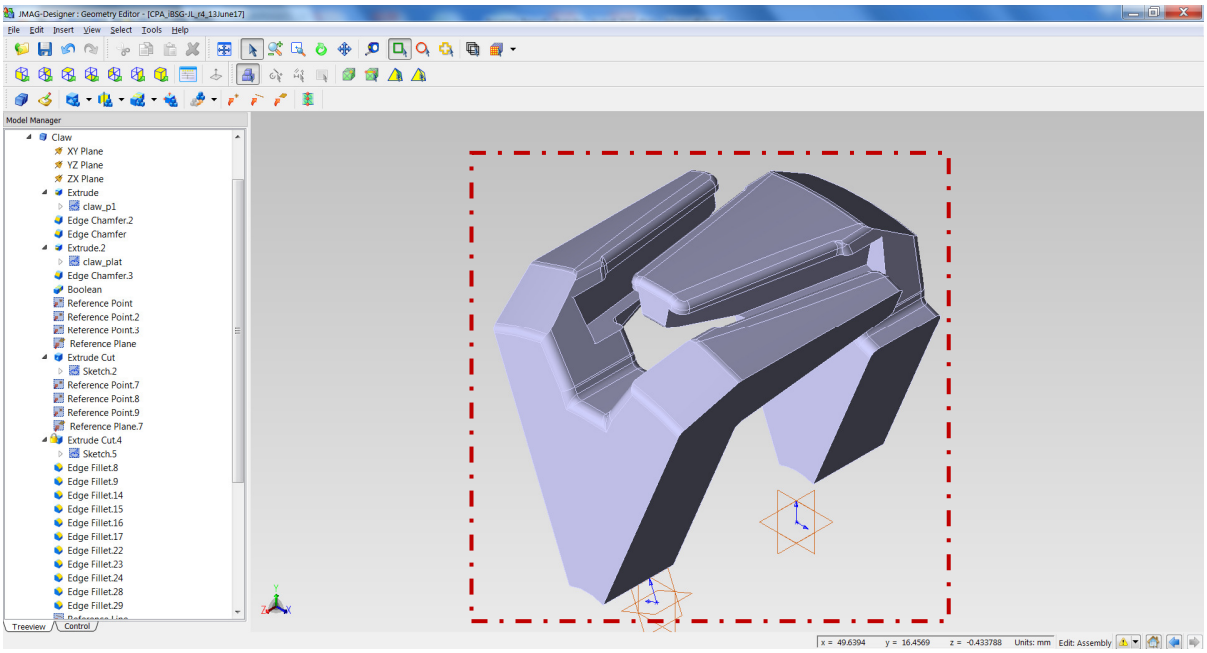


Fig. A1.2 Claw-poles of the machine in geometry editor

## A1.3 Permanent magnets

In Fig. A1.3, the highlighted section shows the two magnets modelled in the inter-claw region of the claw-poles.

## A1.4 Claw core and coil

In Fig. A1.4, the highlighted section shows the claw core and coil of the machine.

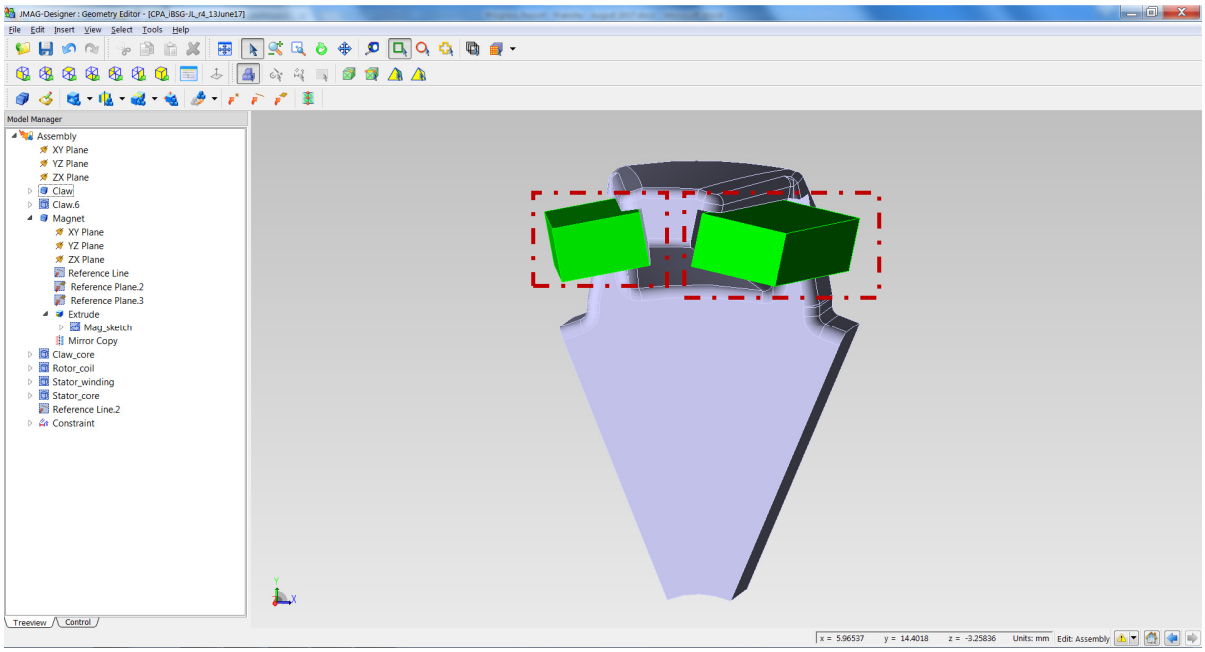


Fig. A1.3 Magnets along with one claw-pole of the machine in geometry editor

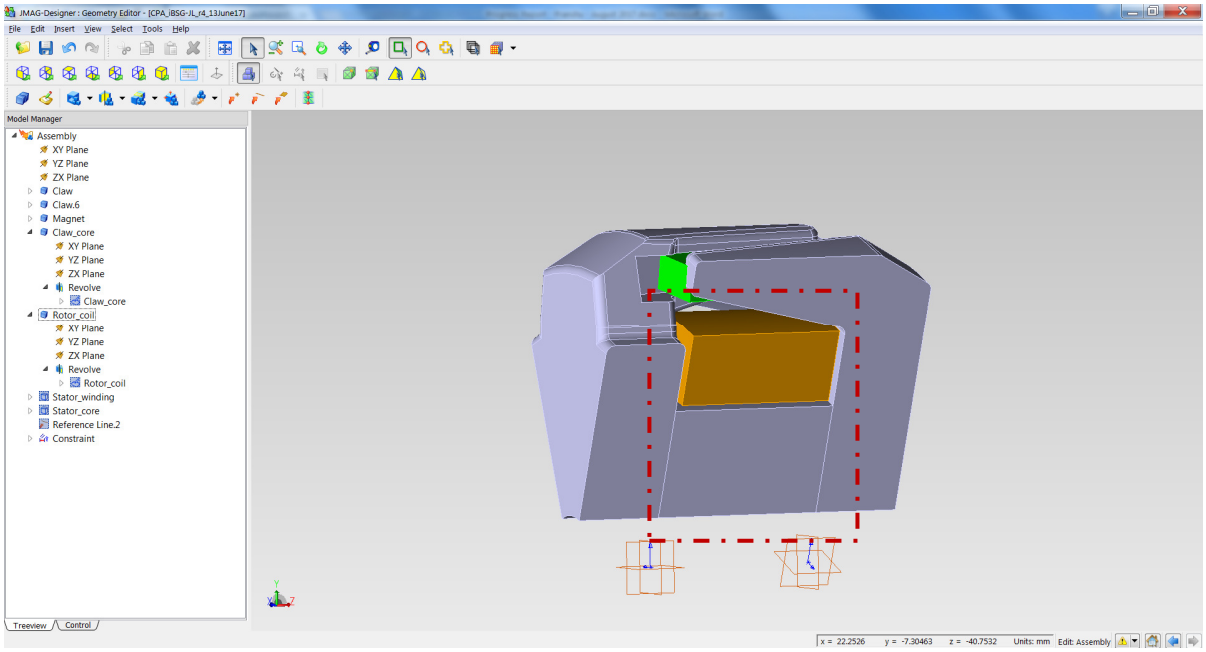


Fig. A1.4 Claw core & coil along with claw-poles & PMs in geometry editor

## A1. 5 Stator core and winding

In Fig. A1.5, the highlighted section shows the stator core and windings of the machine.

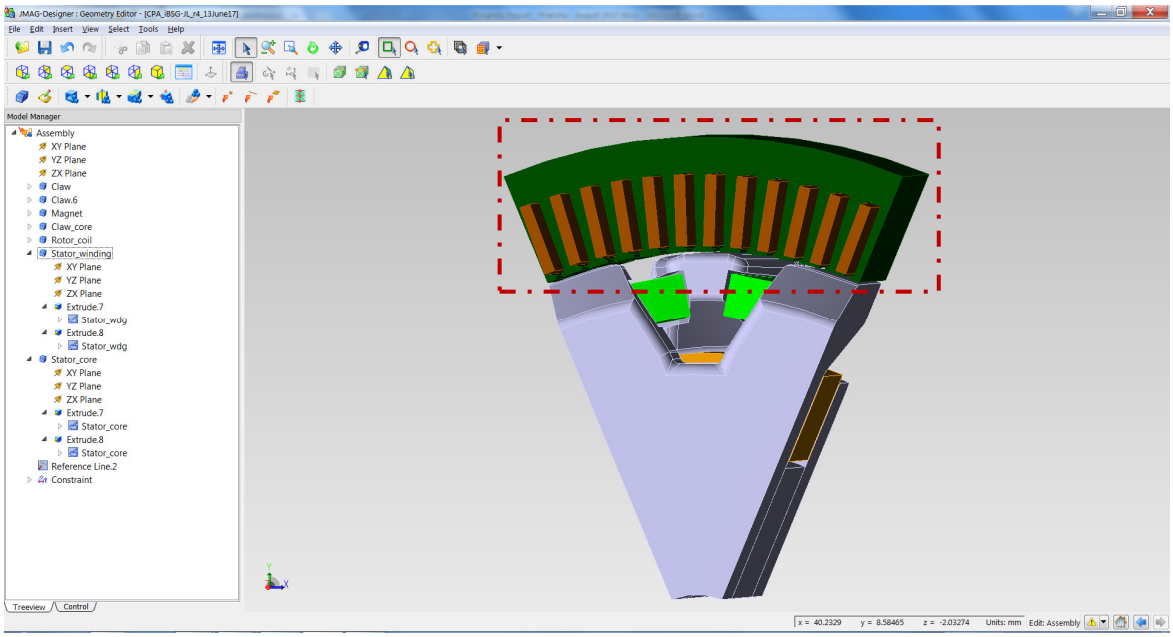


Fig. A1.5 Stator core and windings along with claw-poles, PMs, claw core and claw coil in geometry editor

## A1.6 Geometry Automation using equations and variables

During the process of geometry modelling of the machine in JMAG® geometry editor, geometry constraints were utilized along with variables and equations, so as to automate the geometry modelling of the claw-pole machine. This would help in easy and trouble free modelling of the machine with different value of various geometry parameters, without modelling the complete claw geometry again for a new parameter variation.

Total 79 equations were incorporated in the geometry editor model manager for various parameters like claw outer radius, claw inside radius, claw core radius, claw side plate thickness, distance between the claws, magnet dimensions, stator outside and inside radius, slot dimensions, etc. Figures A1.6 (a), (b) and (c) enlists all the equations and variables utilized for the creation of the geometry.

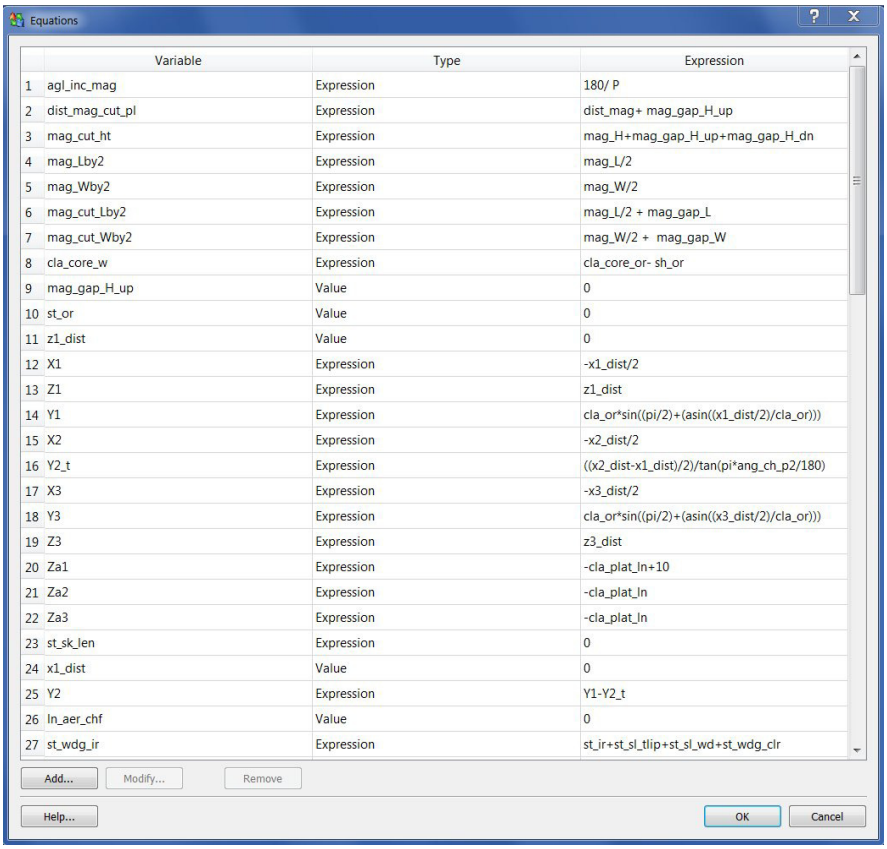


Fig. A1.6 (a) Equations and variables incorporated in JMAG® model manager

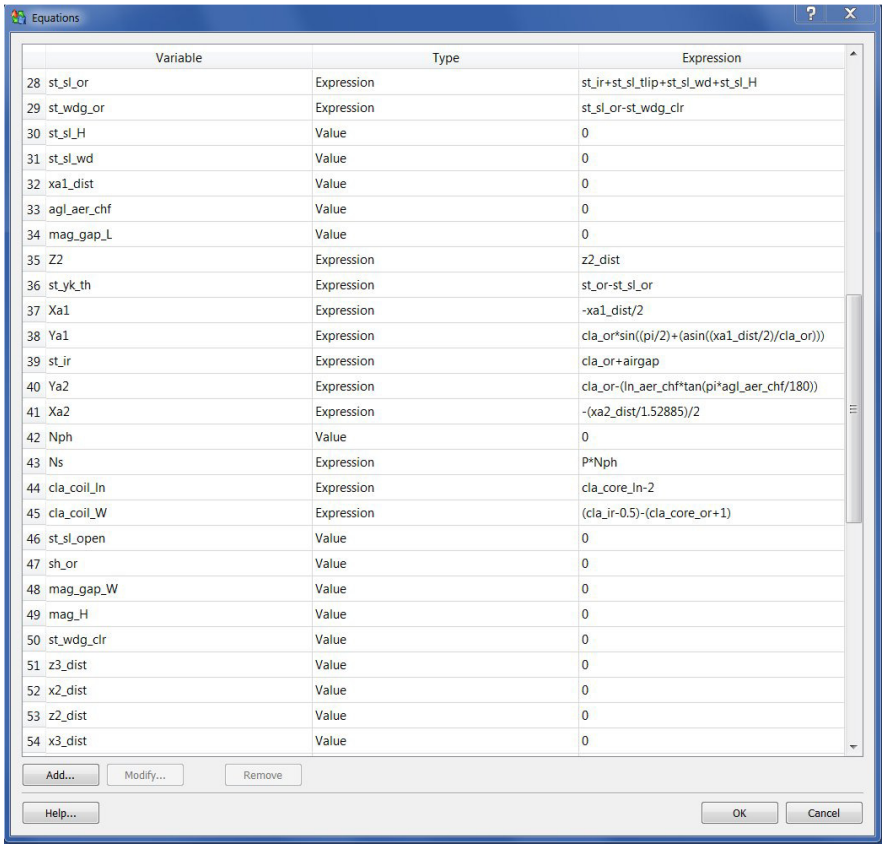


Fig. A1.6 (b) Equations and variables incorporated in JMAG® model manager

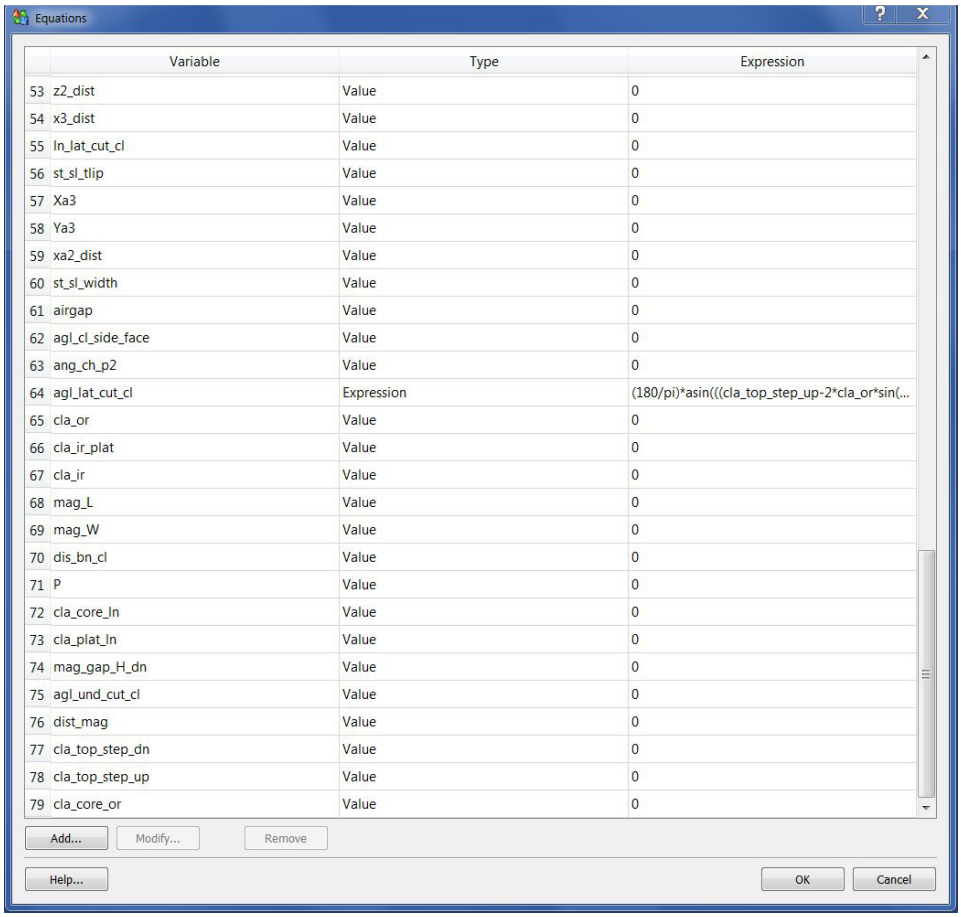


Fig. A1.6 (c) Equations and variables incorporated in JMAG® model manager

# Design & Comparison of a Conventional and Permanent Magnet based Claw-Pole Machine for Automotive Application

Pranshu Upadhayay[1,2], Afef Kedous-Lebouc[1], Lauric Garbuio[1], Jean-Claude Mipo[2], Jean-Marc Dubus[2]

[1]Univ. Grenoble Alpes, CNRS, Grenoble INP, G2Elab, F-38000 Grenoble, France, email: pranshulink@gmail.com
[2]Valeo - Equipements Electriques Moteur, 2 rue André Boulle, 94000 Créteil, France

***Abstract* — This paper presents the design and performance comparison of a conventional claw-pole machine with a permanent magnet based claw-pole machine for automotive application. The magnets are placed in the inter-claw region to decrease the leakage flux and to supply increased magnetic flux in the machine. It has been observed that with the addition of permanent magnets weighing only a few grams, there is a significant increment of more than 22% in output power of the machine. The geometric dimensions of magnets were also varied to verify their effects on performance and it has been observed that with the increase in magnet weight there is a non-linear increment in torque of the machine.**

***Keywords* — *claw-pole; permanent magnet; automotive; motor; alternator; finite element***

## I. INTRODUCTION

Power requirements for automotive applications are increasing day by day with the increase in comfort, safety and luxury in automobiles. With the increase in electric power for various automotive functions, there is also a need of higher fuel efficiency and the automotive applications are moving towards higher voltages of 48 V from erstwhile 12 V systems with increased output power requirements [1]. Generators of output power up to 5 kW and speeds up to 18,000 rpm for these applications are solely dominated, till date, by claw-pole type machines [2]. For mild-hybrid automotive applications, the conventional starter motor and alternator are replaced by an integrated motor-generator set generally known as integrated starter-generator (ISG). The ISG provides its two main functions: (a) starting the internal combustion engine (ICE) by running as inverter driven motor and (b) generating electric power during generator mode by controlled rectification through the inverter. Apart from the main functions, the ISG also provides an auxiliary function of automatic start-stop of ICE during idle standstill, therefore assisting in increased fuel efficiency [2]-[3].

This paper presents design and comparison of a conventional and permanent magnet (PM) based claw-pole machine for mild-hybrid automotive applications. In general, for design and analysis of a belt-driven ISG, the machine design is mainly focused on motoring mode and verifications are done for the generating mode. In this paper the design study for the peak output power of both the machines in motoring mode only has been carried out and comparison of torque vs. speed and power vs. speed for the entire speed range has been evaluated. The generating mode verifications are the scope of future work. It has been observed that the claw-pole machine with PMs provide more than 43% torque in constant torque region and in the range of 22-32% in field weakening or constant power region. The magnet volume is also modified by varying the dimensions of PMs, and it has been observed that there is increment in torque with the increase in magnet weight, but the relationship between torque and PM weight increment is non-linear.

## II. DESIGN AND ANALYSIS OF CLAW-POLE MACHINE USING FINITE ELEMENT METHOD

A conventional claw-pole machine consists of a 3-phase or multi-phase stator with windings and two forged claw-poles as rotor with ring shaped field coil, fed with direct current (DC) via slip rings and carbon brushes. Fig. 1 shows a conventional claw-pole machine [4]-[5]. In a PM based claw-pole machine, the PMs are placed in the inter-claw region i.e. between the two claw poles, to provide increased magnetic flux and reduce flux leakage between the consequent claw poles [6]-[7]. Research work has also demonstrated that by utilizing Iron-Cobalt (FeCo) soft magnetic materials in the claw-pole alternator, there could be considerable gain in the output performance of the machine [8]. But due to high price of FeCo material the research in [8] shows that by utilizing them only in the rotor core also provides output power increment with less rise in machine cost.

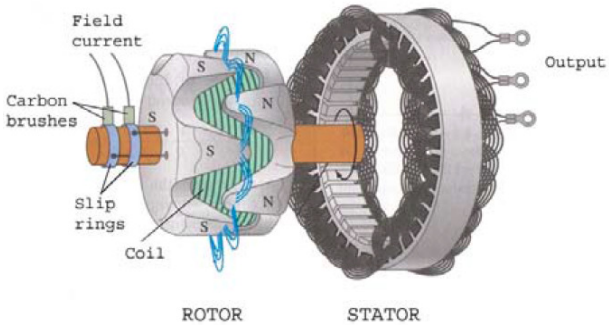


Fig. 1. Conventional claw-pole machine [4]

Literature shows [6] that, with the introduction of PMs in the inter-claw region, there is a torque boost of more than 40% for 42 V DC bus systems with peak output power of around 8 kW for generator operation. Therefore the research carried in this paper is focused on motoring mode during peak power

operation with 48 V DC bus mild-hybrid automotive system with speed range from 600 rpm to 18,000 rpm. The performance comparison of both the machines is carried out for the complete speed range taking into account the contant torque and power regions.

The design analysis of the machines has been carried out using classical electrical machine analysis theory using Park's transformation and later finite element (FE) analysis has been investigated to evaluate the machine performance at various speeds [9]. The *dq* transformation equations utilized are as follows [9]:

$$\begin{bmatrix} F_d \\ F_q \\ F_0 \end{bmatrix} = \frac{2}{3}\begin{bmatrix} \cos\theta & \cos\left(\theta-\frac{2\pi}{3}\right) & \cos\left(\theta+\frac{2\pi}{3}\right) \\ -\sin\theta & -\sin\left(\theta-\frac{2\pi}{3}\right) & -\sin\left(\theta+\frac{2\pi}{3}\right) \\ \frac{1}{2} & \frac{1}{2} & \frac{1}{2} \end{bmatrix}\begin{bmatrix} F_a \\ F_b \\ F_c \end{bmatrix} \quad (1)$$

where, variable $F$ can represent any of the following, i.e. electromotive force (EMF) $e$ in volts, current ($i$) in Amps and flux linkage ($\psi$) in Wb. The $\theta$ is angular displacement of the rotor $d$-axis w.r.t. the $a$-phase.
The voltage equations are as follows:

$$V_d = R_s i_d + \frac{d\psi_d}{dt} - \omega\psi_q \qquad V_q = R_s i_q + \frac{d\psi_q}{dt} + \omega\psi_d \quad (2)$$

where, $V$ is the voltage in volts, $R_s$ is the stator phase resistance in ohms and $\omega$ is the speed in rad/s.
Finally the torque in Nm is as below:

$$T = \frac{m}{2}P\left(\psi_d i_q - \psi_q i_d\right) \quad (3)$$

where, $m$ is the no. of phases and $P$ is the pole pair.

The FE models of both the machines were realized and performance parameters were evaluated by providing appropriate stator and field currents at various speeds for a rotor rotation of one 360° electrical [10]-[11]. In Fig. 2 & Fig. 3 we can observe the magnetic flux density vector plot of the claw-pole rotor without magnets and with magnets respectively. The permanent magnets used in the study are sintered NdFeB with remanent flux density (Br) of 1.3T and coercive field strength of 994 kA/m at 20º C.

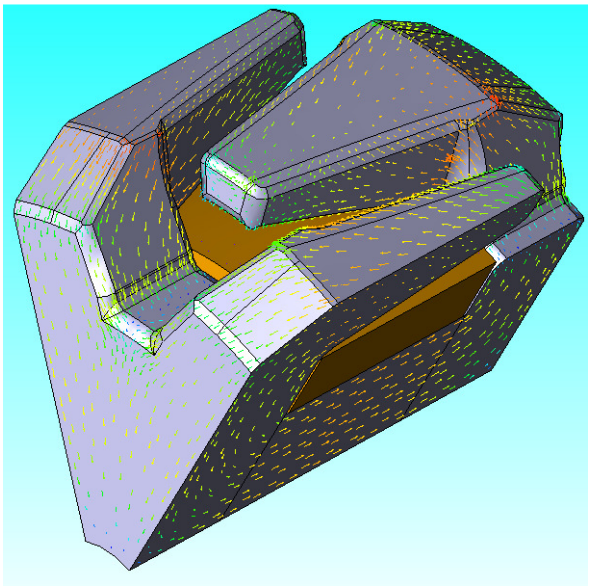

Fig. 2. Magnetic flux density vector plot of claw-pole rotor without magnets

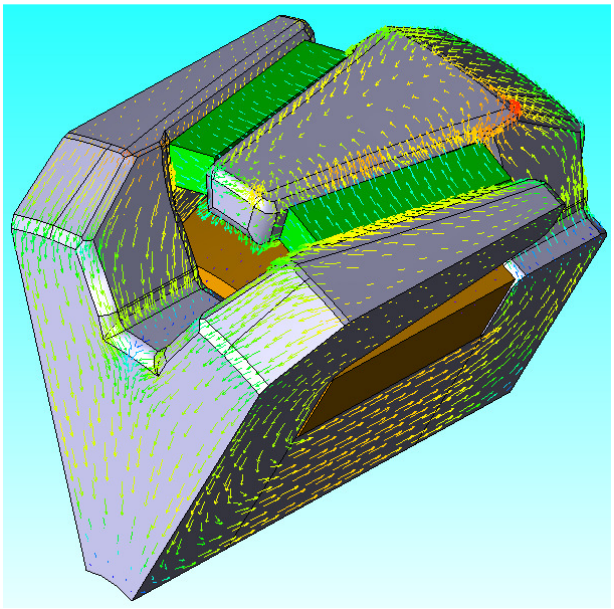

Fig. 3. Magnetic flux density vector plot of claw-pole rotor with magnets

## III. Simulation Results and Comparison

To obtain the complete torque vs. speed and power vs. speed curve for claw-pole machine, it is very important to optimize the stator current, field current and current angle, so as to obtain the constant torque and power region without exceeding the voltage limit of 48V DC. Multi-objective genetic algorithm methodology was adopted for performance evaluation in the complete speed range.

The objective functions in this analysis were:

(i) To maximize the torque.
(ii) To limit the voltage at 48 V DC.

The optimized d-axis current ($I_d$), q-axis current ($I_q$) and field current ($I_f$) are obtained as a result of the optimization convergence; and this process is repeated for different value of speeds so as to obtain the complete torque vs. speed and power vs. speed curve [12]-[13].

Fig. 4 and Fig. 5 shows the torque vs. speed and power vs. speed curves for both the machines respectively. The results thereafter are calculated in per unit (p.u.) method so as to have quick and straightforward comparison of performance. It can be observed from Fig. 4, in the constant torque region, if 1 p.u. torque is obtained for machine without magnet, then over 1.43p.u. torque is obtained for machine with magnets. Therefore this is an increment of more than 43%. In the constant power region it can be observed that this value reduces, however, it is still in the range of 22-32% increased torque as compared to a machine without magnets. Similarly, it can be observed from Fig. 5 that in the constant power region there is a gain of minimum 22% and maximum 45% in the output power of the machine with magnets as compared to machine without magnets.

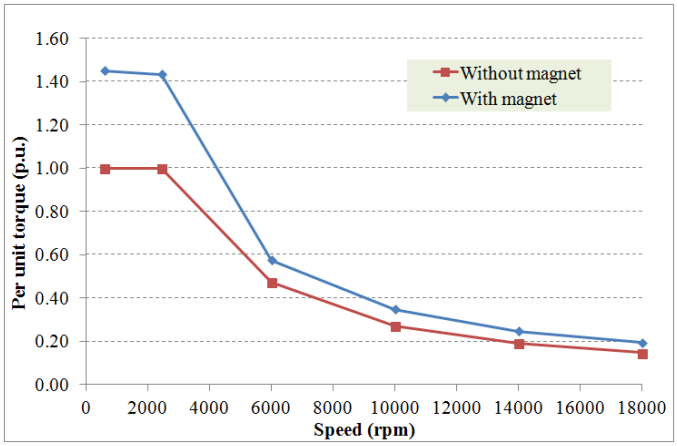


Fig. 4. Torque vs. speed curve for both the machines

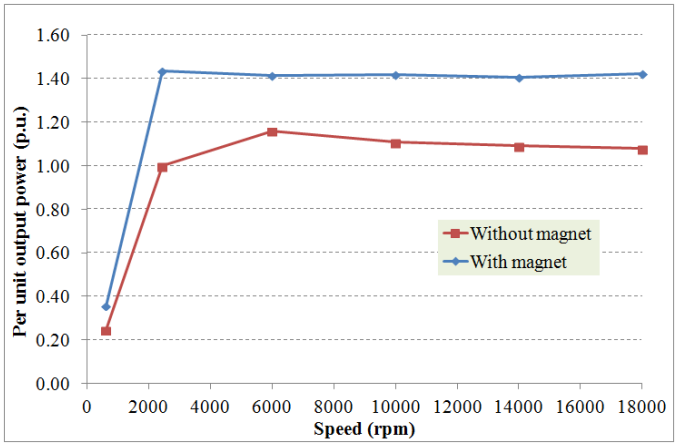


Fig. 5. Power vs. speed curve for both the machines

The objective of this paper is to observe improvements solely due to magnet placement; therefore, the geometry optimization of the claw-poles with magnet is the subject matter of future work. The weight of one PM is 5.64g; hence the total weight of sixteen PMs in the machine with magnets is only 90g. As a result it can be observed that there is a substantial enhancement of more than 22% in the output power of the machine with an addition of only 90g of sixteen magnets.

## IV. Effect of Magnet Weight Variation on the Performance

In the following section, effect of variation in magnet weight on the performance of the machine has been evaluated. In section III we observed that with the introduction of PMs in the claw-pole machine there is a notable increment in the output torque of the machine. Therefore, this provided the motivation to investigate the effect on torque of the machine with change in PM weight. As the percentage gain in torque is highest at low speed of 600 rpm, the following studies are carried out by varying the magnet dimensions and calculating the torque at low speed for each case and observing the effects on performance of the machine. Fig. 6 depicts the width, height and length of the magnets, which are varied to obtain different magnet weights.

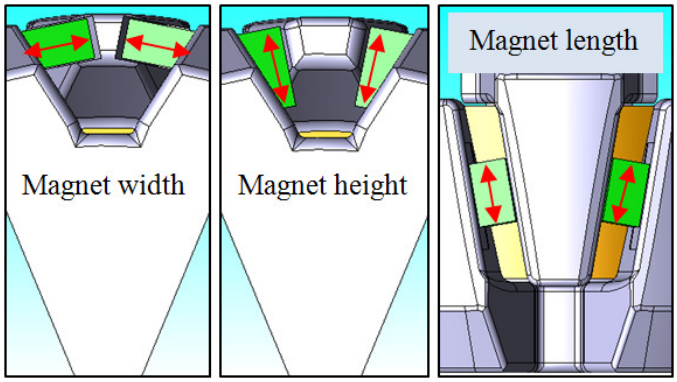


Fig. 6. The width, height and length of magnet utilized for varying the PM weight

### A. *Magnet width variation*

As the first step, the width of the PM was varied to change the weight of PM and observe the consequent effects on the low speed torque of the machine. Here on, torque of 1 p.u. value refers to the base condition of 90g of magnet weight and hence the PM width is increased thereafter till the maximum limit of manufacturing tolerances is achieved. Fig. 7 shows the variation of p.u. torque as a function of PM weight by changing the magnet width. It is observed that the torque increases approximately till the weight of PM is 168g and then reduces till the weight of PM is 184g. This is due to the fact that after a certain value of PM width the claw-pole fingers saturate and subsequently there is an overall reduction of flux in the air gap, hence the torque reduces. It can also be observed that there is 5.45% increase in torque from minimum to maximum value by changing the PM width; however there is 103.4% increment in magnet weight from minimum to maximum, hence depicting non-linear relationship between the increase of torque and weight.

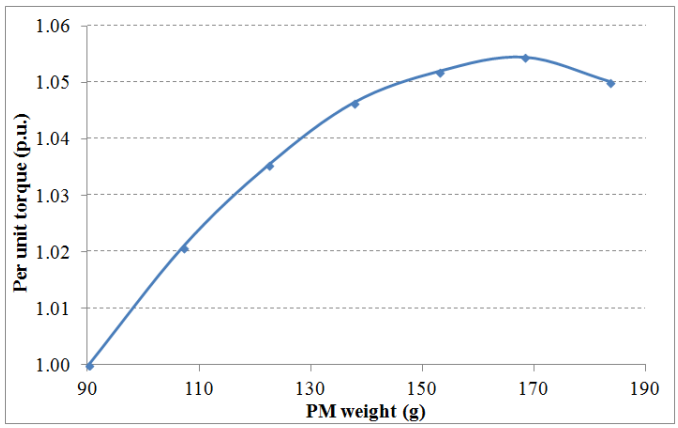


Fig. 7. Variation of torque as a function of PM weight by changing the magnet width

### B. *Magnet height variation*

As a second step, the height of the PM was varied to change the weight of PM and observe the consequent effect on the low speed torque of the machine. In this case also the torque of 1

p.u. value refers to the base condition of 90g of magnet weight and hence the PM height is increased from a minimum to a maximum limit till manufacturing tolerances is achieved. Fig. 8 shows the variation of p.u. torque as a function of PM weight by changing the magnet height. Here, it is observed that the torque increases in a polynomial order with increase in PM weight from 54g to 181g. Hence, illustrating that from minimum to maximum value there is an increment in torque of 34% with a large rise in PM weight of 233%.

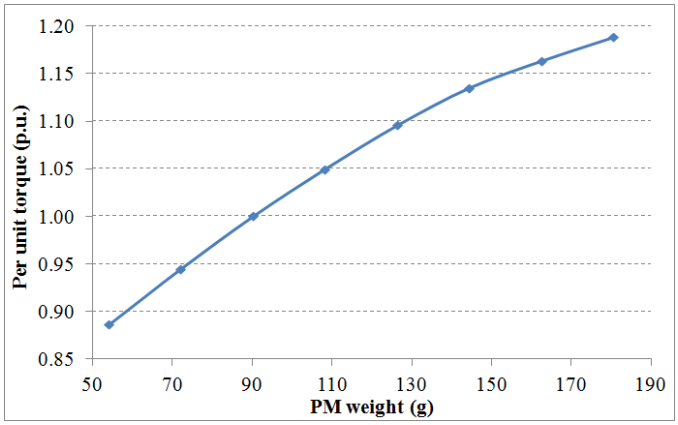


Fig. 8. Variation of torque as a function of PM weight by changing the magnet height

### C. *Magnet length variation*

The length of the PM was varied as the third step to change the weight of PM and observe the consequent effect on the low speed torque of the machine. Similarly in this case the torque of 1 p.u. value refers to the base condition of 90g of magnet weight and hence the PM length is increased from a minimum to a maximum limit till manufacturing tolerances is achieved. Fig. 9 shows the variation of p.u. torque as a function of PM weight by changing the magnet length. Here also it can be observed that the torque increases in a polynomial order with increase in PM weight from 36g to 144g. Therefore, this also shows that the torque increases by 36% from minimum to maximum value, although with a significant rise of almost 300% in PM weight.

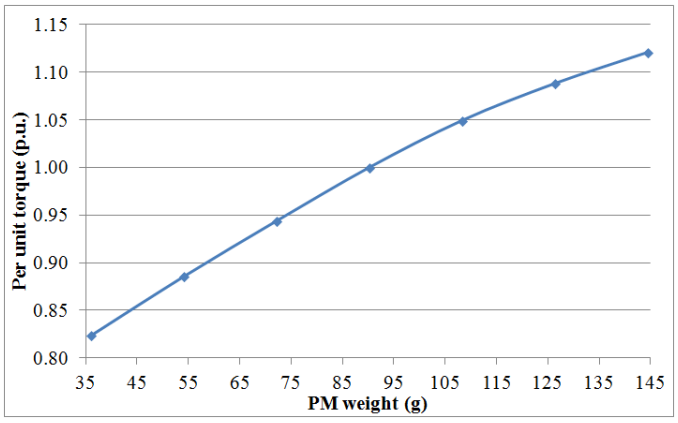


Fig. 9. Variation of torque as a function of PM weight by changing the magnet length

Thus, in continuation to the above three cases; one more scenario is considered where the PM width, height and length are altogether set up to their maximum value. This is done to finally observe the effect on low speed torque by placing maximum PM weight in the machine. Table I shows the total PM weight and p.u. torque of the claw-pole machine with magnets for base model and model with maximum PM width, length and height. It can be observed that the PM weight is increased from 90g to 511g from base model to maximum PM width, length and height model respectively, which translates into 467.78% increment in PM weight. Whereas, the torque is increased from 1 p.u. to 1.39 p.u. from base model to maximum PM width, length and height model respectively, and this translates into 39.35% rise in torque.

TABLE I. COMPARISON OF PM WEIGHT AND P.U. TORQUE BETWEEN BASE MODEL AND MAXIMUM PM WIDTH, LENGTH AND HEIGHT MODEL

| | **Total PM weight (g)** | **Torque (p.u.)** |
|---|---|---|
| **PM model - base** | 90 | 1.00 |
| **PM model - maximum width, length & height of PMs** | 511 | 1.39 |
| **Percentage (%)** | 467.78 | 39.35 |

As a result, from all the above cases it can be observed that the percentage augmentation in torque is comparatively smaller than the percentage increase in PM weight, hence representing non-linear relationship between PM weight and torque increment. This is primarily due to the geometry of claw-pole machine and PM placements in it, since the main role of PM is to reduce leakage flux and assist main flux produced by the rotor DC coil. Thus, optimization of magnet weight with respect to optimum performance of machine is one of the important design criteria in claw-pole machines.

## V. CONCLUSION

In this paper it has be illustrated that there is a considerable torque and power boost of more than 43% in constant torque region and around 22-32% in the constant power region with the introduction of PMs in the inter-claw region of the claw-pole machine. With the placement of only 90g of total magnet weight in the machine we perceive a considerable gain in torque, hence improving output power of the claw-pole machine. This translates into significant power to weight amplification of the machine which is one of the main advantages for mild-hybrid automotive application. It has also been observed that because of claw-pole geometry of the rotor and PM placements in inter-claw region; large PM weight increment transforms into small percentage rise in torque of the machine, thus corresponding to a non-linear correlation between PM weight and torque.

## ACKNOWLEDGMENT

The research leading to these results has received funding from European Community's Horizon 2020 Programme ([H2020/2014-2019)] under Grant Agreement no. 674973 (MSCA-ETN DEMETER). This publication reflects only the author's view, exempting the Community from any liability. Project website: http://etn-demeter.eu/.

## REFERENCES


[1] I. G. Kassakian, H.-C. Wolf, J. M. Miller, and C.J. Hurton, "Automotive electrical systems circa 2005", IEEE Spectrum, 33, 8, August, 1996.

[2] Ion Boldea, Variable Speed Generators, CRC Press, Taylor & Francis Group, 2006, pp. 6-1 – 6-34.

[3] I. A. Viorel, L. Szabó, L. Löwenstein, C. Stet, "Integrated Starter-Generators For Automotive Applications", Acta Electrotehnica, vol. 45, no. 3, pp. 255–260, 2004.

[4] D. M. Whaley, W. L. Soong, and N. Ertugrul, "Extracting more power from the Lundell car alternator", Australian Univ. Power Eng. conf., AUPEC, Brisbane, Australia, 2004.

[5] D. J. Perreault and V. Caliskan, "A new design for automotive alternators", IEEE/SAE International Congress on Transportation Electronics (Convergence), SAE paper 2000-01-C084, 2000.

[6] Lucian Tutelea, Dragos Ursu, Ion Boldea, Sorin Agarlita, "IPM Claw-Pole Alternator System for more Vehicle Braking Energy Recuperation", Journal of Electrical Engineering, vol. 12, no. 3, pp. 211-220, 2012.

[7] S. Kuppers and G. Henneberger, "Numerical procedures for the calculation and design of automotive alternators", IEEE Transactions on Magnetics, vol. 33, no. 2, pp. 2022-2025, March 1997.

[8] Sylvain Perez, "Contribution au dimensionnement optimal d'alternateur à griffes sans aimant - Apport des alliages FeCo", Thèse de doctorat, INP Grenoble, 2014.

[9] R. H. Park, "Two Reaction Theory of Synchronous Machines: Generalized Method of Analysis-Part I", Transactions of the American Institute of Electrical Engineers, vol. 48, no. 3, pp. 716-727, July 1929.

[10] Constantin Stoica, Luminita Mirela Constantinescu, Emilian Lefter and Bogdan Enache, "Computation of the Characteristics of a Claw Pole Alternator through the Finite Element Method", 2013 International Conference on Electronics, Computers and Artificial Intelligence (ECAI), pp. 1-4, June 2013.

[11] G. Henneberger, S. Kuppers and I. Ramesohl, "Numerical Calculation, Simulation and Design Optimisation of Claw Pole Alternators for Automotive Application", IEE Colloquium on Machines for Automotive Applications (Digest No. 1996/166), pp. 3/1-3/5, November 1996.

[12] A. Bruyere, T. Henneron, E. Semai1, F. Locment, A. Bouscayrol, J. M. Dubus, and J. C. Mipo, "Identification of a 7-phase claw-pole starter-alternator for a micro-hybrid automotive application", 18th International Conference on Electrical Machines (ICEM), 2008, pp. 1-6, September 2008.

[13] A. Bruyere, E. Semail, A. Bouscayrol, F. Locment, J. M. Dubus, and J. C. Mipo, "Modeling and Control of a seven-phase Claw-Pole Integrated Starter Alternator for Micro-hybrid Automotive Applications", IEEE Vehicle Power and Propulsion Conference (VPPC), 2008, pp. 1-6, September 2008.

# Appendix A3

## Mechanical Simulations of the Claw-poles

Along with the geometry optimization of the claw-poles as described in Chapter 3 Section 3.4, the mechanical simulations were also carried out to evaluate the Von mises stress and radial displacement of the claw-poles at maximum speeds of 20,000 and 22,000 rpm respectively. Linear static analysis was carried out using Catia V5 software by the mechanical simulation team of Valeo.

The detailed report for the analysis can be observed in below section. It can be observed that after three iterations of minor geometry modifications, the claw-pole design was defined safe for operation at high speeds in terms of maximum Von mises stress @ 20,000 rpm and radial displacement at claw finger tip for non shrinking claw pole @ 22,000 rpm.

| OBJECTIVE | |
|---|---|
| The aim of this study is to perform the mechanical analysis for Claw pole and to study the stress and deformation at 20000 rpm and 22000 rpm respectively. | Demeter_Claw pole centrifugation V3 (following 1608.18 request) |

| | |
|---|---|
| TYPE OF APPLICATION | Non Shrinking |
| TYPE OF MODEL | Half Model |
| | PRESS TO CONFIRM |

| S.No | SUMMARY |
|---|---|
| 1> | At maximum speed of 20000RPM the maximum stress level is below the limit of 521MPa and below the ultimate limit of 570MPa. |
| 2> | At the maximum speed of 22000RPM, the maximum displacement obtained at the clawpole is below the limiting value 0.197. |
| 3> | **From the above points - we can conclude that, the design is considered to be SAFE for Non Shrinking type .** |

| Model | Max- Von mises Stress @ 20000rpm (MPa) | | Displacement at horn tip for Non Shrinking claw pole@ 22000(mm) | | Status |
|---|---|---|---|---|---|
| | Front | Rear | Front | Rear | |
| Demeter_Claw pole centrifugation V3 | 446 | 504 | 0.153 | 0.173 | O.K |
| SIMULATION REFERENCE LIMIT | 521 | | 0.197 | | TEKNO 2004 |

Assembly considered for Simulation

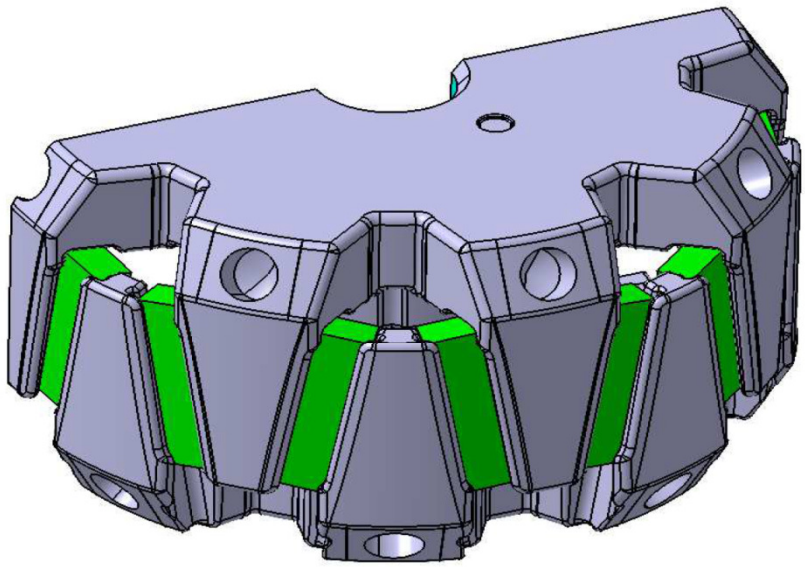

**OBSERVATION:**

**The design modification in the 3rd version is effective and the observations in stuctural point of view is listed below :**

**• The Von mises stress value for rear clawpole is reduced by 181 MPa whereas for front clawpole it is reduced 84 MPa as compared to the 2nd iteration, and the design is found to be SAFE .**

**• The increase in clawpole horn root fillet thickness is effective and the maximum stress value observed in this region is not spreading more than 2 element.**

**• Also, the radial displacement values are within the limits and the design modification is effective in this regard.**

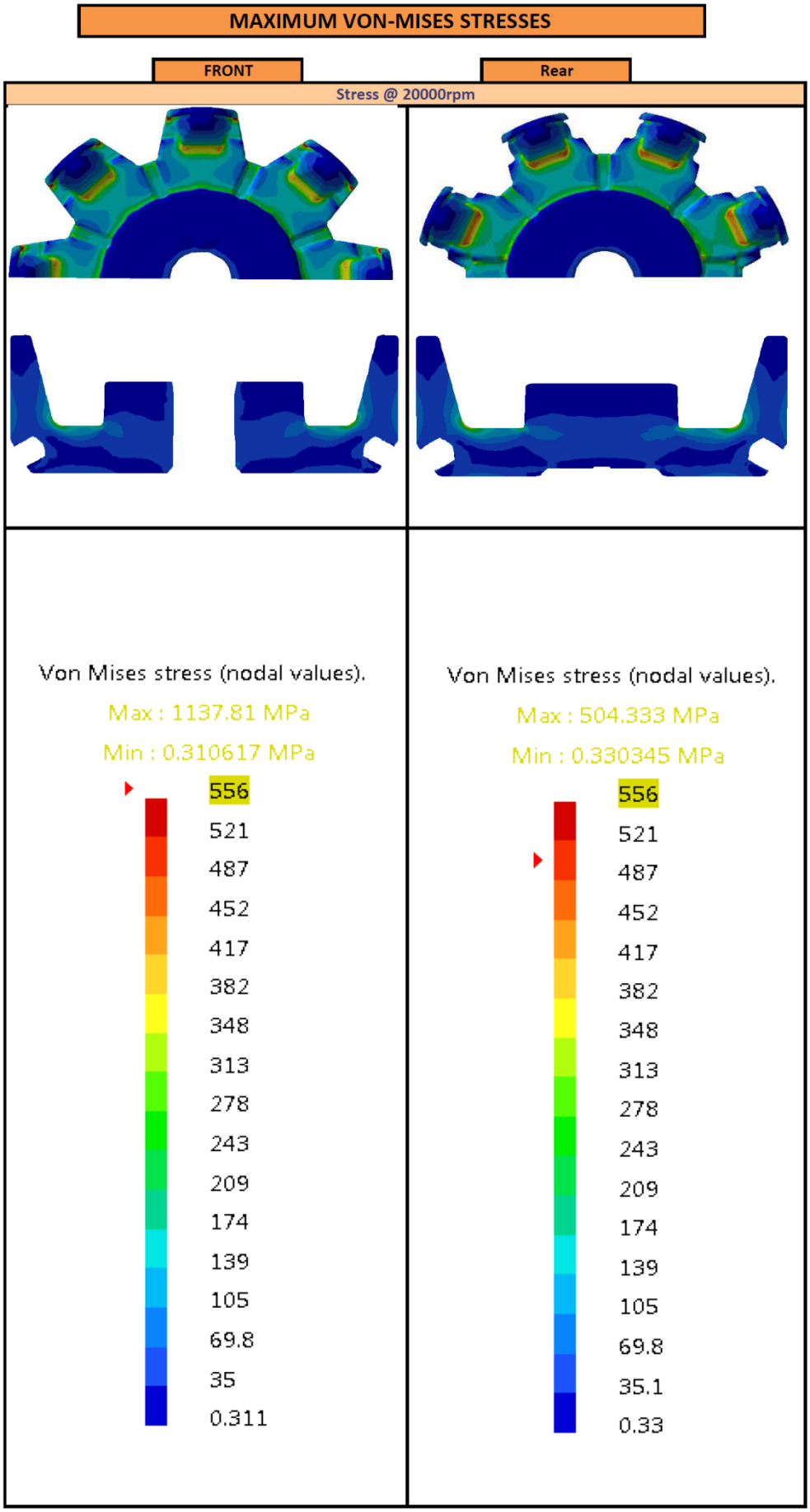
MAXIMUM VON-MISES STRESSES
FRONT
Rear
Stress @ 20000rpm
Von Mises stress (nodal values).
Max : 1137.81 MPa
Min : 0.310617 MPa
556
521
487
452
417
382
348
313
278
243
209
174
139
105
69.8
35
0.311
Von Mises stress (nodal values).
Max : 504.333 MPa
Min : 0.330345 MPa
556
521
487
452
417
382
348
313
278
243
209
174
139
105
69.8
35.1
0.33

| Von-Mises stress at 20,000 RPM in Front Clawpole (MPa) | |
|---|---|
| 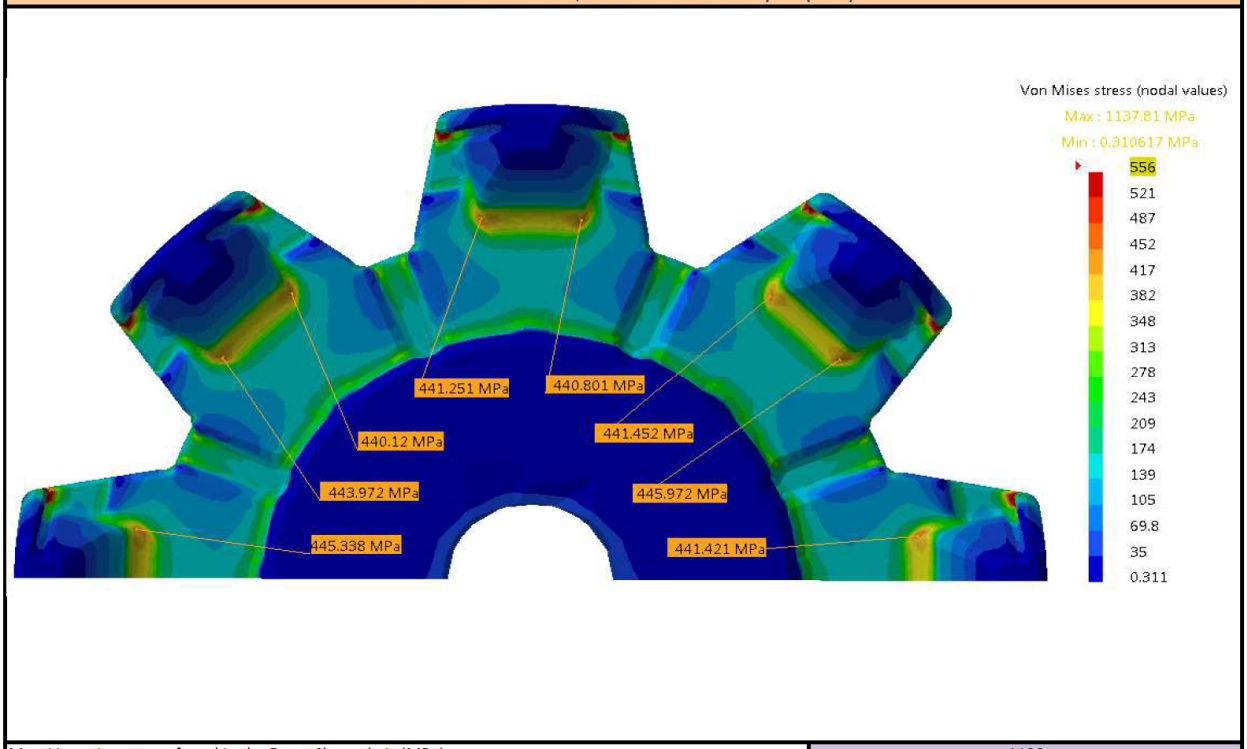 | |
| Max. Von mises stress found in the Front Clawpole is (MPa) | 1138 |
| Max. Von mises stress found in the critical location of Front Clawpole (fillet regions) is (MPa) | 446 |
| REMARKS: | Max. stress in the critical region is below the limit of 521 MPa |

| Von-Mises stress at 20,000 RPM in Rear Clawpole (MPa) | |
|---|---|
| 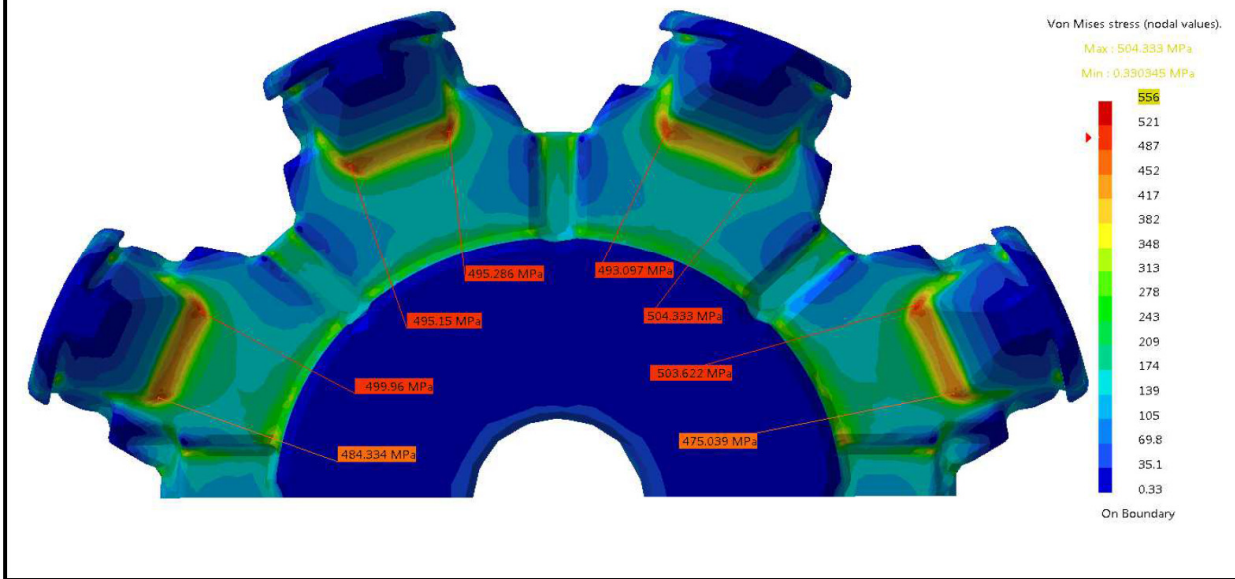 | |
| Max. Von mises stress found in the Rear Clawpole is (MPa) | 504 |
| Max. Von mises stress found in the critical location of Rear Clawpole (fillet regions) is (MPa) | 504 |
| REMARKS: | Max. stress in the critical region is below the limit of 521 MPa |

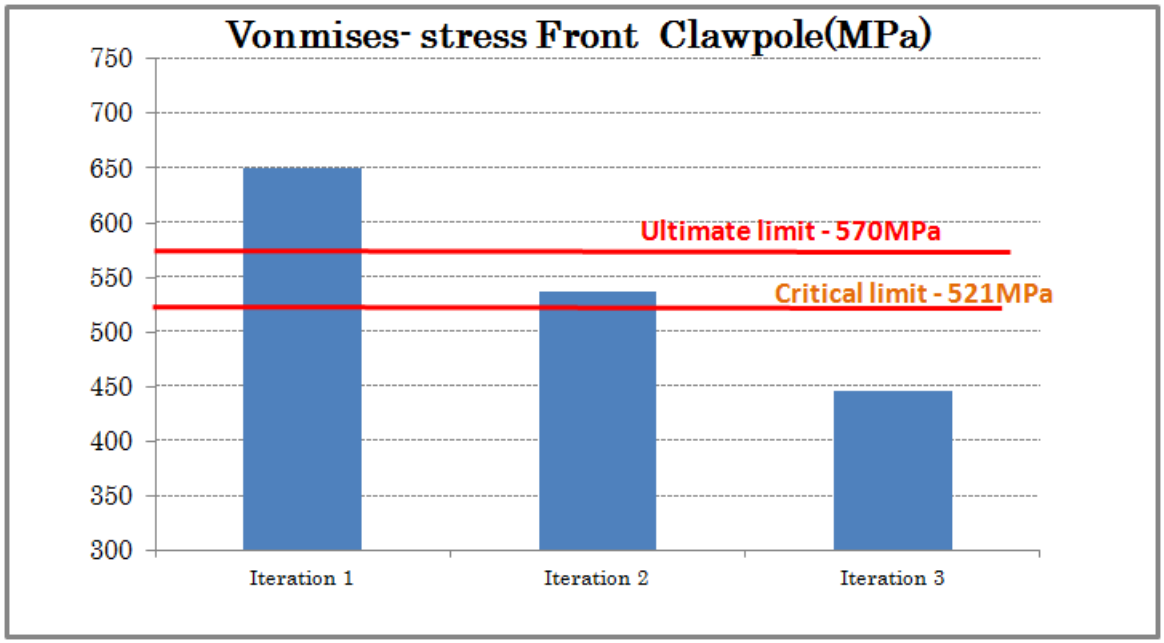
Vonmises- stress Front Clawpole(MPa)
750
700
650
600
550
500
450
400
350
300
Ultimate limit - 570MPa
Critical limit - 521MPa
Iteration 1
Iteration 2
Iteration 3

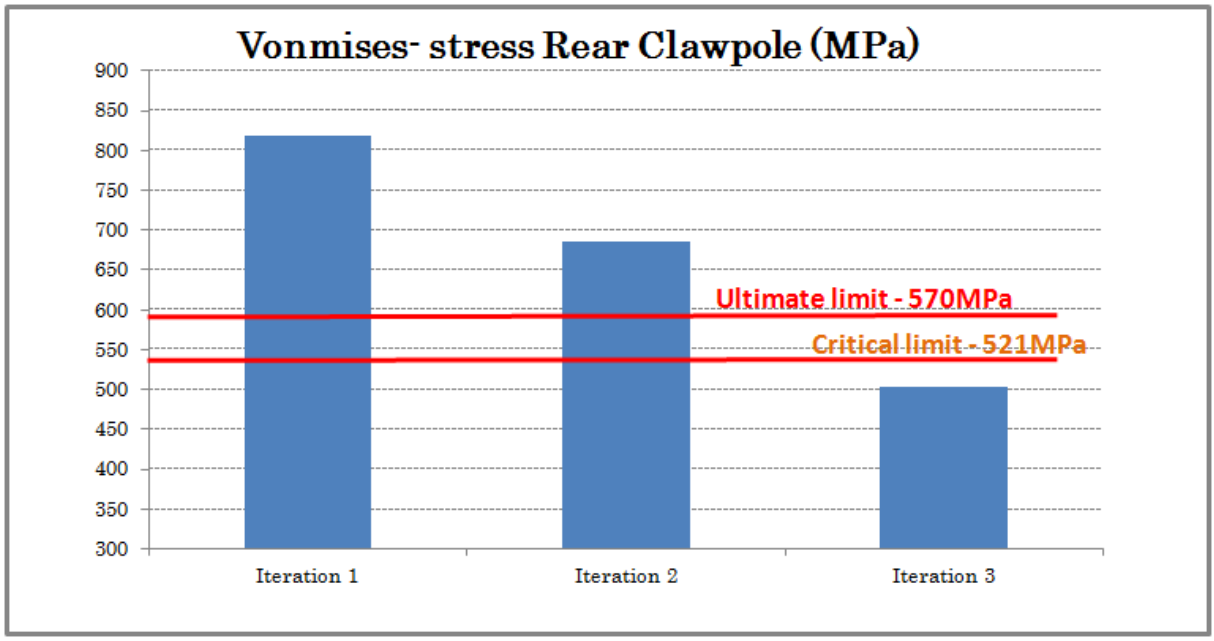
Vonmises- stress Rear Clawpole (MPa)
900
850
800
750
700
650
600
550
500
450
400
350
300
Ultimate limit - 570MPa
Critical limit - 521MPa
Iteration 1
Iteration 2
Iteration 3

# MAXIMUM RADIAL DISPLACEMENT

## Displacement @ 22000rpm

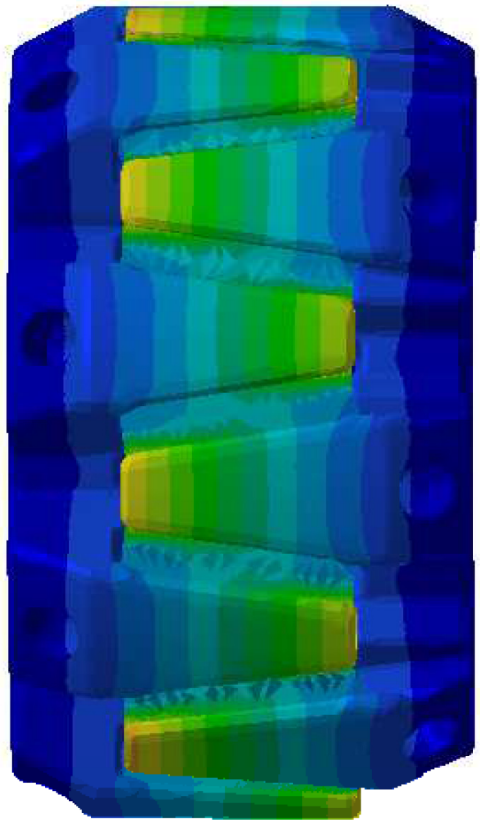

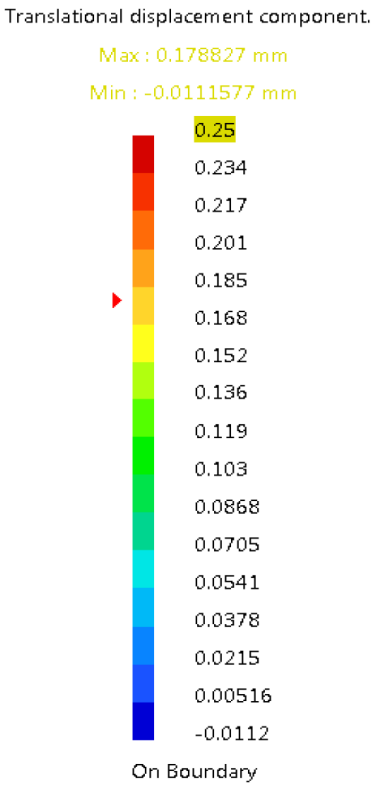

| Radial Deformation at 22,000 RPM in Front Clawpole (mm) | |
|---|---|
| 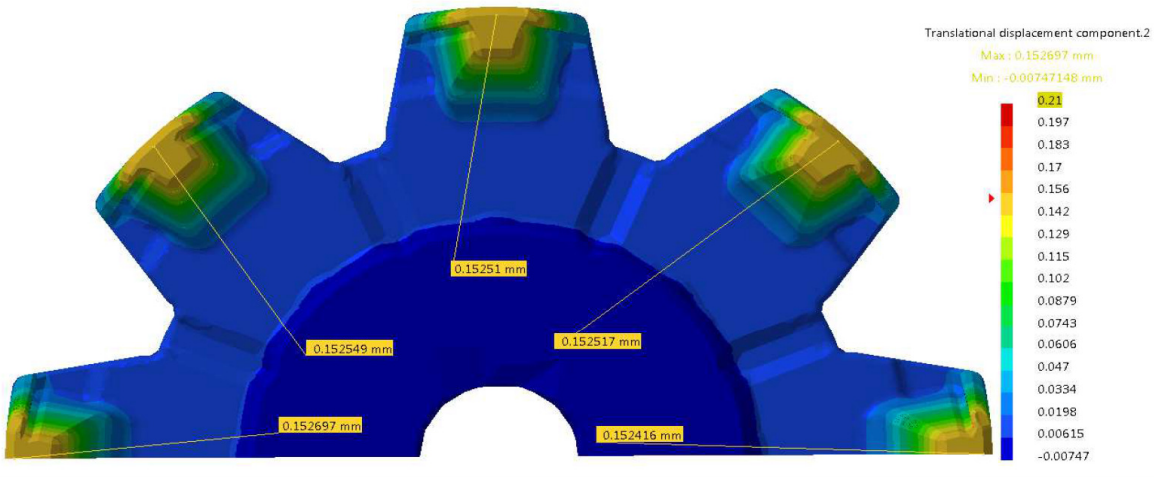 | |
| Maximum radial displacement observed in front claw pole is (mm) | 0.153 |
| REMARKS: | Max. radial displacement observed in the critical regions of front claw pole is 0.153 mm which is less than the limit of 0.197 mm non shrinking. |

| Radial Deformation at 22,000 RPM in Rear Clawpole (mm) | |
|---|---|
| 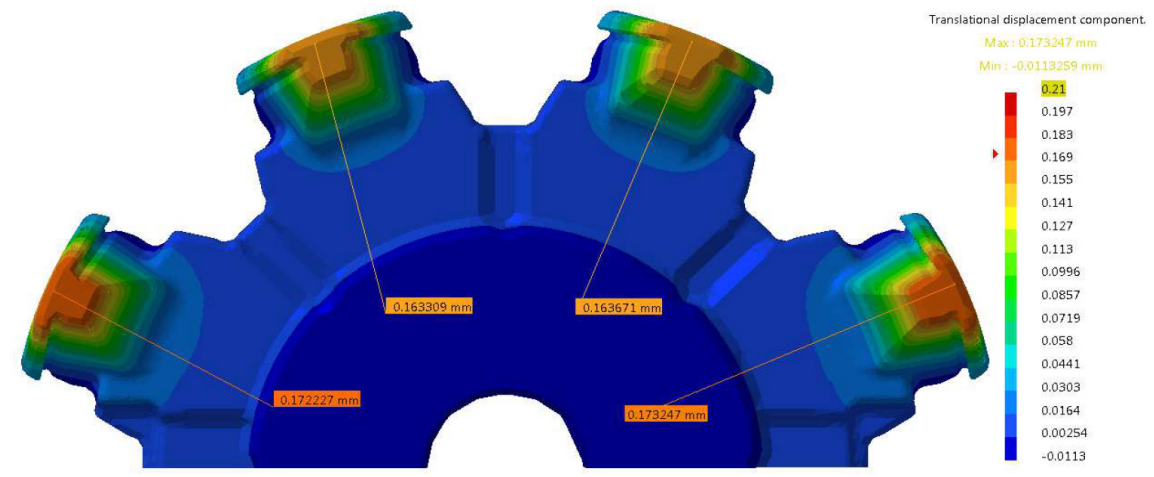 | |
| Maximum radial displacement observed in rear claw pole is (mm) | 0.173 |
| REMARKS: | Max. radial displacement observed in the critical regions of rear claw pole is 0.173 mm which is less than the limit of 0.197 mm non shrinking. |

# Publications

[1] *Pranshu Upadhayay*, Afef Kedous-Lebouc, Lauric Garbuio, Jean-Claude Mipo, Jean-Marc Dubus, "Design & Comparison of a Conventional and Permanent Magnet based Claw-Pole Machine for Automotive Application", 15th International Conference on Electrical Machines, Drives and Power Systems (ELMA), pp. 1-5, June 2017.

[2] *Pranshu Upadhayay*, Afef Kedous-Lebouc, Lauric Garbuio, Jean-Claude Mipo, Jean-Marc Dubus, "Impact of Claw-Pole Geometry Variations on the Performance of Machine used in Automotive Application", 43rd Annual Conference of the IEEE Industrial Electronics Society (IECON), pp. 1990-1995, October/November 2017.

[3] A. G. Gonzalez, A. K. Jha, Z. Li, *P. Upadhayay*, and P. Rasmussen, "Validation of Efficiency Maps of an Outer Rotor Surface Mounted Permanent Magnet Machine for Evaluation of Recyclability of Magnets," IEEE International Magnetics conference (INTERMAG), pp. 1-6, April 2018.

[4] A. K. Jha, Z. Li, A. Garcia, *P. Upadhayay*, P. O. Rasmussen, A. Kedous-Lebouc, and L. Garbuio, "Weighted index of recycling and energy (WIRE) cost for Motors in electric vehicles," International Symposium on Power Electronics, Electrical Drives, Automation and Motion (SPEEDAM), pp. 407-412, June 2018.

[5] *Pranshu Upadhayay*, A. G. Garcia, Z. Li, A. K. Jha, P. O. Rasmussen, A. K. Lebouc, J. C. Mipo, "Evaluation of Energy Cost Index for an Electric Vehicle Motor over a particular Drive Cycle with Recycled Magnet Concept", 23rd International Conference on Electrical Machines (ICEM), pp. 738-744, September 2018.

[6] *Pranshu Upadhayay*, Muhammad Awais, Afef Kedous-Lebouc, Lauric Garbuio, Malik Degri, Allan Walton, Jean-Claude Mipo, Jean-Marc Dubus, "Applicability of Direct Reuse and Recycled Rare Earth Magnets in Electro-mobility", 7th International Conference on Renewable Energy Research & Applications (ICRERA), pp. 846-852, October 2018.

# References


[1] Report on critical raw materials for the European Union – 2011. Available : http://ec.europa.eu/growth/sectors/raw-materials/specific-interest/critical_en

[2] Report on critical raw materials for the European Union – 2014. Available : http://ec.europa.eu/growth/sectors/raw-materials/specific-interest/critical_en

[3] Report on critical raw materials for the European Union – 2017. Available : http://ec.europa.eu/growth/sectors/raw-materials/specific-interest/critical_en

[4] Study on the review of the list of Critical Raw Materials - Criticality Assessments, pp. 14.
Available : https://publications.europa.eu/en/publication-detail/-/publication/08fdab5f-9766-11e7-b92d-01aa75ed71a1/language-en

[5] Periodic table and rare earth elements. Available : http://www.tre-ag.com/commodities/what-are-rare-earths.aspx?sc_lang=en

[6] Electric motors for various functions in an automobile. Available : http://erean.eu/wordpress/the-magnets-of-the-green-cars-motors/

[7] Evolution of PMs with respect to their energy product. Available : http://www.magnetnrg.com/pm-hisory.html

[8] European Training Network for the Design and Recycling of Rare-Earth Permanent Magnet Motors and Generators in Hybrid and Full Electric Vehicles (DEMETER). http://etn-demeter.eu/

[9] A Report by the European Rare Earths Competency Network (ERECON), Strengthening the European rare earths supply-chain: - Challenges and policy options. Available: https://ec.europa.eu/growth/sectors/raw-materials/specific-interest/erecon_en

[10] L. Guzzella & A. Sciarretta, "Vehicle Propulsion Systems: Introduction to Modeling and Optimization", 2nd Edition, Springer-Verlag Berlin Heidelberg, 2013.

[11] D. Cundev, G. Stefanov & V. Sarac, "Configurations of hybrid-electric cars propulsion systems", UGD Repository, 2012.

[12] C. C. Chan, "The state of the art of electric, hybrid, and fuel cell vehicles", Proceedings of the IEEE, vol. 95, no. 4, pp. 704 - 718, April 2007.

[13] M. Ehsani, Y. Gao & A. Emadi, "Modern Electric, Hybrid Electric, and Fuel Cell Vehicles: Fundamentals, Theory, and Design", 2nd Edition, CRC Press, Taylor & Francis Group, 2009.

[14] O. Coppin & N. Devienne, "L'électrification et composants 48V des fonctions moteur et auxiliaires", Valeo Powertrain & Thermal Systems presentation. Available: https://pole-moveo.org/wp-content/uploads/2016/12/MOVEO-Pres_Valeo_DAS_Octobre_2016-V02.pdf

[15] I. G. Kassakian, H. C. Wolf, J. M. Miller, & C. J. Hurton, "Automotive electrical systems circa 2005", IEEE Spectrum, 33, 8, August, 1996.

[16] Ion Boldea, "Variable Speed Generators", Chapter 6, CRC Press, Taylor & Francis Group, 2006.

[17] A. Ibala, R. Rebhi & A. Masmoudi, "MEC-Based Modelling of Claw Pole Machines: Application to Automotive and Wind Generating Systems", International Journal of Renewable Energy Research, IJRER, vol. 1, no. 3, pp.1-8, 2011.

[18] L. Tutelea, D. Ursu, I. Boldea & S. Agarlita, "IPM Claw-Pole Alternator System for more Vehicle Braking Energy Recuperation", Journal of Electrical Engineering, vol. 12, no. 3, pp. 211-220, 2012.

[19] S. Kuppers & G. Henneberger, "Numerical procedures for the calculation and design of automotive alternators", IEEE Transactions on Magnetics, vol. 33, no. 2, pp. 2022-2025, March 1997.

[20] Sylvain Perez, "Contribution au dimensionnement optimal d'alternateur à griffes sans aimant - Apport des alliages FeCo", Thèse de doctorat, INP Grenoble, 2014.

[21] Laurent Albert, "Modélisation et optimisation des alternateurs à griffes - Application au domaine automobile", Thèse de doctorat, INP Grenoble, 2004.

[22] T. Teratani, K. Kuramochi, H. Nakao, T. Tachibana, K. Yagi, & S. Abou, "Development of Toyota mild hybrid systems (THS-M) with 42 V power net", IEEE International Electric Machines and Drives Conference 2003 (IEMDC 2003), Madison, WI, 2003.

[23] K. H. Huebner, D. L. Dewhirst, D. E. Smith & Ted G. Byrom, "The Finite Element Method for Engineers", John Wiley & Sons, 2008.

[24] V. Ostovic, J. M. Miller, V. K. Garg, R. D. Schultz & S. H. Swales, "A Magnetic-Equivalent-Circuit-Based Performance Computation of a Lundell Alternator", IEEE Transactions on Industry Applications, vol. 35, no. 4, pp. 825-830, July/August 1999.

[25] Mamy Rakotova, "Un modèle opérationnel complet pour l'alternateur à griffes dans le domaine automobile", Thèse de doctorat, Cachan, 1996.

[26] M. Hecquet & P. Brochet, "Modeling of a Claw-pole Alternator using Permeance Network Coupled with Electric Circuits", IEEE Transactions on Magnetics, vol. 31, no. 3, pp. 2131-2134, May 1995.

[27] H. Bai, S. D. Pekarek, J. Tichenor, W. Eversman, D. J. Buening, G. R. Holbrook, M. L. Hull, R. J. Krefta, & Steven J. Shields, "Analytical Derivation of a Coupled-Circuit Model of a Claw-Pole Alternator With Concentrated Stator Windings", IEEE Transactions on Energy Conversion, vol. 17, no. 1, pp. 32-38, March 2002.

[28] S. H. Lee, S. O. Kwon, J. J. Lee, & J. P. Hong, "Characteristic Analysis of Claw-Pole Machine Using Improved Equivalent Magnetic Circuit", IEEE Transactions on Magnetics, vol. 45, no. 10, pp. 4570-4573, October 2009.

[29] H. C. Lai & D. Rodger, "Three-dimensional finite element modelling of a claw pole type car alternator", 2nd International Conference on Power Electronics, Machines and Drives (PEMD), pp. 447-451, March 2004.

[30] G. Henneberger & S. Kuppers, "Field Calculation and Dynamic Simulation of a Claw-Pole Alternator", 7th International Conference on Electrical Machines and Drives, 1995 (Conf. Publ. No. 412), pp. 286-290, September 1995.

[31] G. Henneberger, S. Kuppers & I. Ramesohl, "Numerical Calculation, Simulation and Design Optimisation of Claw Pole Alternators for

Automotive Application", IEE Colloquium on Machines for Automotive Applications (Digest No. 1996/166), pp. 3/1-3/5, November 1996.

[32] C. Kaehler & G. Henneberger, "Transient 3-D FEM Computation of Eddy-Current Losses in the Rotor of a Claw-Pole Alternator", IEEE Transactions on Magnetics, vol. 40, no. 2, pp. 1362-1365, March 2004.

[33] C. Barz & C. Oprea, "Study of electromagnetic field in claw-poles alternator", Annals of Faculty Engineering Hunedoara – International Journal of Engineering, Tome IX (Year 2011), fascicule 3, (ISSN 1584 – 2673).

[34] C. Barz, C. Oprea and F. Dragan, "Numerical modeling of claw-poles alternator", Carpathian Journal of Electronic and Computer Engineering, vol. 5, no. 1, pp. 9-12, 2012.

[35] L. Melcesu, M. Cistelecan, O. Craiu & M. Popescu, "Numerical Analysis of Claw Pole Synchronous Machine with Hybrid Contactless Excitation", Przegląd Elektrotechniczny Journal, R. 88, nr 7b/2012, pp. 106-109, 2012.

[36] Y. Kuroda, M. Morita, M. Hazeyama, M. Azuma & M. Inoue, "Improvement of a claw pole motor using additional ferrite magnets for hybrid electric vehicles", 15th International Conference on Electrical Machines (ICEM), pp. 1-3, September 2010.

[37] J. Cros & P. Viarouge, "New structures of polyphase claw-pole machines", IEEE Transactions on Industry Applications, vol. 40, no. 1, pp. 113-120, February 2004.

[38] S. O. Kwon, J. Y. Lee, J. P. Hong, Y. S. Lim & Y. Hur, "Practical Analysis Method for Claw-pole type Generator using 2-Dimensional Equivalent Model", IEEE International Conference on Electric Machines and Drives, pp. 1-4, May 2005.

[39] F. Zhang, H. Bai, H. P. Gruenberger & E. Nolle, "Comparative Study on Claw Pole Electrical Machine with Different Structure", 2nd IEEE Conference on Industrial Electronics and Applications, pp. 1-5, May 2007.

[40] C. Liu, J. Zhu, Y. Wang, Y. Guo & G. Lei, "Comparison of Claw-Pole Machines with Different Rotor Structures", IEEE Transactions on Magnetics, vol. 51, no. 11, pp. 1-4, November 2015.

[41] R. Rebhi, A. Ibala, & A. Masmoudi, "Hybrid Excited Claw Pole Alternators: Attempt to Satisfy the Increasing Power Need on Board", 17th International Conference on Electrical Machines and Systems (ICEMS), pp. 1-5, October 2014.

[42] M. Wardach, "Hybrid excited claw pole generator with skewed and non-skewed permanent magnets", Open Physics, vol. 15, no. 1, pp. 902-906, November 2017.

[43] G. Dajaku, B. Lehner, Xh. Dajaku, A. Pretzer, & D. Gerling, "Hybrid Excited Claw Pole Rotor for High Power Density Automotive Alternators", 22nd International Conference on Electrical Machines (ICEM), pp. 2536-2543, September 2016.

[44] K. Binnemans, P. T. Jones, B. Blanpain, T. V. Gerven, Y. Yang, A. Walton & M. Buchert, "Recycling of rare earths: a critical review", Journal of Cleaner Production, vol. 51, no. 15, pp. 1-22, July 2013.

[45] Y. Yang, A. Walton, R. Sheridan, K. Güth, R. Gauß, O. Gutfleisch, M. Buchert, B. M. Steenari, T. V. Gerven, P. T. Jones & K. Binnemans, "REE Recovery from End-of-Life NdFeB Permanent Magnet Scrap: A Critical Review", Journal of Sustainable Metallurgy, vol. 3, no. 1, pp. 122-149, March 2017.

[46] M. Zakotnik, I. R. Harris, A. J. Williams, "Possible methods of recycling NdFeB-type sintered magnets using the HD/degassing process", Journal of Alloys and Compounds, vol. 450, no. 1-2, pp. 525-531, February 2008.

[47] M. Zakotnik, I. R. Harris, A. J. Williams, "Multiple recycling of NdFeB-type sintered magnets", Journal of Alloys and Compounds, vol. 469, no. 1-2, pp. 314-321, February 2009.

[48] R. S. Sheridan, R. Sillitoe, M. Zakotnik, I. R. Harris, & A. J. Williams, "Anisotropic powder from sintered NdFeB magnets by the HDDR processing route", Journal of Magnetism and Magnetic Materials, vol. 324, no. 1, pp. 63-67, Jan. 2012.

[49] R .S. Sheridan, A. J. Williams, I. R. Harris, & A. Walton, "Improved HDDR processing route for production of anisotropic powder from

sintered NdFeB type magnets", Journal of Magnetism and Magnetic Materials, vol. 350, pp. 114-118, Jan. 2014.

[50] Stig Högberg, "Direct Reuse of Rare Earth Permanent Magnets from Rotating Machines", PhD thesis, Danmarks Tekniske Universitet, 2016.

[51] U. Bast, R. Blank, M. Buchert, T. Elwert, F. Finsterwalder, G. Hornig, T. Klier, S. Langkau, F. Marscheider-Weidemann, J. O. Muller, C. Thurigen, F. Treffer, & T. Walter, "Recycling von komponenten und strategischen metallen aus elektrischen fahrantrieben", (in German) MORE Project report, Aug 2014.

[52] J. Franke, A. Dobroschke, J. Tremel & A. Kühl, "Innovative Processes and Systems for the Automated Manufacture, Assembly and Test of Magnetic Components for Electric Motors", 1st International Electric Drives Production Conference (EDPC), pp. 228-234, September 2011.

[53] B. Karlsson & J. O. Jarrhed, "Recycling of electrical motors by automatic disassembly", Measurement Science and Technology, vol. 11, no. 4, pp. 350-357, January 2000.

[54] T. Yuksel & I. Baylakoglu, "Recycling of Electrical and Electronic Equipment, Benchmarking of Disassembly Methods and Cost Analysis", IEEE International Symposium on Electronics and the Environment 2007, pp. 1-5, May 2007.

[55] M. Bdiwi, A. Rashid & M. Putz, "Autonomous Disassembly of Electric Vehicle Motors Based on Robot Cognition", IEEE International Conference on Robotics and Automation (ICRA) 2016, pp. 2500-2505.

[56] T. Elwert, D. Goldmann, F. Romer, M. Buchert, C. Merz, D. Schueler, and J. Sutter, "Current developments and challenges in the recycling of key components of (hybrid) electric vehicles", Recycling Journal, vol. 1, no. 1, pp. 25– 60, October 2015.

[57] S. T. Lundmark & M. Alatalo, "A segmented claw-pole motor for Traction Applications Considering Recycling Aspects", 8th International Conference and Exhibition on Ecological Vehicles and Renewable Energies (EVER) 2013, pp. 1-6, March 2013.

[58] M. Alatalo, S. T. Lundmark & E. A. Grunditz, “Electric Machine Design for Traction Applications Considering Recycling Aspects Review and New Solution”, 37th Annual Conference of the IEEE Industrial Electronics Society (IECON), pp. 1836-1841, November 2011.

[59] G. Hennenberger, & J. A. Viorel, “Variable Reluctance Electrical Machine”, Shaker Verlag, Aachen, 2001.

[60] R. H. Park, “Two Reaction Theory of Synchronous Machines: Generalized Method of Analysis-Part I”, Transactions of the American Institute of Electrical Engineers, vol. 48, no. 3, pp. 716-727, July 1929.

[61] Andreas Krings, “Iron Losses in Electrical Machines — Influence of Material Properties, Manufacturing Processes, and Inverter Operation”, PhD thesis, KTH School of Electrical Engineering, 2014.

[62] G. Bertotti, “General Properties of Power Losses in Soft Ferromagnetic Materials”, IEEE Transactions on Magnetics, vol. 24, no. 1, pp. 621-630, January 1988.

[63] MATLAB R2016b, Mathworks.

[64] Antoine Tan-Kim, “Contribution à l’étude du bruit acoustique d’origine magnétique en vue de la conception optimal de machines synchrones à griffes pour application automobile”, Thèse de doctorat, l’Université de Technologie de Compiègne, pp. 61-70, 2015.

[65] A. K. Jha, Z. Li, A. Garcia, P. Upadhayay, P. O. Rasmussen, A. Kedous-Lebouc, and L. Garbuio, “Weighted index of recycling and energy (WIRE) cost for Motors in electric vehicles,” International Symposium on Power Electronics, Electrical Drives, Automation and Motion (SPEEDAM) 2018, pp. 407-412, June 2018.

[66] T. J. Barlow, S. Latham, I. S. McCrae, P. G. Boulter, A reference book of driving cycles for use in the measurement of road vehicle emissions, version. 3, United Kingdom: IHS, 2009, pp. 21.

[67] P. Lazari, J. Wang, and L. Chen, "A Computationally Efficient Design Technique for Electric-Vehicle Traction Machines," IEEE Trans. on Industry Applications, vol. 50, no. 5, pp. 3203-3213, Sep.-Oct. 2014.

[68] K. Kiyota, H. Sugimoto, and A. Chiba, "Comparing Electric Motors: An Analysis Using Four Standard Driving Schedules," IEEE Industry Applications Magazine, vol. 20, no. 4, pp. 12-20, July-Aug. 2014.

[69] Qi Li, Tao Fan, Ye Li, Z. Wang, X. Wen, and Jing Guo, "Optimization of external rotor surface permanent magnet machines based on efficiency map over a target driving cycle," 20th International Conference on Electrical Machines and Systems (ICEMS) 2017, pp. 1-5, Aug. 2017.

[70] P. D. Walker, and H. M. Roser, "Energy consumption and cost analysis of hybrid electric powertrain configurations for two wheelers," Applied Energy Journal, vol. 146, pp. 279-287, May 2015.

[71] C. Krasopoulos, M. Beniakar, and A. G. Kladas, "Comparison of Three Different In-Wheel SMPM Motor Configurations Based on the Urban NEDC," Materials Science Forum, vol. 856, pp. 233-238, May 2016.

[72] Ganji B., Kouzani A. Z., Trinh H. M., "Drive Cycle Analysis of the Performance of Hybrid Electric Vehicles," In: Li K., Fei M., Jia L., Irwin G.W. (eds) Life System Modeling and Intelligent Computing. Lecture Notes in Computer Science, vol. 6328, pp. 434-444, Springer, Berlin, Heidelberg, 2010.

[73] J. O. Estima, and A. J. M. Cardoso, "Efficiency Analysis of Drive Train Topologies Applied to Electric/Hybrid Vehicles," IEEE Trans. on Vehicular Technology, vol. 61, no. 3, pp. 1021-1031, Mar. 2012.

[74] E. Carraro, M. Morandin, and N. Bianchi, "Traction PMASR Motor Optimization According to a Given Driving Cycle," IEEE Trans. on Industry Applications, vol. 52, no. 1, pp. 209-216, Jan.-Feb.. 2016.

[75] O. Karabasoglu, and J. Michalek, "Influence of driving patterns on life cycle cost and emissions of hybrid and plug-in electric vehicle powertrains," Energy Policy Journal, vol. 60, pp. 445-461, Sep. 2013.

[76] M. Novak, J. Novak, and Z. Novak, "Methodology for Efficiency Mapping of Permanent Magnet Synchronous Motors," 19th International Conference on Electrical Drives and Power Electronics (EDPE) 2017, pp. 205-210, Oct. 2017.

[77] Electricity price statistics, http://ec.europa.eu/eurostat/statistics-explained/index.php/Electricity_price_statistics

[78] Alliance LLC, Commodity prices. http://www.allianceorg.com/magnetandmaterialcosts.html

[79] H. Jin, P. Afiuny, S. Dove, G. Furlan, M. Zakotnik, Y. Yih, and J. W. Sutherland, "Life Cycle Assessment of Neodymium-Iron-Boron Magnet-to-Magnet Recycling for Electric Vehicle Motors," Environ. Sci. Technol. Journal, 52 (6), pp 3796–3802, 2018.

[80] M. Kimiabeigi, R. S. Sheridan, J. D. Widmer, A. Walton, M. Farr, B. Scholes, and I. R. Harris, "Production and Application of HPMS Recycled Bonded Permanent Magnets for a Traction Motor Application," IEEE Trans. on Industrial Electronics, vol. 65, no. 5, pp. 3795-3804, May 2018.

[81] A. Walton, Han Yi, N. A. Rowson, J. D. Speight, V. S. J. Mann, R. S. Sheridan, A. Bradshaw, I. R. Harris, A. J. Williams "The use of hydrogen to separate and recycle neodymium iron boron-type magnets from electronic waste," Journal of Cleaner Production, vol. 104, no. 1, pp. 236-241, October 2015.

[82] L. U. Lopes, M. A. Carvalho, R. S. Chaves, M. P. Trevisan, Paulo A. P. Wendhausen, H. Takiishi, "Study of Carbon Influence on Magnetic Properties of Metal Injection Molding Nd-Fe-B Based Magnets," Materials Science Forum, vol. 727-728, pp. 124-129, August 2012.

[83] United Nations Economic Commission for Europe (UNECE), World Forum for Harmonization of Vehicle Regulations. http://www.unece.org

[84] Pranshu Upadhayay, A. G. Garcia, Z. Li, A. K. Jha, P. O. Rasmussen, A. K. Lebouc, J. C. Mipo, "Evaluation of Energy Cost Index for an Electric Vehicle Motor over a particular Drive Cycle with Recycled Magnet Concept", 23rd International Conference on Electrical Machines (ICEM), pp. 738-744, September 2018.

[85] Geoffrey Devornique, J. Fontchastagner, D. Netter, and N. Takorabet, "Hybrid Model: Permeance Network and 3-D Finite Element for Modeling Claw-Pole Synchronous Machines", IEEE transactions on Magnetics, vol. 53, no. 6, June 2017.